Synthesis and Biological Characterisation of HPMA copolymer-Mannose Conjugates Designed for Intracellular Delivery of Anti-Leishmanial Compounds to Macrophages

Kerri-Lee Wallom
BSc (Hons.)

A thesis submitted to Cardiff University in partial fulfilment of the requirements for the degree of Doctor of Philosophy

Centre for Polymer Therapeutics
Welsh School of Pharmacy
Cardiff University
United Kingdom

ProQuest LLC
789 East Eisenhower Parkway
P.O. Box 1346
Ann Arbor, MI 48106-1346

DECLARATION

This work has not previously been accepted in substance for any degree and is not concurrently submitted in candidature for any degree.

Signed K Wallon Date 4th August 2008

STATEMENT 1

This thesis is being submitted in partial fulfilment of the requirements for the degree of PhD.

Signed K Wallon Date 4th August 2008

STATEMENT 2

This thesis is the result of my own independent work / investigation, except where otherwise stated. Other sources are acknowledged by explicit references.

Signed K Wallon Date 4th August 2008

STATEMENT 3

I hereby give consent for my thesis, if accepted, to be available for photocopying and for inter-library loan, and for the title and summary to be made available to outside organisations

Signed K Wallon Date 4th August 2008

For David

Acknowledgements

I would like to take this opportunity to thank the many people who have helped me over the last 3 years and in the completion of this thesis. I would first like to thank my supervisor Prof. Ruth Duncan for giving me the opportunity to contribute to this exciting area of research and to work with such a diverse range of people. I am particularly grateful for the constant encouragement throughout my PhD studies. I would also like to thank my second supervisor Prof. Ian Gilbert for his support, and to acknowledge the Wellcome Trust for funding my PhD studentship.

I would not be here today without the support of my family. Great thanks go to my mum and dad, whose belief in me has been unerring. I thank my little sister Hollie and beautiful Charlie, for helping me keep sight of the important things in life. I would also like to thank my new in-laws for making me feel part of their family and always showing an interest in my work.

I would like to thank my friends and colleagues who have been with me over the last few years. During the collaborative aspects of this project Salvatore Nicoletti and Karin Seifert have contributed their knowledge and experience, and thanks to Arwyn, my mentor, for his advice. I would also like to give huge thanks to Jan and Wendy for all their help.

Many thanks are due to Elaine, I am grateful to have had someone fun and understanding to share this experience with from the start. Also, thanks for the cakes. Thanks to Fran, who's inspirational, fabulous Lucile, the new members of CPT, Sam and Cath, for their intellectual discussions and gossip, and to Sian, who's an example of how, with guts and determination, you can overcome all obstacles. I would also like to thank Helena, Jing, Karen, Tom, Neal, Zeena, Maria, Alison, Phil and everyone else who welcomed and advised me during my studies.

Thank you to all my good friends who have provided love and laughs, in particular Jenny and Rachel, and also David, Martin (the quickest PhD in the west), Leyla and all those too numerous to mention.

Most of all, I want to express deep gratitude to my husband David, 'the best boy in the world'. Thank you for your patience and your support throughout the most difficult and the best time of my life. Thank you.

Abstract

Visceral leishmaniasis is the second largest parasitic killer in the world (after malaria) with 59,000 deaths annually. The parasite resides in macrophages, within a compartment called the parasitophorous vacuole, but many anti-leishmanial drugs are toxic and poorly effective due to the low concentrations attained in this compartment. Therefore, the aim of this study was to establish the basis for design of N-(2-hydroxypropyl)methacrylamide (HPMA) copolymer-drug conjugates that would target the parasitophorous vacuole, with potential to deliver improved treatments for leishmaniasis. Mannose was selected as a ligand for macrophage targeting and amphotericin B as a model drug.

First, *in vitro* macrophage models (RAW 264.7 and THP-1 cells) were established that displayed mannose receptor expression and uptake of mannosylated macromolecular ligands. A library of HPMA copolymer-mannose conjugates containing Oregon Green (OG) were then synthesised to define the optimal mannose loading needed for targeting. To define the fate of internalised conjugates a density gradient subcellular fractionation method was developed for THP-1 cells. Finally HPMA copolymer-amphotericin B ± mannose conjugates were synthesised and their cell uptake, intracellular fate and preliminary haemolytic and cytoxicity profiles established.

HPMA copolymer-OG-Man conjugates with a mannose loading ≥ 4 mol % showed significantly higher uptake by THP-1 cells. The subcellular fractionation and confocal fluorescence microscopy confirmed time-dependent trafficking of such conjugates to late endosomes/lysosomes. Release of free OG (as a drug model) from the biodegradable polymer-OG linker was seen. HPMA copolymer-amphotericin B-mannose conjugates were taken up 5-fold faster than the control and accumulated in the late endosome/lysosomal compartment. HPMA copolymer-amphotericin B- mannose conjugates displayed reduced haemolysis and cytotoxicity against the THP-1 cells.

This study has established methods to investigate the intracellular trafficking of polymer-drug conjugates, and has demonstrated the potential of mannose-targeted HPMA copolymer conjugates for effective targeting of anti-leishmanial drugs to macrophages.

Contents

List of Figures

Chapter 1: General Introduction

Chapter 2: Materials and General Methods

Chapter 3: Characterisation of the *in vitro* models used to evaluate macrophage targeting using mannosylated probes

Chapter 6: Synthesis of HPMA copolymer-AmB conjugates and determination of activity and intracellular fate

List of Tables

Abbreviations

AmB	Amphotericin B
ANOVA	Analysis of variance
AP	Aminopropanol
APS	Ammonia persulphate
ASGPR	Asialoglycoprotein receptor
ATCC	American Type Culture Collection
BCA	Bicinchoninic acid
BSA	Bovine serum albumin
CB	Coomassie brilliant blue
CR	Complement receptor
CRD	Carbohydrate recognition domain
DMEM	Dutch modified Eagles medium
DMSO	Dimethylsulphoxide
DNDi	Drugs for Neglected Diseases initiative
Dox	Doxorubicin
DTT	Dithiothreitol
ECACC	European Collection of Cell Cultures
ECL	Enhanced chemiluminescence
EDTA	Ethylenediaminetetraacetic acid
EEA-1	Early endosomal antigen-1
EPR	Enhanced permeability and retention
FBS	Foetal bovine serum
FITC-BSA	FITC-labelled bovine serum albumin
FITC-BSA-Man	FITC-labelled mannosylated bovine serum albumin
GFLG	Gly-Phe-Leu-Gly
GPC	Gel permeation chromatography
HB	Homogenisation buffer
HEPES	N-2-hydroxyethylpiperazine-N`-ethanesulphonic acid
Hex A	N-Acetyl-β-glucosaminidase
HPLC	High performance liquid chromatography
HPMA	N-(2-hydroxypropyl)methacrylamide
HRP	Horse radish peroxidase
INT	2-p-iodonitrotetrazolium violet
IFN	Interferon
IL	Interleukin
LAMP	Lysosome-associated membrane proteins
LDL	Low density liposomes
LPG	Lipophosphoglycan
LPS	Lipopolysaccharide
MA	Methacrylic acid
MHC	Major histocompatibility complex
MLV	Multilameller vesicles
MR	Mannose receptor
MSF	Médecins Sans Frontières
MTD	Maximum tolerated dose
MTT	3-(4,5-dimethylthiazol-2-yl)-2,5-diphenyl-2H-tetrazolium
Mw	Molecular weight
NADH	Reduced nicotinomide adenine dinucleotide

NADPH	ß-nicotinamide adenine dinucleotide reduced disodium salt
NO	Nitric oxide
OG	Oregon green
ONp	P-nitrophenol
OPM	O-palmitoyl mannan
PBS	Phosphate buffered saline
PEG	Polyethylene glycol
PGA	Polyglutamic acid
PNS	Post nuclear supernatant
PAM	P-aminophenyl-mannopyranoside
RBC	Red blood cell
PKC	Protein kinase C
PKDL	Post Kala Azar Dermal Leishmaniasis
PMA	Phorbol 12-myristate 13-acetate
PV	Parasitophorous vacuole
RES	Reticuloendothelial system
SCF	Subcellular fractionation
SDS-PAGE	Sodium dodecyl sulphate polyacrylamide gel electrophoresis
SD	Standard deviation
SEM	Standard error of the mean
TBS	Tris-buffered saline
TEMED	N,N,N,N'-tetra-methyl-ethylenediamine
Th-	T cell helper cell type
TIF	Tagged image file
TLC	Thin layer chromatography
TNF-α	Tumour necrosis factor-α
Tris-Base	Tris(hydroxymethyl)aminomethane
Tris HCl	Tris(hydroxymethyl)aminomethane hydrochloride
Tf-TxR	Transferrin Texas red
TDR	Tropical Diseases Research Programme
UV	Ultraviolet
VL	Visceral Leishmaniasis
WHO	World Health Orghanisation

Chapter 1

General Introduction

1.1 Introduction

The aim of this study was to design and characterise targeted polymer-drug conjugates active against the parasitic disease leishmaniasis. Visceral leishmaniasis (VL) belongs to a group of diseases broad in distribution and phenotype. They are known by an equally broad group of names such as Baghdad Boil, Valley Sickness, Espundia, White Leprosy, Dum-Dum Fever, and most commonly Kala Azar. Leishmaniasis was officially named after the Scottish pathologist William Boog Leishman in 1901 (Herwaldt, 1999), and it falls into a category of what have been termed 'neglected diseases', i.e. those prevalent in developing countries that receive little research funding (Beyrer et al., 2007). Combined with problems such as poor diagnosis, co-infection with HIV and increasing resistance to current therapies, VL is becoming an increasing threat. It is the second largest parasitic killer in the world (after malaria) with 59,000 deaths annually. This leads the World Health Organisation (WHO) to classify it as a Class 1 disease, emerging and uncontrolled (WHO, 2001).

Leishmaniasis results from the bite of a sandfly that transmits the *Leishmania* parasite. The parasite then infects, and resides within, the host macrophage cells (Alexander et al., 1999). After uptake into the macrophage, it lives and multiplies within a specialised vesicle called the parasitophorous vacuole (PV) (Courret et al., 2002). The fact that the parasite resides within such a protected environment presents a major obstacle to therapy. Current drugs used in the treatment of VL include, as first line, long course treatments of pentavalent antimonials (Pentostam, Glucantime). These are highly toxic and have shown growing resistance in endemic areas (Murray, 2000; Sundar et al., 2000). Second line treatments include pentamidine and amphotericin B (Fungizone), which have also shown growing resistance and high toxicity. The problems of systemic toxicity and resistance have led to an interest in methods for targeted delivery of anti-leishmanial drugs to the macrophage.

Liposomal formulations have been explored as a means of improving drug delivery, particularly for Amphotericin B (AmB) (Lopez-Berestein, 1988). Liposomes show increased uptake by macrophages and are the most common

method studied for macrophage drug delivery (Ahsan et al., 2002). The liposomal Ambisome® has been approved for treatment of VL and shows decreased AmB-related toxicity (Bern et al., 2006), however it is also the most expensive and least cost effective drug for VL, even where preferential pricing occurs (Vanlerberghe et al., 2007).

In addition to liposomes, polymers are being increasingly explored as drug delivery agents. A few studies have investigated polymer-drug conjugates as an alternative delivery system for targeted delivery of anti-leishmanials (discussed in further detail in section 1.5.3). There are several advantages of using polymer conjugates for delivering anti-leishmanial agents. By targeting high drug concentration in vicinity of the parasite, they can reduce non-specific toxicity and possibly overcome drug resistance. The polymer-drug linker can also be tailored to give a controlled rate of release in the specific target cell/compartment. Therefore, it is hypothesised that polymers are potentially an ideal way to target anti-leishmanial drugs to the PV of the macrophage. To understand the scope of this project, it is important to understand the pathology of *Leishmania* and the limitations to its treatment, as well as the background to drug targeting and polymer therapeutics. These areas will be discussed in the following sections.

1.2 Leishmaniasis

When designing a drug delivery system it is important to consider the various disease characteristics as these factors may affect the design. The following sections discuss the parasitic life cycle of *Leishmania*, the disease complex in general and then specifically VL.

1.2.1 Epidemiology

An estimated 350 million people are at risk worldwide of leishmaniasis with 12 million currently affected (Desjeux, 2001). This includes both overt disease and symptom-less disease. There are an estimated 1.5 - 2 million new cases of leishmaniasis annually, though only 600,000 are declared. Located mainly in tropics and sub-tropics, the disease is endemic in 88 countries on 5 continents - Africa, Asia, Europe, North America and South America (Figure 1.1). The severity of disease is highly dependent on the location and the species of

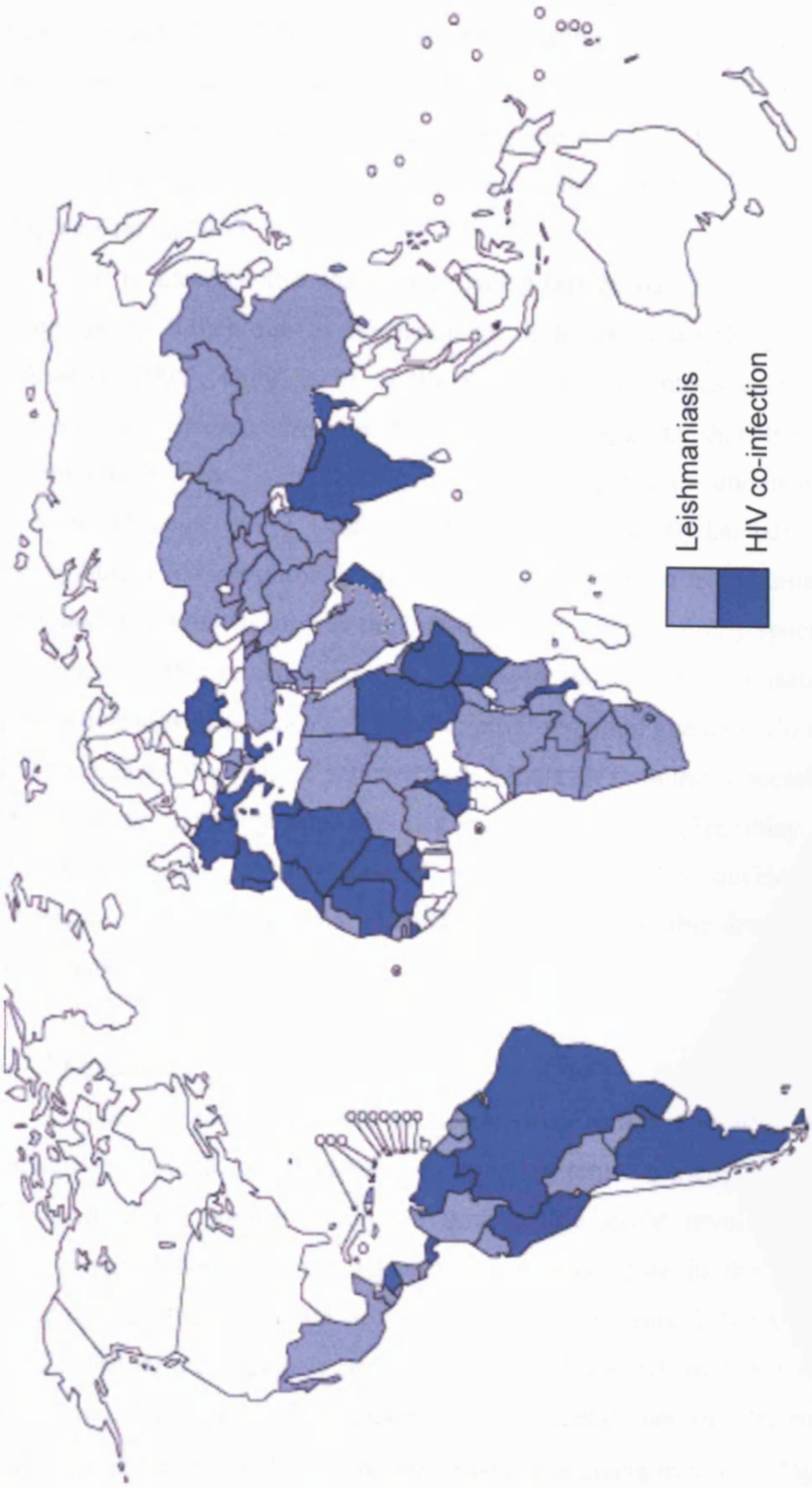

Figure 1.1 Distribution of Leishmaniasis worldwide and its co-infection with HIV (taken from www.who.int/tdr/tropical_diseases/databases/imagelib.pl (2003).

infecting parasite (Table 1.1). Of the 2 million new cases of leishmaniasis annually, the fatal visceral form of the disease makes up 500 000, and of these 90% are located in only 5 countries - Bangladesh, Brazil, India, Nepal and Sudan. Severe epidemics periodically occur, for example in Sudan in the 1990's and Afghanistan in 2002.

It is accepted that the actual disease burden has been underestimated for many years, either due to misdiagnosis or to cases simply going unrecorded (Desjeux, 2001). Only in 32 of the 88 endemic countries is it compulsory to declare this disease. Despite this, evidence suggests that the incidence of leishmaniasis may be increasing, even taking previous underestimations into account (Desjeux, 2001). Until now, spread of the sandfly has been limited by its susceptibility to cold climates, its tendency to take blood from humans or animals only and its ability to support the internal development of only specific species of *Leishmania*. The recent spread is related to increasing urbanisation and large population movements, as well as other environmental changes. Co-infection with HIV increases the risk of infected individuals developing visceral disease, and therefore the mortality rate, and is a growing concern (Tremblay et al., 1996). Again, the spread of co-infection is mainly restricted to developing countries. Therefore it is imperative that effective, safe and affordable drugs be available in these regions.

1.2.2 Life cycle

The complex life cycle of *Leishmania* means that drug access to the parasite is limited, and treatment without systemic toxicity a major obstacle. *Leishmania* are parasitic protozoa with a life cycle involving two distinct morphological forms of the parasite, the promastigote in the vector, and the amastigote in the vertebrate or mammalian host (Figure 1.2) (Alexander et al., 1999). The promastigote is an extracellular, elongated, motile flagellate form, about 10-20 μm long. The amastigote is a round, non-motile, predominantly intracellular form, about 3-7 μm in diameter. The chang in morphology, as well as the various locations inhabited, impacts on the susceptibility of the parasite to therapy.

The female phlebotomine sand fly acts as a vector, becoming infected when feeding on the blood of an infected human or animal reservoir (Bates,

Table 1.1 Species, geographical distribution and disease type of Leishmania parasite[†].

Subgenus	Complex	Subspecies	Geographical Distribution	Disease Type
Leishmania	*Leishmania donovani*	*L.donovani*	China, India, Iran, Sudan, Kenya, Ethiopia	Visceral
		L.infantum	Mediterranean Basin, Central and West Asia	Visceral
		L.chagasi	Brazil, Columbia, Venezuela, Argentina	Visceral
Leishmania	*Leishmania tropica*	*L.minor*	Mediterranean Basin, Afganistan	Cutaneous
		L.major	Central and West Asia, W. N. and Central	Cutaneous
			Africa	Cutaneous
		L.aethipica	Ethiopia, Kenya	
Leishmania	*Leishmania mexicana*	*L.mexicana*	Mexico, Honduras, Guatemala	Cutaneous
		L.amazonensis	Amazon Basin	Cutaneous
		L.pifanoi	Venezuela	Cutaneous
Vianna	*Leishmania*	*L.braziliensis*	Brazil, Peru, Ecuador, Columbia, Venezuela	Cutaneous/mucocutaneous
	braziliensis	*L.guyanensis*	Guyana, Brazil, Venezuela	Cutaneous
		L.panamensis	Panama, Columbia	Cutaneous
		L.peruviana	Peru	Cutaneous

[†] Adapted from 'Bates et al., 2007'

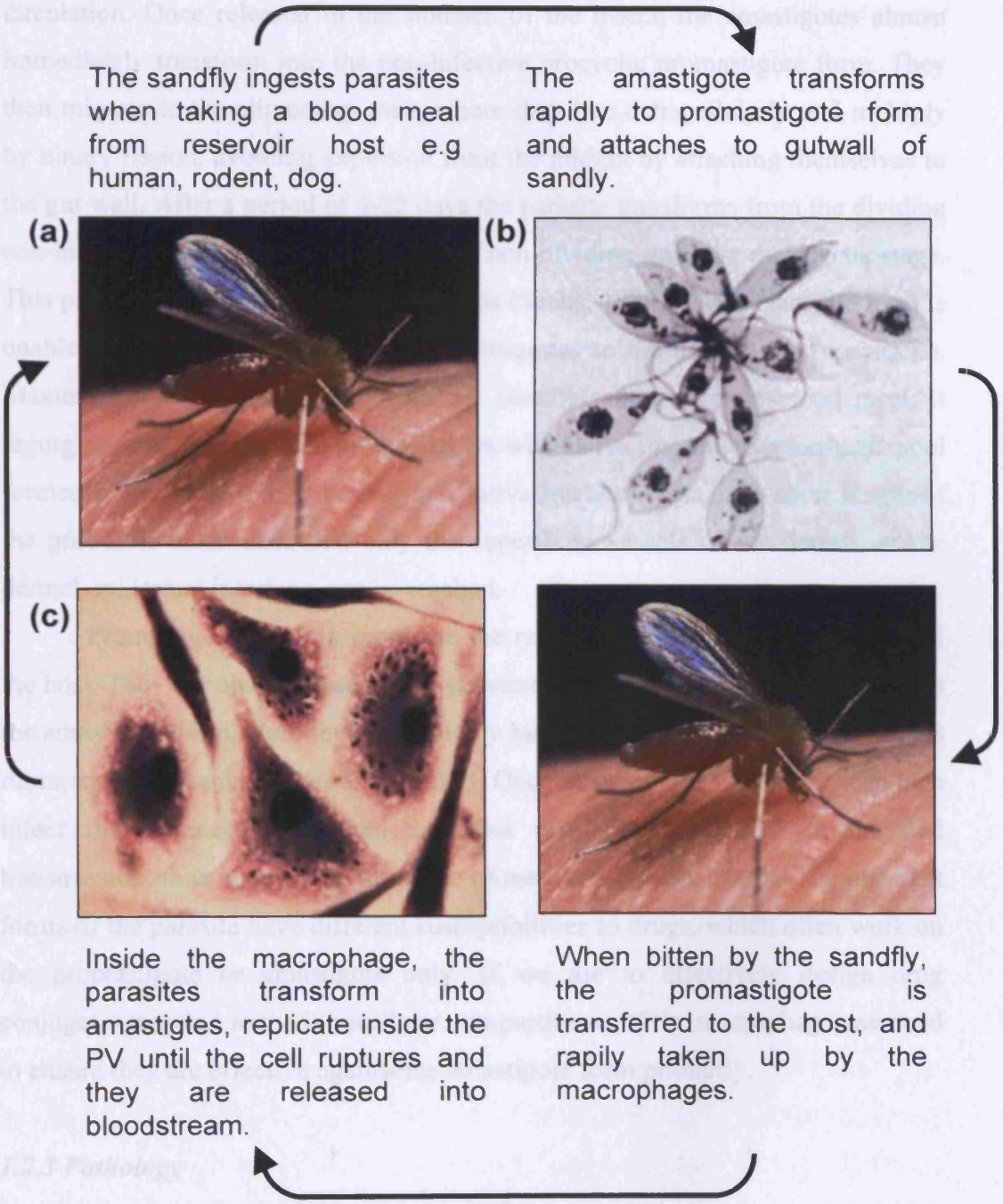

Figure 1.2 The dimorphic life cycle of the *Leishmania* parasite. Stages include infection of its reservoir host and transmission via the sandfly to the human host. Photos were reproduced from www.who.int/tdr/tropical_diseases/databases/imagelib.pl (2003), (a) Phlebotomus sandfly WHO/TDR/Stammers, (b) promastigotes WHO/TDR/Pasteur Inst., and (c) macrophage infected with amastigotes WHO/TDR/Behin.

2007). It ingests either infected macrophages, or released amastigotes in the circulation. Once released in the stomach of the insect, the amastigotes almost immediately transform into the non-infective procyclic promastigote form. They then migrate to the alimentary tract, where they live extracellularly and multiply by binary fission, avoiding expulsion from the midgut by attaching themselves to the gut wall. After a period of 4-25 days the parasite transforms from the dividing non-infective procyclic promastigote to a non-dividing infective metacyclic stage. This process is known as metacyclogenesis (Sacks, 1989). The metacyclic form is unable to attach to the gut wall and so migrates to the mouthparts (proboscis). Maximum infectivity coincides with the sandfly taking its next blood meal. It regurgitates between 1-1000 promastigotes with saliva into the haemorrhagic pool formed by lacerated blood vessels and saliva hyaluronidase. The short length of the proboscis determines that only the superficial vessels of the dermis, at the dermal-epidermal interface, can be reached.

Promastigotes rapidly parasitise the reticulo-endothelial system (RES) of the host. They are phagocytosed by host macrophages, inside which they revert to the amastigote form. Here they replicate by binary fission until the macrophage is ruptured and the amastigotes are released. Once in the blood stream they can then infect other macrophages, and are also available for vector uptake and transmission, thus completing the cycle (Amer & Swanson, 2002). The different forms of the parasite have different susceptibilities to drugs, which often work on the promastigote or amastigote only. If we are to effectively design drug conjugates targeted to the intracellular compartments of the macrophage, we need to ensure they are effective against the amastigote form primarily.

1.2.3 Pathology

The various species of *Leishmania* produce very different phenotypes, which are likely to necessitate specific therapies, as drugs may be active against only certain species and require targeting to different sites. The phenotype varies from the very mild cutaneous form to the fatal visceral form (Murray et al., 2005). The manifestations and outcome depend not only on the infecting species, but is also modulated by the host immune response. There are over 30 species of *Leishmania,* categorised into two subgenera that infect mammals, *Leishmania leishmania* and *Leishmania vianna* (Banuls et al., 2007). The *L. leishmania* group

are primarily located in the Old World and transmitted by *Phlebotomus* sand fly species, whereas *L. vianna* is predominantly in the New World, transmitted by the *Lutzomyia* species. The disease complex can be broadly categorised into three types.

Cutaneous leishmaniasis is the most common form (Figure 1.3a). It is confined to the dermis, usually involving a self-healing lesion, although it can present as a relapsing ulcer, or spread to other cutaneous areas of the body. The *mucocutaneous* form initially appears as a single dermal lesion then multiple lesions that undergo extensive ulceration (Figure 1.3b). After a variable period it will spread to the cartilage and other connective tissues of the nasopharynx, causing extensive tissue destruction and disfiguration. The more serious cases are often fatal.

Visceral leishmaniasis is the most serious form, most commonly known as 'kala azar'. This is where treatment is most clearly needed, and where a targeted therapy could be most effective (Figure 1.3c). Subspecies of the *Leishmania donovani* complex cause systemic infections, resulting in intermittent fever and dysfunction of the liver, spleen, bone marrow and lymph nodes. The manifestations usually appear within 3 months of infection. Fever is the most common symptom, accompanied by tachycardia, and frequently by diarrhoea and cough. The spleen and liver enlargement is dramatic, and there is often immune complex glomerulonephritis and interstitial nephritis. The later manifestation of hyperpigmentation gives the name 'kala azar' or 'black fever' in Hindi. The fatality rate of untreated cases exceeds 80%, but the response to available drugs in non-resistant cases is relatively good. Later relapse occurs in ~ 3 - 10% of patients, presenting as the cutaneous form 'post kala-azar dermal leishamaniasis' (PKDL). This then acts as a readily accessible infection source for the vector.

As VL is caused primarily by the subspecies of *Leishmania donovani* it was therefore decided here to concentrate on this species. Each species has different survival strategies and mechanisms within the host, which may be relevant to choice of therapy. Therefore the following section will concentrate on studies on the *L. donovani* species.

(a) Cutaneous leishmaniasis

- single lesion

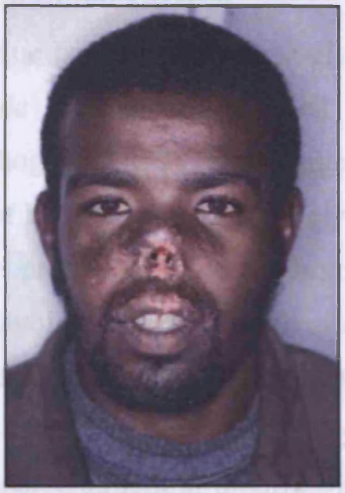

(b) Mucocutaneous leishmaniasis

- nasopharangeal tissue distruction

(c) Visceral leishmaniasis

- splenomegaly

Figure 1.3 The three major clinical manifestations of leishmaniasis. Photos were reproduced from www.who.int/tdr/tropical_diseases/databases/imagelib.pl (2003), (a) WHO/TDR, (b) WHO/TDR/Crump, (c) WHO/TDR/Crump.

1.3 Parasite invasion and survival

Leishmania parasites have evolved to both evade and take advantage of the immune response of the host (Cunningham, 2002). The parasite evades and/or survives the humoral response by living in the macrophage, and also survives the cellular response of the macrophage phagosome (Awasthi et al., 2004). The activity of the polymer conjugate will, in part, depend on its intracellular trafficking in relation to the parasite.

1.3.1 Extracellular survival

Unique parasite membrane glycoconjugates are key to survival both inside and outside the macrophage cell (Ilg, 2000). Promastigotes have a unique lipophosphoglycan (LPG) molecule on their cell surface. They express large amounts of LPG as well as other glycoconjugates, such as gp63, on their surface, thought to protect the parasite from hydrolytic enzymes in the sandfly gut. In order to avoid being excreted after digestion of the blood meal, procyclic amastigotes attach to the midgut epithelium through binding interactions involving LPG with lectins in the gut. As it differentiates into the metacyclic form, extensive structural modifications, involving its size and the expression of terminally exposed sugars, are made to the LPG molecule, reducing the binding affinity for lectins. This leads to detachment from the gut wall, and migration to the pharynx.

Once transmitted to the vertebrate host, the parasite must avoid destruction by the immune system while transiently in the bloodstream. The first attack is by complement. Metacyclic promastigotes not only resist lysis by complement but also use it to gain entry into the macrophage. *L. donovani* metalloprotease gp63 helps prevent complement-mediated lysis and enhances promastigote uptake by cleaving C3b to C3bi, an opsonin that binds the macrophage complement receptor CR3 (Brittingham et al., 1995). Also, sandfly saliva contains a peptide called maxadilan. This has been suggested to inhibit the lipopolysaccharide (LPS) stimulated macrophage from producing tumour necrosis factor-α (TNF-α) and nitric oxide to kill the parasite (Morris et al., 2001). Once inside the macrophage, a variety of protection mechanisms are employed to keep the parasite hidden from

the immune system, and protected from destruction.

1.3.2 The Macrophage

To develop a rationale for the design of macrophage targeted polymer-drug conjugates it is important to review the current knowledge of macrophage biology and the relationship with the *L. donovani* parasite. Life within the macrophage enables *Leishmania* to remain hidden from the host immune system, and consequently also results in protection from any drug given systemically. The macrophage plays a very important role in the innate immune system and this role is what has enabled its parasitism (Amer & Swanson, 2002; Berman et al., 1979; Gordon et al., 1992). Macrophages are phagocytes responsible for removing senescent, dead and damaged cells, and are unique in being able to ingest large microorganisms such as protozoa. They also act as antigen presenting cells, signalling and activating other immune cells.

The tissue macrophages form a network called the reticuloendothelial system found in a number of organs. They exhibit a large degree of phenotypic heterogeneity and include the Kupffer cells in the liver, the intraglomerula mesangium of the kidney, the alveolar macrophages in the lung, the serosal macrophages, the brain microglia, the spleen sinus macrophages and the lymph node sinus macrophages. Macrophages, as part of the innate immune system, are professional phagocytes. The size of the phagosome is determined by the size of the ingested particle and can be almost as large as the cell itself. To initiate phagocytosis by resident macrophages (constitutively in the tissue) or recruited macrophages (monocytes recruited from circulation that are then triggered to differentiate), the cell must be 'triggered' by ligation of its receptors (Aderem & Underhill, 1999b). The mechanisms of uptake and the resulting vacuole are discussed in sections 1.3.4 and 1.3.5.

Numerous receptors are involved in macrophage phagocytosis, recognising both endogenous and exogenous ligands. Altered host cells, apoptotic or infected, are recognised by scavenger-type receptors, which suppress or induce inflammatory responses, though by incompletely understood mechanisms (Pluddemann et al., 2007). Endogenous ligands recognised by macrophage

receptors include modified lipoproteins, lysosomal hydrolases, heat-shock proteins, and proteinase complexes, therefore playing a major role in tissue homeostasis. Exogenous ligands, such as those on micro-organisms, are recognised by receptors that either recognise opsonins that coat the molecule, such as antibody, complement and LPS-binding protein; or that directly recognise ligands such as carbohydrates, proteins, lipids and nucleic acids (Linehan et al., 2000); or both. These receptors include the Fc receptor, complement receptors (CR), and the mannose receptor; which bind ligands such as immunoglobulin, complement and glycoproteins (Table 1.2).

1.3.3 The mannose receptor

The mannose receptor (MR) is a promising target for macrophage delivery, and certainly the most widely used. It is also an important method of entry for the *Leishmania* parasite into the macrophage. The MR is one of the best characterised of the macrophage receptors, first discovered in macrophages (Pontow et al., 1992), then dendritic cells (Sallusto et al., 1995). It is a 165 kD type 1 transmembrane glycoprotein with 8 C-type lectin carbohydrate-recognition domains (CRDs), a fibronectin-like domain, and a cysteine-rich domain (Figure 1.4) (Stahl, 1992). The long cysteine rich 'tail' binds calcium and is known to be critical for MR-mediated endocytosis and sorting in the endosome (Schweizer et al., 2000). The CRDs bind sugar residues with varying affinities: L-fucose > D-mannose > N-acetyl-D-glucosamine >>> D-galactose (Kery et al., 1992; Stahl, 1992). Leishmanial membranes express all of these sugars, in particular mannose-rich glycoconjugates. The high binding affinity for oligosaccharides is generated by cooperative binding of several CRDs, although CDR4 is the only one able to mediate mannose binding alone (Linehan et al., 2000).

The MR is expressed almost exclusively by macrophages, plus dendritic cells (which can also be infected by *Leishmania*) and selected endothelial cells, but not by their precursor monocytes or other immune cells such as neutrophils. Binding of the receptor mediates endocytosis and phagocytosis of mannosylated ligands, including microbial ligands and endogenous ligands such as lysosomal hydrolases, tissue plasminogen activator, myeloperoxidase, thyroglobulin (Gordon, 2003). The receptor binds ligand at the cell surface in a Ca^{++} dependent

Table 1.2 Receptors expressed on human macrophage cells.

Receptor	Expression	Specificity	Reference
β-Glucan / Dectin-1	Macrophage Neutrophil, dendritic cell	β-Glucan (fungal cell walls)	Adachi et al., 2004
CR3 / MAC-1	Monocyte/macrophage Natural Killer, neutrophil	β-Glucan, some mannose and N-acetyl-glucosamine containing oligosaccharides	Ehlers, 2000
Galectin-3	Monocyte/macrophage Epithelial	Galactose bearing oligosaccharides	Sano et al., 2003
Mannose	Macrophage Dendritic Lymphatic and Synusoidal endothelium	Mannose, fucose and N-acetyl-glucosamine containing oligosaccharides	Wileman et al., 1986
NKCL	Monocyte /macrophage Neutrophils	Mannose	Fernandes et al., 1999
Sialoadhesin	Tissue macrophage	Oligosaccharides terminating in sialic acid	Hartnell et al., 2001
Collectin / C1q	Leukocytes Platelets Endothelium	C1q, mannose binding protein, SP-A, conglutinin	Malhotra, 1993

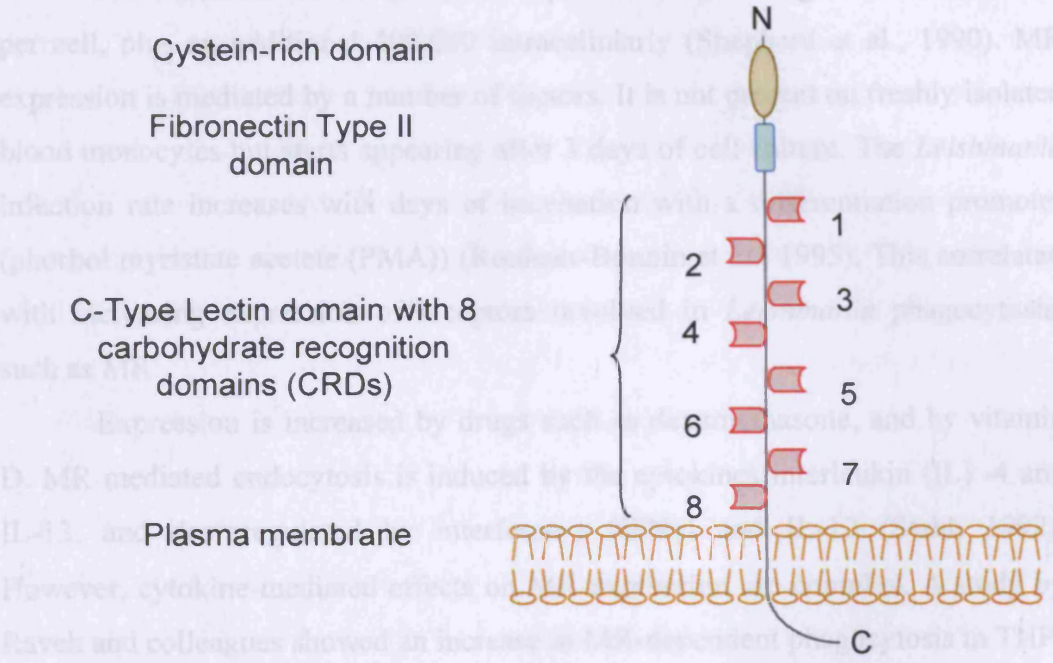

Figure 1.4 Diagram of the structure of the mannose receptor.

manner, and becomes uncoupled from the receptor in the sorting endosome, the receptor being recycled back to the surface. Ligands are directed to the lysosome for degradation. The newly synthesised receptor has a half-life of 33 h and is recycled hundreds of times before being degraded (Lennartz et al., 1989).

The normal level of cell surface expression is in the region of 100,000 MR per cell, plus an additional 400,000 intracellularly (Shepherd et al., 1990). MR expression is mediated by a number of factors. It is not present on freshly isolated blood monocytes but starts appearing after 3 days of cell culture. The *Leishmania* infection rate increases with days of incubation with a differentiation promoter (phorbol myristate acetete (PMA)) (Rouleux-Bonnin et al., 1995). This correlated with increasing expression of receptors involved in *Leishmania* phagocytosis, such as MR.

Expression is increased by drugs such as dexamethasone, and by vitamin D. MR mediated endocytosis is induced by the cytokines interleukin (IL) -4 and IL-13, and downregulated by interferon-γ (IFNγ) and IL-10 (Stahl, 1992). However, cytokine-mediated effects on MR expression are complex. A study by Raveh and colleagues showed an increase in MR-dependent phagocytosis in THP-1 macrophage cells by the cooperative effect of IFNγ and IL4, despite opposing effects on surface expression (Raveh et al., 1998).

Though activation by microorganisms is thought to decrease expression of the MR, the relationship is complicated. Rabinovitch et al. (1985) found no difference in MR-mediated uptake between *L. mexicana amazonensis* infected and non-infected macrophages *in vitro*. However, in a second study, *L. donovani* infection of macrophages resulted in a 50% reduction in surface receptors (Basu et al., 1991). This appeared to have a direct correlation with the parasite burden, as expression decreased with time of infection. However, it has also been shown that when MR expression was reduced by IFNγ, MR-mediated phagocytosis was conversely upregulated (Marodi et al., 1993). The picture is complicated by the fact that MR cannot mediate phagocytosis alone, requiring co-receptors (Le Cabec et al., 2005). Downstream effects of ligation depend on the differentiation stage of the macrophage, and the type of ligand. This may have implications for targeting. MR uptake is dissociated from macrophage activation and therefore could be

considered a 'safe' method of entry for *Leishmania* and a suitable receptor for drug targeting.

1.3.4 Endocytosis

The *Leishmania* parasite enters the macrophage by receptor-mediated phagocytosis, one route being via the MR (Handman & Bullen, 2002). The polymer-drug conjugate can also be targeted to the MR, however once internalised it may or may not localise to the same intracellular compartment as the parasite. It is therefore essential to understand the complexities of the endocytic process, and it will be important to study the trafficking of the polymer-drug conjugates. Endocytosis is a general term used to describe the internalisation of plasma membrane with extracellular material and/or extracellular fluid enclosed in a vesicle (Mukherjee et al., 1997). The process is complex but can be divided into two categories: pinocytosis and phagocytosis (Figure 1.5).

Pinocytosis literally translates as 'cell drinking' and describes the uptake of soluble material and extracellular fluid that occurs in all cell types. Pinocytosis rates vary hugely with cell type and include fluid-phase uptake of molecules in solution, adsorptive uptake involving molecules binding non-specifically to the cell membrane e.g. polar molecules; as well as specific receptor-mediated uptake e.g. transferrin by the transferrin receptor. It is actin independent. Polymer conjugates have been shown to be primarily taken up by pinocytosis, either fluid-phase, non-specific absorptive or receptor-mediated if a targeting residue is used (Duncan et al., 1981).

Phagocytosis means 'cell eating' and describes the internalisation of particulate matter carried out by specialised cells, principally monocytes, macrophages and neutrophils (Aderem & Underhill, 1999). It is characteristically receptor mediated and usually occurs for particles more than 0.75 μm in diameter. Phagocytosis is generally described by the 'zipper' analogy (Swanson & Baer, 1995). After initial particle binding, phagocytosis requires sequential recruitment of cell-surface receptors to bind the rest of the particle surface. This results in the formation of closely opposed pseudopodia extending along the particle, the resulting phagosome conforming to the shape of the particle. Initiation is triggered

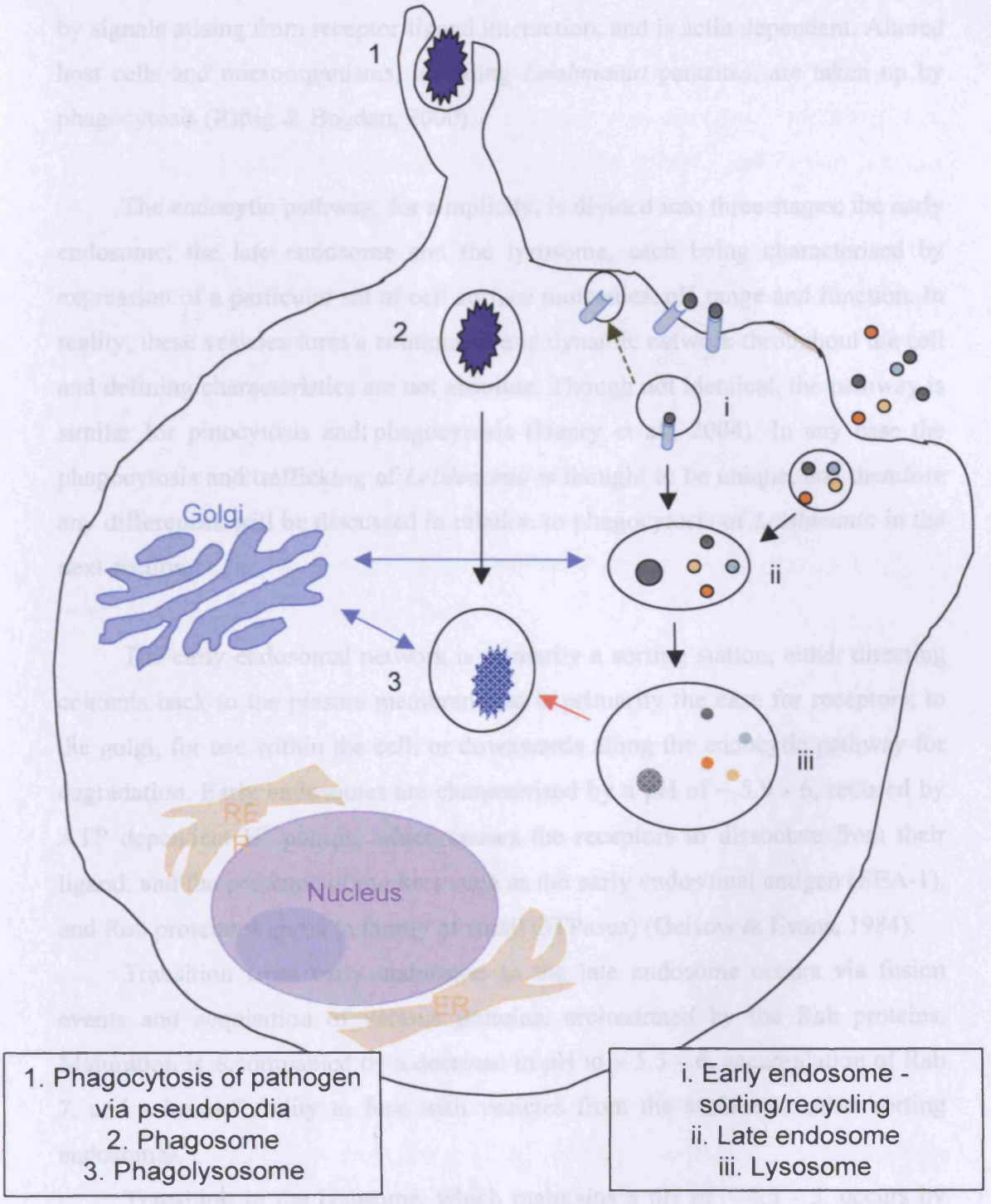

Figure 1.5 Illustration of phagocytosis (1-3) and pinocytosis (i-iii) in the macrophage. The blue arrow indicates traffic between vesicles and golgi, the red arrow indicates fusion of lysosmes and phagosomal vesicles.

by signals arising from receptor-ligand interaction, and is actin dependent. Altered host cells and microorganisms, including *Leishmania* parasites, are taken up by phagocytosis (Rittig & Bogdan, 2000).

The endocytic pathway, for simplicity, is divided into three stages; the early endosome, the late endosome and the lysosome, each being characterised by expression of a particular set of cell surface molecules, pH range and function. In reality, these vesicles form a continuous and dynamic network throughout the cell and defining characteristics are not absolute. Though not identical, the pathway is similar for pinocytosis and phagocytosis (Henry et al., 2004). In any case the phagocytosis and trafficking of *Leishmania* is thought to be unique, and therefore any differences will be discussed in relation to phagocytosis of *Leishmania* in the next section.

The early endosomal network is primarily a sorting station, either directing contents back to the plasma membrane, as is primarily the case for receptors; to the golgi, for use within the cell; or downwards along the endocytic pathway for degradation. Early endosomes are characterised by a pH of ~ 5.9 - 6, reduced by ATP dependent H^+ pumps, which causes the receptors to dissociate from their ligand, and the presence of markers such as the early endosomal antigen (EEA-1), and Rab proteins 4 and 5 (a family of small GTPases) (Geisow & Evans, 1984).

Transition from early endosome to the late endosome occurs via fusion events and acquisition of various proteins, orchestrated by the Rab proteins. Maturation is accompanied by a decrease in pH to ~ 5.5 – 6, accumulation of Rab 7, and a loss of ability to fuse with vesicles from the surface or other sorting endosomes.

Transition to the lysosome, which maintains a pH of ~ 4.5 - 5, occurs by similar maturation as well as fusion with existing (dense core) lysosomes. There is some debate over whether these fusion events are 'kiss and run' events (transient membrane attachment for transfer) or complete fusion resulting in hybrid oraganelles (Luzio et al., 2007). Lysosomes contain about 40 types of hydrolytic enzymes including proteinases, nucleases, glycosidases, lipases, phospholipases, phosphatases and sulphatases. All are acid hydrolases, i.e. work optimally in acid environment, and would do little damage in the neutral cytosol (pH 7.2).

The lysosome is responsible for the degradation of macromolecules, after which the final products e.g. amino acids, sugars, and nucleotides are transported to the cytosol, excreted or released by the cell. Undegradable particles are retained in lysosomes forming residual bodies. It is important that drug conjugates delivered to the lysosome are not retained, which could lead to the development of lysosomal storage disease. There is, as yet, no evidence of this with any polymer drug conjugates, though none have been clinically tested for chronic administration.

Whether the conjugate ends up in the same compartment as the parasite will depend on the specific route of entry and the trafficking pathway taken inside the cell. Therefore, it is important to carefully investigate the intracellular trafficking of the conjugate in relation to the parasite.

1.3.5 The parasitophorous vacuole

The *Leishmania*-containing phagolysosome, or PV, has a distinct set of characteristics in part determined by the parasite (Russell et al., 1992). Polymer delivery of the drug to the PV will depend on the intracellular trafficking in infected macrophages and the enzyme content of the PV. *Leishmania* promastigotes are 10 – 20 μm in diameter and are phagocytosed by the macrophage at the site of infection, as well as by dendritic cells and fibroblasts. Released amastigotes (3-7 μm) are also phagocytosed by macrophages after the initial infection. Both are phagocytosed via either opsonic or non-opsonic receptors on the macrophage surface. Opsonisation with C3b and C3bi, which bind to macrophage receptors CR1 and CR3, is the predominant method by which the promastigote enters the macrophage (Wilson & Pearson, 1986). CR1 and CR3 ligation promote phagocytosis without eliciting oxidative burst, and CR3 mediated uptake inhibits IL-12 induced cell-mediated immunity. *L. donovani* also use the Fc receptor after opsonisation with immunoglobulin (Blackwell, 1985), and the MR, as discussed earlier.

To design a therapeutic that can target the PV, it is important to better understand its nature and composition. The parasite-infected phagosome generally

matures into a phagolysosome (or PV). However, *L. donovani* infection delays maturation of the vesicle and alters its properties, causing it to arrest in a late endosomal-like state. It exhibits both late endosomal and lysosomal characteristics. The pH is ~ 4.7 – 5.2, and it contains the lysosomal hydrolases cathepsins D, B, H and L, and the lysosome-associated membrane proteins LAMP-1 and LAMP-2, ATPase and major histocompatibility complex (MHC) class II (Antoine et al., 1998; Courret et al., 2002; Henry et al., 2004).

The *Leishmania*-containing PV exhibits a number of features that enable and enhance survival. *L. donovani* is thought to delay phagosome-endosome fusion by reducing fusogenic properties of the membranes to allow time for amastigote differentiation. The PV accumulates an F-actin coat instead of shedding it which may physically block vesicle fusion (Lodge & Descoteaux, 2005a). However, this appears to be transient or limited as transfer of lysosomal contents has been shown in numerous studies (Berman et al., 1979; Berman et al., 1981; Weldon et al., 1983) The parasite is also able to either withstand or inhibit the enzymes present in phagosomes (Lewis & Peters, 1977). The Gp63 protease on the *Leishmania* membrane exhibits optimal activity under acidic conditions and can actually degrade lysosomal enzymes (Chaudhuri et al., 1989; Lewis & Peters, 1977). LPG may act as barrier as it is highly anionic and has unique galactose-β1,4-mannose linkages within the repeating units, rendering it resistant to lysosomal enzyme (Lodge & Descoteaux, 2005b; Lodge et al., 2006). LPG can also bind calcium and impairs signal transduction (protein kinase C (PKC) activation) and hence may prevent activation of the macrophage. As the parasitophorous vacuole has the characteristics of a late endosomal vacuole it would be expected to allow MHC class II presentation. MHC class II is expressed but presentation by infected macrophages decreases rapidly with time post-infection with *L. donovani* and correlates with transformation to the amastigote form (Lang et al., 1994). It also suppresses expression of B7-1 co-stimulatory molecule.

The overall clinical outcome of *Leishmania* infection is highly dependent on the cytokine response (Awasthi et al., 2004). IL-12 production stimulates a T helper cell type 1 (Th1) response and induces nitric oxide killing of the parasite.

However, if IL-4 is produced a Th2 response is elicited and the host is left susceptible to infection (Miralles et al., 1994). The principle mechanism for killing the *Leishmania* parasite is nitric oxide (NO). Although there are differences in response between infecting species, the requirement for IFNγ is a constant. If IFNγ is present before infection, macrophages are stimulated to produce NO, but if infection occurs first, NO production is inhibited. The microbicidal oxidative burst has also been shown to be suppressed by LPG (Lodge & Descoteaux, 2005b; Lodge et al., 2006). As stated earlier, the response is dependent on both host genetic factors and the infecting species, though the exact mechanisms are not wholly elucidated. Amastigotes have been shown to downregulate macrophage IL-12 production (Carrera et al., 1996). *L.donovani* also induces IL-10, which suppresses macrophage activation, cytokine production and expression of co-stimulatory molecules (Bhattacharya et al., 2001). A diagrammatic view of the uptake into the PV and subsequent modulation of the immune response is shown in Figure 1.6.

Combined, these strategies enable *Leishmania* to parasitise the host successfully and establish disease. To successfully treat leishmaniasis, new therapies, whether small molecules, liposomes or polymer-drug conjugates, must be taken up by macrophages, gain access to the PV and be active against the amastigote form. Current therapies and new strategies that have informed this work will be discussed below.

1.4 Anti-leishmanial therapy

The limitations of current therapies highlight the need for new therapies, and the potential importance of drug targeting to reduce toxicity and potentially overcome resistance. The following section describes commercially available drugs, those in pre-clinical development, and the most promising drug or drug combinations for delivery using polymer-drug conjugates.

1.4.1 Diagnosis and prevention

Early diagnosis is essential in the control of leishmaniasis. Diagnosis is laboratory based and therefore often impractical and unreliable in rural areas. The gold standard is parasite diagnosis from a biopsy (e.g. bone marrow) though PCR

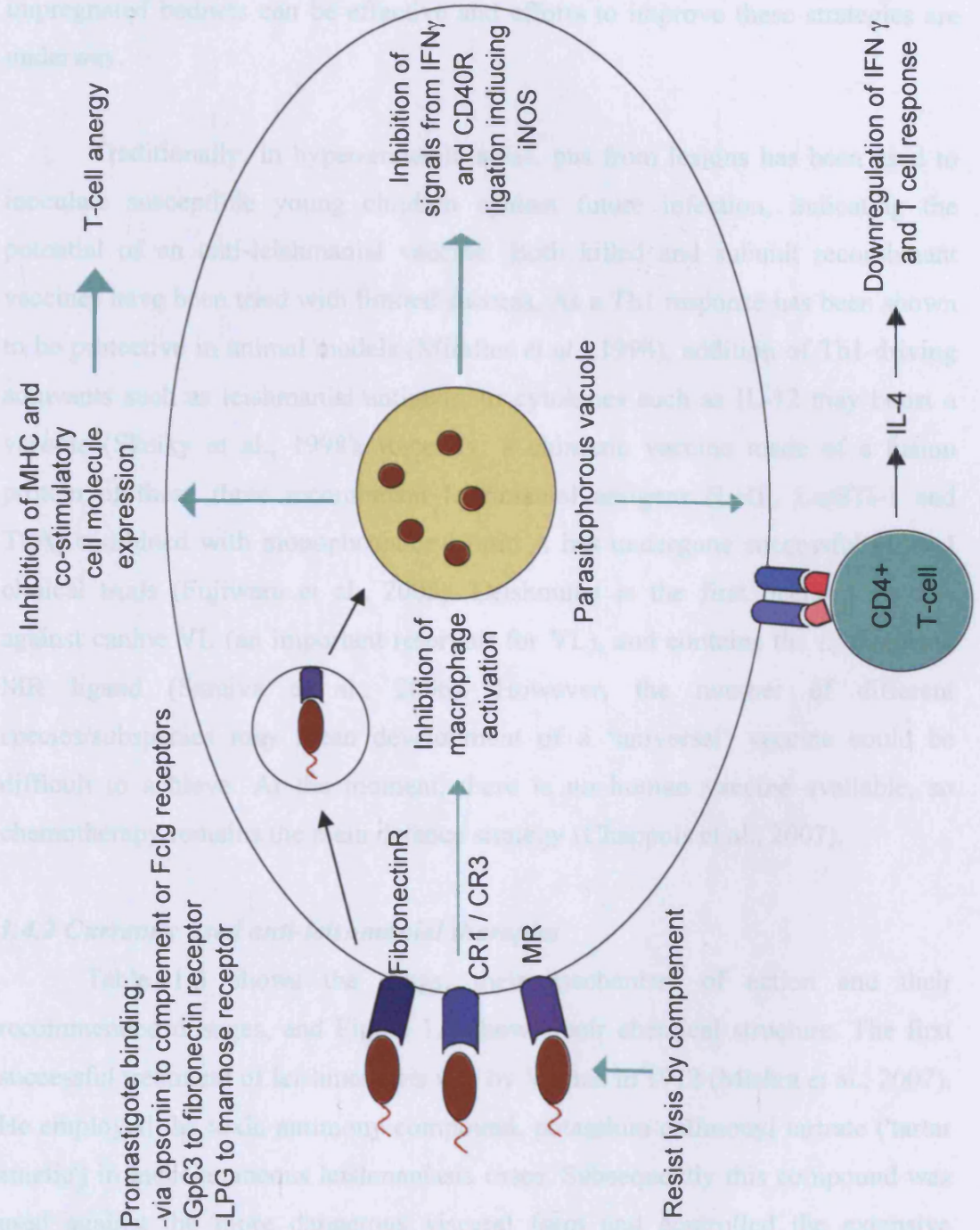

Figure 1.6 *Leishmania* parasite entry into macrophage by receptor mediated phagocytosis, replication inside the parasitophorous vacuole and modulation of the host immune response

based techniques are increasingly prevalent (WHO, 2001). Vector and reservoir control have also been tried with some success (Kishore et al., 2006). Insecticide impregnated bednets can be effective and efforts to improve these strategies are underway.

Traditionally, in hyper-endemic areas, pus from lesions has been used to inoculate susceptible young children against future infection, indicating the potential of an anti-leishmanial vaccine. Both killed and subunit recombinant vaccines have been tried with limited success. As a Th1 response has been shown to be protective in animal models (Miralles et al., 1994), addition of Th1-driving adjuvants such as leishmanial antigens, or cytokines such as IL-12 may boost a vaccine (Skeiky et al., 1998). Recently, a chimeric vaccine made of a fusion protein of these three recombinant leishmanial antigens (LeIF, LmSTI-1 and TSA) combined with monophosphoryl lipid A has undergone successful phase I clinical trials (Fujiwara et al., 2005). Leishmune is the first licensed vaccine against canine VL (an important reservoir for VL), and contains the *L. donovani* MR ligand (Saraiva et al., 2006). However, the number of different species/subspecies may mean development of a 'universal' vaccine could be difficult to achieve. At the moment, there is no human vaccine available, so chemotherapy remains the main defence strategy (Chappuis et al., 2007).

1.4.2 Currently used anti-leishmanial therapies

Table 1.3 shows the drugs, their mechanism of action and their recommended dosages, and Figure 1.7 shows their chemical structure. The first successful treatment of leishmaniasis was by Vianna in 1912 (Mishra et al., 2007). He employed the toxic antimony compound, potassium antimonyl tartrate ('tartar emetic') in mucocutaneous leishmaniasis cases. Subsequently this compound was used against the more dangerous visceral form and controlled the extensive epidemics in Assam in 1915 (Dye & Wolpert, 1988). Antimonials are still the main treatment for leishmaniasis, with sodium stibogluconate (pentostam) and meglumine antimonate (glucantime) being first line treatments. However, resistance is now widespread in some areas.

Table 1.3 Current anti-leishmanial drugs, their mechanism of action and suggested dosage[†].

Drug	Mechanism of action	Dosage
Meglumine antimoniate	Acivated in amastigote by conversion to trivalent form. MoA	20 $mg/kg^{-1}/day^{-1}$ IV/IM
Sodium stibogluconate	unknown.	20 – 28 days
Amphotericin B	Complexes with ergosterol in parasite membrane, causing pore	1-3 $mg/kg^{-1}/day^{-1}$ IV
	formation leading to ion imbalance and death.	20 days
Ambisome	As above, plus enhanced uptake into macrophages and	2 $mg/kg^{-1}/day^{-1}$ IV
	intracellular release.	3 days
Pentamidine	Uncertain but can bind to kinetoplast DNA	2 - 4 $mg/kg^{-1}/day^{-1}$ IV/IM
		Alternate days for 15 days
Paromoycin (phase III)	Thought to bind to 30S subunit of ribosomes, causing misreading	15 $mg/kg^{-1}/day^{-1}$ IM
	and termination of protein synthesis.	21 days
Miltefosine (phase IV;	Possible inhibition of phospatidylcholine biosynthesis, signal	2.5 $mg/kg^{-1}/day^{-1}$ orally
registered in India)	transduction and calcium homeostasis.	28 days

[†] Adapted from 'Mishra et al., 2007

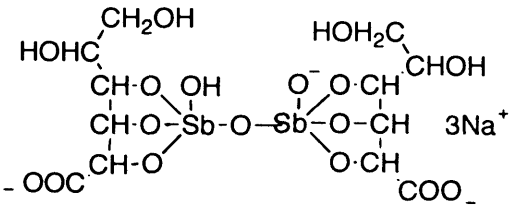

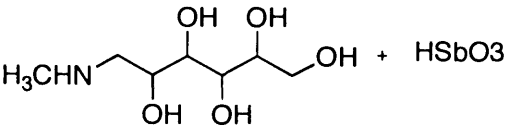

(a) The antimony compounds sodium antimoniate and meglumine antimonate

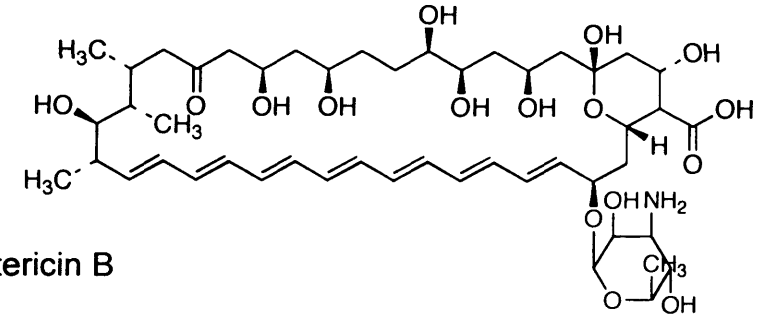

(b) Amphotericin B

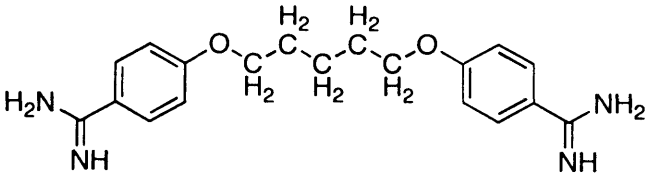

(c) Pentamidine

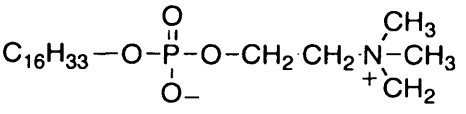

(d) Miltefosine

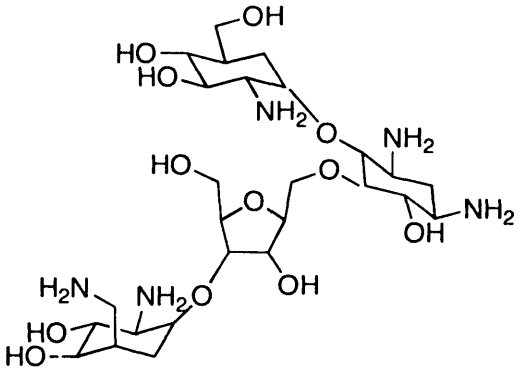

(e) Paromomicin

Figure 1.7 Chemical structure of current anti-leishmanial drugs.

The diamidines have reasonable tolerability, the preferred drug being pentamidine, and are generally used as second line treatment. Unfortunately pentamidine has greater toxicity, common side effects and resistance has developed in parts of India, leading to its abandonment in this area (Jha, 1983).

Most recently, the polyene macrolide antibiotics have been employed, amphotericin B (AmB) being most predominant (Giri, 1994). AmB consists of a glycosidic molecule containing a large lactone ring linked to an amino sugar, mycosamine. Its mechanism of action involves increasing cell membrane permeability leading to loss by leakage, first of ions, then other cellular contents. It binds to ergosterol in the parasite membrane, forming pores, and leading to cell death. However, use is limited by the drugs systemic toxicity (it is the most toxic antibiotic available for clinical use) to those cases that are refractory to both the antimonials and pentamidine.

Paromomycin is an aminoglycoside antibiotic, and acts by binding to ribosomes, inhibiting protein synthesis and causing misreading and premature termination of mRNA translation. It is used as an affective alternative to, or in combination with, antimonials, as a topical ointment for treatment of cutaneous disease. It was approved in India for injectable treatment of VL in 2006 (Sundar et al., 2007). However it is less active against VL than AmB and pentamidine (Thakur et al., 2000).

An orally administered drug, miltefosine, is in advanced clinical trials, with promising results, and was registered in India in 2002 (Sundar et al., 2006; Sundar et al., 1998). However, it has a small therapeutic window and there are implications in women of childbearing age due to teratogenic effects (Murray, 2000). It has a long half life (~ 150 h) and resistance is easily induced *in vitro* (Perez-Victoria et al., 2006).

Successful chemotherapy cannot be guaranteed for any form of leishmaniasis with the present limited range of available drugs. All are toxic, and most have the disadvantage of requiring parenteral administration and hospitalisation. There is no evidence of clinical resistance to AmB as yet, however

resistance to the other anti-leishmanials is on the increase, particularly the antimonials and pentamidine, as well as concerns over miltefosine (Ouellette et al., 2004). The response to these drugs is again dependent mainly on the strain of the infecting parasite but also the degree of host susceptibility and immune response. Recently there has been development of several new drugs, and drug delivery strategies in an attempt to overcome these difficulties.

1.4.3 New anti-leishmanial therapies

Improved anti-leishmanial therapies. These must be non-toxic, highly effective drugs preferably administered by the oral route or as a single or low dose parenteral. The search has been largely unsuccessful. One exception is the increased activity of AmB seen when delivered within a liposome (vesicle composed of phospolipid bilayers surrounding an aqueous compartment) (Davidson et al., 1991; New et al., 1981; Yardley & Croft, 2000). Ambisome® is highly active and is well tolerated (Dupont, 2002; Yardley & Croft, 2000).

In Ambisome® AmB is intercalated into a unilamelar bilayer membrane consisting of phospholipids with saturated fatty acid side chains of hydrogenated soy phosphatidylcholine, distearoylphosphatidylglycerol, and cholesterol. The incorporation of cholesterol stabilizes the liposome and has been postulated to bind to the AmB, minimising the interaction with mammalian cell membrane (Adler-Moore & Proffitt, 2002). It has shown no acute or chronic toxicity up to 15 mg/ml and has a 90-100 % efficacy. However, infusion related toxicity and leakage of drugs from such systems could be problematic with AmB's high toxicity. The main problem is that it is prohibitively expensive. Its increased efficacy and tolerance, is matched by its increase in cost. It is widely used in Europe but not available for most of Asia and Africa where disease burden is highest. Recent cost analysis studies of drugs for VL found Ambisome® to be the least cost effective treatment (Sundar & Chatterjee, 2006; Vanlerberghe et al., 2007). A course of conventional AmB was the most effective and costs around US$ 70, whereas Ambisome® costs US$ 1500 (Kshirsagar et al., 2005). The success of the liposomal therapy does, however, suggest a method of reducing systemic toxicity by cell targeting.

Recent work has brought knowledge of a number of potential parasite

specific enzyme or metabolites that could be targeted, e.g. inhibitors of dihydrofolate reductase (Gilbert, 2002). Such compounds have shown activity against the cell-free amastigotes, but lower activity against the intracellular amastigotes.

A second option is to combine chemotherapy with cytokine therapy. IFNγ is sometimes used in combination with antimonials and does increase the cure rate, but the cost of such treatments is prohibitive for use in undeveloped nations (Li et al., 1997). Another factor to be taken into consideration is HIV co-infection. In co-infected individuals, cure rates drop to around 60-70 % for antimonials, AmB and its lipid complexes (Laguna, 2003) and also for miltefosine (Sindermann et al., 2004), increasing the need for new drugs.

1.5 Drug delivery strategies

It is important to bear in mind that new drug molecules will have little effect if they are unable to penetrate the PV. One way to ensure that drugs will cross host cell membrane barriers is to use a drug delivery agent that will constitutively enter via endocytosis rather than diffusion into the cytoplasm. The benefits of using drug delivery strategies, for example liposomal encapsulation, are well known, including the possibility of enhanced specificity and reduced toxicity. This is how Ambisome® exerts its effect and avoids systemic toxicity. Studies have demonstrated successful treatment of multidrug resistant patients with Ambisome® (Davidson et al., 1991).

There have been several studies on drug delivery of anti-leishmanial drugs (Table 1.4). Liposomes have been the most common delivery method employed, particularly for macrophage delivery, though other studies have included protein- and polysaccharide drug conjugates. The ease of formulation and high drug encapsulation into liposomes has allowed a wide variety of drugs to be delivered in this manner. The first studies mainly used antimonials (Black et al., 1977; New et al., 1978), but also, as discussed in the previous section, liposomal AmB that has since proved very effective (Berman et al., 1986b; New et al., 1981). Specific targeting has been shown to further increase uptake of liposomes, using such targeting residues as parasite specific antibody (Mukherjee et al., 2004) and

Table 1.4 Anti-cancer polymer-drug conjugates in clinical trials, their status and indication.

Compound	Clinical Status (Phase)	Reference
Polyglutamate-paclitaxel (Xyotax)	III	Li et al., 1998
Polyglutamate-camptothecin	I	Bhatt et al., 2003
HPMA copolymer-doxirubicin (PK1)	III	Vasey et al., 1999
HPMA-copolymer-dox-galactosamine (PK2)	I/II	Duncan et al., 1983; 1986
HPMA-copolymer-paclitaxel	I	Meerum-Terwogt et al., 2001
HPMA-copolymer-camptothecin	I	Caiolfa et al., 2000
HPMA-copolymercarboplatin platinate	I/II	Rademaker-Lakhai et al., 2004
HPMA-copolymer-DACH platinate	I/II	Lin et al., 2004
Dextran-doxorubicin	I	Danhauser-Riedl et al., 1993
Modified dextran-camptothecin	I	Inoue et al., 2003
PEG-camptothecin (Prothecan|)	II	Posey et al., 2005

DACH, diaminocyclohexane; HPMA, N-(2-hydroxypropyl)methacrylamide; PEG, poly(ethyleneglycol).

phosphatidylserine (Tempone et al., 2004). Banerjee and colleagues tested sugar grafted liposomes *in vivo* and found mannose-grafted liposomes were the most efficient in comparison with either glucose or galactose-grafted ones, in reducing spleen parasite load (Banerjee et al., 1996). However, the combined problems of poor stability and high cost of preparation mean liposomes are less than ideal as a drug delivery method. Also, the drugs are not covalently bound; therefore the release kinetics cannot be customised for specific needs.

There are now more sophisticated delivery methods being developed, and polymer conjugates have many advantages over liposomes, as discussed in the next section.

1.5.1 Polymer therapeutics

Polymer therapeutics offer great flexibility in terms of architecture and loading. There is large scope for different combinations of drugs, targeting residues and linkages. This enables controlled pharmacokinetics with the design of agents with specific size, charge, body distribution and drug release patterns. This section will concentrate on polymer therapeutics, their background, applications and potential for anti-leishmanial therapies.

Polymers are already widely used biomedical materials in medicine, for example, hip prostheses, contact lenses, vascular grafts and as scaffolds for tissue engineering. Pharmaceutical uses include excipients in oral formulations (alginates, celluloses, dextrin, dextran or synthetic polymers), solubilisers in parenteral formulations and in controlled release products. Such polymers are considered inert, they are simply carriers without being covalently bound to a drug or exerting any biological effect themselves.

A more recent approach to the use of polymers in pharmaceuticals has been to exploit the properties of natural or synthetic water-soluble polymers for use as drugs or pro-drugs themselves. The idea stemmed from Christian de Duve's realisation in the 70's that drug delivery might make use of the endocytic pathway (de Duve et al., 1974), termed 'lysosomotropic drug delivery'. In 1975, Ringsdorf introduced the concept of the targeted drug carrier in which water-soluble polymers, modified with both targeting agents and drugs, could be used to deliver the drugs to appropriate disease sites (Ringsdorf, 1975). The term

'polymer therapeutics', coined by Duncan (Duncan, 2003), is used to distinguish this new class.

Defining properties of these polymers are that they are water soluble, biologically active and/or covalently bound to a drug, and are usually administered either by intravenous or subcutaneous injection. The term 'polymer therapeutics' includes polymeric drugs, polymer-protein conjugates, polymer-drug conjugates, block polymeric micelles (to which drug is covalently bound) and multi-component polyplexes that are being developed as non-viral gene delivery systems (Figure 1.8). Most are designed for intracellular drug delivery, either lysosomotropic, diffusing out of the lysosome, or endosomotropic, diffusing out of the endosome before it reaches the lysosomal compartments, though some may be designed to act on the surface. Recent developments in the design of polymer therapeutics have focused on increasingly complex architectures to give multivalent multibranched structures such as graft and block copolymers, dendrimers and star polymers. These new structures provide multivalent surfaces for attaching drugs as well as imaging agents, targeting molecules and peptide epitopes. However most polymer-drug conjugates have, to date, been based on linear polymers.

1.5.2 Polymer-drug conjugates

Although considered drug delivery agents, polymer-drug conjugates are defined as macromolecular drugs or pro-drugs in their own right as they are chemically conjugated to the drug and therefore new chemical entities. Polymer conjugates can be used to deliver nucleic acids, proteins and drugs. The basic principle is to reduce the immunogenicity or toxicity, increase the stability and solubility, and prevent the rapid clearance from the circulation by the RES or the kidney. They can also enhance targeting and site-specific delivery.

Despite a growing number of polymer-drug conjugates now in clinical trials, there are none yet on the market (Table 1.5). The first polymer drug conjugates, developed in the early 1980's by Duncan and colleagues, went into clinical trial in 1994 (Duncan, 2005; Duncan et al., 1998; Vasey et al., 1999). The conjugates were based on N-(2-hydroxypropyl)methacrylamide (HPMA) copolymers bound to the anti-cancer drug doxorubicin. The simplified structure of

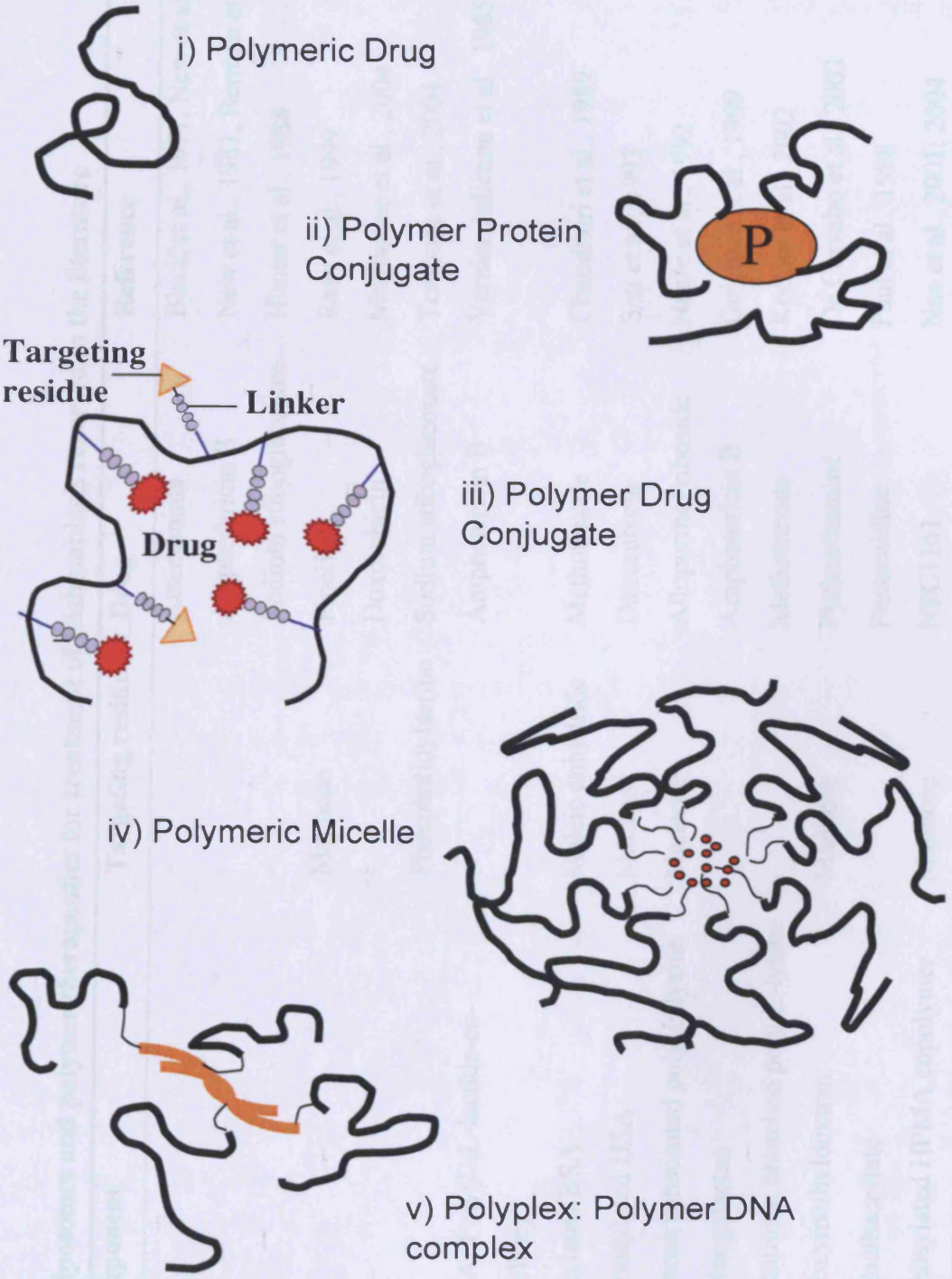

Figure 1.8 Simplified diagram of polymer therapeutics. Adapted from Duncan R., 2003 .

Table 1.5 Examples of liposomes and polymer therapeutics for treatment of leishmaniasis reported in the literature

Type of carrier	Component	Targeting residue	Drug	Reference
Liposome		-	Antimonials	Black et al., 1977, New et al., 1978
		-	Amphotericin B	New et al., 1981, Berman et al., 1986
		-	Sodium stibogluconate	Hunter et al., 1988
		Mannose	Piperine	Raay et al., 1999
		-	Doxorubicin	Mukherjee et al., 2004
		Phosphatidylserine	Sodium stibogluconate	Tempone et al., 2004
Microsphere	PLGA: Poly(D,L-lactide-co-glycolide)	-	Amphotericin B	Vernier-Julienne et al., 1985
Protein	Maleylated BSA	Maleic anhydride	Methotrexate	Chaudhuri et al., 1989
	Mannosylated HSA	Mannose	Doxorubicin	Sett et al., 1993
Polysaccharide	Mannose substituted poly-L-lysine	Mannose	Allopurinol riboside	Negre et al., 1992
	Arabinogalactan		Amphotericin B	Golenser et al., 1999
	Polycationic branched poly-L-lysine	-	Methotrexate	Koczan et al., 2002
	Carboxymethyldextran	Mannose	Pyrimethamine	De Carvaho et al., 2003
Synthetic polymer	Polymethacrylate		Pentamidine	Paul et al., 1998
	Mannosylated HPMA copolymer	Mannose	NPC1161	Nan et al., 2001; 2004

a targeted HPMA copolymer-drug conjugate showing the polymer backbone covalently bound to a drug or targeting residue via a linker, is shown schematically in Figure 1.9.

As the first polymer therapeutics, HPMA copolymer drug conjugates have been widely studied. HPMA copolymer is a synthetic water soluble polymer, first developed in Czekoslovakia as a plasma expander (Sterba et al., 1976). There has been no evidence of accumulation with HPMA below 40 kD and it is considered non-toxic. It increases the water solubility of hydrophobic drugs such as doxorubicin (Dox). The plasma half-life is increased leading to higher accumulation in target sites and reduced side effects and toxicity. The first polymer-drug conjugates to enter clinical trial were Dox conjugates, PK1, and the second PK2, which also contains a liver-targeting residue. Dox was linked via a peptide linker, designed to be cleaved by lysosomal enzymes.

PK1 has activity against non-small-cell lung cancer and anthracycline resistant breast cancer. No immunogenicity or polymer-related toxicity was seen, the dose-limiting toxicity being the same as that of Dox alone. PK2 has a galactosamine molecule bound to the backbone, which targets liver cells by binding the asialoglycoprotein receptor (ASGPR) (Duncan et al., 1983; Duncan et al., 1986). It has proved effective against liver cancer, and is the first polymer therapeutic designed for receptor-mediated uptake to be tested clinically. Hepatoma concentrations were significantly higher than could be achieved with Dox alone (Seymour et al., 2002).

Most polymer-drug conjugates to date have been anticancer agents. The first generation were mainly anthracyclines, the second generation now entering clinical trials are paclitaxel and camptothecin, which are normally poorly water soluble and lead to hypersensitivity reactions. The HPMA-camptothecin conjugates produced side effects and have poor drug loading, but a polyethelene glycol (PEG) conjugate has provided more promising results (Caiolfa et al., 2000; Posey et al., 2005). PEG has not been widely used for drug conjugates as it has only two terminal end groups with which to bind drug, polymers with higher loading capacities are normally required. HPMA copolymer-paclitaxel has also shown dose limiting toxicity similar to paclitaxel alone (Meerum Terwogt et al., 2001). These results likely result from the ester linkage used, which, unlike the

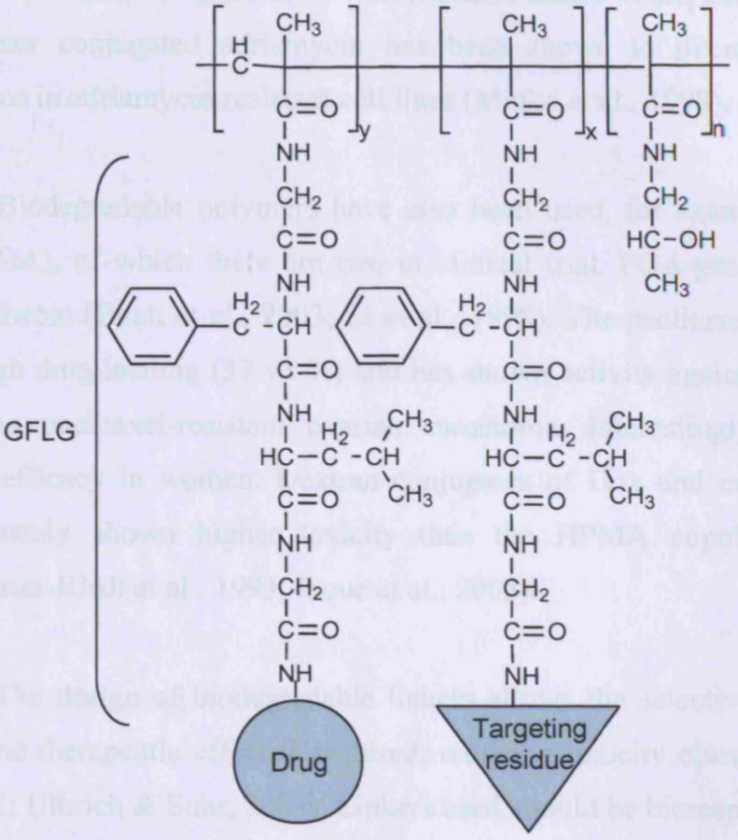

Figure 1.9 Simplified structure of a polymer-drug conjugate. The diagram shows a linear HPMA copolymer with drug and targeting residue attached via a peptide linker (GFLG).

peptide linkers designed for lysosomotropic delivery, is cleaved in the bloodstream. HPMA copolymer-platinates have shown good activity and reduced toxicity as with the Dox conjugates (Lin et al., 2004; Rademaker-Lakhai et al., 2004). The first anti-angiogenic drug conjugate, HPMA copolymer conjugated to TNP-470, is now being tested *in vivo* (Satchi-Fainaro et al., 2004). Also, HPMA copolymer conjugated adriamycin has been shown to overcome multi drug resistance in adriamycin resistant cell lines (Minko et al., 1998).

Biodegradable polymers have also been used, for example polyglutamic acid (PGA), of which there are two in clinical trial, PGA-paclitaxel and PGA-camptothecin (Bhatt et al., 2003; Li et al., 1998). The paclitaxel conjugate has a very high drug loading (37 wt %) and has shown activity against several cancers including paclitaxel-resistant ovarian carcinoma. Interestingly, it has shown greater efficacy in women. Dextran conjugates of Dox and camptothecin have unfortunately shown higher toxicity than the HPMA copolymer conjugates (Danhauser-Riedl et al., 1993; Inoue et al., 2003).

The design of biodegradable linkers allows the selective release of drug where the therapeutic effect is required, reducing toxicity elsewhere (Duncan et al., 1982; Ulbrich & Subr, 2004). Linkers used should be bioresponsive, i.e. stable during transport through the plasma, but preferentially degraded at the target site. The drug must also be released in its native/active form, as any chemical modification of the structure may result in loss or change of therapeutic activity. There are two main types of linkers used. Acid labile or pH sensitive linkers make use of the decreasing pH of the endosome, or the low pH associated with tumour tissue (the hydrazone or the N-cis-aconityl linker). Peptide linkers have been developed to be enzyme degradable, making use of tumour associated enzymes, or lysosomal hydrolases and proteases (Duncan et al., 1980). HPMA copolymer conjugates are taken up by endocytosis, and trafficked to the lysosome (Duncan et al., 1981). PK1 and PK2 have an endocyticly cleaved linker, Gly-Phe-Leu-Gly (GFLG). The choice of linker will depend primarily on the intracellular trafficking of the conjugates in the macrophage.

1.5.3 Targeting of polymer-drug conjugates

Polymer conjugation allows targeting of the drug to its site of action, either by an active or passive mechanism. Passive mechanisms use pathophysiological properties of the intended site; the most well documented being the properties of tumour tissues. Conjugates are easily able to access the tumour tissue due to leaky vasculature, and are retained longer due to lack of lymphatic drainage. This is termed the enhanced permeability and retention (EPR) effect and leads to accumulation of drug in the tumour tissue (Matsumura & Maeda, 1986).

Other potentially useful properties of tumour tissue or other pathologies include reduced pH or secreted enzymes. However, most disease sites do not have such easily exploited properties, hence most polymer therapeutics to date have been anti-cancer agents. Intracellular infections, such as leishmaniasis, are likely to require active targeting. This usually involves conjugation of a targeting moiety that will bind a specific receptor on a particular cell type or tissue. If conjugates lack a targeting ligand they are usually internalised slowly as a solute by fluid phase pinocytosis, though hydrophobic polymers may interact with the plasma membrane in some cell types, leading to non-specific adsorptive uptake. A high loading of a hydrophobic drug could increase this non-specific binding. If a ligand with low specificity is used, cross-reactivity of the targeting moiety with other tissue may result in severe side effects. Therefore targeting to any particular site requires careful verification, to ensure non-specific toxicity is reduced and that there is no unexpected targeting to other sites.

Targeting can be achieved using a virtually infinite number of molecules, but the two types that have shown most promise are antibodies and sugars, for example the MR discussed in section 1.3.3. PK2 has had success in clinical trials and is a good model for sugar targeting. Using this method of targeting it may be possible to achieve higher drug concentrations in the macrophage.

1.5.4 Polymer-drug conjugates – applications for anti-leishmanial therapies

A number of polymers have been studied for anti-leishmanial drug delivery including proteins, polysaccharides and synthetic polymers including HPMA (Table 1.5). Those that have had most success have included mannose as a targeting residue. Previous studies using this sugar have shown it can selectively

localise polymers to macrophages. Duncan and colleagues demonstrated the targeting effect of mannose conjugated to HPMA, and the concentration of these conjugates in cells of the RES in the liver and spleen (Duncan et al., 1983). They also showed that the increasing sugar content resulted in increased uptake (Duncan et al., 1986).

Most recently, Ghandehari's group have used HPMA with mannose targeting residues conjugated to anti-leishmanial 8-aminoquinoline analogues (Nan et al., 2004; Nan et al., 2001). Though the cytotoxicity was halved compared to that of free drug, the conjugates were toxic to KB cells at levels required to match the efficacy of free drug. The conjugates were, however, significantly more effective against *Leishmania in vivo* compared to free drug in mice models. These studies demonstrate the potential of HPMA copolymer-drug conjugates as anti-leishmanial therapeutics. The uptake of polymers by endocytosis, the selectivity of targeted conjugates for macrophages and the delivery of the drug to the PV are of prime importance in the design of such therapeutics.

In summary, there are several advantages of polymer therapeutics that make them a good prospect for treating leishmaniasis:

- Solubilise poorly soluble anti-leishmanial compounds.
- Can incorporate multiple drugs for combination therapy.
- Allow targeting of macrophages, where the parasite resides.
- Enter the macrophage by endocytosis delivering a high drug concentration in the vicinity of the parasite.
- Could potentially overcome resistance mechanisms.
- Release kinetics can be tailored depending on the drug/drugs used and the trafficking.

1.6 Aims of the project

There is a pressing need for new anti-leishmanial therapies, the essential criteria of any new agent being the ability to gain access to the PV. One way to achieve this is using targeted polymer-drug conjugates. The main aim of the work described in this thesis was therefore to synthesise and characterise HPMA copolymer-drug conjugates with mannose as targeting residues for macrophage-specific endocytic anti-leishmanial drug delivery. An important part of this work

was to set up both the macrophage models for the targeting studies, and the methods necessary to study the trafficking of the conjugates in these models.

1.7 Summary of the project

First, suitable in vitro macrophage cell models were established (Chapter 3). A library of HPMA copolymer conjugates with a range of mannose loadings were synthesised in order to ascertain the optimal loading for significant receptor-mediated uptake (Chapter 4). It was next important to investigate the intracellular trafficking of the conjugates. A novel subcellullar fractionation method was optimised for the THP-1 macrophage cell line to study the localisation of the HPMA copolymer-Man conjugates in these cells. Confocal fluorescent microscopy was used to support these studies and confirm the intracellular fate of the conjugates (Chapter 5). To the selected conjugate the chosen model drug was conjugated to the polymer backbone. AmB was chosen as it has near 100% cure rate and resistance is rare. Though it has very high toxicity, studies have shown this can be overcome using drug delivery vehicles such as liposomes (Ambisome®). *In vitro* cytotoxiciy and activity in infected macrophages was performed (Chapter 6) with the aim of providing candidates for further testing *in vivo* and eventually for clinical trial.

Chapter 2

Materials and General Methods

2.1 Equipment

2.1.1 Equipment for cell culture

Costar cell culture consumables (sterile flasks and plates) were supplied by Corning Inc, USA. Serological pipettes, Bijoux and universal containers were from Elkay, Ireland. Galaxy S incubators and a Procell incubator were from Wolf laboratories and Jencons-PLS, UK respectively. Bioair and Microflow class II laminar flow hoods were from Bioair, Italy and Servicecare, UK. Routine cell culture and counting was performed using a silver stained Neubauer haemocytometer, Germany, on an inverted DM IL Leica bright field microscope (Leica, Germany). Cell scrapers (1.8 cm swivel blade) were from Fisher Scientific, UK. A Varifuge 3.0 RS with swing out rotor buckets (type 8080, r_{max} 21.1 cm) and Eppendorf 5417 R bench-top centrifuge with standard fixed angle rotor (model 5417 C/R) were from Heraeus Instruments and Eppendorf, Germany respectively. The Mr. Frosty cryovial container was from Wessington Cryogenics, UK.

2.1.2 General analytical equipment

Ultraviolet (UV) absorbance was measured with a sunrise UV absorbance plate reader from Tecan, Austria, and a Cary 1G UV-visible spectrophotometer from Varian, Australia, using Cary Win UV software package for data acquisition and analysis. Fluorescence was measured using a Fluostar optima fluorescent plate reader from BMG Labtechnologies, Germany, and an Aminco-Bowman Series 2 luminescence spectrophotometer from Spectronic instruments, USA. Thin layer chromatography (TLC) silica plates coated with Alugram SIL-G/UV_{254} were from Macherey-Nagel, Germany and visualised under a multiband UV lamp (254/365 nm) from Upland, USA.

Polymer conjugates were freeze dried before analysis using a Flexi Dry FD-1.540 freeze-dryer from FTS Systems, USA, connected to a DD75 double stage, high vacuum pump from Javac, Australia. Gravitational gel permeation chromatography (GPC) was performed with sephadex G25 PD10 columns that were supplied by Amersham Biosciences, Sweden.

2.1.3 Flow cytometry and fluorescent microscopy equipment

Images were acquired by fluorescence microscopy using an inverted Leica TCS SP5 confocal microscope equipped with 40 x oil immersion objective and Argon (488 nm), GHe/Ne (543 nm) and blue diode (405 nm) lasers. Images were processed with LAS (Leica, Germany) software.

Flow cytometry data was collected on a Becton Dickenson FACScalibur flow cytometer equipped with an argon laser (excitation wavelength 488 nm) using manufacturers instructions. Logarithmic-transformed data was acquired in 1024 channels with band pass filters FL-1 (530 ± 30 nm) and FL-2 (585 nm ± 42 nm) and subsequently processed with Cell Quest software (version 3.3).

2.1.4 Subcellular fractionation equipment

The automated gradient maker and piston fractionator were from Biocomp instruments (Canada). The samples were spun on a Beckman SW 41 TI rota ultracentrifuge. The refractometer was from Abbe 60/DR, Bellingham and Stanley Ltd. The cells were homogenised using the cell cracker from the European Molecular Biology Laboratory (EMBL, Germany). Ultracentrifugation was performed with a Beckman SW 41 TI rota on an Optima LE-80K centrifuge from Beckman Coulter, USA. Polyclear™ (14 x 89 mm) ultracentrifuge tubes were from Seton Scientific, CA, USA.

2.1.5 Western and dot blotting

All electrophoresis equipment was from Bio-Rad, UK. Protan® 0.45 μm nitrocellulose membrane was from Schleicher and Schuell Biosciences, Germany. The Bellydancer automated shaker was from Stovall Life Science, USA.

2.2 Materials

2.2.1 General chemicals and reagents

Ethanol, methanol, acetone, ethyl acetate, hydrochloric acid, triethylamine, sodium hydroxide pellets, sodium chloride, disodium hydrogen orthophosphate, sodium dihydrate orthophosphate, citric acid monohydrate and trisodium citrate dihydrate were from Fisher Chemicals, UK. Dimethylsulphoxide (DMSO), triton X-100, ninhidrin, 4 % w/v copper (II) sulphate solution, 3-amino-1-propanol (AP),

citric acid monohydrate, N-2-hydroxyethylpiperazine-N'-ethanesulphonic acid (HEPES), ethylenediaminetetraacetic acid (EDTA), tris(hydroxymethyl)aminomethane (Tris-Base), p-nitrophenyl phosphate, sodium borate, ß-nicotinamide adenine dinucleotide reduced disodium salt (NADPH), leupeptin, bovine serum albumin (BSA) and glycine were from Sigma Aldrich, UK. All other general chemicals, unless otherwise specified, were from Sigma Aldrich, UK.

2.2.2 Cells and tissue culture reagents

RAW 264.7, a mouse monocyte macrophage cell line (established from an ascites of a tumour induced in a male mouse by intraperitoneal injection of Abselon Leukaemia Virus) and THP-1, a human monocytic cell line (established from an acute monocytic leukaemia of a male 1yr infant), were obtained in frozen ampules from European Collection of Cell Cultures (ECACC) and American Type Culture Collection (ATCC) respectively. Dutch modified Eagles medium (DMEM) with glutamax (with and without phenol red pH indicator) and RPMI 1640 with glutamax (with and without phenol red), and foetal bovine serum (FBS) were from Invitrogen, UK. Medical grade CO_2, N_2 (95 % v/v) and liquid nitrogen were supplied by BOC, UK. Trypan Blue reagent, tissue culture grade DMSO, 3-(4,5-dimethylthiazol-2-yl)-2,5-diphenyl-2H-tetrazolium (MTT) and phorbol 12-myristate 13-acetate (PMA) were obtained from Sigma Aldrich, UK.

2.2.3 Chemicals and reagents for flow cytometry and fluorescent microscopy

Mannan (Saccharomyces Cerevisiae) was obtained from Sigma Aldrich, UK. FACS Flow, Clean and Rinse formulations and falcon FACS tubes were from Becton Dickenson, UK. FITC-labelled bovine serum albumin (FITC-BSA) and mannosylated FITC-BSA (FITC-BSA-Man) were obtained from Sigma Aldrich, UK and DQ-ovalbumin from Molecular Probes, UK. Mouse anti-EEA-1 antibody was from BD Biosciences, UK and mouse anti-transferin and anti-LAMP-1 antibody were from DSHB, USA. Alexa Fluor 488- and Cy5- labelled anti-mouse antibodies were from Molecular Probes, UK. Frosted microscope slides and 16 mm coverslips were purchased from Chance Propper, UK. Vectashield was obtained from Vector,

USA and clear nail varnish from Rimmel, UK. Immersion oil was obtained from Leica, Germany.

2.2.4 Reagents for subcellular fractionation

Optiprep™ was from Axis-Sheild Diagnostics, UK. The protease inhibitor complex tablets were from Roche Diagnostics, UK. Texas Red-labelled Transferrin was from Molecular Probes, UK. Sucrose was from Sigma Aldrich, UK.

The following reagents for the biochemical assays; N-Acetyl-β-glucosaminidase (Hex A), 2-p-iodonitrotetrazolium violet (INT), tris(hydroxymethyl)aminomethane hydrochloride (Tris-HCl), succinic acid tris(hydroxymethyl)aminomethane (Tris base), β-nicotinomide adenine dinucleotide reduced disodium salt (NADH), pyruvic acid (crystallised monosodium salt), sodium citrate, citric acid, 4-methylumbelliferyl, 4-methylumbelliferyl-N-acetamido-β-D-glucosaminide, sodium hydroxide pellets, p-nitrophenol phosphate (aq.), sodium borate and magnesium chloride were from Sigma Aldrich, UK.

2.2.5 Sodium dodecyl sulphate polyacrylamide gel electrophoresis (SDS PAGE), Western and dot blot reagents

Prestained SDS-PAGE standards, broad range (7,331 – 211,806 g/mol) were obtained from Bio-Rad, USA. Acrylamide / Bis-acrylamide (30 % solution), ammonia persulphate (APS), dithiothreitol (DTT), bicinchoninic acid (BCA) solution, copper (II) sulfate and glycerol were purchased from Sigma Aldrich, UK. Coomassie brilliant blue (CB), bromophenol blue, 2-mercaptoethanol, sodium dodecyl sulphate and N,N,N,N'-tetra-methyl-ethylenediamine (TEMED) were supplied by Bio-Rad, USA. Glycine (electrophoresis grade) was from ICN Biomedicals, USA. Mouse anti-EEA-1 antibody was from BD Biosciences, UK and mouse anti-LAMP-1 antibody was from DSHB, USA. Alexa Fluor 488- and Cy5-labelled anti-mouse antibodies were from Molecular Probes, UK. HRP-conjugated anti-mouse and anti-rabbit antibodies were from Dakocytomation, UK. The enhanced chemiluminescence detection reagent kit was from Pierce, USA.

2.2.6 Polymers and reagents used in conjugation of HPMA copolymer

Batches of HPMA copolymer-GFLG-ONp containing 9.03 mol % side chains terminating in p-nitrophenoxy (ONp) (Batch PP10/22/277 Mw 37,427 Mw/Mn 1.58) were obtained from Polymer Laboratories Ltd., UK. Oregon Green (OG) 488 cadaverine was from Molecular probes, UK. Dry triethylamine and dry DMSO were obtained from Sigma Aldrich, UK in sure-sealed bottles. All other reagents and solvents were from Sigma Aldrich, UK. Spectra/Pore 7-regenerated cellulose dialysis membrane (Mw cut-off 2000 g/mol) was obtained from Spectrum Laboratories Inc, USA.

2.3 General methods

All the general methods used in these studies are described below, however, where necessary, specific methods and steps taken to tailor details of the methods, are given in the related experimental chapters. Where the development of a method is considered an important part of the results, such as the synthesis of HPMA copolymer-OG ± Man and HPMA copolymer-Man ± AmB conjugates, the method is detailed in the respective chapter. All buffers were made up in double distilled water as detailed in the Data for Biochemical Research reference book (Dawson et al., 1986).

2.3.1 General cell culture

2.3.1.1 Maintenance of cell lines

Routine cell culture was performed in a laminar flow hood under sterile conditions. RAW 264.7 cells were maintained in DMEM with glutamax and phenol red pH indicator supplemented with 10 % foetal bovine serum (complete medium) at 37 °C and 5 % CO_2. Sub-confluent subcultures (~ 80 %) were split and passaged, as described below, approximately every 3-4 days. This cell line is semi-adherent i.e. some adhere strongly, some loosely and some grow in suspension. Therefore, adherent cells were removed mechanically by scraping, and then the suspension spun down to collect all cells. All cells were resuspended in fresh complete medium, counted and seeded at a density of 10^5 cells per ml.

THP-1 cells were maintained in RPMI 1640 medium with glutamax and phenol red supplemented with 10% foetal bovine serum (complete medium) at 37

°C and 5 % CO_2. These cells grow in suspension and so were subcultured by replacement of medium. This was done either by removing medium from flask and topping up with fresh complete medium or by centrifugation, and resuspension in fresh complete medium after counting. Cells were maintained between 5 x 10^4 and 10^6 cells per ml and passaged approximately every 3 - 4 days.

Suspension cells were differentiated using PMA into adherent macrophage cells. PMA (stock solution of 2 mM in DMSO) was added to the cell suspension when seeding to give a final concentration of 20 nM. Cells were incubated for 48 h at 37 °C, at 5 % CO_2 before changing for fresh complete medium. Cell adherence (differentiated) was confirmed visually by light microscopy.

2.3.1.2 Cell counting and viability assessment using trypan blue

Trypan blue is a dye that does not penetrate the membrane of living cells but is taken up into dead cells, and is therefore used to assess viability. After centrifugation, cells were resuspended to give a homogeneous suspension. 100 µl of this solution in a bijou bottle was mixed with an equal amount of trypan blue solution added (sterile filtered and diluted 1:1 in phosphate buffered saline (PBS)). Cell counting was performed microscopically using a haemocytometer slide. The slide has a grid of 9 large squares with an area of 1 mm^2, and a depth of 0.1 mm. Therefore, when 10 µl of cell suspension was added, the total volume of fluid over each square is 10^{-4} ml. The non-blue cells were counted in 5 squares and the mean number obtained multiplied by 2 x 10^4 to obtain the number of cells per ml of solution. The percentage of cells that had taken up blue dye was used to calculate cell viability.

2.3.1.3 Evaluation of cell growth using the MTT assay

The MTT assay was first introduced by Mosmann as a means of measuring cell viability (Mosmann, 1983). MTT is a yellow solution that is reduced in viable cells by mitochondrial dehydrogenase enzymes. It then forms insoluble blue crystals of formazan salt, which can be solubilised in a solvent. The absorbance at 550 nm is proportional to cell number. Cells were seeded in a 96 well plate at a density of 10^3 (RAW 264.7) or 10^4 (THP-1) cells per well (100 µl) in triplicate and left to adhere

for 24 h or differentiated as above. Every day for 10 days, the MTT assay was performed to obtain a growth curve for each cell line.

MTT (20 µl of a sterile filtered solution (5 mg/ml) in PBS) was added to each well, and incubated with the cells for 5 h at 37 °C and 5 % CO_2. The plates were then centrifuged and the supernatant removed, carefully avoiding the precipitated crystals. The crystals were left to dissolve in 100 µl of sterile DMSO for 30 min at 37°C and 5% CO_2 and absorbance was read using a plate reader at 550 nm. The growth curves are shown in Figure 2.1.

2.3.1.4 Freezing, thawing and storage of viable cells

To preserve the cell lines long-term, cells taken from the log phase growth of early passages were frozen and stored in liquid nitrogen. DMSO was used for freezing as a cryoprotectant to allow a slower cooling rate and thus preventing the formation of ice crystals that can damage the cell. Cells were resuspended in freezing medium (10^6 –10^8 cells/ml in medium containing 20 % FBS plus 10 % DMSO) in 2 ml cryovials. The vials were placed in a Mr Frosty overnight at –70 °C, then into the liquid nitrogen storage container. When required, ampules were thawed rapidly, 10 ml warmed complete medium added, centrifuged and supernatant discarded as quickly as possible to remove DMSO. Cells were resuspended in warmed complete medium and cultured as previously described.

2.3.2 Fluorescence characterisation of fluorophores and fluorescent conjugates/probes

The absorbance and emmision spectra for each probe or fluorophore were measured to determine the peak maxima and degree of overlap. FITC-BSA, FITC-BSA-Man and DQ Ovalbumin and OG were dissolved in phosphate buffer (pH 7.4). 1 ml of a 0.1 mg/ml solution was placed in a polystyrene cuvette. Emission and absorbance curves were obtained using the Amico Bowman series 2 fluorescence spectrophotometer. To assess the effect of pH on fluorescence output, samples of each fluorescent probe/fluorophore were dissolved in buffers at three physiological pH (0.1M sodium citrate buffer at pH 5.5 and 6.2, and 0.1 M sodium phosphate buffer at pH 7.4). Concentration curves were prepared at each condition (0.001 to 1 µg/ml of probe/fluorophore) in a black 96 well plate. Fluorescence was measured

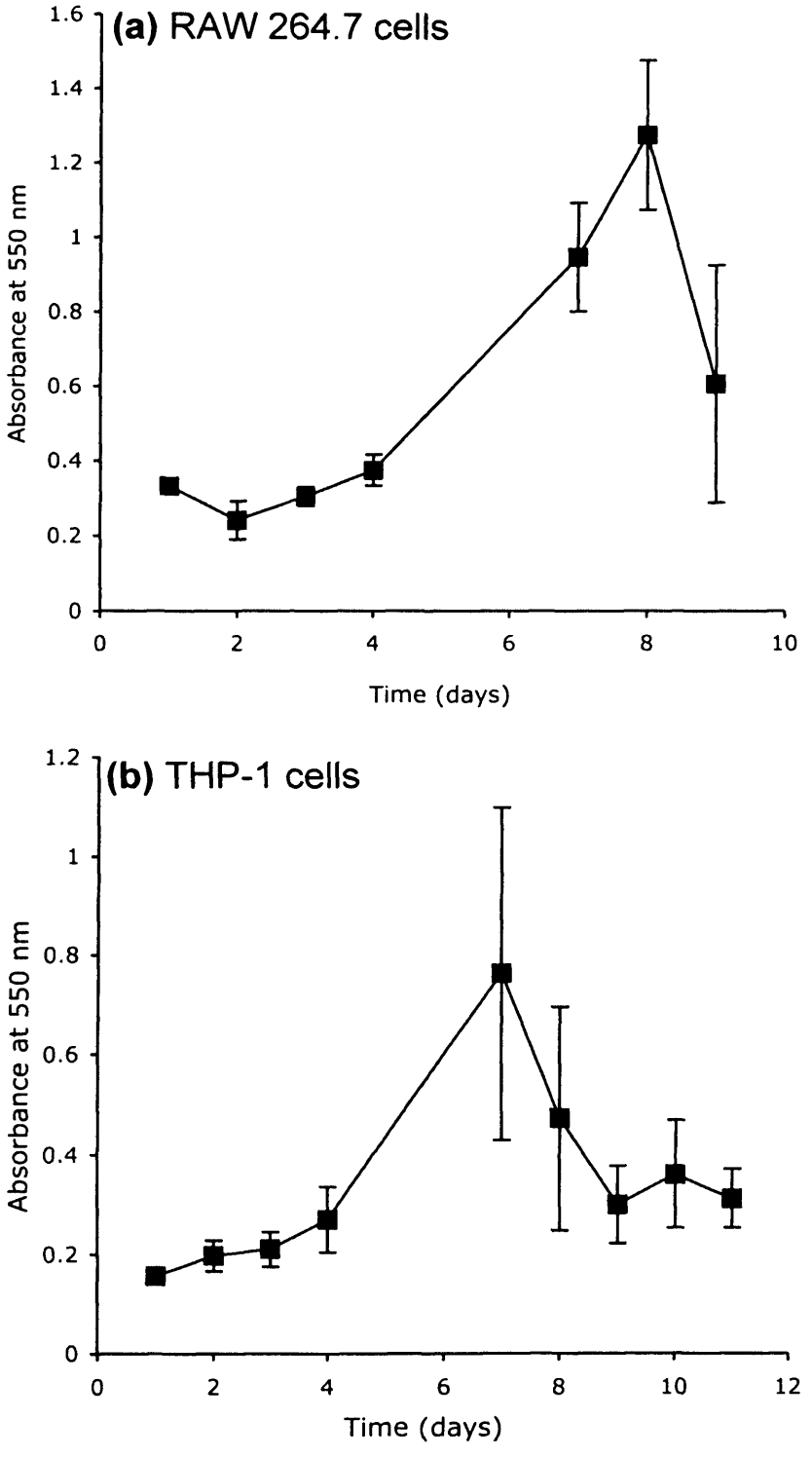

Figure 2.1 Cell growth curves. Cell proliferation of (a) RAW 264.7 cells (seeded at 10^3/well) and (b) THP-1 cells (suspension) (seeded at 10^4/well) measured using MTT assay. Data represent mean (n = 6) ± SD.

using a Fluostar optima fluorescence plate reader using filters for 492/520 nm. The degree of fluorescence labelling was calculated using the UV absorbance at 494 nm.

2.3.3 General flow cytometry protocol to assess binding and endocytosis in RAW 246.7 and THP-1 cells

Cell-associated fluorescence at both 4 °C and 37 °C over time was measured to assess binding only, and binding plus uptake respectively. Cells were seeded at a concentration of 5 x 10^5 cells per ml in complete clear media in 6 well plates. RAW 264.7 cells were incubated at 37 °C, at 5 % CO_2 for 24 h to adhere. THP-1 cells were differentiated using PMA as described in section 2.3.1, and then incubated for 24 h in clear complete media. After experimental procedures (described in the respective chapters), incubations were stopped by adding ice cold PBS and putting the plates on ice. RAW 264.7 cells were scraped using a rubber policeman, pipetted into FACS tubes and centrifuged at 500 r.c.f. for 5 min at 4 °C. They were then washed in PBS and centrifuged twice more before re-suspending the cell pellet in a final volume of 200 µl ice cold PBS. Using THP-1 cells the experiment was performed as above except the cells were washed three times with ice cold PBS in the plates and collected into FACS tubes as above. For the binding experiments conducted at 4 °C plates were pre-incubated on ice in the cold room for 30 min before the experiment.

20,000 counts (cells) per sample were collected. Cells were gated on the forward scatter/side scatter plot to exclude the non-viable cells (Figure 2.2 (a)) and fluorescence measured on FL1 channel (520 nm) (Figure 2.2 (b)). The geometric mean was used to establish the degree of fluorescence, which equates to the median of the original data (as log-transformed data was acquired). The fluorescent plot was arbitrarily gated for positive (M2) and negative cells (M1), negative being the viable control cells. The percentage positive takes account of the autofluorescence of the control cells, as well as the degree of exogenous cell-associated fluorescence. The term 'derived cell-associated fluorescence' will be used to describe the binding and uptake and was determined by the following equation:

Derived cell-associated fluorescence = (% cells that are positive x geometric mean of the fluorescence)/100

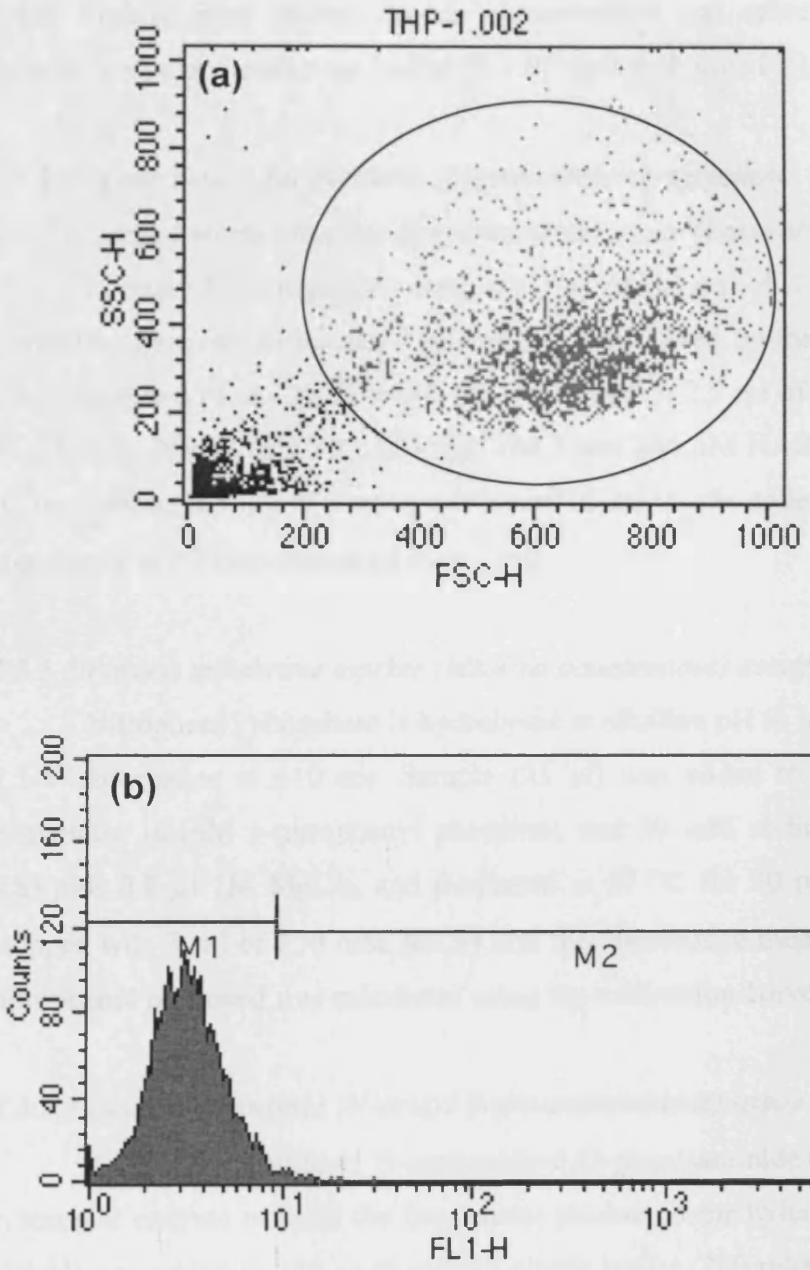

Figure 2.2 Typical flow cytometry plots of THP-1 cells. Panels show a) gating of viable cells (circled) and b) autofluorescence of control cells and gating of negative (M1) and positive cells (M2).

2.3.4 Bradford assay for protein (Bradford, 1976)

Samples (30 µl) were added to 200 µl Bradford reagent in a 96 well plate and incubated at room temperature for 5 min. Absorbance was measured at 595 nm on Tecan Sunrise plate reader. Protein concentration was calculated from the BSA standard curve in the relevant buffer (0 – 20 µg/ml) (Figure 2.3).

2.3.5 Enzyme assays for markers of intracellular organelles

2.3.5.1 Cytosol marker (lactate dehydrogenase) assay (Vassault, 1983)

Lactate dehydrogenase catalyses the oxidation of NADH to NAD+ by converting pyruvate to lactate. The reaction is followed by the reduction of NADH absorbance at 339 nm. Sample (50 µl) was added to 2.5 ml of a solution containing 81 mM Tris-NaOH (pH 7.2), 203 mM NaCl and 244 µM NADH (equilibrated to 30 °C in cuvette). To this 0.5 ml of pyruvate (10 mM) was added and the decrease in absorbance at 339 nm measured over 1 min.

2.3.5.2 Plasma membrane marker (alkaline phosphatase) assay (Graham, 1993)

Nitrophenyl phosphate is hydrolysed at alkaline pH to nitrophenol, which has a UV absorbance at 410 nm. Sample (25 µl) was added to 200 µl of a solution containing 16 mM p-nitrophenyl phosphate and 50 mM sodium borate-NaOH (pH 9.8) plus 0.8 µl 1M $MgCl_2$, and incubated at 37 °C for 30 min. The reaction was stopped with 1 ml of 250 mM NaOH and the absorbance measured. The amount of nitrophenol produced was calculated using the calibration curve (Figure 2.4).

2.3.5.3 Lysosomal enzyme (N-acetyl-β-glucosaminidase) assay (Klemm et al., 1998)

4-methylumbelliferyl-N-acetamido-ß-D-glucosaminide is hydrolysed by the lysosomal enzyme to yield the fluorescent product, 4-methylumbelliferone. Samples (50 µl) was added to 250 µl of sodium citrate buffer (200 mM; pH 5), plus 75 µl of l250 mM sucrose containing 0.1 % TX-100. The substrate (100 µl) was then added and the reaction incubated at 37 °C for exactly 1 min. The reaction was terminated by addition of 2.5 ml of glycine-NaOH (250 mM; pH10.4). The concentration of liberated product (methylumbelliferone) was determined on the fluorimeter (absorbance 357 nm, emission 444 nm) using a calibration curve of 4-

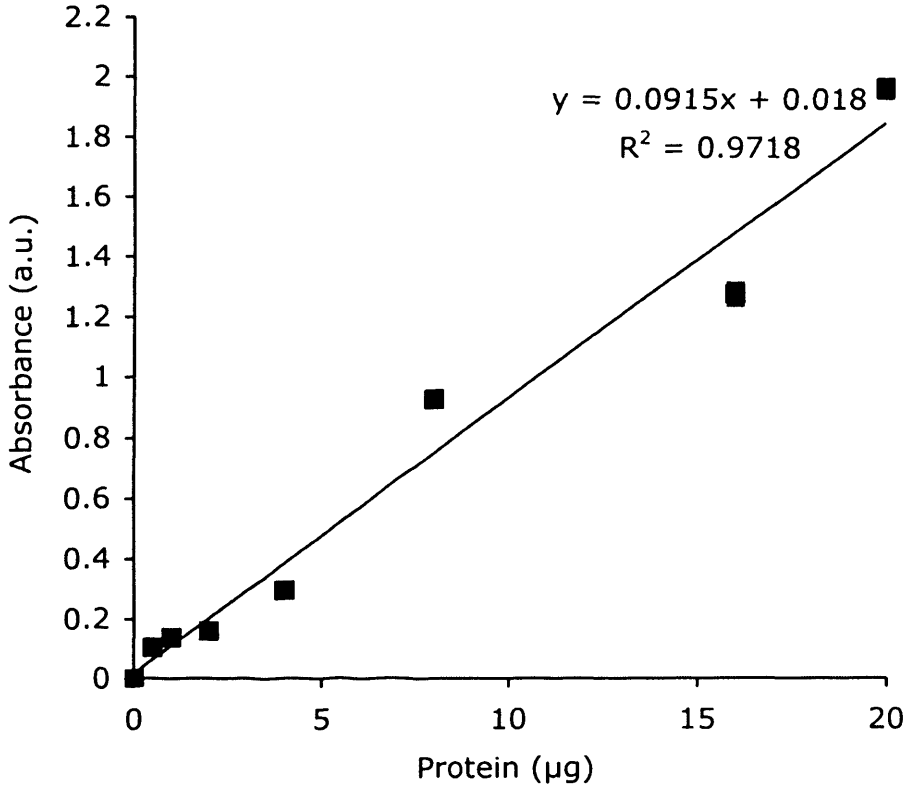

Figure 2.3 Bradford protein assay. Calibration curve of BSA in HB. Data represents mean ± SD (n=3), and when error bars are not visible they fall within the data points.

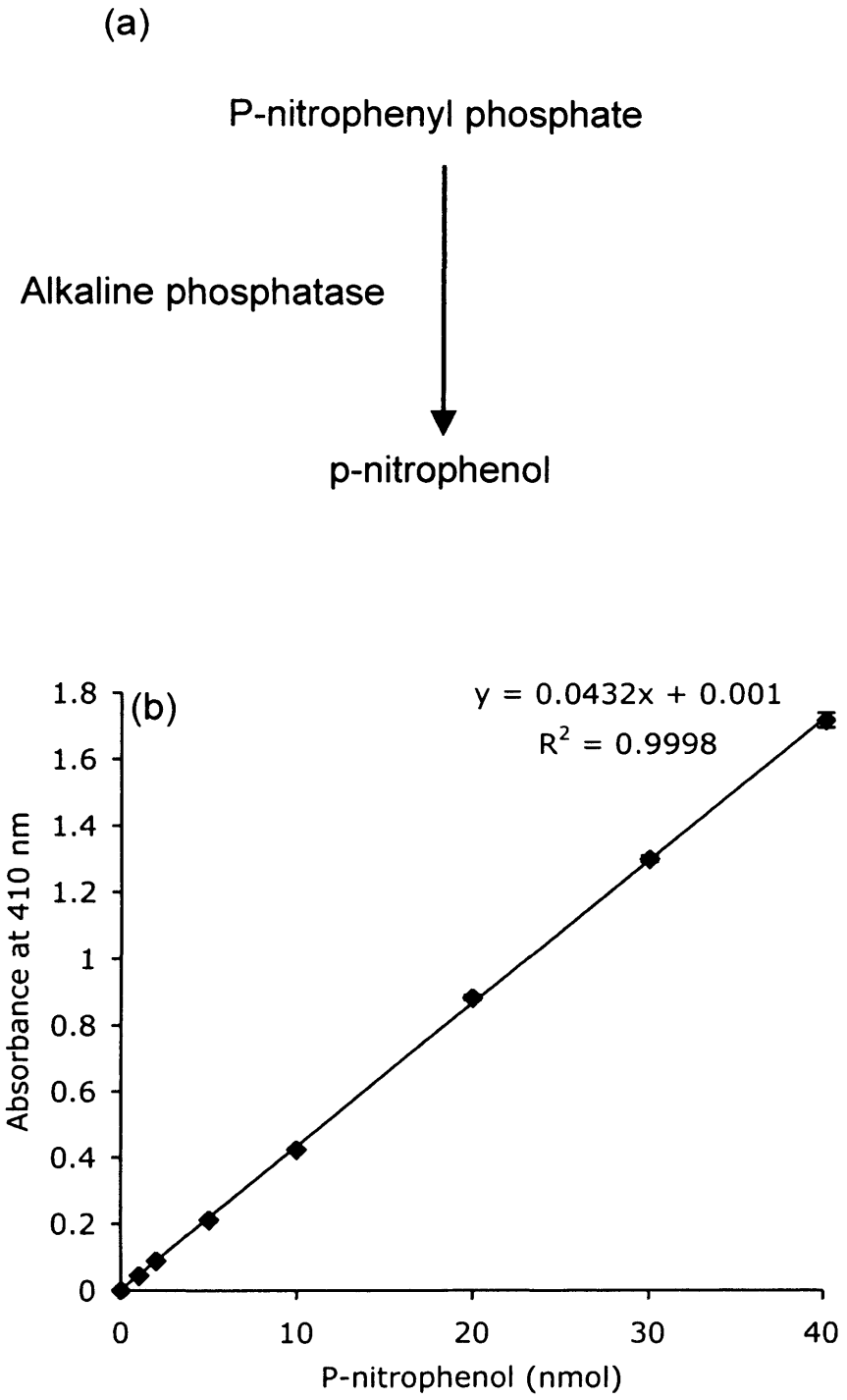

Figure 2.4 Plasma membrane enzyme marker alkaline phosphatase assay. Panel (a) enzyme reaction and (b) calibration curve of product p-nitrophenol. Data represents average ± standard deviation (n = 3) and error bars are within data points where not visable.

methylumbelliferone (Figure 2.5). Blanks contained either no biological material or no substrate.

2.3.6 SDS-PAGE to separate proteins by size

A 10% SDS-PAGE gel was prepared (Table 2.1) in the gel apparatus assembled according to manufacturers instructions (Bio-Rad, UK). The running gel was first prepared, pippetted into the space between the glass plates with a layer of isopropanol on top of the gel and left to set for 30 min. The stacking gel was made up, the isopropanol discarded, and applied carefully to the top of the running gel. An appropiate comb was then pushed into the stacking gel and left to set for approximately 30 min. Samples (50 µl) were diluted 6:1 in sample buffer (6x to give a final concentration of 62.5 mM Tris-HCl, pH 6.8 containing 2 % SDS, 100 mM DTT, 10 % glycerol and 0.001 % bromophenol blue) and boiled for 5 mins (100 °C). Samples (30 µl or protein concentration specified in specific chapter) were then placed in each well and run in Tris running buffer (25 mM Tris (pH 8.3), 192 mM glycine, 0.1 % SDS) for ~ 1 h at 200 V.

2.3.7 General Western blotting protocol

The proteins were wet transferred from the gel onto nitrocellulose membranes in cold transfer buffer (25 mM Tris (pH 8.3), 192 mM glycine plus 20 % MeOH) at 350mA for 1 h. Transfer apparatus was assembled according to the manufacturer's instructions (Bio-Rad, UK). Confirmation of transfer was performed using Ponceau Red stain (0.2%) for 5 min then washed with water until the membrane is clean but bands are clear. Membranes were destained by washing extensively with TBS-T (Tris buffered saline (TBS) 20 mM Tris-HCl, 150 mM NaCl, adjusted to pH 7.5 plus 0.1 % Tween-20). The gel was stained with Coomassie stain (25 % MeOH, 10 % acetic acid plus 0.18 % w/v CB) for 30 min, then de-stained with a weak solution of acetic acid and methanol solution (25 % MeOH 10 % acetic acid) to confirm transfer.

Non-specific binding sites were blocked by incubation with 10 % skimmed milk in TBS for 1 h at room temperature. The membranes were the incubated with the appropriate primary antibody in TBS-T for 2 hrs at room temperature. Enough

(a)

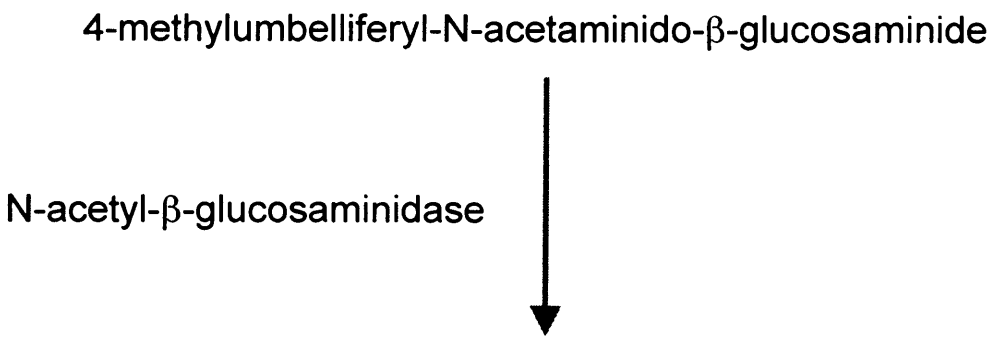

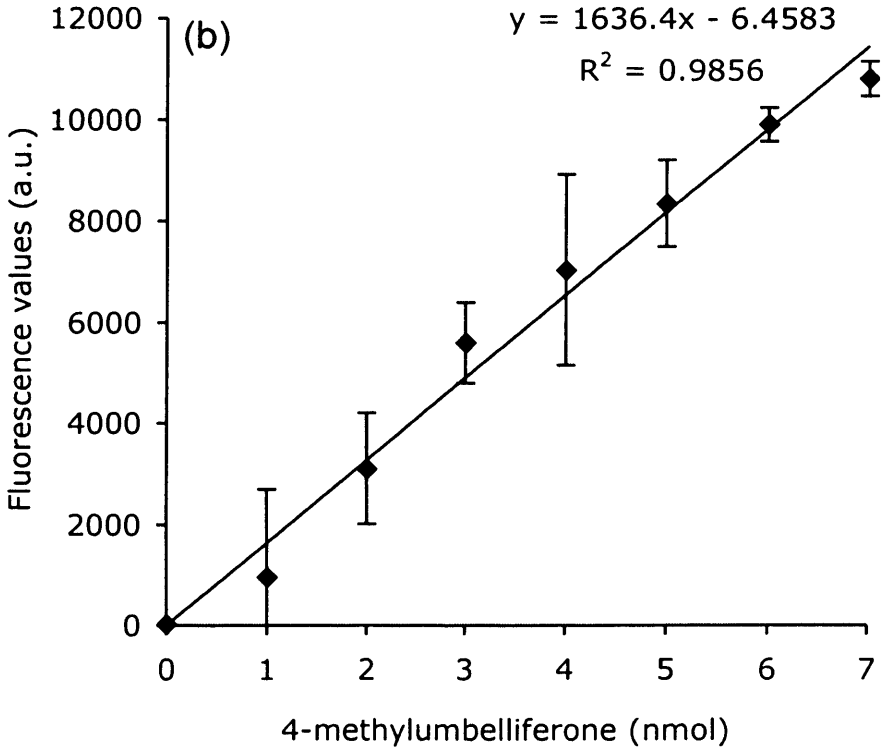

Figure 2.5 Lysosomal enzyme marker N-acetyl-b-glucosaminidase assay. Panel (a) enzyme reaction and (b) calibration curve of product 4-methylumbelliferone. Data represents average ± standard deviation (n = 3).

Table 2.1 Composition of polyacrylamide gels for SDS PAGE

Reagent	Running Gel (ml)	Stacking Gel (ml)
ddH2O	9.69	5.85
Tris HCl	5 (1.5 M)	2.5 (0.5 M)
10 % SDS	0.2	0.1
40 % Acryl/Bis	5	1
10 % APS	0.1	0.05
TEMED	0.01	0.005

solution was prepared to completely cover the membrane so as not to dry out and was gently agitated on an orbital shaker (bellydancer). Membranes were washed three times with TBS-T before incubation with the appropriate secondary antibody, conjugated with either horseradish peroxidase (HRP) or Alexa Fluor 488, for 1 h at room temperature. The membranes were washed as above and either fluorescent bands visualised directly on the Typhoon or, to detect HRP activity, the membrane bands were developed using enhanced chemiluminescence (ECL) reagent and exposed to X-ray film in the dark room for various lengths of exposure (10 s – 5 min).

2.3.8 Dot blot protocol

A grid was drawn in pencil on the nitrocellulose membrane, to indicate the region to blot. Using a narrow-mouth pipette tip, 2 µl of samples was spotted slowly onto the nitrocellulose membrane at the centre of the grid and left to dry. Non-specific sites were blocked by soaking in 5% BSA in TBS-T (1 h, RT). Membranes were incubated with primary antibody (1:100) dissolved in BSA/TBS-Tween for 1 h at RT, then washed three times with TBS-T (3 x 5 min). Incubation with secondary antibody conjugated with HRP (1:5000) was for 1 h at room temperature, before washing three times with TBS-T (15 min x 1, 5 min x 2), then once with TBS (5 min). Membranes were then incubated with ECL reagent for 1 min, and exposed to X-ray film in the dark room for various lengths of exposure (10 s – 5 min).

2.3.9 Fixation of cells for confocal microscopy

Cells were seeded at 5 x 10^5 cells/well on coverslips (ethanol immersed and washed in sterile PBS) in 6 well plates. Cells were placed on ice and washed 3 x with ice cold PBS, fixed either by immersion in methanol (20 °C for 5 min) or 20 min in 3% w/v paraformaldehyde in PBS, washed 3 times in PBS before being permeabilized with Triton extraction buffer for 5 min at 25°C (0.2% v/v TX-100 and 50 mM glycine in PBS pH 7.2). After washing in PBS the coverslips were mounted on slides with 40 µl Vectashield, the edges sealed with clear nail varnish, and stored at 4 °C for imaging within 72 h.

2.3.10 Immunolabeling of cells for confocal microscopy

When cells were to be immunolabeled, after fixation and washing with PBS above slides were incubated for 1 h in blocking buffer (2% goat serum in PBS). The cells were then incubated at room temperature with mouse anti-EEA 1 (1: 600) or anti-LAMP 1 (1: 300) antibodies in blocking buffer for 1 h. Following further 3 x 5 min washes in PBS, the cells were incubated for 1 h with either Alexa Fluor 488 or 534 anti-mouse antibodies in blocking buffer. After washing in PBS the coverslips were mounted on slides with 40 µl Vectashield, the edges sealed with clear nail varnish, and stored at 4 °C for imaging within 72 h.

2.3.11 Fluorescence confocal microscopy of macrophage cells

Confocal microscopy was performed on a Leica SP5 system. Data was collected using dedicated software supplied by the manufacturers and exported as tagged image files (TIF); at least three representative images were obtained for each sample. Every effort was made to control for the false positives that may be associated with "bleed" from one channel to another. This was done by switching off the appropriate laser and adjusting the gain settings and laser power until no signal was visible in the corresponding photodetection channel. Images in separate channels were also acquired sequentially.

2.3.12 Statistical Analysis

Samples were analysed in a minimum of three replicates where possible and the error calculated as either standard deviation (SD) or standard error of the mean (SEM) where appropriate. Typically, either a students t-test, or a one way analysis of variance (ANOVA) followed by a Bonferroni post hoc test, were used to analyse the statistical significance of the results where appropriate. Unless otherwise stated, probability (p) of < 0.05 was deemed to indicate significance.

Chapter 3

Characterisation of the *in vitro* models used to evaluate macrophage targeting using mannosylated probes

3.1 Introduction

To design polymer drug conjugates suitable for macrophage-specific targeting of anti-leishmanial drugs, it was first necessary to set up the *in vitro* models. There were two important considerations when choosing the macrophage models. First, it was essential that the cell line was susceptible to infection by the *Leishmania* parasite so that it could later be used to test the conjugates activity. Second, it was important that the cell express MR in sufficient number to enable targeting. The murine RAW 264.7 macrophage-monocyte and the human THP-1 cell lines were chosen for these studies. The rationale for their choice and the fluorescent probes used is discussed below.

3.1.1 The mannose receptor

The MR structure, characteristics and physiological function have been described in detail in section 1.6. MR expression is an indicator of macrophage maturity as the MR is not expressed on monocyte precursors. Many cell lines e.g. J774-2, J774-B10 and P338-D1 do not seem to express the MR or express low receptor levels (Stahl & Gordon, 1982). Therefore it was considered important to ensure the cell lines chosen here expressed the MR, and would be able to endocytose mannosylated polymer conjugates.

3.1.2 The RAW 264.7 cell line

The RAW 264.7 murine monocyte-macrophage cell line was used in part because planned later *in vivo* studies were going be performed in a murine model. This cell line has been shown to exhibit similar characteristics to normal macrophages including the phagocytosis of bacteria and antibody-coated red blood cells (Frankenberg et al., 2008; Henry et al., 2004) and secretion of lysozyme (Raschke et al., 1978). It has been shown to be a good model of inflammatory macrophages, capable of Fc-γR mediated phagocytosis, respiratory burst and cytokine secretion (Loegering & Lennartz, 2004). Importantly, RAW 264.7 cells are able to phagocytose and maintain *Leismania donovani* infections (St-Denis et al., 1999).

This cell line has been used to study the pharmacological activity of anti-leishmanials (Kayser & Kiderlen, 2003; Radtke et al., 2003) and literature on RAW 264.7 cell lines indirectly suggests some level of MR expression as HPMA copolymer conjugates containing mannose were taken up to a higher degree than those without

(Nan et al., 2004). However, the level of MR expression in this cell line had not been extensively studied.

3.1.3 The THP-1 cell line

The THP-1 cell line is a human cell line. It resembles the blood monocyte, in that it has no MR expression and these cells do not phagocytose parasites. Treatment of THP-1 monocytes with the phorbol ester PMA results in a differentiated phenotype displaying macrophage characteristics (Schwende et al., 1996). These include adherence, loss of proliferation, phagocytosis of latex beads, expression of CR3 and CD14 (LPS receptor), and release of superoxide anions and TNF-α (Tsuchiya et al., 1980). PMA is an analogue of diacylglycerol, an activator of PKC, therefore its actions are thought to be mediated by PKC. It should also be noted that Korho and colleagues (2004) found that although many morphological and other characteristics are similar to macrophages, there are many differences at the transcriptional level.

Therefore it was considered important to characterise these cells carefully for MR expression. Some studies have suggested MR expression in THP-1 cells, for example Raveh et al. (1998) studied the effect of cytokines on MR-dependent phagocytosis. They found that the prototypical Th2 cytokine, IL-4, increases both surface expression and MR-mediated endocytosis; whereas the Th1 cytokine, IFN-γ, decreases them both. However, both alone and together, these same cytokines act to increase MR-mediated phagocytosis. The expression of the MR is complicated and depends on the inflammatory state of the macrophage. In addition, THP-1 cells have been shown to phagocytose and maintain *Leishmania* infection *in vitro* (Croft et al., 2006; Dasgupta et al., 2003; Ogunkolade et al., 1990) and this cell line has been used as an *in vitro* model for screening the pharmacological activity of anti-leishmanial drugs (Gebre-Hiwot et al., 1992).

3.1.4 Choice of fluorescent probes

To study endocytosis via the MR it was necessary to choose suitable fluorescent probes. The structures of the proteins (BSA and ovalbumin) used as probes are shown in Figure 3.1, and the chemical structures of the fluorophores used in Figure 3.2. FITC-labelled BSA was primarily used in these experiments. Albumin is the most abundant protein in blood plasma, being chiefly responsible for

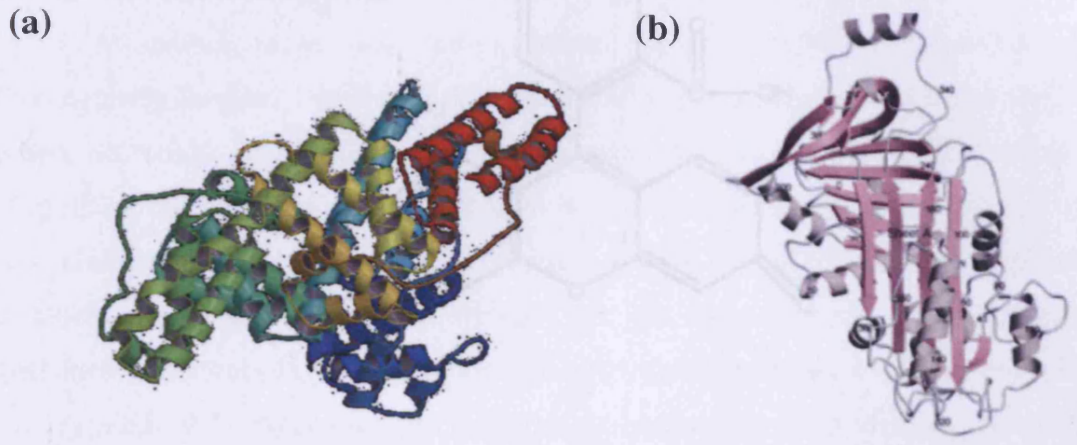

Figure 3.1 Structures of the protein probes. Panel (a) bovine serum albumin (taken from Schreiber, 2004) and panel (b) ovalbumin (taken from Yamasaki, 2003).

(a)

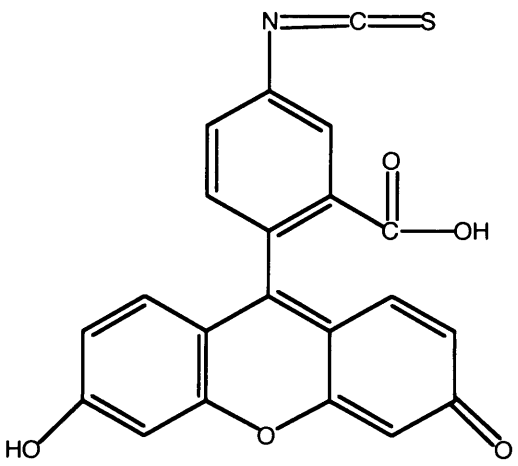

(b)

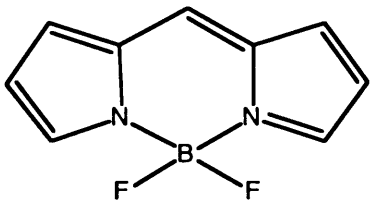

Figure 3.2 Chemical structure of the fluorophores. Panel (a) FITC and (b) BODIPY.

maintaining blood pH. It is not rapidly degraded in the circulation, and although there are macrophage receptors for albumin, such as the scavenger receptors gp18 and gp30, these primarily recognise modified albumins and only weakly bind the native form (Schnitzer and Bravo, 1993). However, when conjugated to mannose residues albumin can be used as a marker of mannose receptor-mediated uptake (Monsigny et al., 1984). Thus, FITC-labelled BSA was used here to indicate the degree of targeting achievable using the MR in THP-1 and RAW 264.7 cells, and to compare the specific and non-specific binding/uptake.

A second probe was also chosen for these studies, DQ-ovalbumin. Fluorescently-labelled ovalbumin is commercially available and has been used by others to study MR-mediated uptake in mycobacterium-infected macrophages (Teitelbaum et al., 1999). DQ-ovalbumin is another albumin protein, derived from egg protein (45 kDa) with an inherently high degree of mannosylation. DQ ovalbumin is labelled with a BODIPY fluorophore that has the advantage of being highly quenched at neutral pH, and therefore relatively non-fluorescent. However, once it is endocytosed and transported to endosomal compartments containing lysosomal enzymes the protein is degraded and the released BODIPY begins to fluoresce. Therefore this probe can be used to assess whether MR delivers its payload to the late endosomal/lysosomal compartment.

3.1.5 Techniques used to study cellular uptake and binding

Flow cytometry

Flow cytometry was used to measure the cellular binding and uptake of the probes, being a rapid, reliable and widely used technique. It is possible to measure both the physical and chemical characteristics of the cells, examining the scatter properties and the fluorescent emission without fixation. Also large cell numbers can be analysed. Fluorescence is proportional to the amount of probe bound and/or internalised, provided it is within the linear range of concentration and at a defined pH.

Cell-surface binding of probes to the THP-1 cells was assessed by incubation at 4 °C, as endocytosis is largely inhibited at this temperature. At 37 °C, both binding and endocytosis occur, and the fluorescence measured was used to indicate uptake into the cells. Receptor-specificity was also investigated by assessing the concentration dependence of the binding and the effect of competitors. Mannan (yeast

poly-mannose) can be used as competitor of mannose receptor mediated binding, and therefore endocytosis (Stahl et al. 1980). Competition experiments have co-incubated unlabelled mannan and FITC-BSA-Man to determine whether the uptake is specifically mannose receptor-mediated.

Fluorescence microscopy

Once taken up into the macrophage, it was considered important to ascertain the intracellular trafficking of the probes and whether they accumulate in late endosomal and/or lysosomal compartments. The disadvantage of flow cytometry is that it gives no indication as to where in the cell the compound is localised. Fluorescence microscopy has frequently been used to determine cell accumulation and localisation of fluorescently labelled compounds though it is not quantitative and care must be taken in interpreting such images (North, 2006; Zwier et al., 2004). Also, it allows any changes in cell morphology to be visualised. Macrophage cells were observed, by both light and fluorescence microscopy, after incubation with the above fluorescent probes, then by confocal fluorescence microscopy, using antibodies to label of the early endosomes and late endosome/lysosome.

Western blotting

The above techniques use indirect methods to investigate MR-dependent uptake and provide no direct evidence of receptor expression. To directly determine MR expression in these cell lines, a specific MR antibody was used. Western blotting is the most common method used to study expression of a receptor, and was used here to establish comparative levels of the mannose receptor on theTHP-1 cell line. However, it should be noted that this technique can only measure the total cell MR content and does not demonstrate either surface expression or functionality of the receptor.

3.1.6 Summary of aims

The aim of this study is to establish macrophage models suitable to investigate MR-mediated uptake. The specific technical aims were as follows:

- Characterise the pH-dependence of the fluorescence output of the probes.

- Establish flow cytometry protocols to study the binding (4 °C) and uptake (37 °C) of various fluorescent probes ± Man in THP-1 and RAW 264.7 cell lines.
- Use MR competitor (mannan) to investigate specific and non-specific uptake.
- Use fluorescence microscopy to visualise the distribution of the fluorescent probes within the macrophage models.
- Use western blotting with an MR specific antibody, as well as microscopy of the THP-1 cells to visualise total MR expression in the cell lines.

3.2 Methods

The general methods used in these studies have already been described in chapter 2. The RAW 264.7 and THP-1 cells were maintained as in section 2.3.1.1. SDS-PAGE and Western blotting was performed using the general protocol described in sections 2.3.6 and 2.3.7, and the MR antibody was used at a dilution 1:10.

3.2.1 Fluorescence characterisation of FITC-BSA, FITC-BSA-Man and DQ ovalbumin probes

The absorbance and emmision spectra, the pH and concentration dependence of fluorescence of FITC-BSA, FITC-BSA-Man and DQ Ovalbumin was measured using the protocols outlined in section 2.3.2.

3.2.2 Binding and endocytosis of probes into RAW 246.7 and THP-1 cells using flow cytometry

Derived cell-associated fluorescence was measured with time using flow cytometry to assess binding at 4 °C, and binding plus uptake at 37 °C. The flow cytometry protocol is described in section 2.3.3. Cells were seeded at 5 x 10^5 cells per ml in clear media in 6 well plates overnight. They were then incubated with FITC-BSA, FITC-BSA-Man or DQ ovalbumin in clear media (at either 0.1 mg/ml of protein or 10 μg/ml of fluorophore) and cell-associated fluorescence was measured every 10 min for 60 min. 10 000 cells were counted, and data expressed as (the % of positive cells x geometric mean of the fluorescence)/100.

Flow cytometry experiments were carried also out using a competitive ligand, unlabelled yeast mannan (poly-mannose) to determine the degree of specific mannose

receptor-mediated uptake and to establish the number of receptors present. Cells were incubated with mannan (2 mg/ml) 30 min prior to the addition of FITC-BSA or FITC-BSA-Man (10 μg/ml FITC equivalent). The cells incubated in the dark at 37 °C, 5 % CO_2 for a further 60 min. Mannan alone was also incubated with the cells as a control.

3.2.3 Live-cell imaging of binding and endocytosis of probes in THP-1 cells using fluorescent microscopy

THP-1 cells were plated at a seeding density of 5 x 10^5 cells per ml in clear media into small optical petri dishes. After incubation with the fluorescent probes at equivalent fluorophore concentration (10 μg/ml of FITC) at 37 °C the cells were washed with ice cold PBS three times, then 1 ml ice cold PBS was left covering the cells in the dish. Dishes were covered and taken directly to the microscope. Phase contrast and fluorescent images of samples were captured using a Leica DMIRB at x 40 using filters set for FITC or BODIPY dyes.

3.2.4 Fixed-cell imaging of binding and endocytosis of probes in THP-1 cells using confocal fluorescent microscopy

THP-1 cells were at a seeding density of 5 x 10^5 cells per ml in 6 well plates, each with a sterile coverslip on the bottom of the well, and incubated with fluorescent probes as for live cell imaging (section 3.2.3). After washing, cells were fixed and labelled with EEA-1 and LAMP-1 antibodies as described in section 2.3.9, 2.3.10 and 2.3.11.

3.3 Results

3.3.1 Absorbance and fluorescence characteristics of FITC-BSA, FITC-BSA-Man and DQ-ovalbumin probes

The absorbance and emission peaks of the fluorescence spectra were measured at pH 7.4. The FITC-BSA conjugates have a wide absorbance range, consisting of three separate peaks, but a single emission peak. The absorption maxima were at 492 nm and the emission 521 nm (Figure 3.3a,b). In contrast, DQ-ovalbumin had broad absorbance and emission peaks, but had absorption maxima of 505 nm and emission maxima of 517 nm (Figure 3.3c). These wavelengths were then used to monitor the probes fluorescence output.

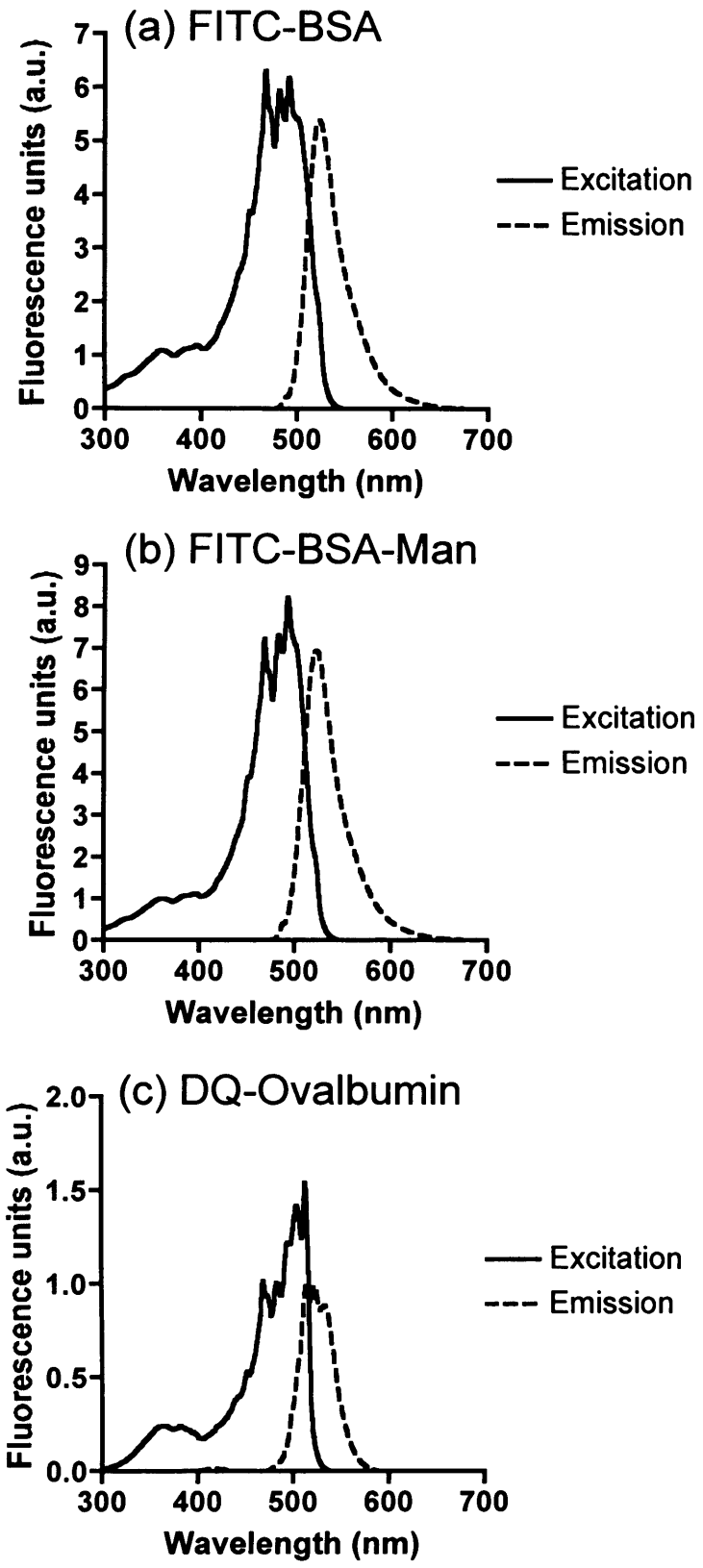

Figure 3.3 Excitation and emission spectra of the fluorescent probes used. Panel (a) FITC-BSA, (b) FITC-BSA-Man and (c) DQ-Ovalbumin in clear media at pH 7.4 (0.1 mg/ml).

When the effect of pH on the fluorescence emission was examined, it was found that as the pH decreased from 7.4 to 6.5 to 5.5, the fluorescence of the FITC conjugates decreased markedly at all concentrations (Figure 3.4a,b). The fluorescence output of FITC also exhibited concentration-dependent quenching and it was quenched at concentrations > 0.02 mg/ml FITC-equivalent. This equates to approximately 0.6 mg/ml of FITC-BSA and 0.2 mg/ml of FITC-BSA-Man. DQ-ovalbumin, conjugated to the fluorophore BODIPY, exhibited a linear increase in fluorescence with concentration up to 0.6 mg/ml (Figure 3.4c). Only a small decrease in fluorescence output was seen at the lower pH. It was decided, in the following flow cytometry experiments comparing the FITC-BSA ± Man probes, that the concentration of each probes would be standardised to the same FITC concentration (calculated using the UV absorbance readings), rather than concentration of protein. All subsequent uptake experiments were conducted using low concentrations of FITC (i.e. 10 μg/ml).

3.3.2 Binding and cellular uptake of uptake of fluorescent probes using flow cytometry

When the derived cell-associated fluorescence was measured large differences were seen for the different cell lines and probes. Both the number of cells that were gated positive and the mean fluorescence intensity were significantly increased when the RAW 264.7 cells were incubated with FITC-BSA-Man compared to FITC-BSA, at both 4 °C and 37 °C (Figures 3.5 and 3.6). The increase in derived cell-associated fluorescence of RAW 264.7 cells incubated with FITC-BSA was linear over 60 min at 37 °C, whereas at 4 °C it remained level (Figure 3.7a). However, RAW 264.7 cells incubated with FITC-BSA-Man exhibited derived cell-associated fluorescence at 37 °C that levelled off at 40 min (Figure 3.7b). The comparison between the two albumin probes at 37 °C, and a 4 °C (Figure 3.8a, b), shows the manosylated probe had significantly higher derived cell-associated fluorescence than FITC-BSA ($p < 0.05$, students t-test). There was a 4-fold increase at 37 °C and a 5-fold increase at 4 °C.

Similar patterns were found in the THP-1 cell line. Both the number of cells that were gated positive and the mean fluorescence intensity were significantly increased when the THP-1 cells were incubated with FITC-BSA-Man compared to FITC-BSA, at both 4 °C and 37 °C (Figures 3.9 and 3.10). THP-1 cells incubated with

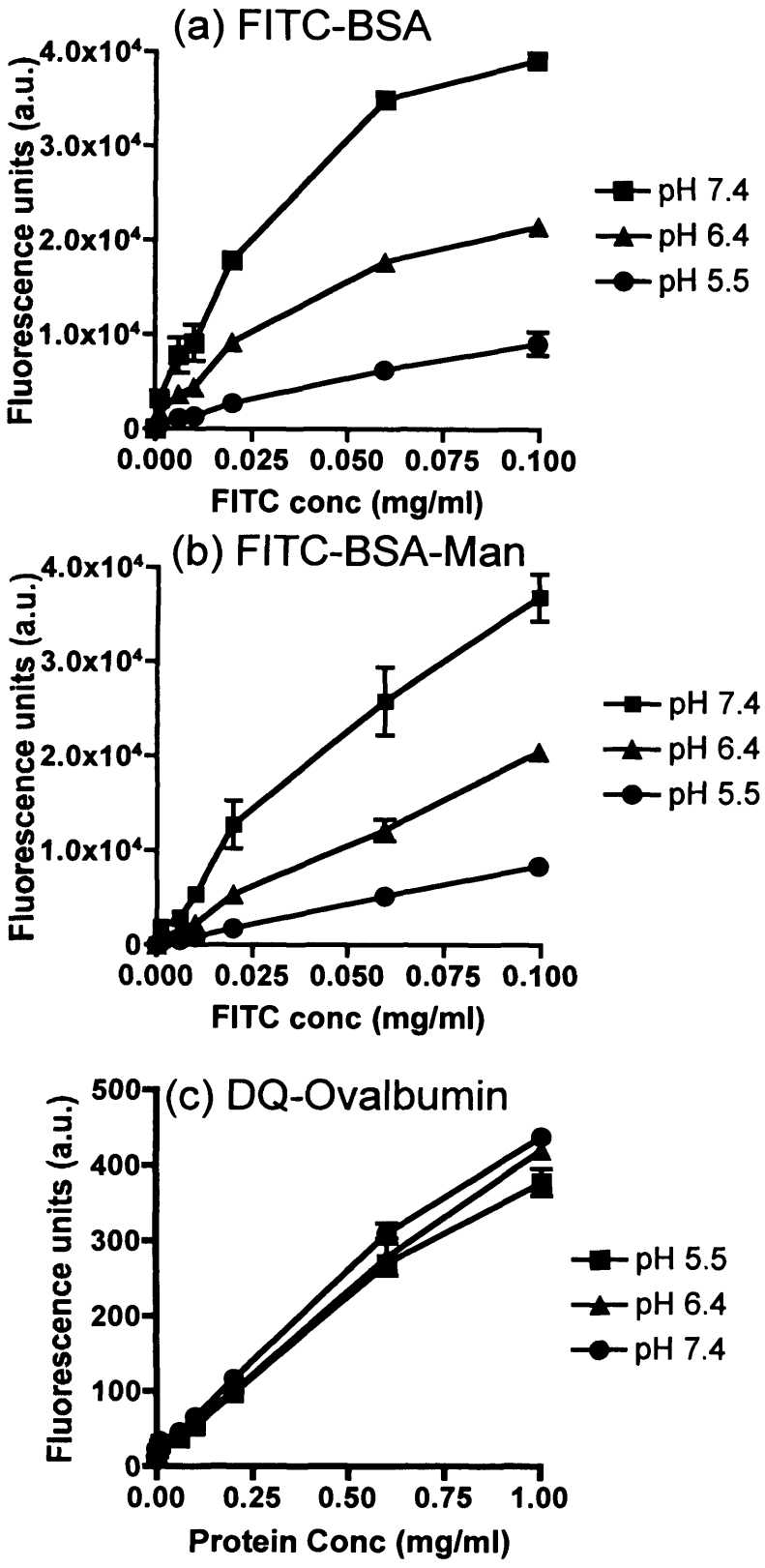

Figure 3.4 Effect of pH on the fluorescence of probes. Panel (a) FITC-BSA, (b) FITC-BSA-Man and (c) DQ-Ovalbumin. The data represent the mean ± SD (n = 3) and where the error bars are not visable they fall within the data points.

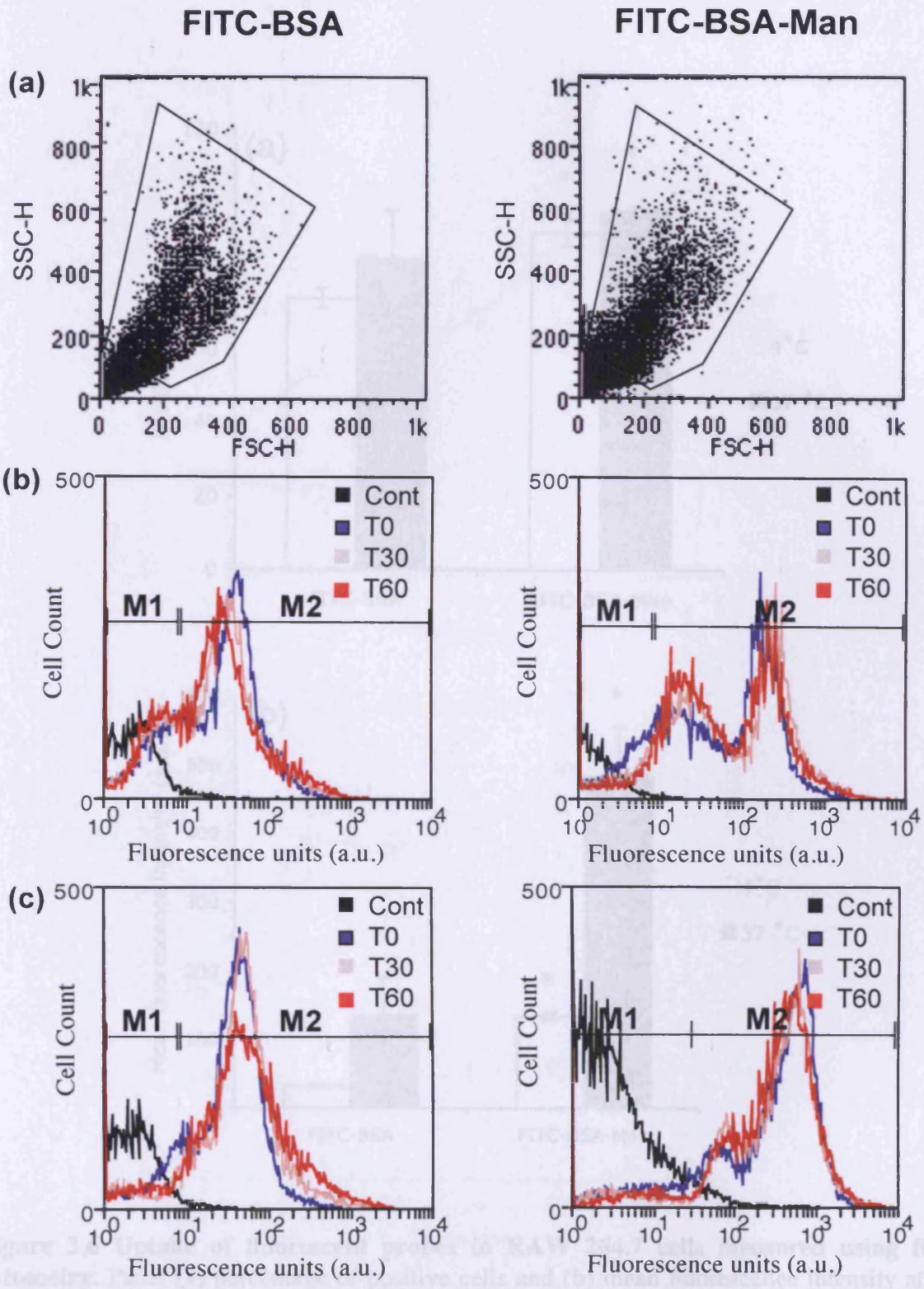

Figure 3.5 Typical raw data obtained from flow cytometry of RAW 264.7 cells incubated with FITC-BSA and FITC-BSA-Man. Panel (a) shows cell scatter and panel (b) the change in fluorescence with time over 60 min at 4 °C and (c) 37 °C.

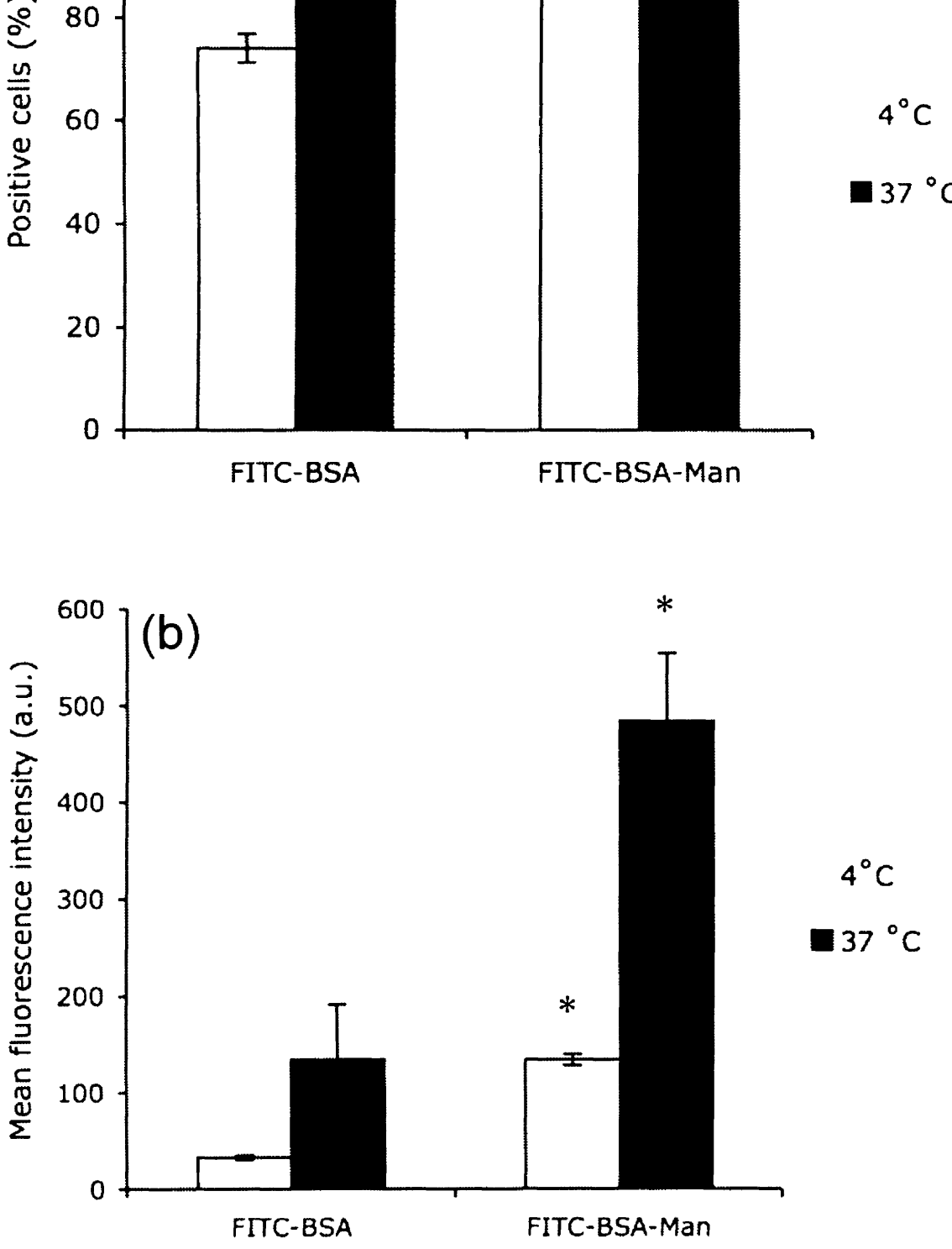

Figure 3.6 Uptake of fluorescent probes in RAW 264.7 cells measured cytometry. Panel (a) percentage of positive cells and (b) mean fluorescence in °C and 4 °C. The data represent the mean ± SD (n = 3 (4 °C), n = 9 (37 °C)) a error bars are not visible they fall within the data points. Statistical significance FITC-BSA and FITC-BSA-Man was determined at $p < 0.05$ for all both (students t-test).

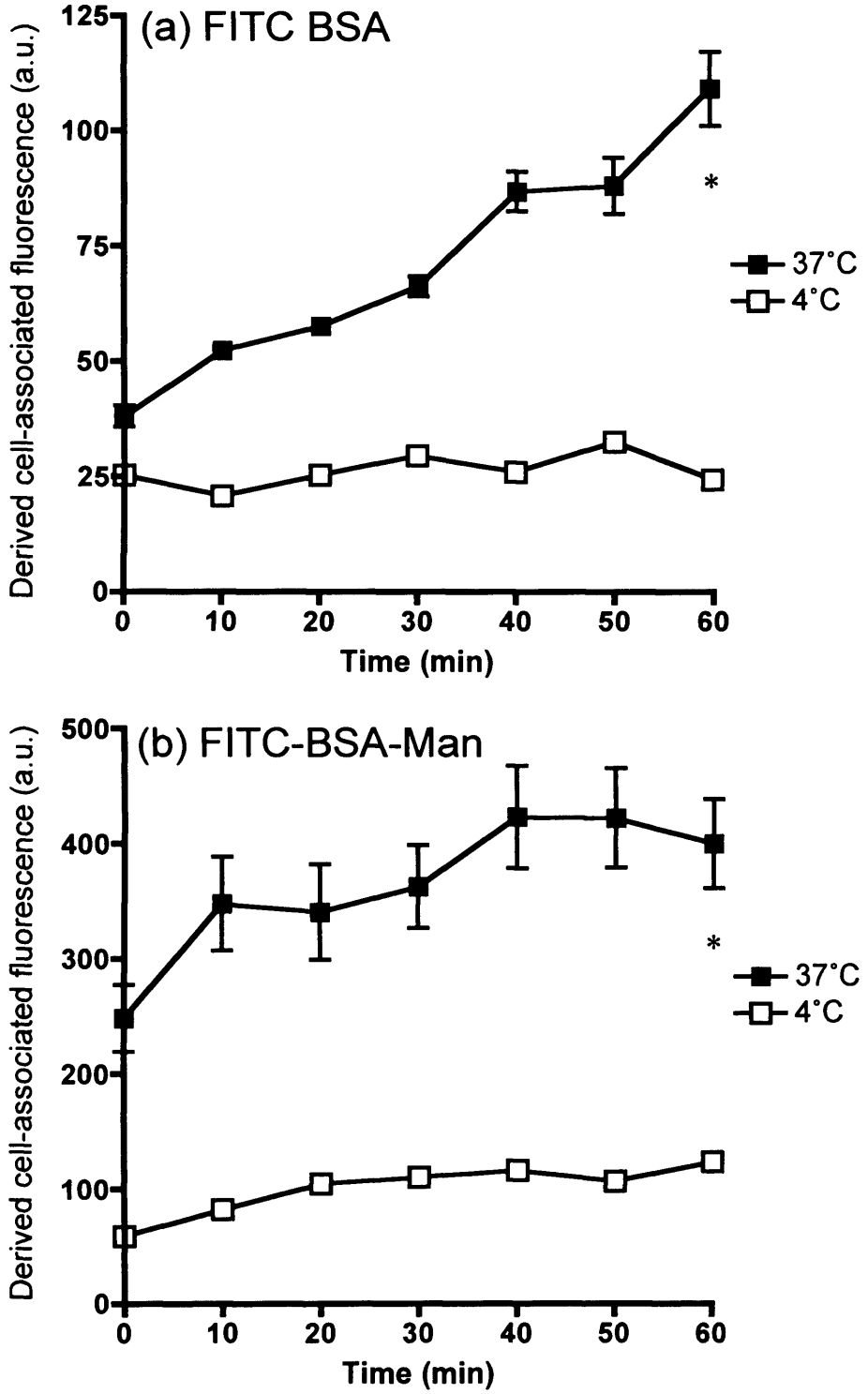

Figure 3.7 Time-dependent uptake of fluorescent probes in RAW 264.7 cells measured using flow cytometry. Panel (a) FITC-BSA and (b) FITC-BSA-Man at 37 °C and 4 °C. The data represent the mean ± SD (n = 3 (4 °C), n = 9 (37 °C)) and where the error bars are not visible they fall within the data points. Statistical significance (*) between 37 and 4 °C was determined at $p < 0.05$ for all data points (ANOVA with Bonferroni *post hoc* test).

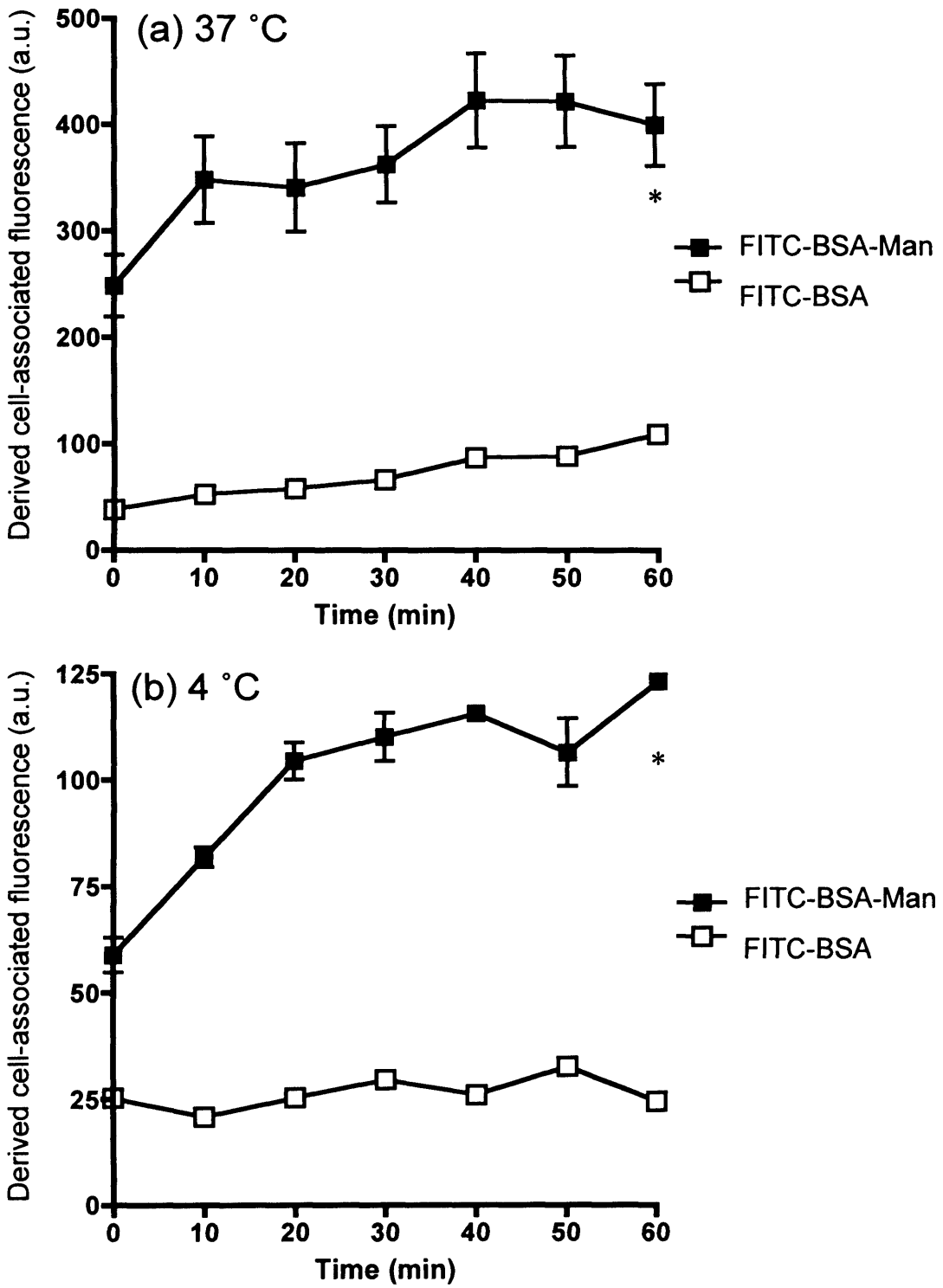

Figure 3.8 Comparison of binding/uptake of FITC-BSA±Man in RAW 264.7 cells. Panel (a) 37 °C and (b) 4 °C. The data represent the mean ± SD (n = 3) and where the error bars are not visible they fall within the data points. Statistical significance (*) between 37 and 4 °C was determined at $p < 0.05$ for all data points (ANOVA with Bonferroni *post hoc* test).

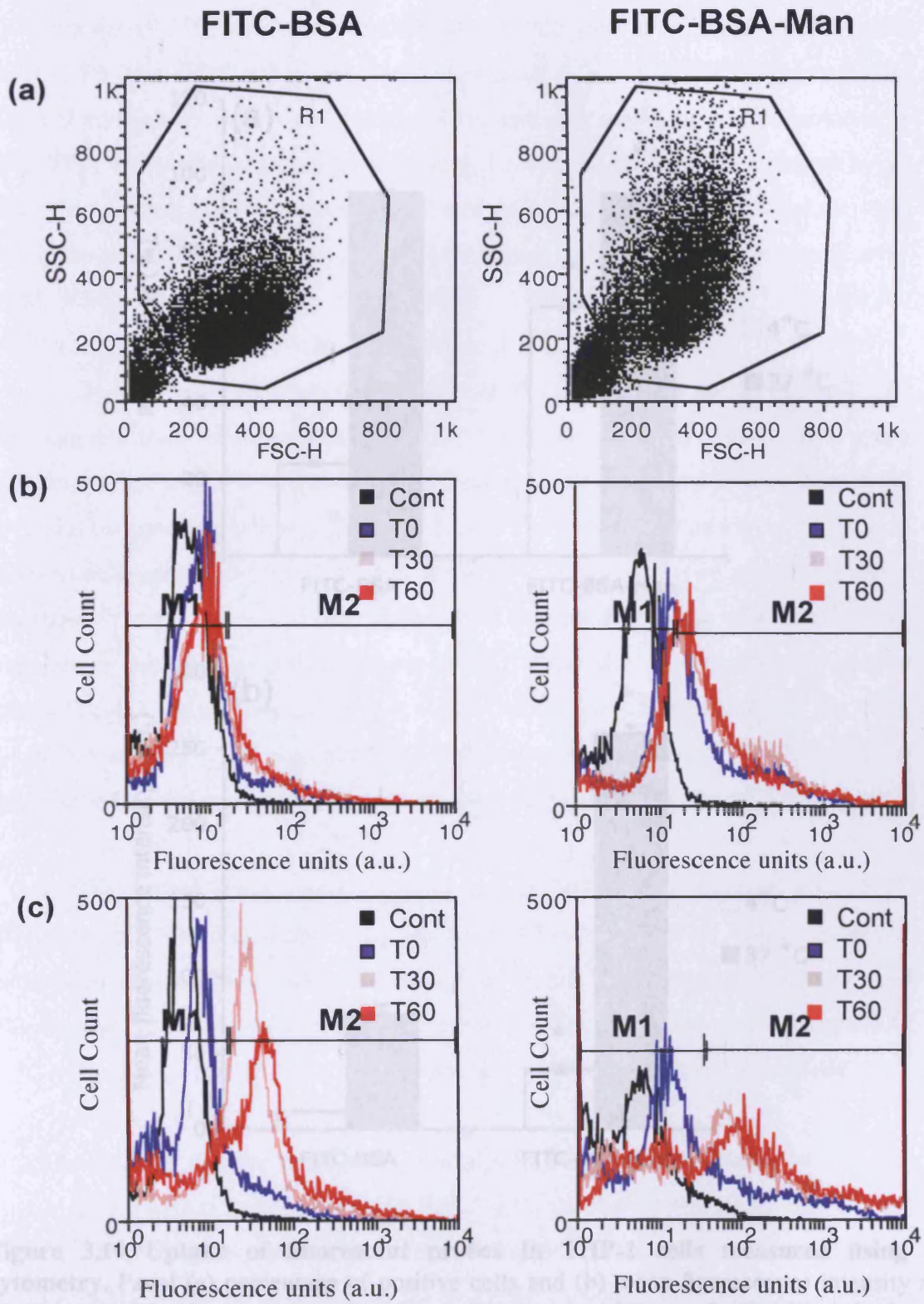

Figure 3.9 Typical raw data obtained from flow cytometry of THP-1 cells with FITC-BSA and FITC-BSA-Man. Panel (a) shows cell scatter and panel (b) the change in fluorescence with time over 60 min at 4 °C and (c) 37 °C.

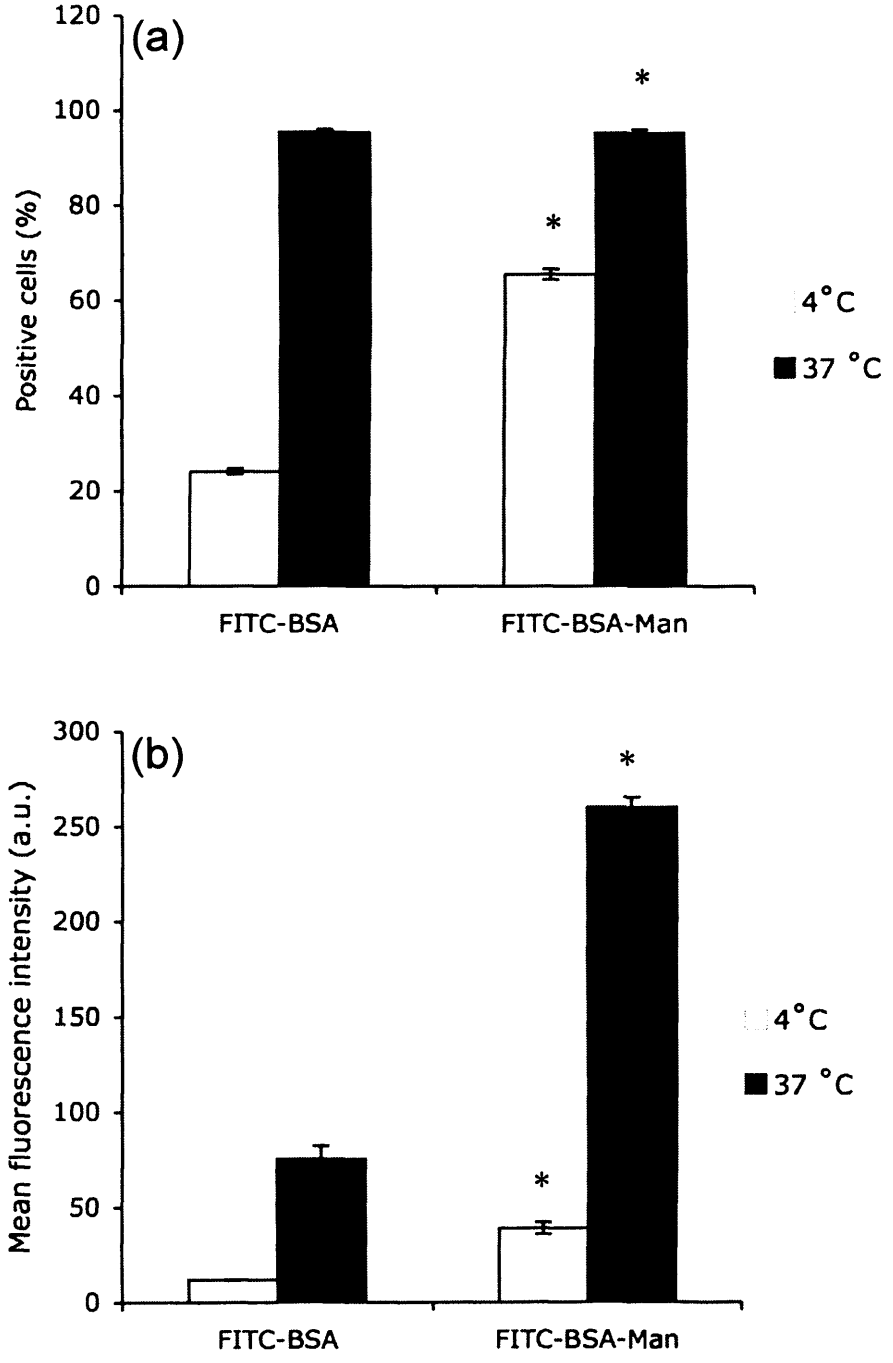

Figure 3.10 Uptake of fluorescent probes in THP-1 cells measured using flow cytometry. Panel (a) percentage of positive cells and (b) mean fluorescence intensity at 37 °C and 4 °C. The data represent the mean ± SD (n = 3 (4 °C), n = 9 (37 °C)) and where the error bars are not visible they fall within the data points. Statistical significance (*) between FITC-BSA and FITC-BSA-Man was determined at $p < 0.05$ for all both time points (students t-test).

both FITC-BSA and FITC-BSA-Man showed a low level of derived cell-associated fluorescence at 4 °C that did not significantly increase over time (Figure 3.11). Again FITC-BSA-Man displayed a very slight increase at 4 °C. FITC-BSA-incubated cells showed a linear increase in cell associated fluorescence with time whilst the increase with FITC-BSA-Man began to level out after 10 min and had reached a plateau by 50 min. Comparison of the patterns of uptake of both albumin probes demonstrates that the mannosylated probe shows significantly higher cell associated fluorescence over FITC-BSA, a 5-fold increase at 37 °C and a 10-fold increase at 4 °C ($p < 0.05$, ANOVA plus Bonferoni *post hoc* test) (Figure 3.12).

Derived cell-associated fluorescence at 37 °C increased rapidly over 60 min for both cell lines when incubated with DQ Ovalbumin. In THP-1 cells, there was a maximum increase of 8-fold over the 4 °C derived cell-associated fluorescence at 60 min and the uptake was linear (Figure 3.13 and Figure 3.14a). The rate of increase in derived cell-associated fluorescence in RAW 264.7 cells increased with time, with a maximum increase of 6-fold over that at 4 °C (Figure 3.14b). At both temperatures the derived cell-associated fluorescence of FITC-BSA-Man was significantly greater than FITC-BSA at all time points ($p < 0.05$, ANOVA with Bonferroni *post hoc* test). It should also be noted that the RAW cells have almost double the derived cell-associated fluorescence at 60 min, with all three probes, compared with THP-1 cells.

The derived cell-associated fluorescence of THP-1 cells incubated with FITC-BSA-Man at 37 °C was significantly decreased when co-incubated with an excess of unlabelled mannan ($p < 0.05$, students t-test) (Figure 3.15). Derived cell-associated fluorescence of cells incubated with mannan alone was equivalent to control cells. At 4 °C little effect was seen but at 37 °C there was a 44 % decrease in fluorescence.

3.3.3 Imaging of binding and uptake of probes by fluorescence microscopy

Fluorescence images of RAW 264.7 cells incubated with BSA-FITC, man-BSA-FITC and DQ-ovalbumin show the distribution of probes after 60 min at 37 °C (Figure 3.16). Each panel compares the standard widefield light microscope image with the fluorescent image of the same cells. Probes have clearly been taken up into numerous small vesicles throughout the cytoplasm whereas the nuclei are not stained. DQ ovalbumin (Panel c) shows the brightest vesicles in the perinuclear region,

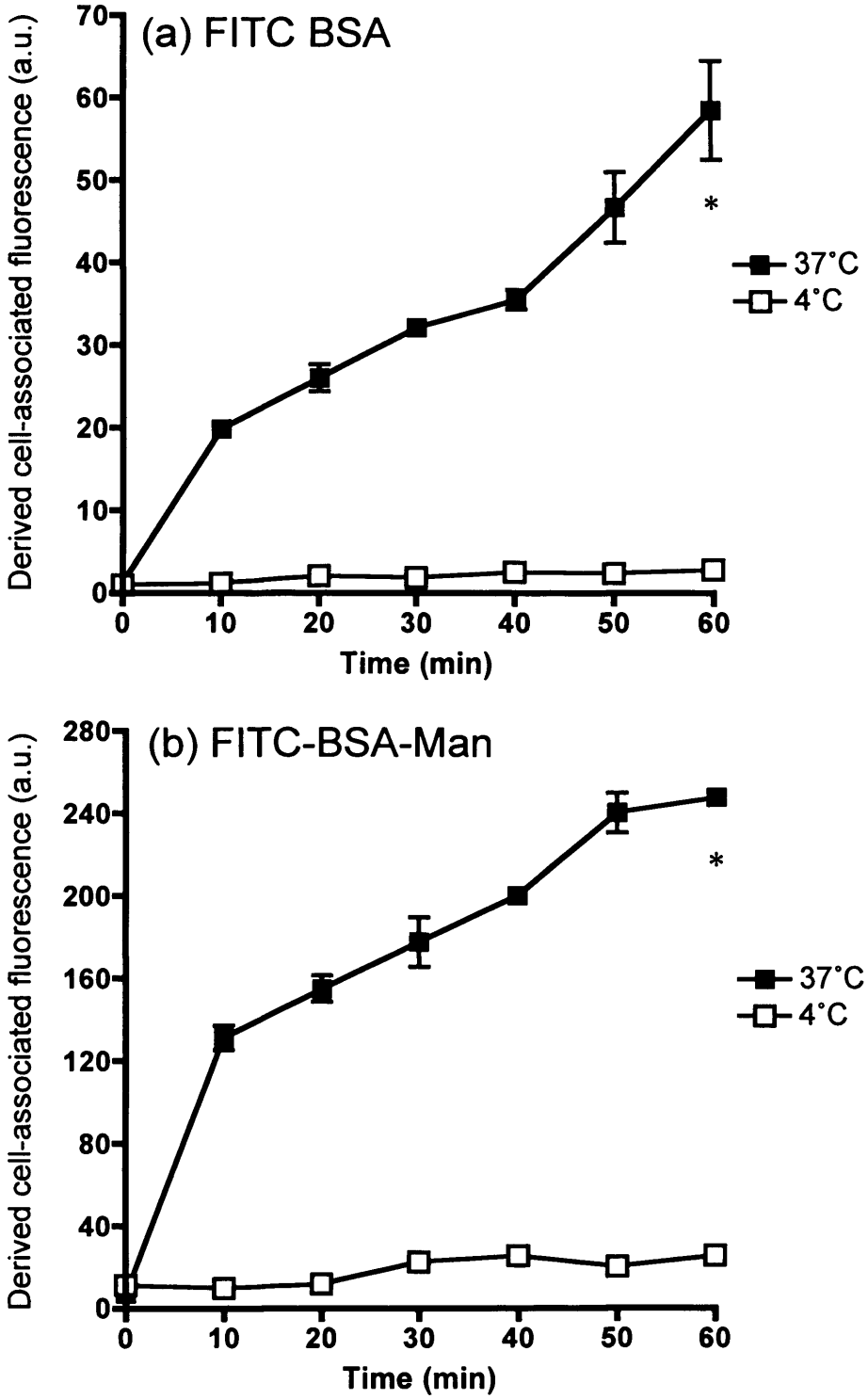

Figure 3.11 Time-dependent uptake of fluorescent probes in THP-1 cells. Panel (a) FITC-BSA and (b) FITC-BSA-Man at 37 °C and 4 °C. The data represent the mean ± SD (n = 3 (4 °C), n = 9 (37 °C)) and where the error bars are not visible they fall within the data points. Statistical significance (*) between 37 and 4 °C was determined at $p < 0.05$ for all data points (ANOVA with Bonferroni *post hoc* test).

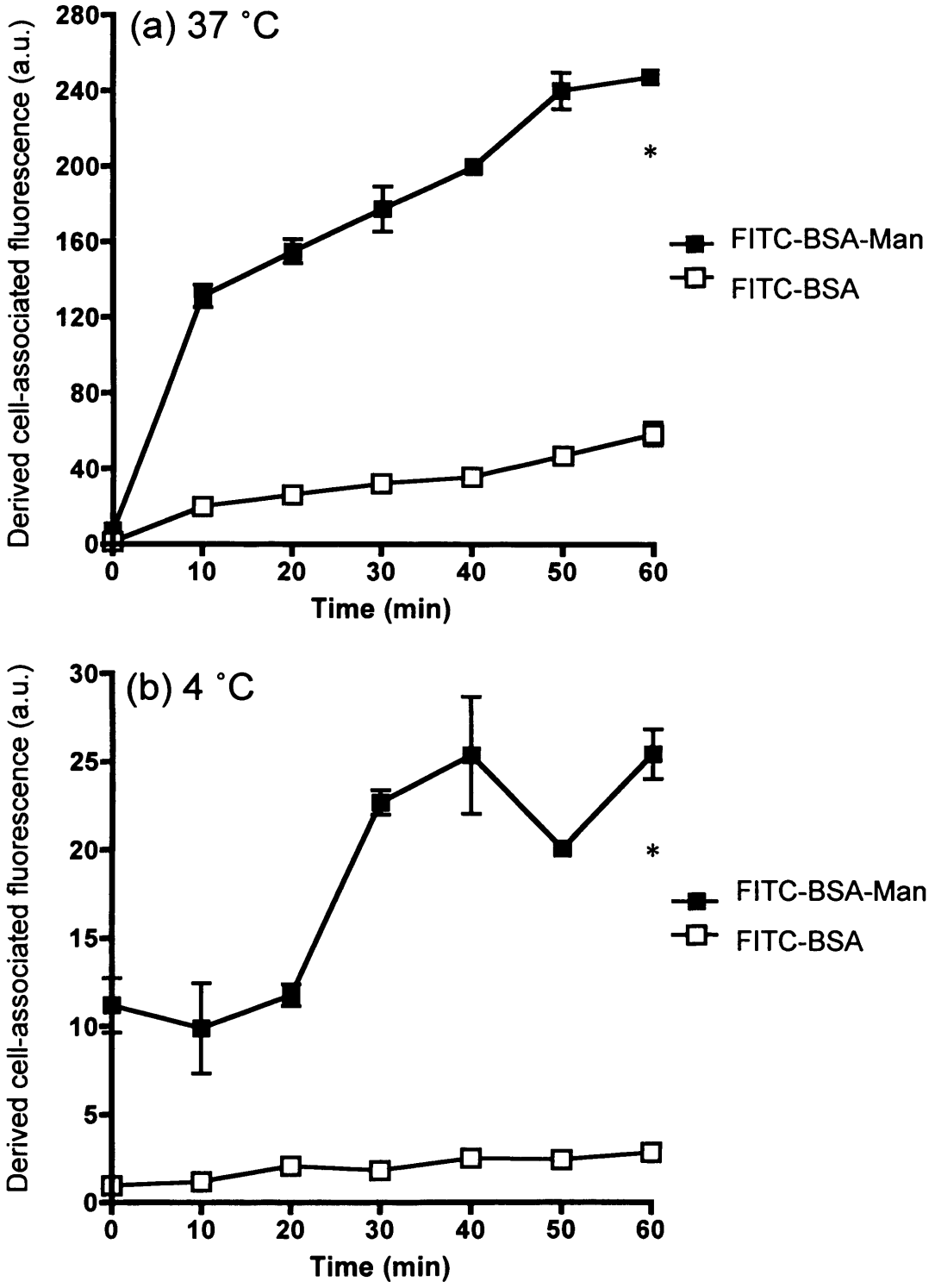

Figure 3.12 Comparison of binding/uptake of FITC-BSA±Man in THP-1 cells. Panel (a) 37 °C and (b) 4 °C. The data represent the mean ± SD (n = 3) and where the error bars are not visible they fall within the data points. Statistical significance (*) between 37 and 4 °C was determined at $p < 0.05$ for all data points (ANOVA with Bonferroni *post hoc* test).

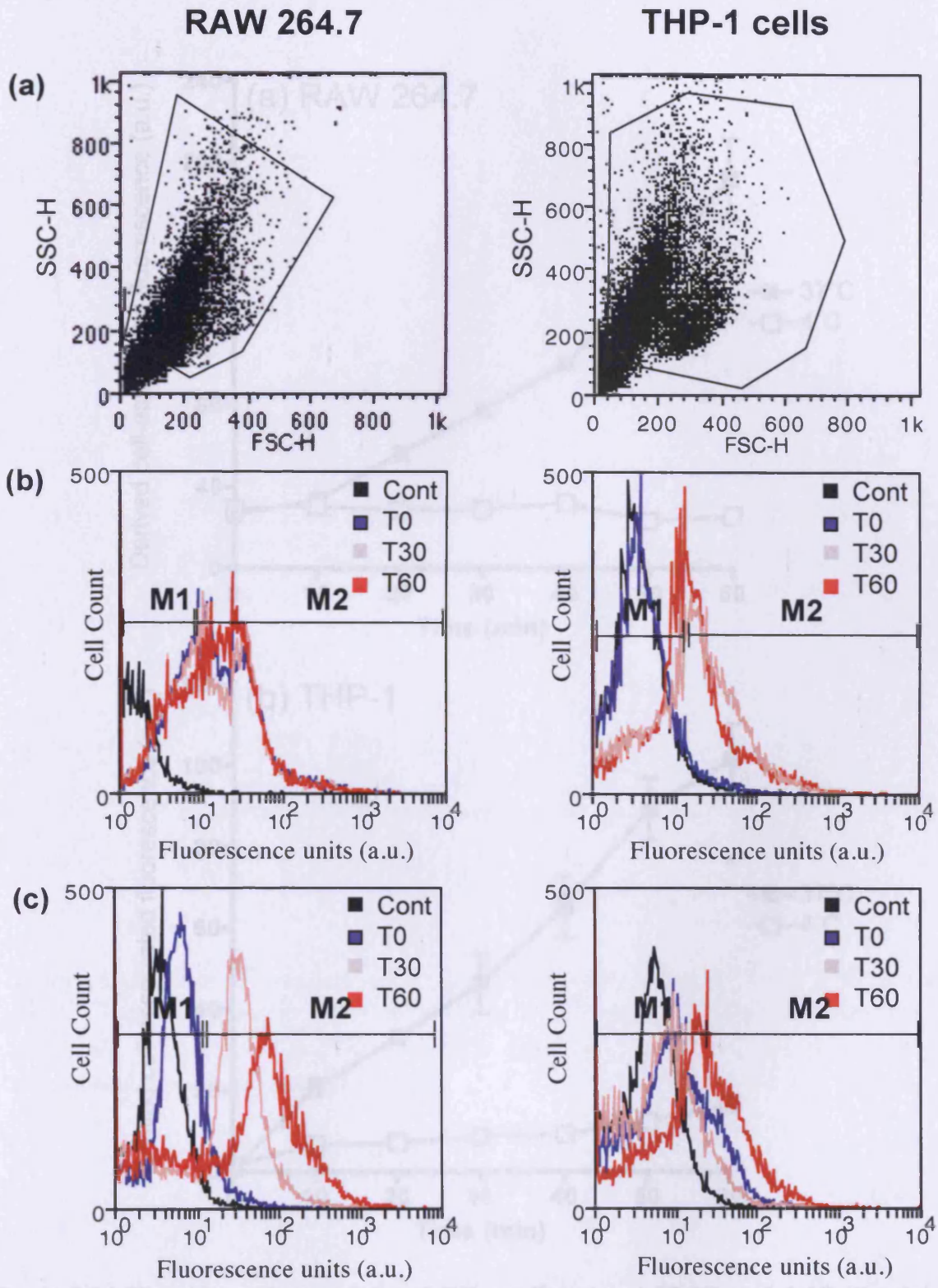

Figure 3.13 Typical raw data obtained from flow cytometry of RAW 264.7 and THP-1 cells with DQ-ovalbumin. Panel (a) shows cell scatter and panel (b) the change in fluorescence with time over 60 min at 4 °C and (c) at 37 °C.

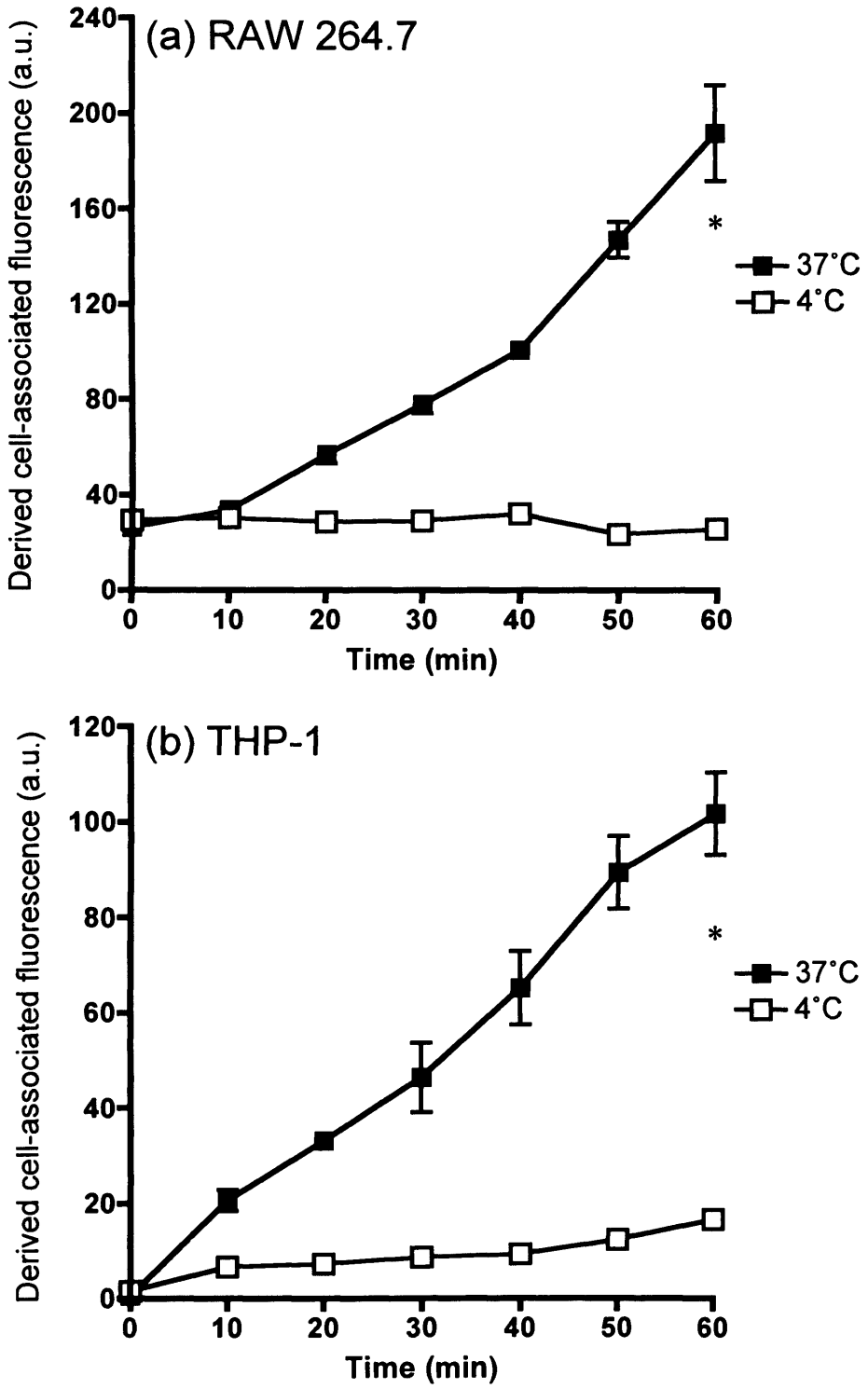

Figure 3.14 Time-dependent uptake of DQ ovalbumin at 37 °C and 4 °C. Panel (a) RAW 264.7 (b) THP-1 cells. The data represent the mean ± SD (n = 3 (4 °C), n = 9 (37 °C)) and where the error bars are not visable they fall within the data points. Statistical significance (*) between 37 and 4 °C was determined at $p < 0.05$ for all data points (ANOVA with Bonferroni *post hoc* test).

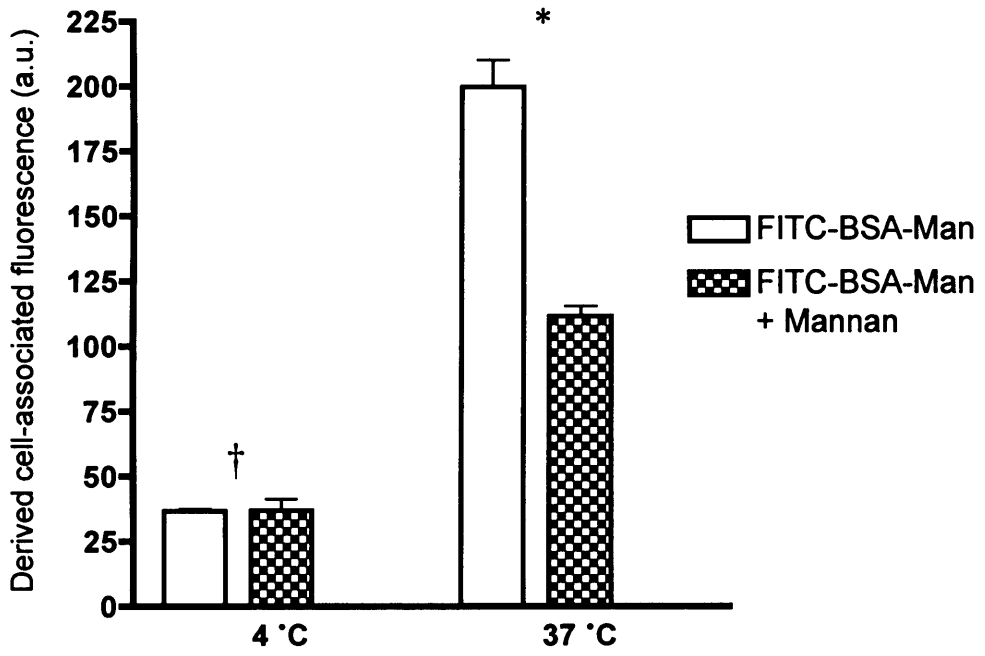

Figure 3.15 Effect of mannan on uptake of FITC-BSA-Man in THP-1 cells at 4 and 37 °C. The data represent the mean ± SD (n = 3). Statistical significance between cell associated fluorescence of FITC-BSA-Man ± mannan at 37 (*) and 4 °C (†) was determined at $p < 0.05$ (students t-test).

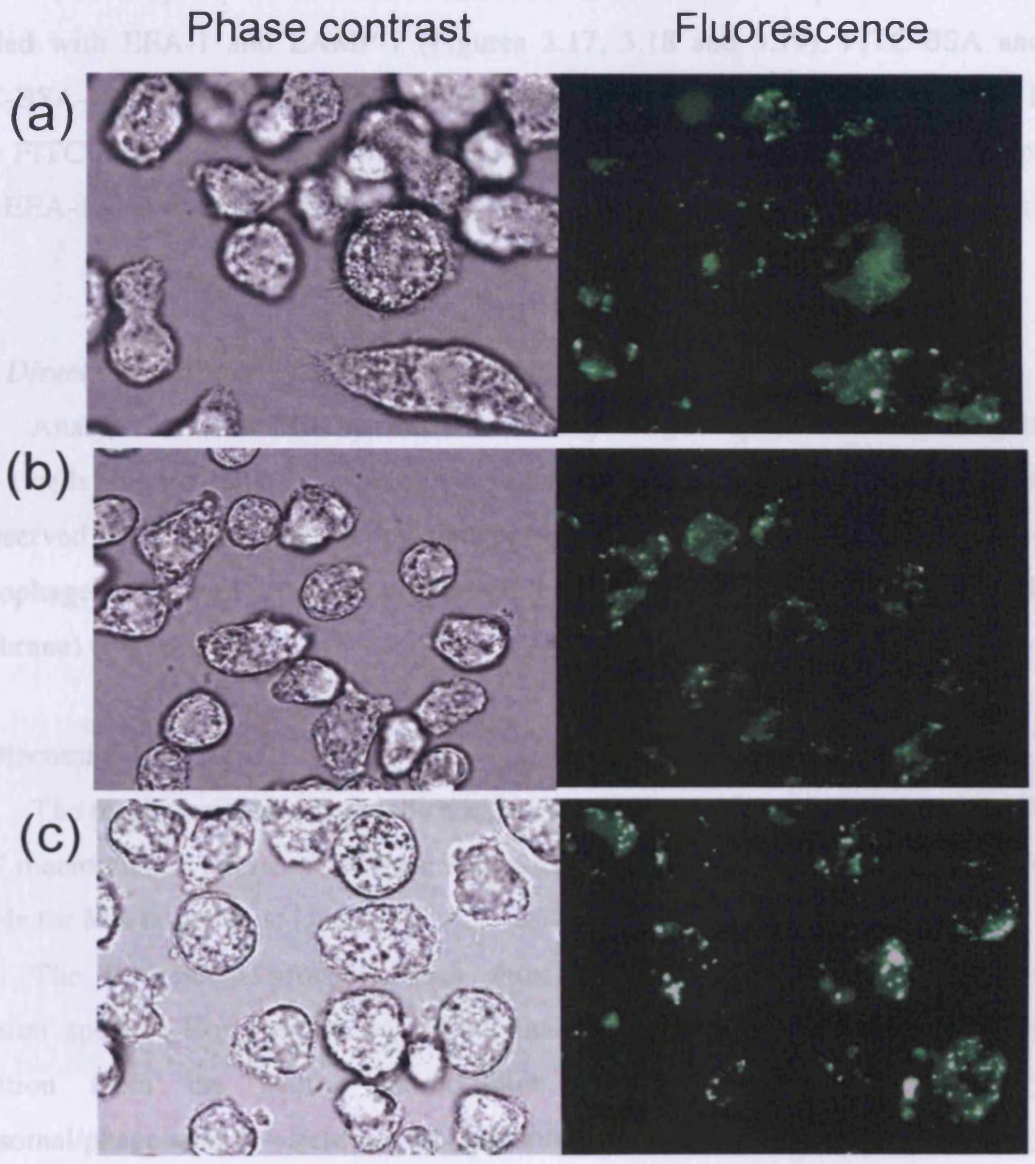

Figure 3.16 Phase contrast and fluorescent microscope images of THP-1 cells incubated for 1 h with fluorescent probes. Panel (a) FITC-BSA (b) FITC-BSA-Man and (c) DQ-Ovalbumin.

whereas the BSA probes are more diffuse (Panels a,b). There is some hazy fluorescence throughout the cell, and vesicles can be more clearly seen in the fixed cells.

To identify the intracellular localisation of the fluorescent probes cells were labelled with EEA-1 and LAMP-1 (Figures 3.17, 3.18 and 3.19). FITC-BSA and FITC-BSA-Man were seen in distinct vesicular structures. After a 1 h pulse and 3 h chase FITC-BSA or FITC-BSA-Man fluorescence co-localised with LAMP-1 but not with EEA-1. No evidence of plasma membrane, nuclear or cytosolic labelling was seen.

3.3.4 Direct visualisation of MR in THP-1 cells

Analysis of total MR by western blotting showed specific MR staining in THP-1 cells (Figure 3.20a). Further direct visualisation of expression and distribution as observed by confocal microscopy showed the MR was distributed throughout the macrophage cell, with a small proportion being located on the periphery (cell membrane) (Figure 3.20b).

3.4 Discussion

The results presented here indicate the two cell lines chosen, THP-1 and RAW 264.7 macrophages, express functional receptors for mannose and are suitable *in vitro* models for MR targeting studies.

The fluorescent probes chosen show reasonably narrow excitation and emission spectra. However, it was found that a reduction in pH, mimicking the transition from the neutral extracellular environment, through the early endosomal/phagosomal vesicle to the lysosomal/phagolysosomal vesicle radically altered the fluorescence characteristics. The FITC fluorescence was highly quenched below pH 7.4. Though commonly used in fluorescent studies of uptake, these results indicate the poor suitability of FITC as an endocytosis marker. A decrease in pH may be due to reduced uptake or simply the acidic environment of the endosomal vesicle. In addition, the fluorescence of FITC exhibited concentration-dependent quenching. However, as BSA is rapidly degraded once taken up into the endosome, it may no longer be quenched (Stahl et al. 1980). Also, though the fluorescence values measured

(a) EEA-1

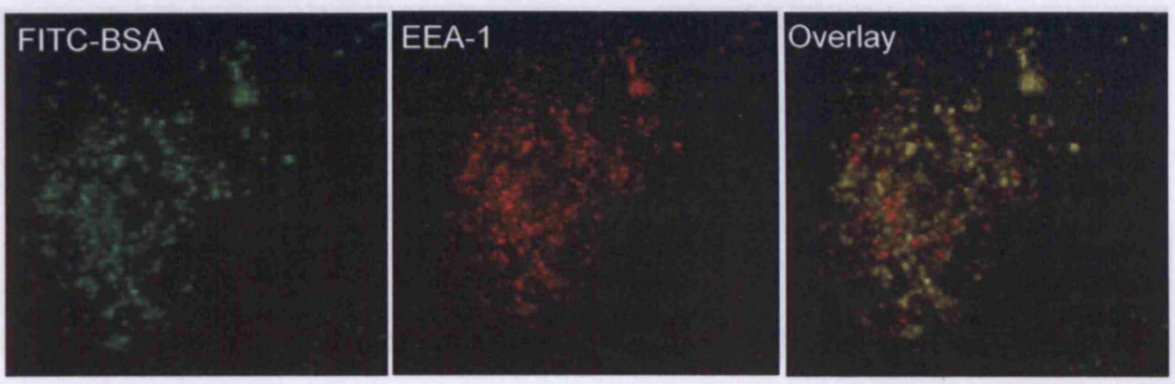

(b) LAMP-1

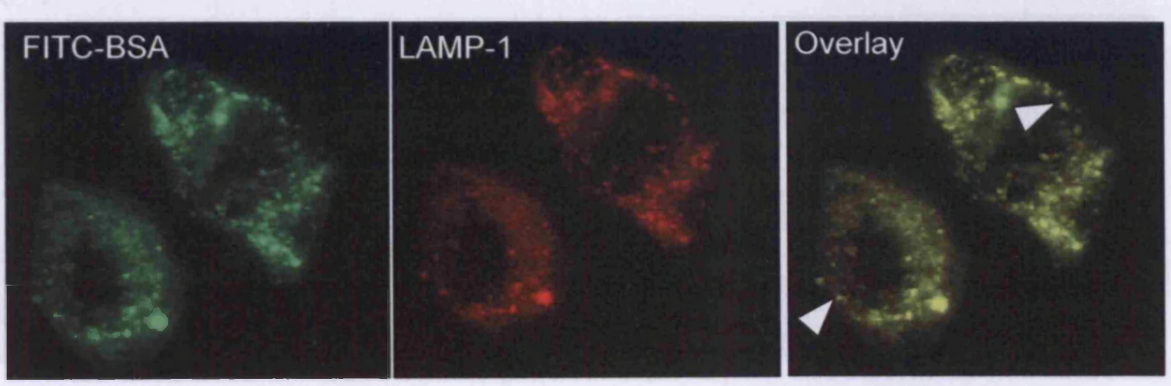

Figure 3.17 Confocal fluorescent microscope images of THP-1 cells incubated for a 1 h pulse and a 3 h chase with FITC-BSA. Panels represent cells co-stained with (a) anti-EEA-1 antibody and (b) anti-LAMP-1 antibody. Examples of co-localisation between compartment marker and BSA-TxR are indicated using white arrows.

(a) EEA-1

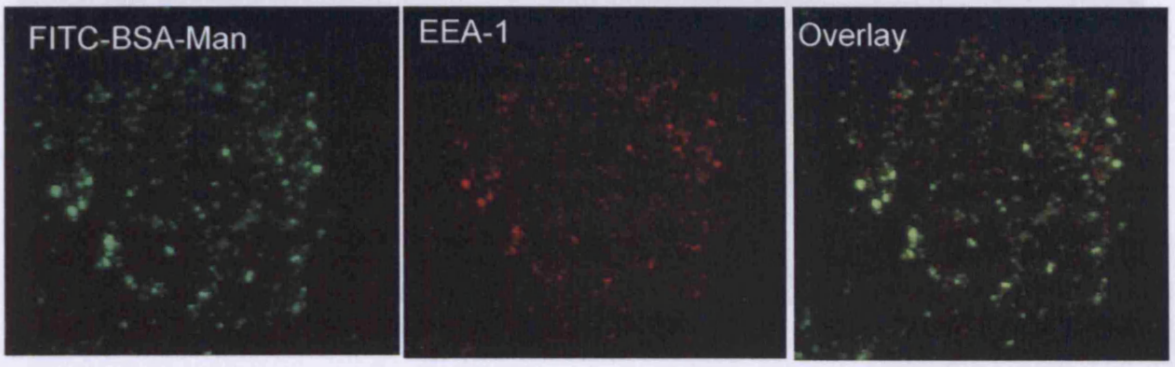

(b) LAMP-1

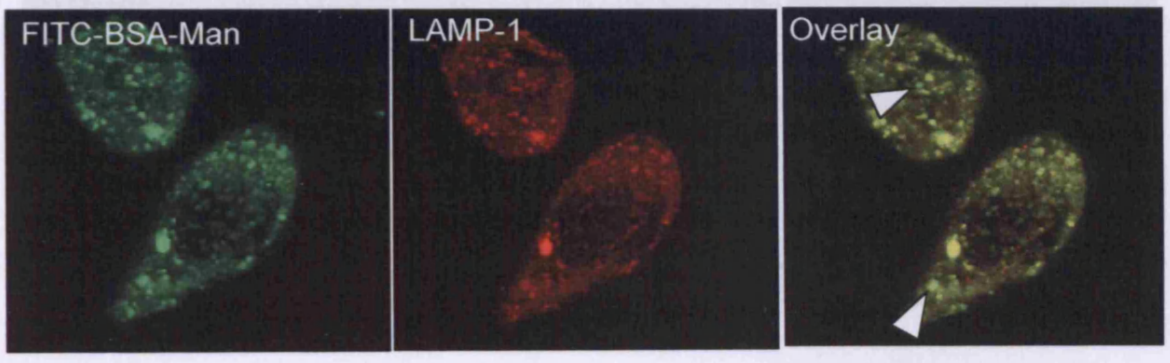

Figure 3.18 Confocal fluorescent microscope images of THP-1 cells incubated for a 1 h pulse and a 3 h chase with FITC-BSA-Man. Panels represent cells co-stained with (a) anti-EEA-1 antibody and (b) anti-LAMP-1 antibody. Examples of co-localisation between compartment marker and BSA-TxR are indicated using white arrows.

(a) EEA-1

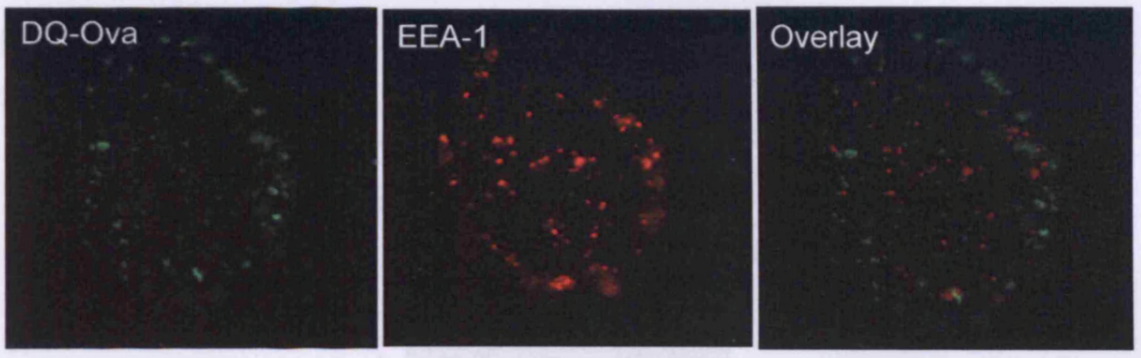

(b) LAMP-1

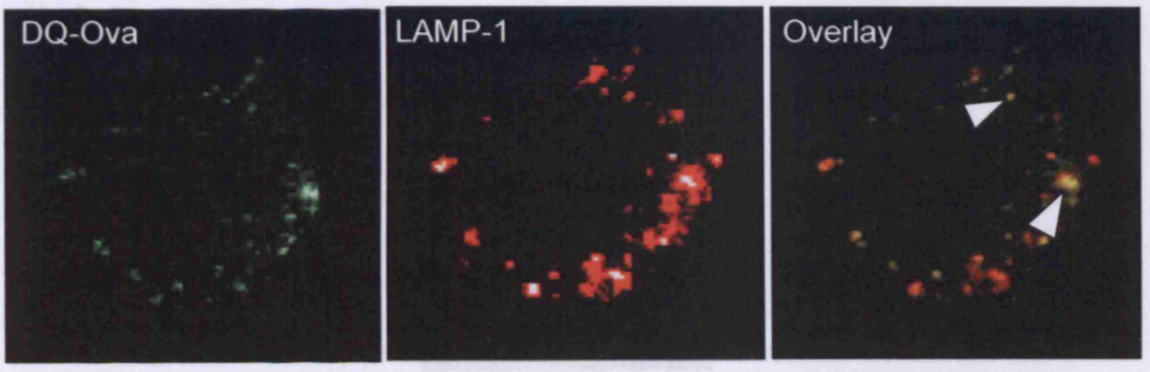

Figure 3.19 Confocal fluorescent microscope images THP-1 cells incubated for a 1 h pulse and a 3 h chase with DQ-ovalbumin. Panels represent cells co-stained with (a) anti-EEA-1 antibody and (b) anti-LAMP-1 antibody. Examples of co-localisation between compartment marker and BSA-TxR are indicated using white arrows.

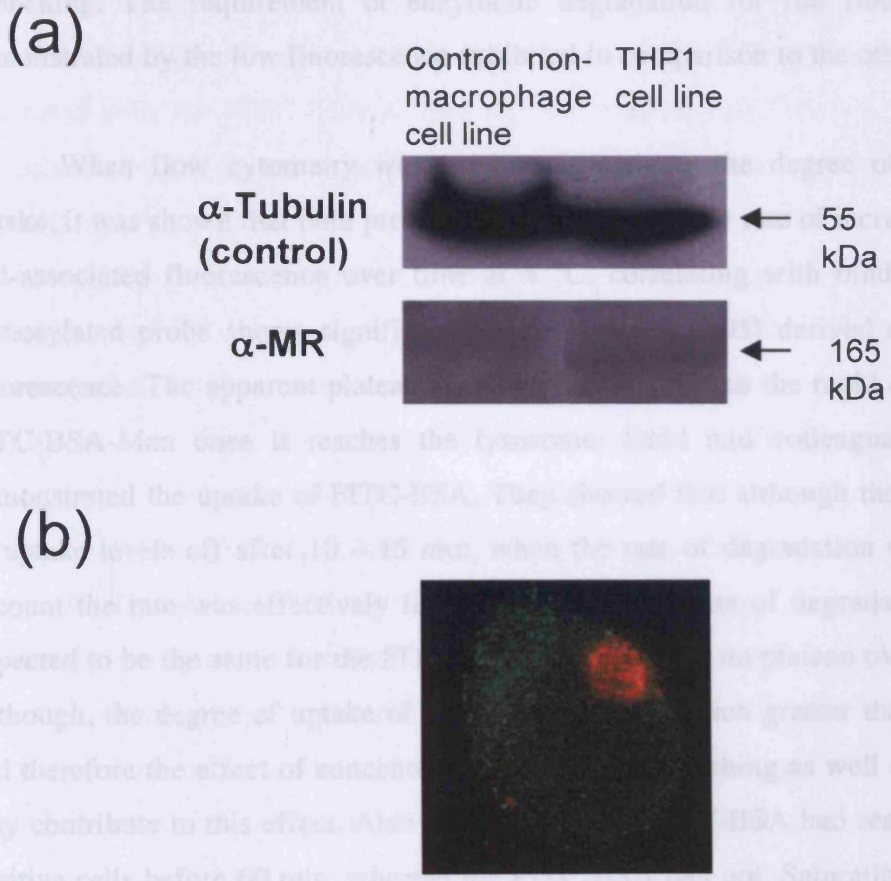

Figure 3.20 Expression of the mannose receptor in THP-1 cells. Panel a) western blotting for mannose receptor and panel b) staining of cells using an anti-mannose receptor antibody (clone 19.2) (trans-golgi anti-TGN46 staining in red).

cannot be taken as absolute values, FITC-BSA and FITC-BSA-Man uptake was still comparable as long as the amount of FITC in the incubation medium was equivalent.

The DQ Ovalbumin probe takes advantage of this rapid degradation in the endocytic pathway. In contrast to FITC, the fluorophore BODIPY exhibited the advantage of a linear increase in fluorescence with concentration, and little pH quenching. The requirement of enzymatic degradation for full fluorescence was demonstrated by the low fluorescence exhibited in comparison to the other probes.

When flow cytometry was used to investigate the degree of binding and uptake, it was shown that both probes exhibited a fairly low rate of increase in derived cell-associated fluorescence over time at 4 °C, correlating with binding only. The manosylated probe shows significantly higher ($p = < 0.05$) derived cell-associated fluorescence. The apparent plateau seen may also be due to the rapid degradation of FITC-BSA-Man once it reaches the lysosome. Stahl and colleagues (1980) first demonstrated the uptake of FITC-BSA. They showed that although the apparent rate of uptake levels off after 10 – 15 min, when the rate of degradation was taken into account the rate was effectively linear. However, the rate of degradation would be expected to be the same for the FITC-BSA, which shows no plateau over the 60 min. Although, the degree of uptake of FITC-BSA-Man is much greater than FITC-BSA, and therefore the effect of concentration-dependent quenching as well as degradation may contribute to this effect. Also the manosylated FITC-BSA had reached ~ 100 % positive cells before 60 min, whereas the FITC-BSA had not. Saturation studies with increasing concentrations of probe would have given more information on the receptor binding specificity, however due to time constraints, it was decided to do these studies using the mannose targeted polymers in the next chapter.

Derived cell-associated fluorescence of THP-1 cells and RAW 264.7 cells with DQ Ovalbumin demonstrated similar binding kinetics at 4 °C to the BSA probes, though a more rapid rate at 37 °C. It is likely to be due to the low fluorescence on binding and initial uptake, and a correlation with the rate of degradation of the probe and release of fluorescence as it reaches the lysosome. It does, however, support the

hypothesis that the probe is taken up by the endocytic pathway and delivered to the lysosome.

Comparison between THP-1 and RAW 264.7 cells shows that, although the RAW cells have almost double the apparent uptake of all probes compared with THP-1 cells, the difference between FITC-BSA and FITC-BSA-Man is greater in the THP-1 cells. These results may indicate differences in MR expression or any number of differences between the cell lines such as differing levels of non-specific uptake or rate of degradation of albumin. The RAW 264.7 cells showed double peaks when incubated with the FITC-BSA ± Man probes, whereas the THP-1 cells were more uniform in uptake. This is most likely to be due to the fact that they are a uniform cell population, whereas the RAW cells are heterogeneous. The adherent and suspension cells are likely to exhibit different characteristics, including possibly MR expression. Although the THP-1 cells could display different characteristics due to the degree of differentiation. There was a longer tail on the THP-1 cell peak, particularly with the Man probe, and there was a spike of fluorescence at the highest point measured, although this could be an artefact of the way the fluorescence is measured. The initial (time zero) derived cell-associated fluorescence is significantly lower in THP-1 cells than in RAW 264.7 cells. Time zero refers to the first time point to be measured after addition of probe and immediate removal and washing, and therefore is not strictly zero but the earliest time point it was possible to measure. Using the RAW 264.7 cells this was longer as it required scraping the cells before spinning down and washing in fresh PBS rather than removal of the solution immediately as with the THP-1 cells. This may explain the higher fluorescence values. These factors make the THP-1 cells both easier and more accurate to use for the flow cytometry experiments. For this reason THP-1 cells were used as the macrophage model for subsequent studies with the polymer-mannose conjugates.

The reduction in uptake caused by the competitive inhibitor mannan supports the conclusion that the uptake was mannose-specific. The data should indicate the non-specific and mannose-specific uptake as all the mannose binding sites should be blocked. This inhibition should be more pronounced at 4 °C, as at 37 °C there is constant replenishment by intracellular pools of MR (Stahl et al., 1980). The lack of inhibition in binding is contrary to most published studies (Linehan et al., 2000; Stahl & Gordon, 1982; Stahl et al., 1980), though the 4 °C binding is affected to a small

degree. Also, most studies have found non-specific uptake to be about 20 % rather than 50 %. Higher concentrations mannan may give more accurate results, as all the MR's may not be saturated. Still, these results are a good indication that mannose targeting should be able to increase uptake of conjugates significantly.

Corroboration of the uptake by endocytosis and visualisation of the distribution within the cell, fluorescent microscopy was used. The probes are clearly located in vesicles located throughout the cell. The brighter vesicles in the perinuclear region of the DQ ovalbumin-containing vesicles correlate with the increased fluorescence in the lysosomal compartments. However, presumably due to pH-dependent quenching along the endosomal pathway, FITC-BSA is brighter along the periphery of the cell. This did not occur when a chase time was included (fixed cells) and vesicular labelling was clear. FITC-BSA and FITC-BSA-Man was located primarily in the late endosome/lysosome (labelled with LAMP-1) and not endosomes (EEA-1). There is likely to be some bleed-through of the green channel into the red, which may account for the apparent co-localisation of some green EEA-1 with the probes. However the large amount of red labelled vesicles could not be bleed-through and the limited amount of non-colocalised red in the LAMP-1 labelled cells.

Finally, the specific anti-MR antibody has shown MR expression on the THP-1 cells. The previous data indirectly support the hypothesis of MR expression, showing receptor-specific uptake of mannosylated conjugates, but not the involvement of the MR itself. Direct visualisation of the MR in these cells showed a diffuse distribution, which correlates with previous studies showing that a large proportion of MR is located intracellularly, rather than on the cell surface (Diaz-Silvestre et al., 2005; Stahl et al., 1980). However, this can be rapidly deployed to the cell surface when needed, resulting in virtually continual uptake of mannosylated ligands. The non-reliance on *de novo* synthesis is of benefit to the design of mannosylated conjugates for uptake into macrophages. However, the MR antibody used only poorly stained the THP-1 cells, and did not stain the RAW 264.7 cells. Further studies with positive and negative controls would be necessary to confirm MR expression.

There is evidence that when infected with *Leishmania* parasites the surface mannose receptor expression on macrophages is reduced (Basu et al., 1991). However, other studies have found no difference in MR-mediated uptake between infected and non-infected macrophages (Rabinovitch et al., 1985; Shepherd et al., 1990). It would be interesting to determine whether in both our macrophage models and in the in vivo situation the mannose receptor show changes in receptor expression after infection. However, unfortunately these experiments were not undertaken.

3.5 Conclusions

From the data presented we can conclude that the THP-1 and RAW 264.7 cell lines are suitable models for use in these mannose-targeting studies. Use of probes has shown that binding and uptake are both temperature- and time-dependent. Mannose conjugation significantly increased both binding and uptake by both cell types. The results suggest that both RAW and THP-1 cells express MR, and in sufficient numbers to study receptor specific targeting of polymer conjugates. Also, MR ligands are trafficked to the endosome/lysosome as indicated by the DQ ovalbumin degradation and fluorescence, and the microscopy images. Specificity was further confirmed by competitive inhibition by mannan. It was decided for reasons of time to concentrate on one of the models for the bulk of the further studies. The THP-1 cell line was chosen for further studies as it has shown greater reproducibility, and is more representative of the intended target, the human macrophage.

Chapter 4

Synthesis and Characterisation of OG-labelled HPMA Copolymer-Mannose Conjugates

4.1 Introduction

The studies on the uptake of model fluorescent probes in Chapter 3 confirmed that MR targeting could be achieved in both THP-1 and RAW 264.7 cells. The aim of these studies was to synthesise mannose-targeted polymer conjugates, and to investigate the mannose loading needed for MR targeting of a polymeric carrier. In these studies HPMA copolymer with a GFLG linker ± mannose, with OG as a fluorescent marker, and THP-1 cells as a macrophage model, were used. As discussed in section 1.5.1, HPMA copolymers have been widely developed as drug carriers and for gene delivery (reviewed in Duncan, 2005). The design behind these conjugates will now be discussed in more detail.

4.1.1 History and development of the HPMA polymer and HPMA-drug conjugates

HPMA polymers were first investigated as biomedical polymers in the 70's (reviewed in Duncan, 2005; Kopecek, 1977). HPMA homopolymer was initially developed as a plasma expander. However, the subsequent studies during the 70's and 80's systematically developed HPMA copolymers as drug carriers. Kopecek and Bazilova (1973) developed methods for free radical polymerisation and copolymerisation of the HPMA monomer with different co-monomers. Subsequently, Rejmanová et al. (1977) defined the polymerisation methods for incorporation of methacrylic acid (MA) monomer bearing peptides terminating in 4-nitrophenol ester (ONp). The polymer intermediates prepared in this way can be easily reacted with amine groups by a process called aminolysis. This enables drugs or targeting residues that have an aliphatic amino group to be conjugated via an amide bond.

HPMA copolymer conjugates were originally designed for lysosomotropic drug delivery (reviewed in Duncan, 2005). The importance of enzymatically cleavable side chains for intracellular drug release was apparent, and several studies led to the design of appropriate peptide sequences, including GFLG, which is cleaved by lysosomal enzymes particularly cathepsin B (Duncan et al., 1983; Duncan et al., 1984; Duncan et al., 1980; Duncan et al., 1981; Rejmanova et al., 1985). An optimum HPMA copolymer structure for drug delivery, including molecular weight and optimum drug loading to retain solubility, was thus established. The synthetic

methods, the biodistribution of the HPMA copolymer drug conjugates (with and without targeting ligands) and the use of such conjugates are reviewed in the next sections.

4.1.2 Synthetic methods used to prepare HPMA copolymer conjugates

The synthesis of HPMA copolymer-drug conjugates containing peptide side chains is now well established. It is commonly achieved by free radical copolymerisation of HPMA monomer by either of two methods (shown schematically in Figure 4.1):

i) Copolymerisation of HPMA monomer and MA-peptide (e.g. GFLG) terminating in reactive ONp. This polymeric intermediate can then be easily modified with drug or targeting ligand, providing they have an aliphatic amino group (Figure 4.1a). This is termed the *polymer analogous reaction.*

ii) Copolymerisation of HPMA monomers and MA-peptide monomers terminating in the drug/ligand (Figure 4.1b).

Most HPMA copolymer conjugates have been prepared by the polymer analogous reaction and this technique was used to prepare the conjugates described here. This allows libraries to be made using a common intermediate of specific molecular weight. This ensured reproducibility of Mw and polydispersity and gives better control of drug loading. Copolymerisation of drug bearing monomers that can have different reactivities can lead to conjugates of widely different molecular weight and/or polydispersity. One potential disadvantage of the polymer analogous reaction is the possibility of free drug in the final conjugate. Also, there will inevitably be a random distribution of drug and/or ligand along the polymer chain. Although copolymerisation using method (ii) would, also lead to a random distribution of the drug-carrying monomer; and that carrying a targeting ligand.

Using an HPMA copolymer intermediate containing many reactive ONp groups it is possible to bind more than one drug or ligand at relatively high loadings. However, the highest practical loading is governed by the drug/conjugate solubility.

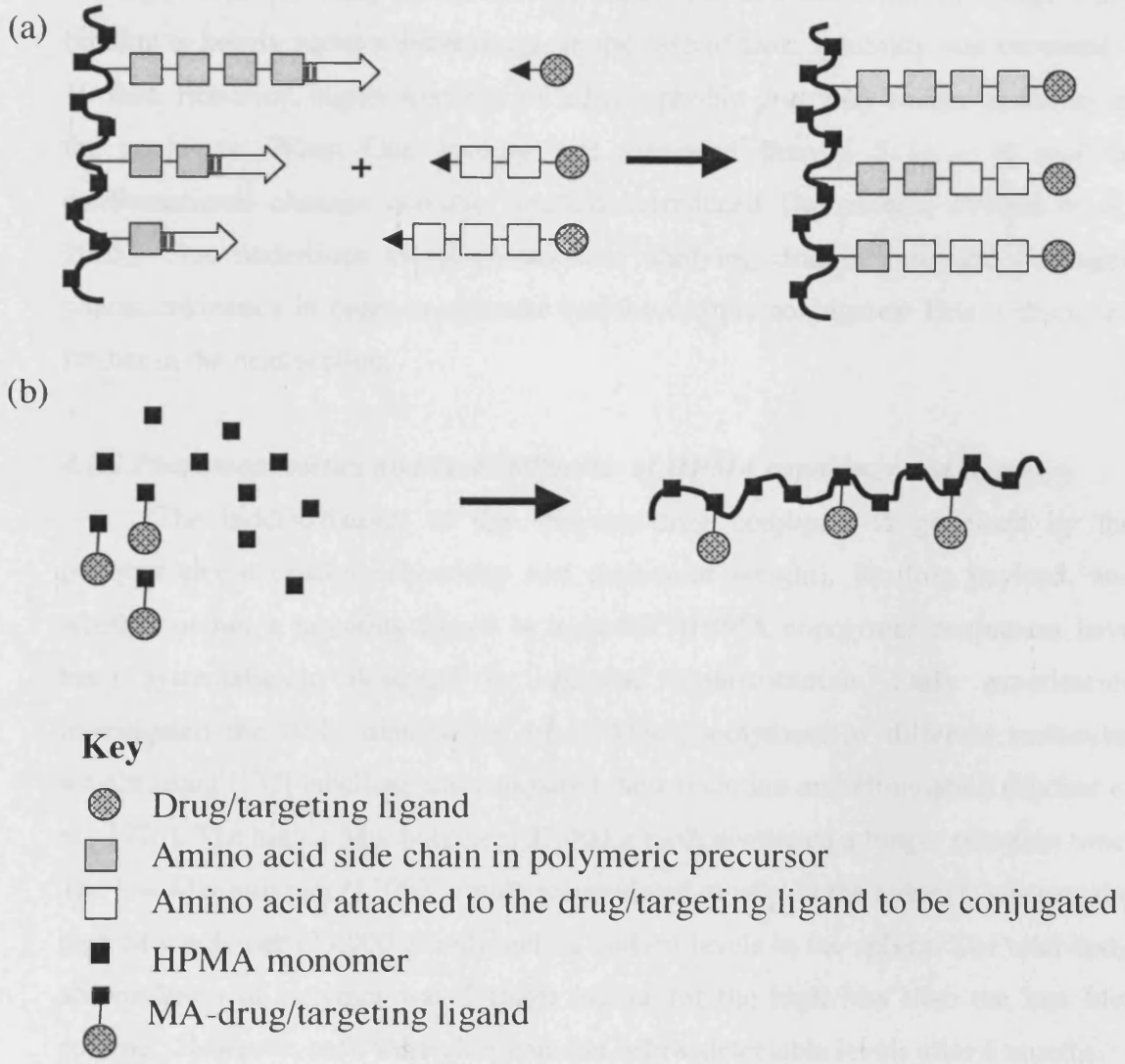

Figure 4.1 Scheme showing synthetic methods for producing HPMA copolymer-drug conjugates. Panel (a) polymer-analogous reaction and panel (b) polymerisation of modified monomers. Taken from Duncan (2005).

For example, the anti-cancer conjugate HPMA copolymer-GFLG-Dox (PK1) had a Dox loading of around 8 wt %, and HPMA copolymer-GFLG-Dox-Gal (PK2) a Dox loading of 7.5 wt %. The latter also had a Gal loading of 4 mol %. The benefits of HPMA copolymers as carriers for drug delivery are discussed in section 1.5.1, but the high water solubility of the HPMA copolymer is a particular advantage when binding to poorly water-soluble drugs. In the case of Dox, solubility was increased > 10 fold. However, higher loadings of a hydrophobic drug may reduce solubility of the conjugate. When Dox loading was increased from ~ 5 to ~ 10 mol %, conformational changes actually resulted in reduced Dox release (Vicent et al., 2005). This underlines the importance of studying drug release and conjugate pharmacokinetics in order to optimise lysosomotropic conjugates. This is discussed further in the next section.

4.1.3 Pharmacokinetics and biodistribution of HPMA copolymer conjugates

The biodistribution of any polymer-drug conjugate is governed by the polymer characteristics (chemistry and molecular weight), its drug payload, and whether or not a targeting ligand is included. HPMA copolymer conjugates have been systematically designed to optimise biodistribution. Early experiments investigated the body distribution of HPMA copolymers of different molecular weight using [^{14}C] labelling and compared their retention and elimination (Sprincl et al., 1976). The higher Mw polymer (33,000 g/mol) displayed a longer retention time. The low Mw polymer (1, 000 g/mol) accumulated mostly in the kidneys, whereas the high Mw polymer (33,000 g/mol) had its highest levels in the spleen. The total body accumulation of polymer was 5 times higher for the high Mw than the low Mw polymer. However, both were eliminated to below detectable levels after 6 months.

Using ^{125}I-labelled HPMA copolymer fractions of Mw 12,000 – 778,000 g/mol, Seymour et al. (1987) further defined the effect of polymer Mw on biodistribution and tumour targeting. The distribution of polymers showed size-dependent accumulation, and higher Mw polymers were taken up by the RES. Also, the largest Mw polymer was retained at the site of administration. The smallest was eliminated rapidly from the body. This study showed that the optimisation of Mw could increase plasma circulation times and allow tissue and organ penetration.

Rapid renal elimination of HPMA copolymer conjugates without a specific targeting residue occurs below a Mw threshold of 45,000 g/mol (Seymour et al., 1987). The pharmacokinetic studies undertaken in phase I clinical trials of PK1 confirmed preclinical experiments and showed that > 50 % of the conjugate was excreted within 24 h, with a blood clearance of $t_{1/2}\alpha$ of 1-2 h, and a $t_{1/2}\beta$ of 93 h (Vasey et al., 1999). Drug access to areas such as the bone marrow and heart was limited by polymer conjugation, therefore reducing the non-specific Dox toxicity. The maximum tolerated dose was 320 mg/m^2 Dox-equivalent; five times higher than that of free Dox. Most anti-cancer polymer-drug conjugates tested clinically so far have relied on passive targeting. The altered pharmacokinetics of polymer conjugates designed for cell-specific targeting will be discussed in the next section.

4.1.4 Targeting by HPMA copolymer conjugates

The studies described here build on previous work that has tried to establish targeted delivery of HPMA copolymer conjugates. As discussed in section 1.5.3, a large number of targeted HPMA copolymer conjugates have been described. Typically they contain antibodies, proteins, peptides and sugar residues to promote receptor-specific targeting (reviewed in Duncan, 2005) (see Table 4.1), however, the only targeted polymer conjugate to enter clinical trials to date is HPMA copolymer-GFLG-Dox bearing galactosamine (PK2).

PK2 was designed to target primary liver cancer as the ligand galactose (bound by the amino sugar) binds to the ASGPR found on both normal hepatocytes and hepatocellular carcinoma cells. This conjugate contained ~ 7.5 wt % Dox and ~ 4 mol % galactose. In Phase 1 clinical trials < 5 % of the conjugate dose was excreted by 24 h, and achieved a 12-50 fold higher hepatoma-associated drug than equivalent free Dox (Seymour et al., 2002). PK2 had a maximum tolerated dose of 160 mg/m^2 Dox-equivalent. Although still approximately 3 fold higher than seen for free Dox, it was approximately half the value found for PK1, presumably due to the higher liver concentration. In PK2 a cleavable GFLG linker was used to bind galactose as well as Dox to the polymer backbone to prevent continuous uptake (recycling) of polymer, as this would lead to accumulation of the polymer backbone rather than its hepatobiliary elimination.

Table 4.1 Anticancer HPMA copolymer-drug conjugates with targeting residues in the literature.

Drug	Linker	Targeting Residue	Indication	References
Doxorubicin	GFLG	Tat	Cancer	Nori et al., 2003a ;2003b,
	GFLG	Hsp47/CBP2 binding peptide	Cancer	Tijerina et al., 2001; 2003
	Hydrazone	ATG antibody	Cancer	Nan et al., 2005
	GFLG	Transferrin/CD71 antibody	Cancer	Ulbrich et al., 2004
	GFLG	Hyaluronan	Cancer	Kovar et al., 2002
	GFLG	Melanocyte stimulating hormone	Cancer	Luo et al., 2002
				O'Hare et al., 1993
Dox/Mce6	GFLG	OV-TL16 antibody	Ovarian cancer	Shiah et al., 2001
Adriamycin	GFLG	OV-TL16 antibody	Ovarian cancer	Omelyanenko et al., 1998
Daunomycin/ puromycin	GFLG	Fucose	Cancer	Duncan et al., 1987, 1988
Radiotherapy β-emitter	Chelators GG-DPK for ^{99m}Tc CHX-A"-DPTA for ^{90}Y	$\alpha_v\beta_3$ integrin-targeting peptide	Cancer (angiogenesis)	Mitra et al., 2006

CHX-A"-DPTA Cyclohexyl derivative of Diethylenetriamine Pentaacetic acid; DPK = N-epsilon-bis(2-pyridylmethyl)lysine

During the systematic design of PK2, HPMA copolymers bearing D-galactose, D-glucose and D-mannose, attached to the polymer via a GFLG linker were prepared. All these sugars were bound using the amino derivatives (e.g. galactosamine) to allow conjugation by aminolysis. To study their pharmacokinetics (and to allow gamma-camera imaging) copolymers were prepared additionally containing MA-Gly-Tyr to allow radio-iodination (Duncan et al., 1983). Both the galactose-targeted and the mannose-targeted conjugates were found to be predominantly in the liver after intravenous administration. The galactose-targeted conjugates were found predominantly in hepatocytes, whereas the mannose-targeted HPMA copolymers were found largely localised to the Kupffer cells (RES macrophages).

Subsequent studies used a library of conjugates bearing 1-11 mol % galactose to investigate the minimum galactose loading necessary for increased hepatocyte targeting. Increased galactose content resulted in increased uptake, but a loading of only 4 mol % gave significantly increased targeting to liver cells (Duncan et al., 1986). When using receptor-mediated approaches for drug targeting it is also important to define when receptor saturation occurs. In preclinical *in vivo* studies with PK2 it was found that liver targeting was dose-dependent and saturation occurred at > 0.68 mg/ml (Seymour et al., 1991). At higher doses the conjugates will simply distribute randomly around the body. Therefore in the phase 1 clinical trials, patient gamma-camera imaging was used to guide the dosing regime, moving from bolus injection to infusion at higher doses. There were no signs of saturation or inhibition of hepatic targeting after intravenous administration with increasing drug doses (Seymour et al., 2002).

The various targeting residues that have been incorporated into HPMA copolymer-drug conjugates have mostly been directed at cancer (Table 4.1), however, ligands targeting other diseases, including leishmaniasis, have been proposed (Table 4.2). Ghandahari's group (Nan et al., 2004; Nan et al., 2001) synthesised a library of HPMA copolymer-8-aminoquinoline conjugates with a mannose loading of 2, 5, 10, 15 and 20 mol %. Increased uptake of the conjugates into RAW 264 murine macrophages *in vitro* was evident at 5 mol % mannose. Further successive increases in mannose content above 5 mol % did not, however,

Table 4.2 HPMA copolymer-drug conjugates with targeting residues in the literature with non-cancer applications.

Drug	Linker	Targeting Residue	Indication	References
Dexamethasone	Hydrazone	D-aspartic acid octapeptide	Rheumatoid Arthritis	Wang et al., 2006
8-aminoquinoline	GFLG	Mannose	Leishmaniasis	Nan et al. 2004
Cyclosporin	GFLG	α-CD3 antibody	Immunosuppression	Šťastný et al., 1997

significantly increase uptake. Here, it was considered important to investigate the effect of the mannose content of HPMA copolymer-8-aminoquinoline conjugates on targeting to THP-1 cells as this had not been reported before in this cell type.

4.1.5 Synthesis and Characterisation of the HPMA copolymer ± Man Conjugates

Here, the same systematic approach used to develop PK2 was used to optimise the mannose loading of the proposed HPMA copolymer conjugates. An HPMA copolymer precursor of Mw 30,000 g/mol containing ~ 10 mol % GFLG side chains were used for this study (as for PK2). Again it was decided to use cleavable linkers for both drug and mannose binding to prevent accumulation of HPMA copolymer-Man in the macrophage.

In order to determine the minimum mannose content necessary for MR targeting in THP-1 cells, a library of HPMA copolymer conjugates was prepared containing a range of loadings of D-mannosamine (2, 4, 6 and 8 mol %), and, in addition, OG-cadaverine as a fluorescent marker (1 mol %) to monitor cell uptake. OG was chosen as it has similar fluorescent qualities to FITC but is less susceptible to pH quenching (pK_a = 4.7 Invitrogen). Use of mannosamine and OG-cadaverine allows direct aminolysis of the polymeric precursor to prepare the conjugates.

Chemical Characterisation of the Conjugates

The conjugates were first characterised in terms of total OG and free OG content. As they were used to monitor endocytic uptake, it was also important to determine the pH and concentration dependent fluorescence output.

Quantification of mannose content proved more difficult. Sugar quantification is complicated as it first involves hydrolysis of the sugar from the polymer backbone using harsh conditions, and then chemical modification of the sugar to allow indirect measurement. Previous studies with PK2 used hydrolysis conditions of 4M HCl at 100 °C for 4 h to release the galactosamine sugar. The sugar content in the hydrolysate was then quantified using an amino acid analyzer (Cheng & Boat, 1978; Duncan et al., 1986). This method, however, proved difficult due to degradation of the sugar before measurement.

Elson and Morgan originally developed a method to determine free glucosamine by acetylation, transformation into a coloured solution by Erlich reagent, and measurement by UV (Elson & Morgan, 1933). Configliacchi et al. (1996) used this method to determine the total galactosamine content in PK2. Following its hydrolysis from the polymer using HCl 6N at 60 °C for 5 h, transformation of the sugar using a modified Elson Morgan method, it was measured by HPLC.

Here, the mannose content of the conjugates was determined using the Configliacchi method but the derivitised sugar was measured by UV, as this was quicker than HPLC and prevented degradation of the sugar. This method was developed by Salvatore Nicoletti (University of Dundee).

Biological Characterisation of the Conjugates

Flow cytometry was used here to investigate the effect of mannose loading on the binding and uptake of the conjugate library using THP-1 cells as a macrophage model. Derived cell association at 37 °C and 4 °C was used to distinguish binding and uptake, and to define the minimum mannose content necessary to promote MR targeting. The concentration dependence of uptake of the HPMA copolymer-OG-Man conjugates was also investigated, and effect of the competitive inhibitor mannan on uptake.

4.1.6 Summary of aims

- To synthesise a library of HPMA copolymer conjugates bearing a range of mannose loading (0 – 8 mol %), and also OG (1 mol %) to enable measurement of derived cell association.
- To characterise the conjugates with respect of mannose content by the modified Elson and Morgan method, the total and free OG fluorescence using PD10 column chromatography and UV absorbance respectively.
- To measure the cell-association of the library at 37 and 4 °C in THP-1 cells using flow cytometry and define the minimum mannose content necessary to promote MR targeting.
- To investigate the specific and non-specific cell-association of HPMA copolymer-OG-Man by co-incubation with mannan as a competitor for the MR.

4.2 Methods

The conjugation protocol for HPMA copolymer-GFLG-ONp and Man was initially adapted from Kopecek et al., (1986), and Salvatore Nicoletti (University of Dundee) provided help with modifications to the protocol.

4.2.1 Optimisation of reaction time using TLC

To optimise the reaction times for mannose conjugation, first, reactions were carried out with HPMA copolymer precursor and mannosamine alone. HPMA copolymer containing GFLG-ONp side chains (9.03 mol %) was dissolved in DMSO (5 mg in 0.5 ml). To this solution, after stirring at room temperature for 30 min, a solution of mannosamine.HCl in dry DMSO (19.6 μl of 12 mg/ml), along with 2 molar equivalents (0.15 μl) of triethylamine. The reaction mixture was stirred at room temperature under nitrogen and monitored every hour using TLC.

The mannosamine aminolysis reaction was monitored by TLC using reverse phase silica gel plates in a solution of potassium orthophosphate and acetonitrile (9/1 v/v). The plate was treated with ninhydrin reagent to visualise the amine group on the sugar (as a purple spot). The disappearance of this spot showed that the mannosamine was reacting with the polymer. TLC was performed every hour from the start of the reaction for 5 h, and then again after 16 h. After 4 h the spot had completely disappeared.

The same procedure was used to monitor OG-cadaverine binding. First, mannosamine was reacted as described above, and then, after 4 h, OG-cadaverine was added and the reaction left over night. Aminolysis by OG-cadaverine was monitored using silica gel plates in a mixture of methanol and triethylamine (9.5/0.5 v/v). The endpoint of the reaction was taken as the point where the spot of free OG had disappeared and there was visible OG at the baseline (i.e. co-localised with the polymer). TLC was performed at the start of the reaction and at 16 h to ensure the OG had bound to the HPMA copolymer.

4.2.2 General method for preparation of HPMA copolymer GFLG-OG conjugates

The method used to prepare the HPMA copolymer-OG conjugates is shown in Figure 4.2. Typically, 102.8 mg of HPMA copolymer-GFLG-ONp (9.03 mol % side chains) was dissolved in DMSO (1 ml). After stirring at room temperature for 30 min, 444 μl of a solution of OG-cadaverine in dry DMSO was added (6.3 mg/ml) to this solution, estimated to give a final theoretical loading of 1 mol %. The mixture was stirred in the dark for 16 h at room temperature under a nitrogen atmosphere and then an excess of aminopropanol (2 μl) was added to remove any remaining ONp groups.

4.2.3 General method for preparation of HPMA copolymer GFLG-OG-Man conjugates

The method used to prepare the HPMA copolymer-OG-Man conjugates is shown in Figure 4.3. HPMA copolymer-GFLG-ONp (9.03 mol % side chains) was dissolved in DMSO (99.8 mg in 1 ml). To this solution, after stirring at room temperature for 30 min, a solution of mannosamine hydrochloride in dry DMSO (12 mg/ml) was added (estimated to give theoretical final loadings of 2 (98 μl), 4 (196 μl), 6 (294 μl) or 8 (392 μl) mol % on the side chains) along with 2 molar equivalents (3.1 μl) of triethylamine. The reaction mixture was stirred at room temperature for 4 h. Then, 430 μl of a solution of OG-cadaverine in dry DMSO (5 mg/ml) was added to give final loading of 1 mol %. The mixture was stirred at room temperature in the dark for 16 h under a nitrogen atmosphere and then an excess of aminopropanol (2 μl) was added to remove any remaining -ONp groups.

4.2.4 Purification of HPMA copolymer-OG ± Man conjugates

The conjugates were then precipitated by pouring the reaction mixture into 50 ml of a rapidly stirring ice-cold acetone: diethylether solution (9/1 v/v), and stirring on ice for 10 min. The precipitate was then filtered off, thoroughly washed again with the acetone and ether solution, and dried. Acetone and diethyl ether fumes were trapped in a liquid nitrogen cold trap. The product was dissolved in water and then lyophilised before characterisation.

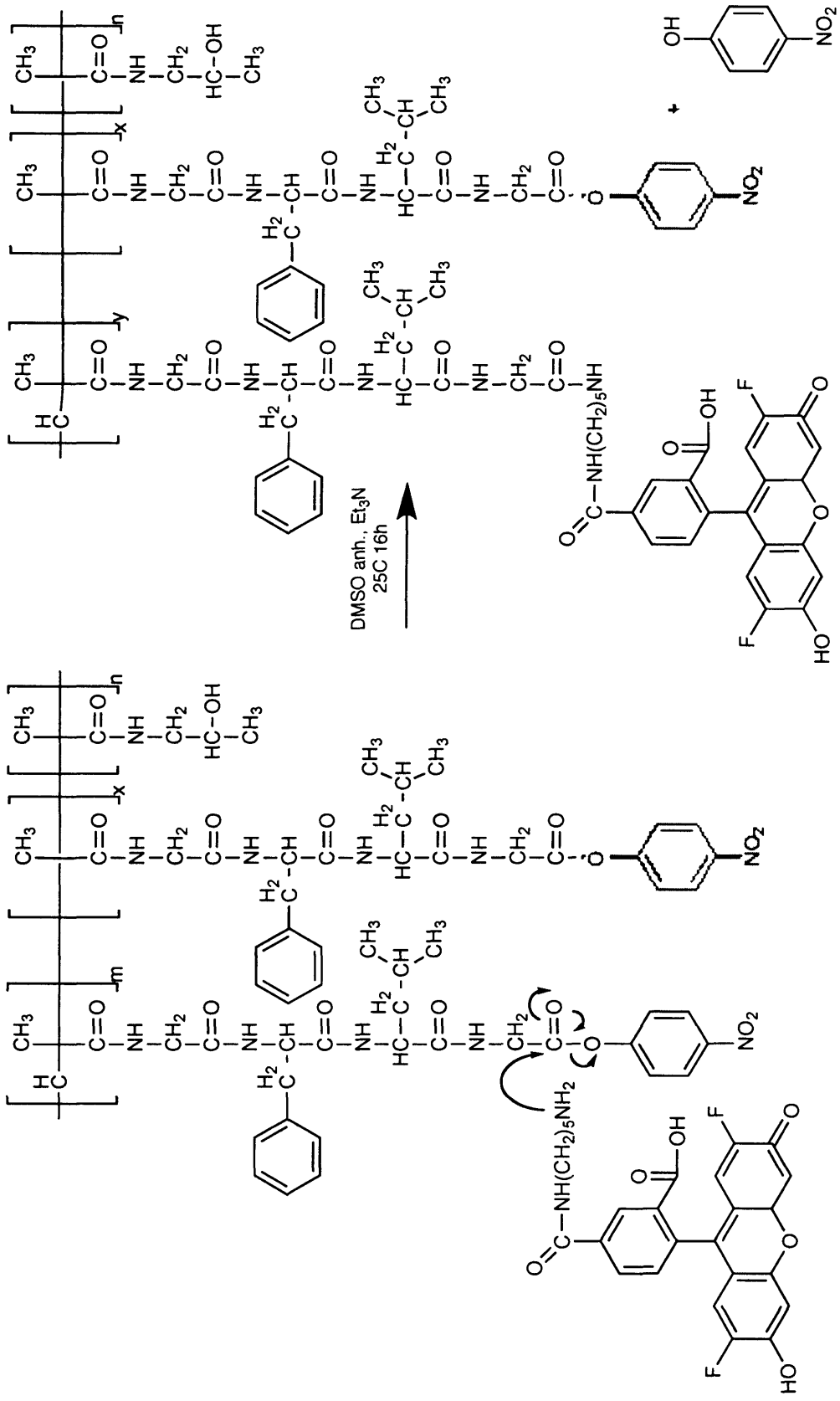

Figure 4.2 Synthesis reaction scheme of HPMA copolymer-GFLG-ONp (Mw 37,000 g/mol, Mw/Mn 1.58) with OG cadaverine. n = 90.07 mol %; m + x = 9.03 mol %.

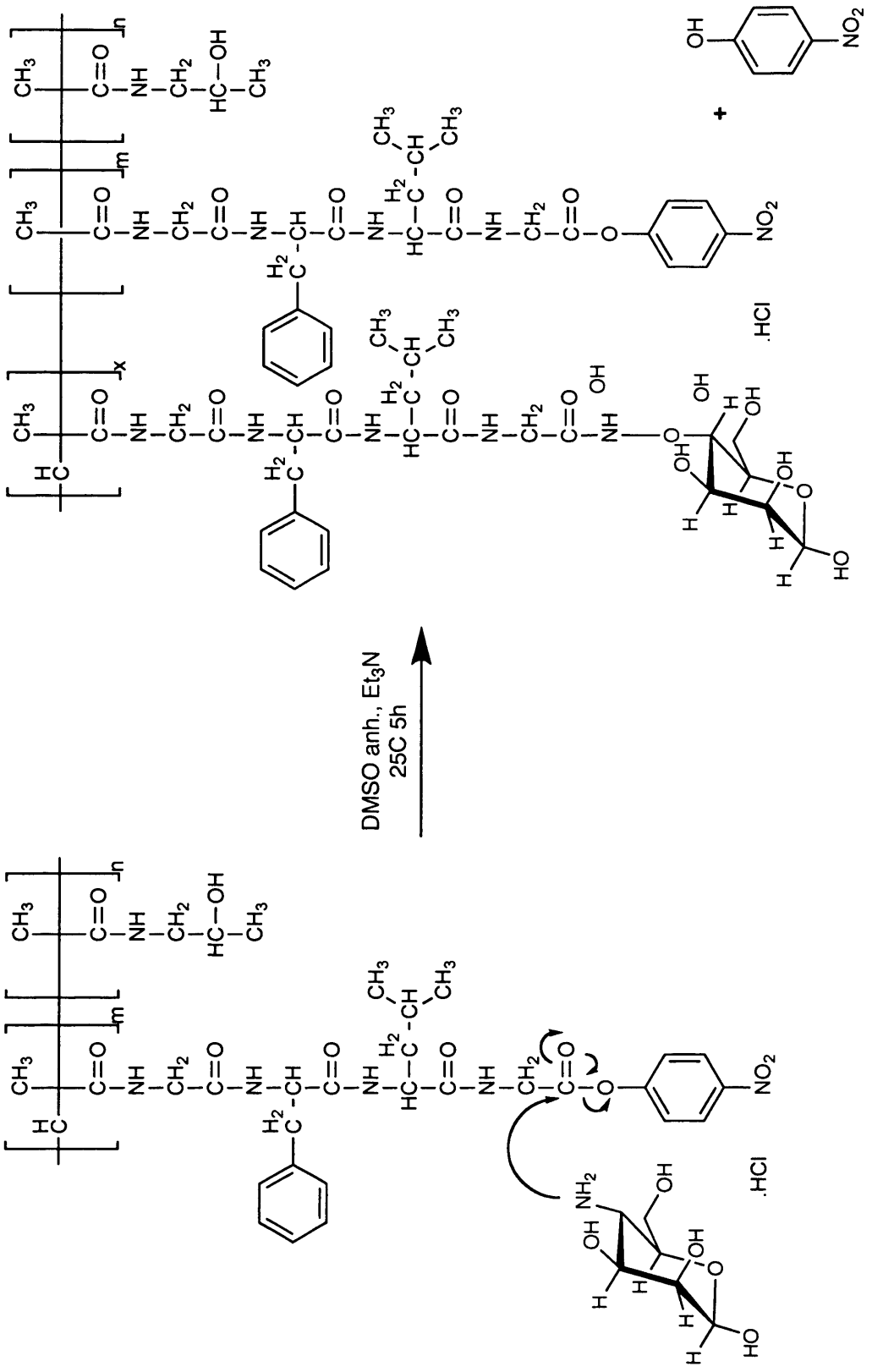

Figure 4.3 (a) Synthesis reaction scheme of HPMA copolymer-GFLG-ONp (Mw 37,000 g/mol Mw/Mn 1.58) with mannosamine hydrochloride. n = 90.07 mol %; m + x = 9.03 mol %.

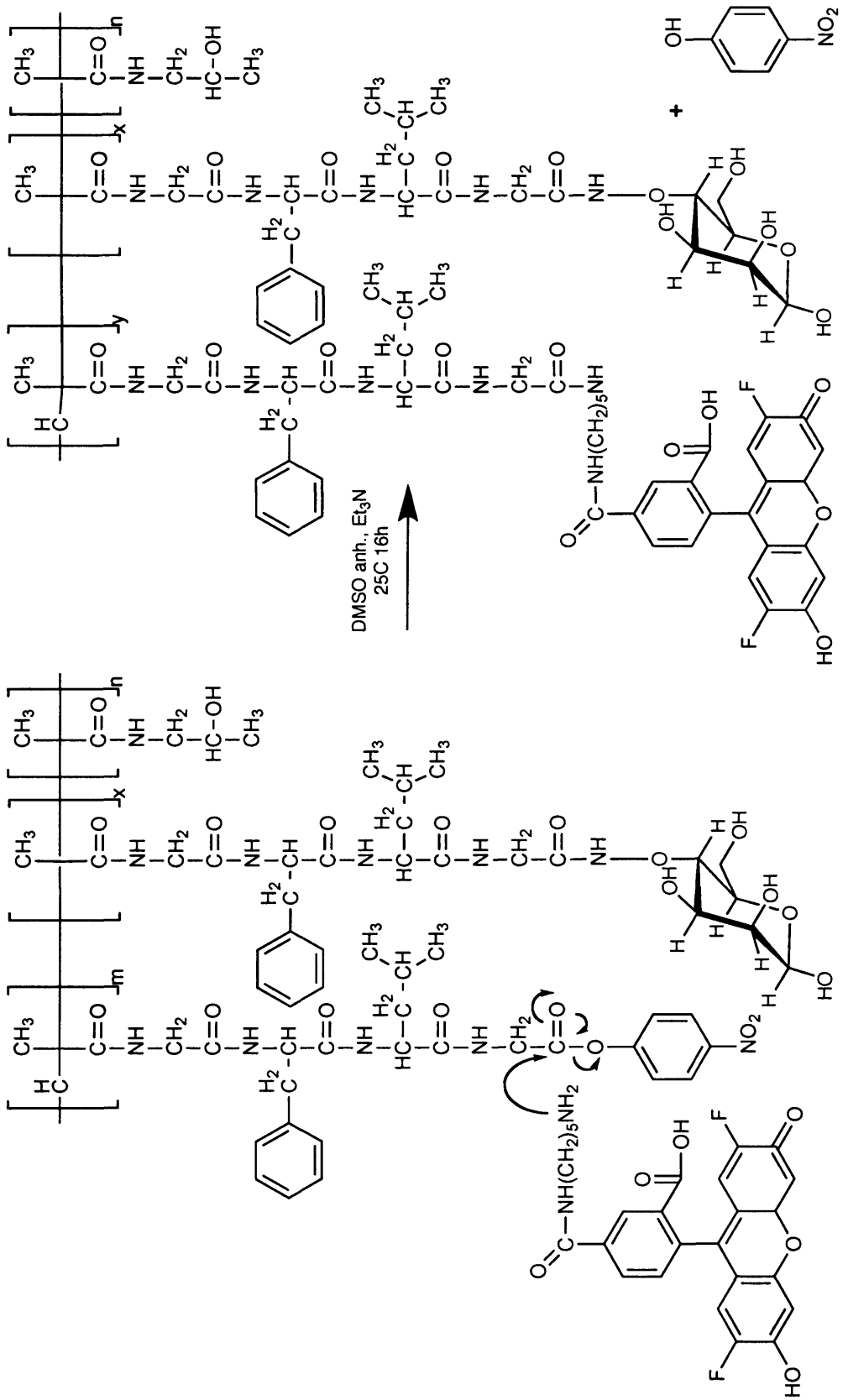

Figure 4.3 (b) Synthesis reaction scheme of HPMA copolymer-GFLG-Man (Mw 37,000 g/mol, Mw/Mn 1.58) with OG cadaverine. n = 90.07 mol %; m + x = 9.03 mol %.

4.2.5 Characterisation of the conjugates in respect of total and free OG

The OG content of the HPMA copolymer conjugates was estimated using the UV absorbance. A concentration curve of free OG-cadaverine was prepared (0.001 to 1 μg/ml) in phosphate buffer at pH 7.4. Conjugate samples were also dissolved at in phosphate buffer (0.1 mg/ml). The absorbance was then measured at 494 nm and the amount of conjugated OG calculated using the calibration curve.

The free OG content of the conjugates was measured using a PD10 size exclusion column with PBS as the eluent. A sample of the conjugate (1 ml at 5 μg/ml OG-equivalent) was applied to the column and then 0.5 ml PBS added sequentially until 48 fractions (0.5 ml) were collected. A sample of each fraction (200 μl) was then assayed in a 96 well plate by measuring the UV absorbance at 494 nm. Free OG elutes separately from the conjugate, the conjugate elutes in the void volume (i.e. fraction 1 – 14), and therefore allows estimation of the free OG as a percentage of the total OG content. Those conjugates that contained a significant amount of free OG were re-purified using a PD10 column. Fractions 1 – 14 were collected and the remainder (containing free OG) was discarded. All the conjugates used in the biological assays contained less than 5 % free OG.

4.2.6 Determination of mannose loading on HPMA copolymer conjugates

The measurements of mannose content in the HPMA copolymer-OG-Man conjugates were performed with an assay set up by Salvatore Nicoletti (University of Dundee). Analysis of conjugates 6 – 10 were performed with Salvatore Nicoletti at Cardiff University, but then subsequent analysis of conjugates 11 and 12 was performed by Salvatore Nicoletti at the University of Dundee. The method used is described below.

First, standards of D-mannosamine hydrochloride were prepared by dilution of the stock solution in water (0.63 mg/ml in 10 ml water) to give various concentrations between 0 and 16 μg/ml. To determine the mannose content of the conjugates, first the glycosidic linkage between the D-mannosamine and the glycine of the tetrapeptide was cleaved. A sample (1 ml) of the standard or conjugate (0.1 mg/ml) was transferred to a 10 ml glass tube, and mixed with 1 ml of HCl (6 M). The

tubes were capped and the solutions were stirred for 5 h at 60 °C, and then dried under vacuum.

The free mannose was then derivitised using acetylacetone and Ehrlich reagent. The dry residues were dissolved with 0.5 ml of water and 0.5 ml of acetyl acetone reagent (4.8 % (v/v) acetyl acetone in 1 M sodium carbonate buffer). The resulting mixtures were stirred for 20 min at 96 °C and then cooled on ice. Subsequently 2.5 ml of absolute ethanol and 0.5 ml of Ehrlich reagent (0.8 mg of p-dimethylaminobenzaldehyde dissolved in 30 ml of absolute ethanol and 30 ml of HCl) were added. The samples were then stirred for 10 min at 65 °C, and the UV absorbance measured at 530 nm. The mannose content was calculated from the calibration curve.

4.2.7 Absorbance and fluorescence characteristics of conjugates

The concentration and pH dependence of the HPMA copolymer-OG ± Man conjugate fluorescence were measured as described in section 2.3.2.

4.2.8 Measurement of binding and endocytosis of HPMA copolymer-OG ± Man in THP-1 Cells by flow cytometry

The derived cell association of HPMA copolymer-OG ± Man was determined using clear tissue culture media at an OG concentration of 1 μg/ml of OG-equivalent for all polymer conjugates in differentiated THP-1 cells with time. Derived cell association was measured using flow cytometry as described in section 2.3.3.

It should be noted that the PMA used to differentiate THP-1 cells from monocytes to macrophages can, at high levels, activate macrophages and this can lead to inhibition of internalisation by the MR (Bozeman et al., 1988). However, the low levels of PMA used here for differentiation would be unlikely to have this effect. Never the less, it was important to make sure all the PMA was removed.

First, the cell-association of HPMA copolymer-OG and HPMA copolymer-OG-Man (with a theoretical 8 mol % mannose content) at 37 °C after 60 min incubation with THP-1 cells was compared. To determine the OG release the

incubation media was retained and the free OG content was measured using a PD10 column as described in section 4.2.5.

To investigate the effect of the presence of serum on the cell-association of HPMA copolymer-OG-Man, THP-1 cells were incubated with media containing HPMA copolymer-OG or HPMA copolymer-OG-Man, with or without serum present. Additionally, THP-1 cells were incubated overnight without serum to investigate the effect of serum starvation.

The concentration-dependence of conjugate uptake was measured by incubating THP-1 cells with increasing amounts of HPMA copolymer-OG-Man (0 – 1 mg/ml) for 60 min. To investigate the effect of mannose competition cells were co-incubated with and without mannan (10 mg/ml) as a competitive inhibitor. Cells incubated with mannan were also pre-incubated for 30 min with mannan before polymer solutions were added.

To define the minimum mannose content necessary to promote MR targeting, cell-association with time of the HPMA copolymer-OG conjugates bearing a range of mannose loadings (0 – 8 mol %) was measured over 60 min at 37 °C. The cell-association at 4 °C was then measured to distinguish the cell binding from the cell uptake.

4.3 Results

4.3.1 Characteristics of HPMA copolymer-OG ± Man conjugates

Aminolysis of HPMA copolymer-GFLG-ONp with mannosamine was complete within 4 h. OG-cadaverine added at this time was found on the baseline i.e. polymer-bound, with no visible free OG after 16 h.

The HPMA copolymer-OG-Man conjugates synthesised using this protocol are summarised in Table 4.3.

For the preliminary biological experiments, a control HPMA copolymer conjugate was prepared with ~ 1 mol % OG (code number 3), and two batches of

Table 4.3 Characteristics of HPMA copolymer-OG ± Man conjugates.

Code n°	Conjugate Structure	Total OG † (mol %)	Total OG † (wt %)	Free OG †† (%)	Mannose (mol % theoretical)	Mannose * (mol % measured)
3	HPMA copolymer-GFLG-OG	0.32	0.93	3.7	0	N/A
11	HPMA copolymer-GFLG-OG	1.05	2.8	4.2	0	N/A
6	HPMA copolymer-GFLG-OG	0.56	1.53	2.6	0	N/A
7	HPMA copolymer-GFLG-OG-Man	0.54	1.46	1.7	2	1.4
8	HPMA copolymer-GFLG-OG-Man	0.68	1.85	2.1	4	3.6
12	HPMA copolymer-GFLG-OG-Man	0.59	1.6	1.5	4	4.8
9	HPMA copolymer-GFLG-OG-Man	0.58	1.57	2.0	6	5.0
10	HPMA copolymer-GFLG-OG-Man	0.83	2.25	1.9	8	4.7
4	HPMA copolymer-GFLG-OG-Man	0.35	1.04	2.4	8	Not measured
5	HPMA copolymer-GFLG-OG-Man	0.98	2.89	1.1	8	Not measured

† Estimated by UV absorbance at 494 nm †† Estimated by PD-10 chromatography * Estimated by Elson Morgon method

HPMA copolymer conjugate with ~ 1 mol % OG and a theoretical loading of ~ 8 mol % mannose (code number 4 and 5). This is the maximum amount that could be loaded on the HPMA copolymer precursor (9.03 mol % ONp groups).

Subsequently, a library of conjugates containing a range of mannose loadings (0, 2, 4, 6 and 8 mol %) was successfully synthesised (code numbers 6-10). Again conjugates contained ~ 1 mol % OG. A further batch of conjugates (HPMA copolymer-OG and HPMA copolymer-OG-Man containing 4 mol % mannose) was then synthesised.

Free OG-cadaverine (in phosphate buffer, pH 7.4) had an absorbance maximum of 494 nm (Figure 4.4a) and the calibration curve showed a linear dependence (r^2 = 0.9996) of absorbance related to concentration over the range of concentrations tested (0 – 10 μg/ml) (Figure 4.4b). The total OG content of all conjugates was in the range of 0.32 – 1.05 mol % (0.93 – 2.8 wt %) (Table 4.3). The HPMA copolymer-OG conjugates had an identical absorbance spectrum (Figure 4.5).

The free OG content of the conjugates was determined using PD10 size exclusion chromatography. The conjugate eluted in the first 14 fractions (7 ml), whereas free OG eluted in fractions 14 - 48 (7 - 24 ml) (Figure 4.6). The free OG content was between 1.1 – 4.2 % of the total for all of the conjugates. The first conjugates (Table 4.3, code numbers 3 - 5) initially showed high free OG content (10 – 12 %). However, it was decided for all biological experiments that only conjugates with levels less than 5 % free OG would be used, and therefore conjugates were re-purified using the PD10 column. The library of conjugates containing 0, 2, 4, 6 and 8 mol % mannose (code numbers 6 – 10) contained a similar amount of free OG (1.7 – 2.6 %) (Figure 4.7).

The calibration curve of mannose showed a linear dependence (r^2 = 0.9996) of absorbance related to concentration over the range of concentrations tested (0 – 16 μg/ml) (Figure 4.8). The mannose content of conjugates 4 and 5 were not measured. The measured mannosamine content of the library of HPMA copolymer conjugates

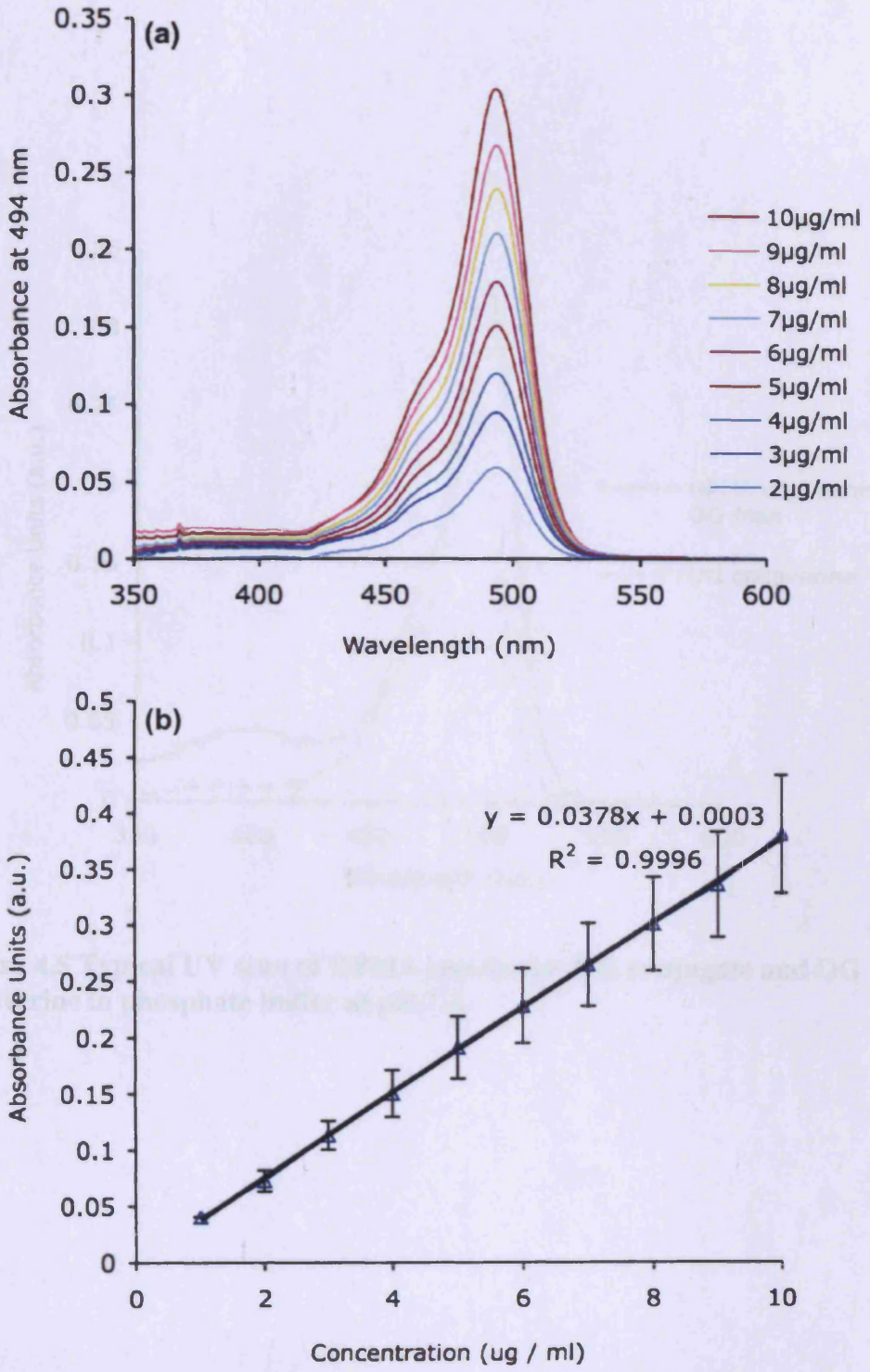

Fig 4.4 Calibration curve for OG cadavarine. The calibration curve was measured over a range of concentrations in pH 7.4 phosphate buffer. Panel (a) UV scans of absorbance spectra and (b) the calibration curve at an absorbance of 494 nm. The data represent the mean ± SD (n = 4).

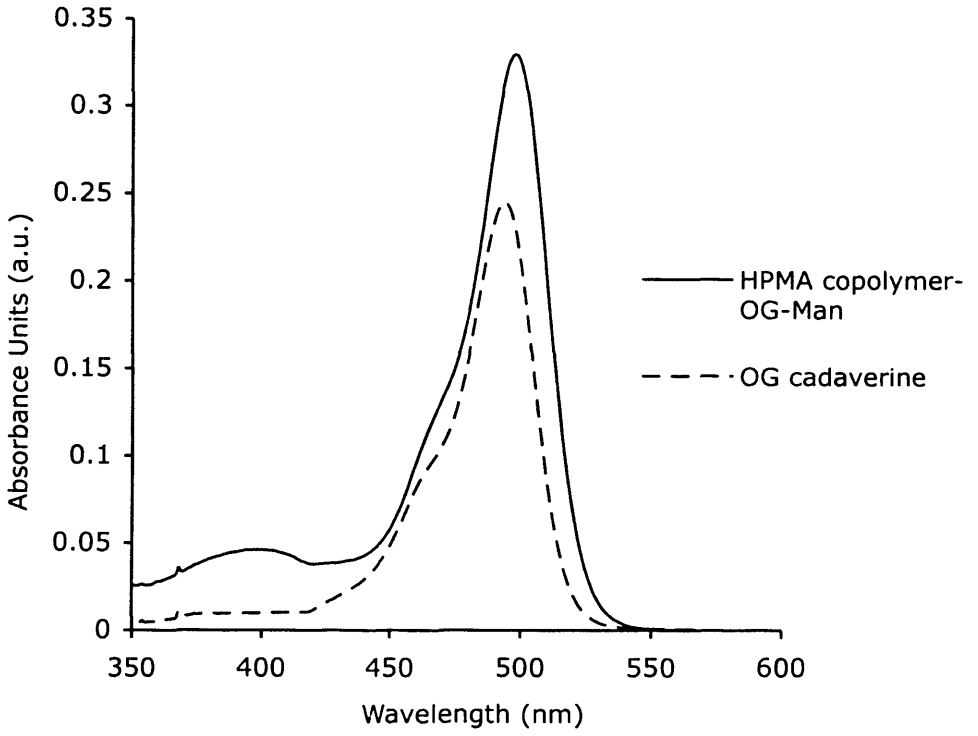

Figure 4.5 Typical UV scan of HPMA copolymer-OG conjugate and OG cadaverine in phosphate buffer at pH 7.4.

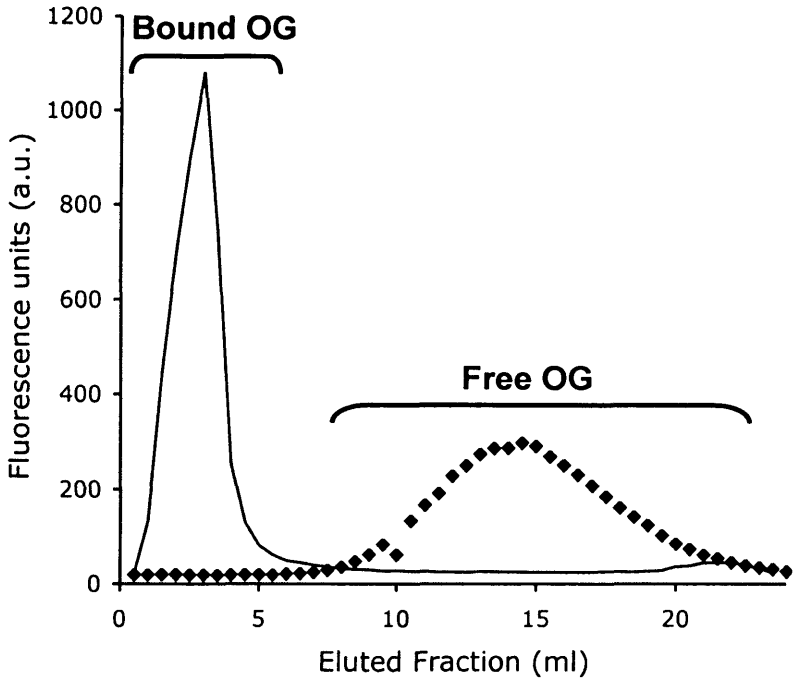

Figure 4.6 PD10 elution of HPMA copolymer-OG conjugates. HPMA copolymer-OG and free OG cadaverine were eluted in PBS through a PD10 column and fluorescence measured at 520 nm.

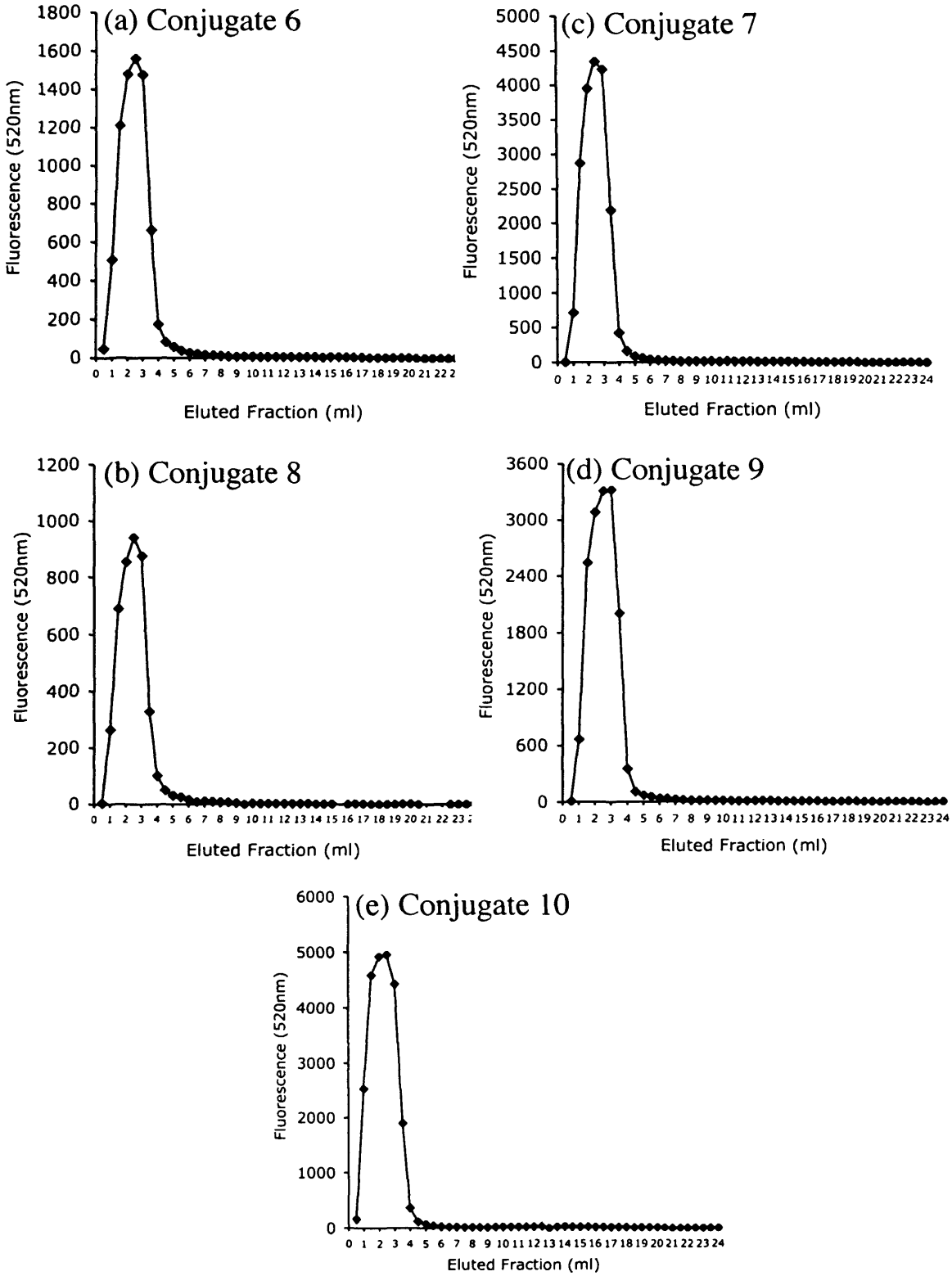

Figure 4.7 PD-10 profiles of HPMA copolymer-OG conjugates. The conjugate was eluted in PBS and the fractions collected were assayed for fluorescence measured (Abs 494 nm Em 520 nm).

(0 – 8 mol %) correlated reasonably well with the theoretical values except at the highest value of 8 mol % containing between 0 – 5 mol % mannose (2 mol % theoretical gave 1.43 mol % measured, 4 measured 3.55, 6 measured 5.02, 8 measured 4.71 mol %) (Table 4.3).

It was confirmed that pH had a relatively small effect on the fluorescence output of OG (Figure 4.9). A small reduction in fluorescence output was seen from pH 7 to pH 6.2 (about 16 % at 1 mg/ml), but not from 6.2 to 5.5. Concentration dependent quenching was seen at concentrations > 0.2 – 0.6 mg/ml, but this was minimal.

4.3.2 Comparison of the derived cell-associated fluorescence of HPMA copolymer-OG-Man conjugates in THP-1 cells

Incubation of cells with the HPMA copolymer-OG for 1 h at 37 °C showed a clear increase in derived cell-associated fluorescence with time when compared to cells incubated without conjugate (Figure 4.10a) ($p < 0.05$, students t-test). Derived cell-associated fluorescence was 3-fold greater for the HPMA copolymer-OG-Man conjugate (Figure 4.10b). When the cell culture media (collected after 1 h incubation) was subject to PD10 chromatography, there was no significant difference in the amount of free OG seen at the end of the incubation compared to the control (~ 5 % to ~ 7 % free OG) (Figure 4.11).

When experiments were conducted to examine the effect of serum on derived cell association, greater uptake of HPMA copolymer-OG-Man was seen when the cells were incubated without serum; however, similar and significant differences were seen between HPMA copolymer-OG and HPMA copolymer-OG-Man derived cell association with and without serum present (Figure 4.12). Serum starving the cells overnight significantly reduced the difference in derived cell association between the targeted and the non-targeted conjugate.

There was an increase in concentration-dependent cell-association of HPMA copolymer-OG-Man compared to HPMA copolymer-OG after 1 h at 37 °C. This was

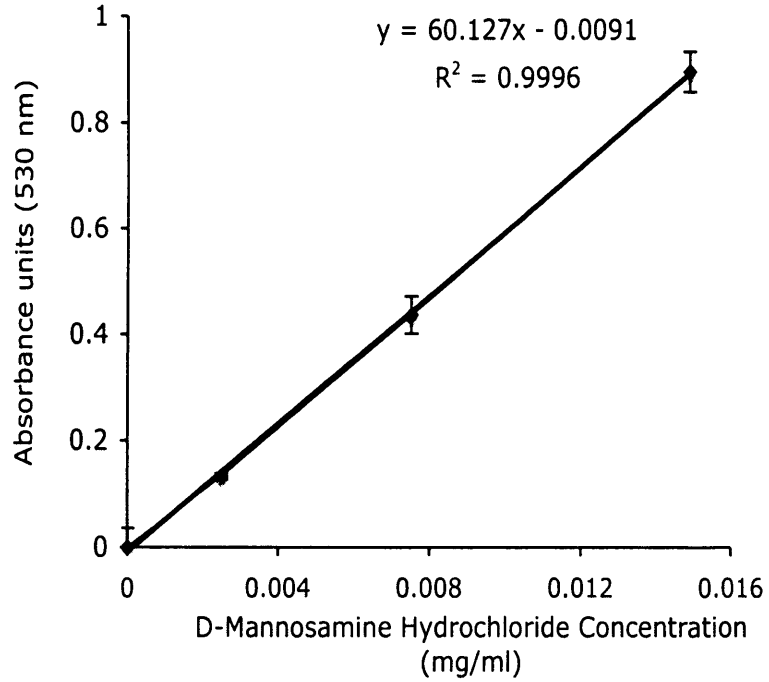

Figure 4.8 Calibration curve of mannose measured at 530 nm on UV spectrophotometer. Data represent mean ± SD (n = 3).

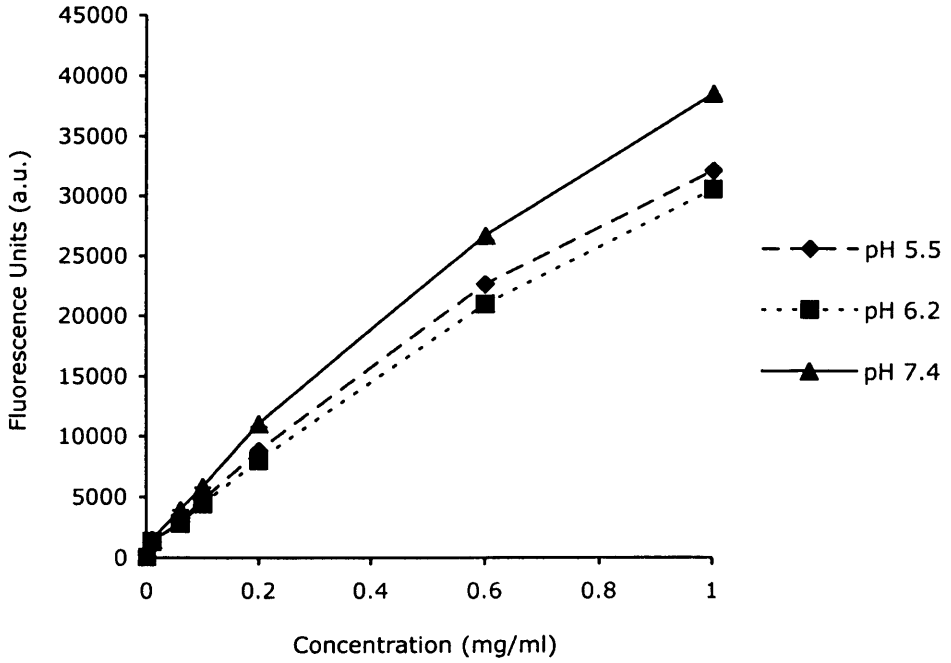

Figure 4.9 Effect of concentration and pH on HPMA copolymer-OG-Man fluorescence. HPMA copolymer-OG was dissolved in buffers at pH 7.4, 6.2 and 5.5 and measured at 520 nm on a fluorescent plate reader. The data represent the mean ± SD (n = 3). Where the error bars are not visible they fall within the data points.

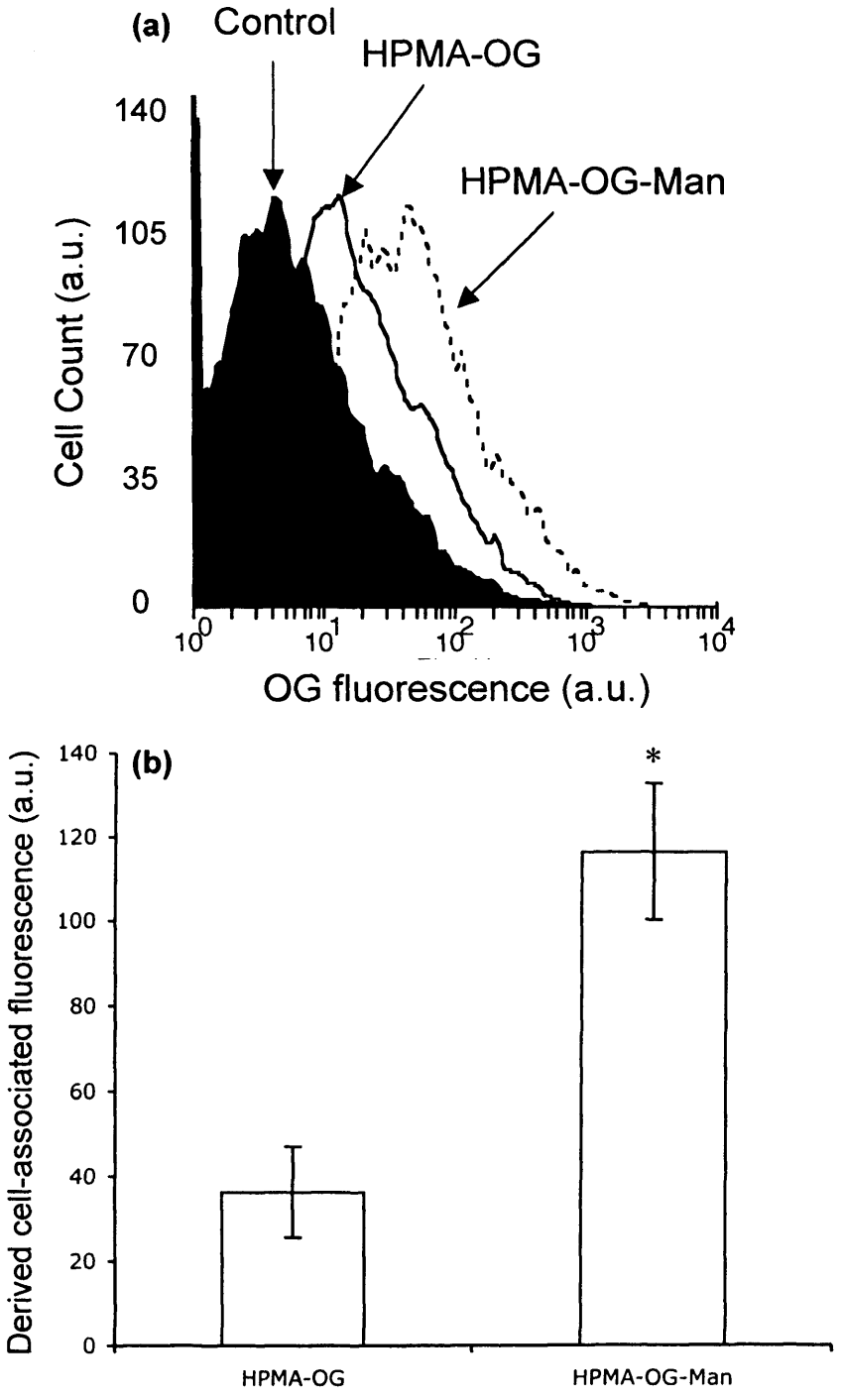

Figure 4.10 Comparison of cell-association of HPMA copolymer-OG and HPMA copolymer-OG-Man (8 mol %) at 37 °C after 60 min incubation with THP-1 cells by flow cytometry. Panel (a) flow cytometry raw data and (b) calculated cell associated fluorescence. The data represent the mean ± SD (n = 3). Statistical significance (*) was determined at $p < 0.05$ (students t-test).

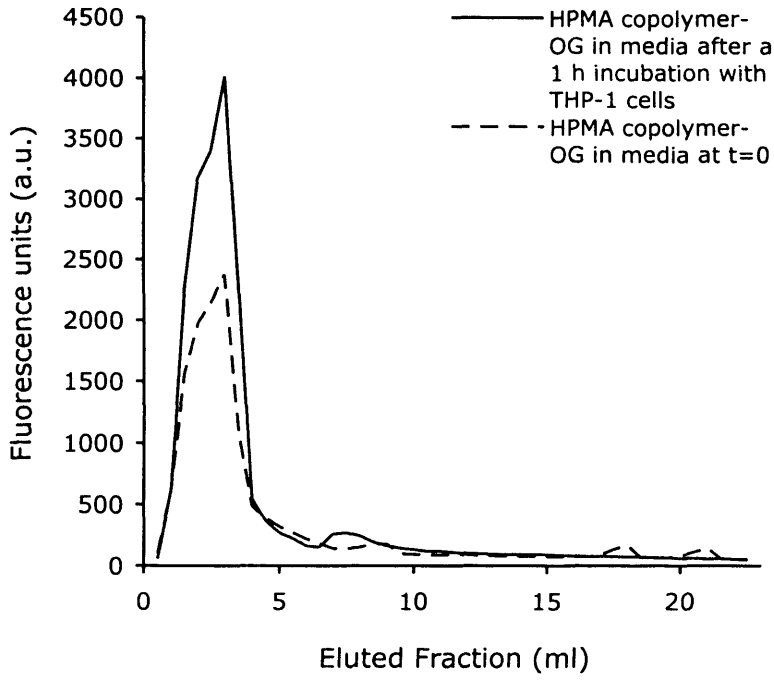

Figure 4.11 Stability of HPMA-OG conjugates during incubation with THP-1 cells. PD-10 profiles of HPMA copolymer-OG conjugate after 60 min incubation with THP-1 cells at 37 °C. were obtained by elution in PBS and the fractions collected were assayed for fluorescence measured (Abs 494 nm Em 520 nm).

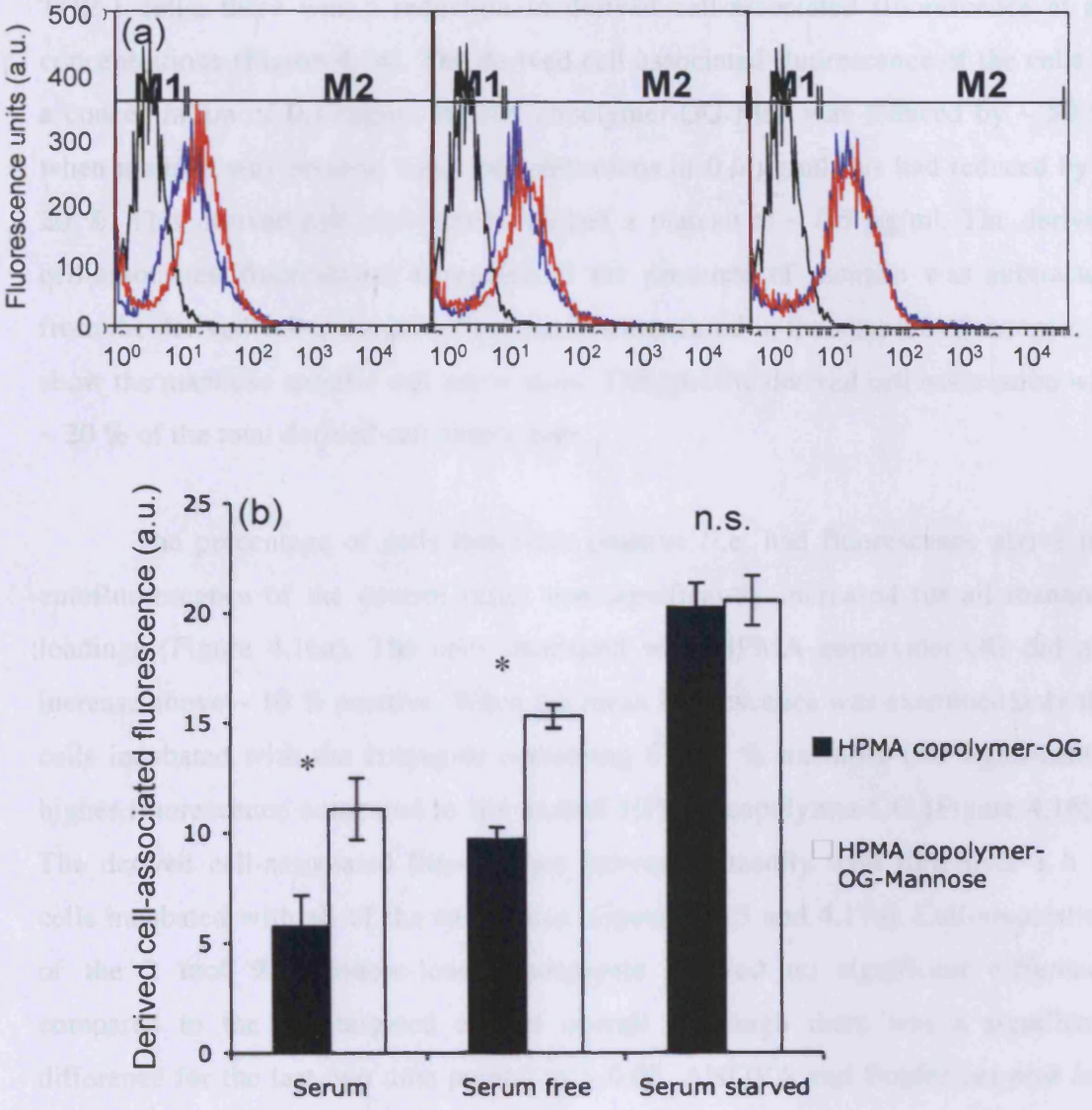

Figure 4.12 Comparison of cell-association of HPMA-OG and HPMA-OG-Man with and without serum present, and serum starved overnight. Panel (a) shows the raw data and panel (b) shows the transformed data. Flow cytometry at 37 °C at 60 min. The data represent the mean ± SD (n = 3). Statistical significance (*) between HPMA copolymer-OG and HPMA copolymer-OG-Man was determined as $p < 0.05$ (ANOVA and Bonferroni *post hoc* test).

not linear, the rate increasing with concentration, and did not plateau over the range studied (Figure 4.13).

When mannan was co-incubated with HPMA copolymer-OG-Man in the THP-1 cells, there was a reduction in derived cell-associated fluorescence at all concentrations (Figure 4.14). The derived cell-associated fluorescence of the cells at a concentration of 0.1 mg/ml HPMA copolymer-OG-Man was reduced by ~ 50 % when mannan was present, but at concentrations of 0.6 μg/ml this had reduced by ~ 20 %. This derived cell association reached a plateau at ~ 0.5 μg/ml. The derived cell-associated fluorescence measured in the presence of mannan was subtracted from the derived cell-associated fluorescence measured in the absence of mannan, to show the mannose specific cell-association. The specific derived cell association was ~ 20 % of the total derived cell association.

The percentage of cells that were positive (i.e. had fluorescence above the autofluorescence of the control cells) was significantly increased for all mannose loadings (Figure 4.16a). The cells incubated with HPMA copolymer-OG did not increase above ~ 10 % positive. When the mean fluorescence was examined only the cells incubated with the conjugate containing 8 mol % mannose had significantly higher fluorescence compared to the control HPMA copolymer-OG (Figure 4.16b). The derived cell-associated fluorescence increased steadily with time over 1 h in cells incubated with all of the conjugates (Figures 4.15 and 4.17a). Cell-association of the 2 mol % mannose-loaded conjugate showed no significant difference compared to the non-targeted control overall (although there was a significant difference for the last two time points) ($p > 0.05$, ANOVA and Bonferroni *post hoc* test) (Figure 4.17b). However, at mannose loadings of 4 mol % mannose and above, the cells showed significant differences in derived cell association compared to the control. The uptake was rapid over the first 10 min, slowed after 10 min but did not reach a plateau. The increase in derived cell association correlated with mannose loading but it was not linear. The conjugates containing 2, 4, 6 and 8 mol % loadings showing a 2, 5, 6 and 18-fold increases in uptake at 60 min respectively. There was minimal derived cell association at 4 °C (Figure 4.18).

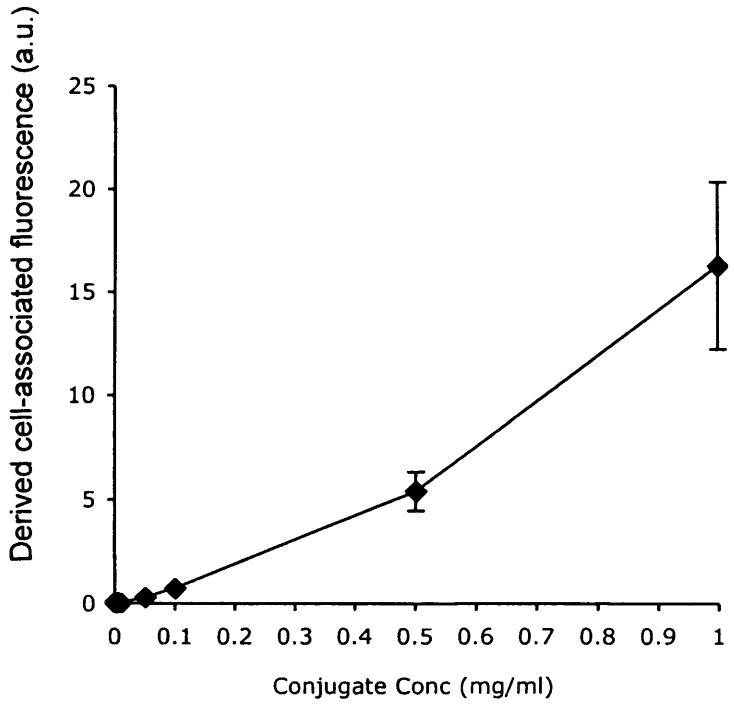

Figure 4.13 Concentration-dependence of the cell-associated fluorescence in THP-1 cells incubated with HPMA copolymer-OG-Man (8 mol %) at 37 °C for 60 min. The data represent the mean ± SD (n = 3).

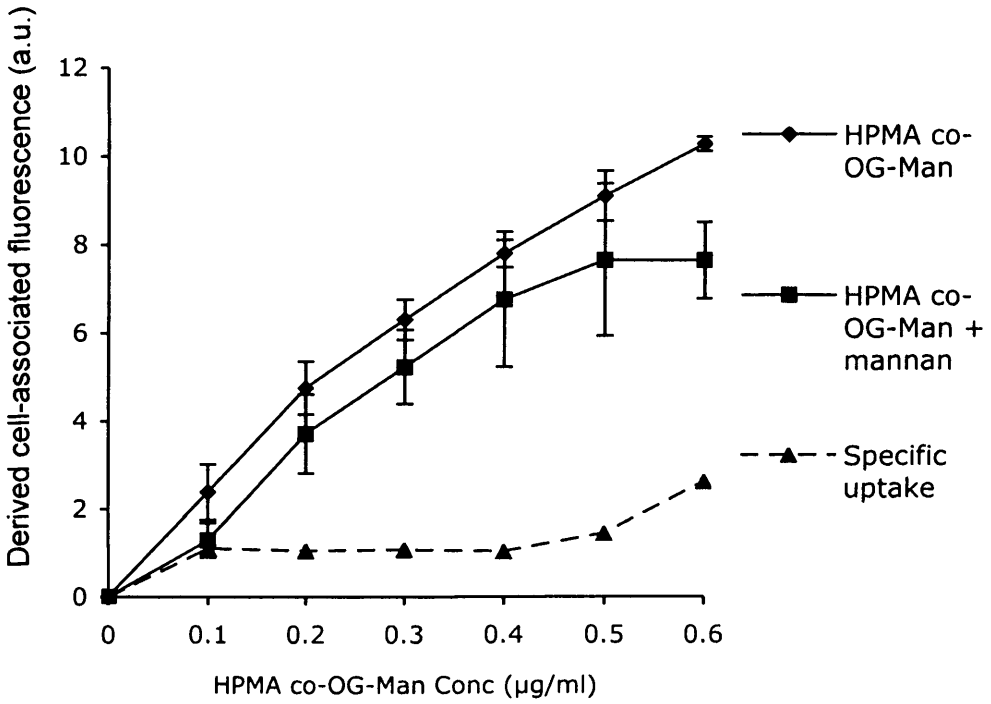

Figure 4.14 Competition assay to determine specific cell-association. Concentration-dependence of the cell-associated fluorescence of THP-1 cells incubated with HPMA copolymer-OG-Man (8 mol %) ± mannan at 37 °C for 60 min. The difference i.e. the specific uptake is shown (n = 3).

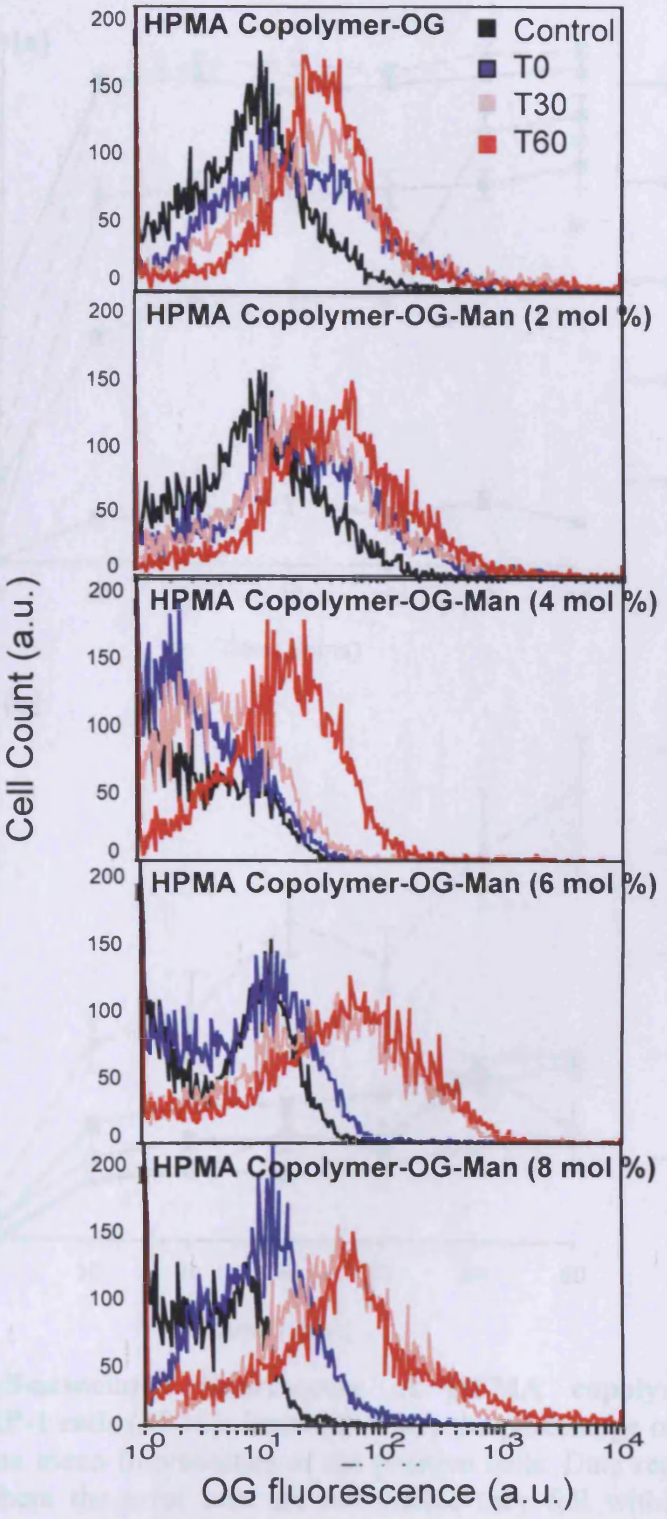

Figure 4.15 Flow cytometric raw data of cell-associated fluorescence of HPMA-OG ± Man conjugates in THP-1 cells at 37 °C.

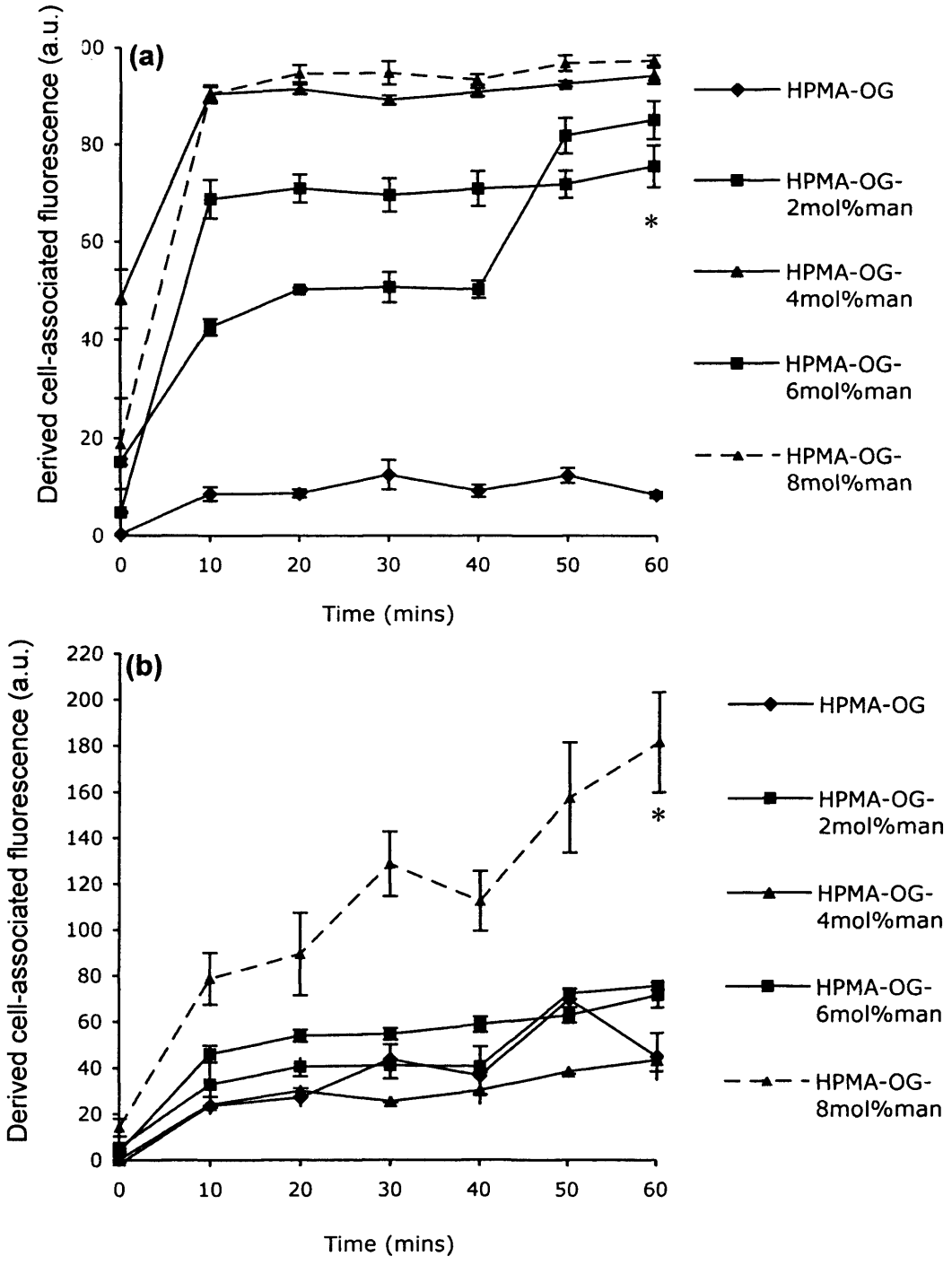

Figure 4.16 Cell-associated fluorescence of HPMA copolymer-OG ± Man conjugates in THP-1 cells (37 °C). Panel (a) shows the percentage of positive cells and panel (b) shows the mean fluorescence of the positive cells. Data represent the mean ± SEM (n = 3). Where the error bars are not visible they fall within the data points. Statistical significance (*) between the percent of HPMA copolymer-OG and HPMA copolymer-OG-Man (4, 6 or 8 mol%) positive cells; and between mean fluorescence of HPMA copolymer-OG-Man (8 mol %) and all other conjugates was determined as $p < 0.05$ (ANOVA and Bonferroni *post hoc* test).

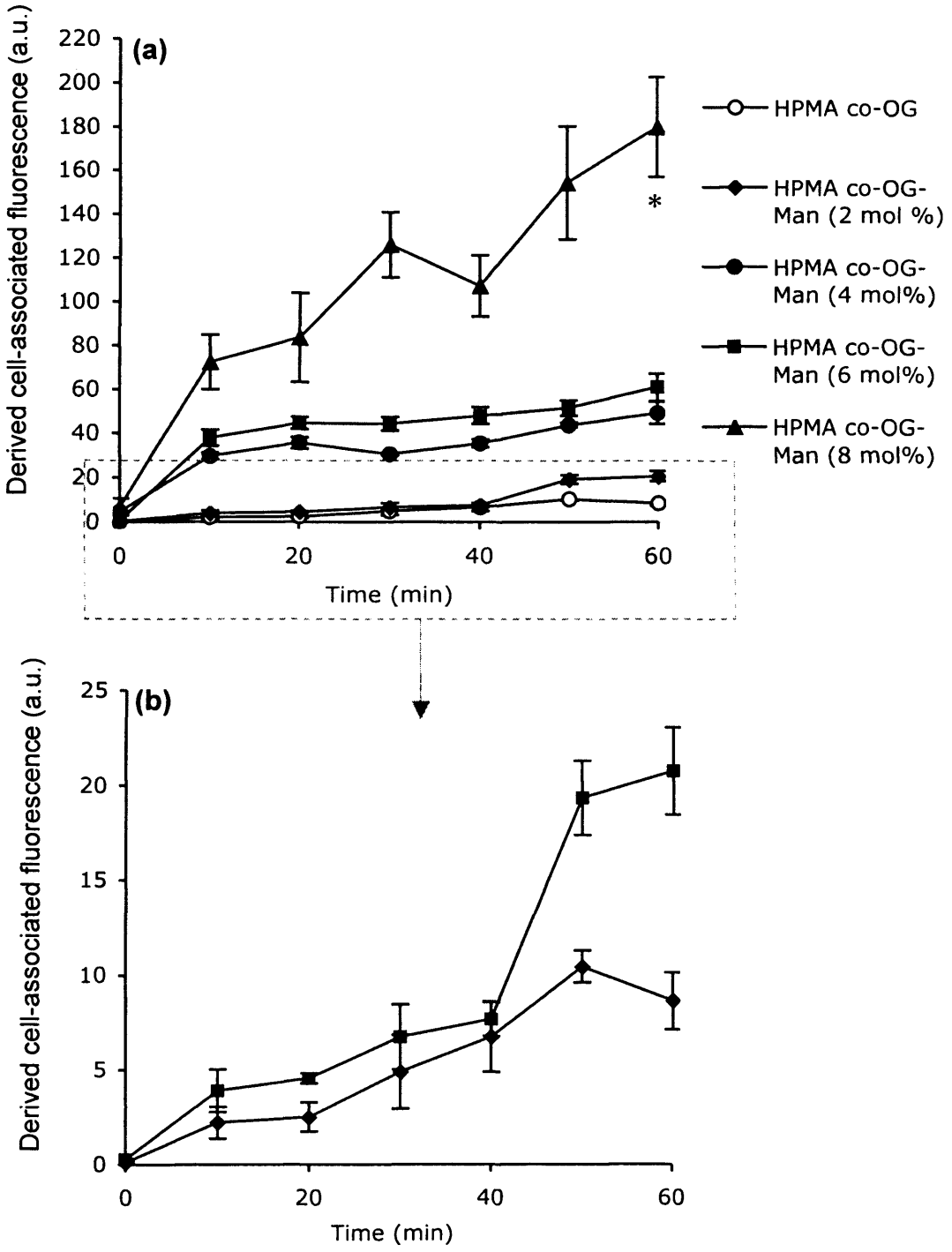

Figure 4.17 Cell-associated fluorescence of HPMA copolymer-OG ± Man conjugates in THP-1 cells (37 °C). Panel (a) shows the cell-association of a library of conjugates with a range of mannose loadings of 0 - 8 mol %, and panel (b) shows the cell association of HPMA copolymer-OG-Man (2 mol%) compared to control on a larger scale. Data represent the mean ± SEM (n = 3). Where the error bars are not visible they fall within the data points. Statistical significance (*) between HPMA copolymer-OG and HPMA copolymer-OG-Man (4, 6 or 8 mol%) was determined as $p < 0.05$ (ANOVA and Bonferroni *post hoc* test).

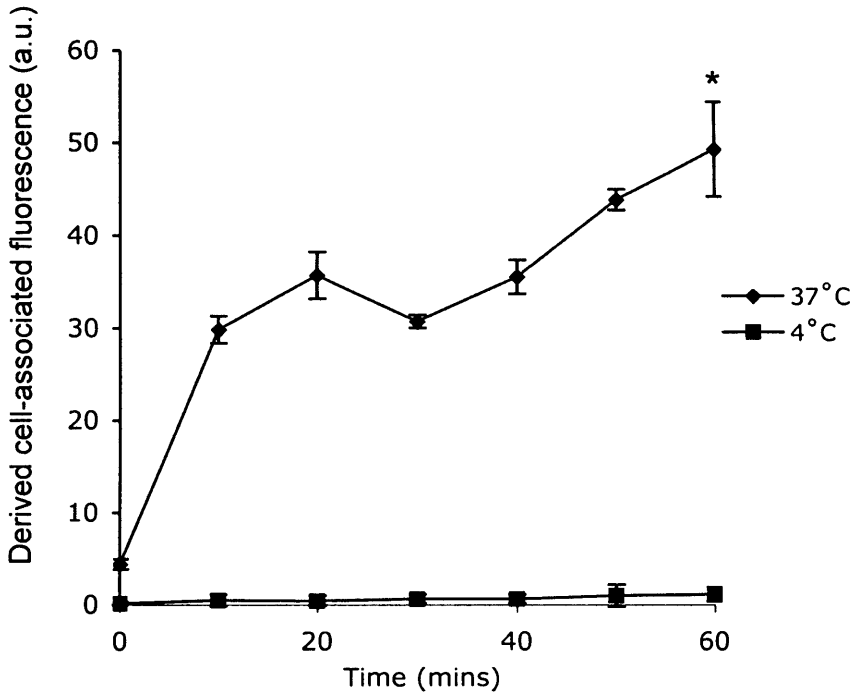

Figure 4.18 Time-dependent uptake of HPMA copolymer-OG-Man (4 mol %) in THP-1 cells. Panel (a) 37 °C and (b) 4 °C. The data represent the mean ± SD (n = 3) and where the error bars are not visible they fall within the data points. Statistical significance (*) between 37 and 4 °C was determined at $p < 0.05$ (students t-test).

4.4 Discussion

4.4.1 Conjugate synthesis and characterisation

The methodology for conjugation of galactosamine to HPMA copolymer-GFLG-ONp by aminolysis has been well established (Duncan et al., 1983; Kopecek, 1986), but it was still necessary to determine the optimal reaction conditions for synthesis of HPMA copolymer-Man conjugates. The initial reaction conditions and timings chosen here for mannosamine were based on PK2 synthesis and it was found that 4 h was optimal for mannose conjugation. This is much less than that used to bind galactosamine to HPMA copolymer precursor (16 h) (Kopecek, 1986). Subsequently, a library of OG-labelled conjugates with a range of mannose loading (0 – 8 mol %) was prepared.

The total OG content achieved was reproducible, with only a small batch-to-batch variation. The loading was kept low ($\leq$ 1 mol % which equates to ~ 1 – 3 μg/mg polymer). This was similar to that reported for other polymer conjugates (e.g. hyaluronic acid (3.4 μg/mg) (Duncan et al., 2008) and dextrin (5 μg/mg) (Richardson et al., 2008)). This low OG loading was used to allow higher mannose and drug loadings, and also to minimise the possibility that the OG fluorophore would itself would change the binding or uptake rate.

The PD10 column chromatography showed that the conjugates had only very low levels of free OG (< 5 % of total fluorescence) and as this free OG level was similar for all conjugates, the impact on the measured total fluorescence would be minimal. Also, no significant pH-quenching of OG fluorophore was observed with pH. Therefore, the measured cellular fluorescence would be expected to be independent of the cellular compartment to which the conjugate was localised. Although higher concentrations (> 0.2 - 0.6 mg/ml) of OG did show a small reduction in fluorescence output, the cell uptake experiments used a much lower concentration (1 μg/ml OG equivalent in the incubation medium). It is important to note that the concentration of fluorescent conjugate in endocytic compartments may be very high due to vesicle fusion. However, the intracellular concentrations were unlikely to reach 0.2 mg/ml.

Although the total and free OG content of the HPMA copolymer conjugates synthesised here was easy to determine, accurate Man quantification was much more difficult. The TLC showed no free mannosamine left after a 4 h reaction for any of the conjugates. However, the modified Morgan Elson method used here suggested that the maximum Man loading achievable was ~ 5 mol %, compared to a theoretical loading of 8 mol % hoped for.

This discrepancy could have resulted from a low reaction yield. However this is unlikely, as PK2 has been prepared on an industrial scale without such problems. Alternatively, the values measured could be an artefact of the quantification method. Configliacchi et al. (1996) optimised the hydrolysis conditions for PK2, which contained ~ 4 mol% galactose. They noted that higher temperatures and longer reaction times could lead to decomposition of the sugar. The balance between hydrolysis and sugar decomposition is likely to vary for each sugar type. Possible issues here include the Man was not released optimally at this time and temperature, and/or the released sugar was subject is degradation. The solution conformation of polymer-drug conjugates has been shown to affect the drug release of drug from HPMA copolymer conjugates (Vicent et al., 2005). Perhaps this was also a factor here. It may have been better to further standardise the sugar analysis method for the Man conjugates but unfortunately time did not allow it. Another option that could have been used to accurately define Man content would have used [^{14}C] mannosamine to prepare the conjugates. This would have had the added benefit of negating the need for fluorescence labelling, to measure cell uptake, which has inherent disadvantages, but these experiments were also not possible for various reasons. NMR of the conjugates could also have provided information on the conjugation of mannosamine and OG. However, the ^{1}H-NMR analysis identified the proton of the polymer backbone and of the protons of the GFLG peptide chain, but the spectroscopic profile did not show any signal related to the protons of the amino sugar or the fluorescent probe (not shown).

Never the less, as the synthetic methods used to prepare the HPMA copolymer-sugar conjugates have been well documented in the past and the TLC detected no free mannosamine in the reaction mixture, it was decided to progress to the biological experiments with these conjugates, assuming the theoretical loading to be correct.

4.4.2 Cell uptake and evidence for MR-specific interaction

The biological experiments did provide indirect evidence to support the conclusion that the mannose had indeed been successfully bound to the polymer at the theoretical loadings. The derived cell association of HPMA copolymer-OG conjugates with THP-1 macrophages measured using flow cytometry was significantly higher for the mannose-targeted conjugates. The percentage of positive cells reached a maximum after 10 min for conjugates with 4, 6 and 8 mol % Man. The cells incubated with the conjugate loaded with 2 mol % Man had significantly more positive cells than the control but didn't reach a maximum over the time course studied. The mean fluorescence didn't show discernable differences except for the conjugate loaded with 8 mol % Man. Differences may have been seen more clearly if the cells were incubated with a greater concentration of conjugate or for a longer time course.

When both the percentage of positive cells and the mean fluorescence of the cells was taken into account (as described in section 2.3.3) the differences were more clearly seen. Cell uptake was progressive with time, but not linear as a plateau of fluorescence was seen for all mannose loadings with time (Figure 4.17a). This may be due to the release of free fluorophore or exocytosis of the conjugate. Exocytosis rates were not measured, but the PD10 analysis of the media after incubation with the cells showed no significant increase in free OG after 1 h (Figure 4.11), so release of free OG is unlikely to account for the decreased rate of uptake. Internalisation of surface MR with limited replacement from intracellular MR stores could be rate limiting. However, as no plateau was seen despite significantly increased conjugate concentration (~ 10 times more than used for time-dependent studies) (Figure 4.13), this is unlikely. The macrophage has massive intracellular MR stores, which can be mobilised rapidly (Stahl et al., 1980). Conjugates were clearly internalised as derived cell association was almost completely inhibited at 4 °C. However no concentration dependent specific uptake was seen at below 0.4 μg/ml. This might indicate a large amount of non-specific uptake or that the MR were not adequately blocked by the mannan.

The picture is complicated. Although the differences between the conjugates may be exaggerated using the derived cell-associated fluorescence, the results still indicate enhanced uptake of the mannose targeted conjugates. The cells incubated with conjugates loaded with 2 - 6 mol % Man did not significantly different fluorescence values, however more cells took up the conjugates with 4 - 8 mol % Man and more rapidly (10 mins). The combined results showed that the derived cell association of HPMA copolymer-OG-Man was enhanced when the mannose loading was at 4 mol % and above (Figure 4.17a). This is consistent with Nan et al. (2004) who reported that 5 mol %, but not 2 mol %, mannose was sufficient for targeting. These observations here were also comparable to the studies of Duncan et al. (1986) that found ~ 4 mol % galactosamine was able to target the ASGPR. The MR is expressed on macrophages at a similar level (5 x 10^5 receptors/cell) to the ASGPR on liver cells. The MR-targeting residue was bound to the conjugate by a GFLG linker and therefore conjugate would be expected to release Man, leaving just the polymeric carrier. This would then be excreted rather than continually being targeted to more macrophages.

It was found that doubling the Man content of the conjugates produced more than a doubling of uptake by THP-1 cells. These observations correlate with studies that have shown that multiple Man residues are necessary for MR interaction (Mammen et al., 1998). The MR has multiple binding sites, as discussed earlier (Section 1.6). Ligand interaction via individual saccharide groups is of low affinity, but high affinity binding is achieved through multivalent cooperative binding. When multiple ligands are incorporated into one macromolecule, biorecognition and binding should be enhanced (Mammen et al., 1998). This has previously been described as the 'glycoside cluster effect' - affinity enhancement over and above what was expected from the increased concentration of sugar (Lee and Lee, 2000).

Oligomannosides with three branches have a greater inhibitory potency in preventing MR-mannan binding than linear oligomannosides or those with higher branching (Kery et al., 1992). It has also shown that the incorporation of trimannose residues stimulated endocytosis of FITC-dextran as well as increasing expression of other adhesion molecules and co-stimulatory molecules (Kanbe et al., 2001). When investigating specificity of HPMA copolymer-Dox-galactose conjugates, multivalent

'TriGal' targeting residues produced greatly increased biorecognition when compared to the galactose (David et al., 2004). Linking a trimannose residue to each HPMA copolymer-GFLG side chain may be a possible future method of increasing targeting efficacy.

When studying the uptake of HPMA copolymer conjugates the THP-1 derived cell-associated fluorescence was routinely measured in serum-free media. Serum has been shown to reduce uptake of mannose-targeted liposomes into mouse peritoneal macrophages in vitro, by competitively binding the mannose conjugate (Opanasopit et al., 2001). However, in these studies, serum competition for MR-specific binding was probably not important as there was no change in the relative difference between HPMA copolymer-OG and HPMA copolymer-OG-Man derived cell association when cells were incubated with or without serum. A general decrease in uptake of both conjugates was seen in the presence of serum but this was not specific to MR-mediated uptake. Reduced targeting via the MR was only seen after serum starvation, which is known to effect receptor expression, and may have reduced surface expression of the MR. There was also greatly enhanced non-specific cell-association, which could be attributed to the induction of apoptosis and loss of cell integrity rather than endocytosis.

4.5 Conclusions

In conclusion, a library of HPMA copolymers containing OG and mannose loadings of 2, 4, 6 and 8 mol % was synthesised and characterised. Although quantitative estimation of the Man content proved difficult, the theoretical values did seem to correlate with the biological properties. A Man content threshold of 4 mol % seemed to be necessary to achieve reproducible targeting. For this reason the HPMA copolymer-Man (4 mol %) conjugate was chosen to study further the intracellular trafficking (chapter 5) and for AmB conjugation (chapter 6).

Chapter 5

Intracellular fate of HPMA copolymer conjugates: Establishment of a subcellular fractionation method in THP-1 cells

5.1 Introduction

When polymer-drug conjugates are designed for intracellular delivery, it is important to study their intracellular trafficking. The MR-targeted anti-leishmanial drug conjugate, once endocytosed by the macrophage, must be able to access the PV and not be routed to the recycling/secretory pathways (Figure 5.1). The precise intracellular localisation of the conjugate and/or drug may also influence the choice of drug and linker. This would also depend on the drug's mode of action. Therefore, the aim of this study was to establish a subcellular fractionation (SCF) method that could be used to investigate, and ideally quantify, the intracellular trafficking of the MR-targeted HPMA copolymer-drug conjugates. Fluorescence microscopy was used to support these studies. The SCF method was set up in the uninfected THP-1 macrophage model, but with the aim of transferring the technique to the infected model (at LSHTM). It was hypothesised that if the conjugate was delivered to the PV, then it would directly access the parasite. However, if the conjugate was delivered to the lysosomal compartments, and the lysosomes did not fuse with the PV, it may then be necessary to include a linker that could release the drug here so it would diffuse to the PV.

5.1.1 Subcellular fractionation

Since the pioneering work in the 40's and 50's on cell fractionation, both cell fractionation and microscopy techniques have evolved side by side (De Duve & Beaufay, 1981). The first attempts to fractionate tissue or cells by applying sedimentation rates to separate organelles, used differential centrifugation (Bensley & Hoerr, 1934; de Duve, 1969; Hogeboom et al., 1948). Differential centrifugation involves homogenisation of tissue or cells in an isotonic solution (preventing vesicle ruption or changes in sedimentaion due to osmosis (Schneider, 1948)), and fractionation of the homogenate by means of successive centrifugations and washings. Increasing centrifugal force and centrifugation times can be used to yield fractions containing "nuclei", "mitochondria", "microsomes" and finally the cytosolic supernatant. Claude first investigated enzyme markers as a method to assess the purity each of the fractions and developed a 'quantitative' fractionation method (Claude, 1946a; Claude, 1946b).

Hogeboom with Kuff pioneered the use of density gradient centrifugation rather than differential centrifugation for quantitative fractionation of cells (Schneider &

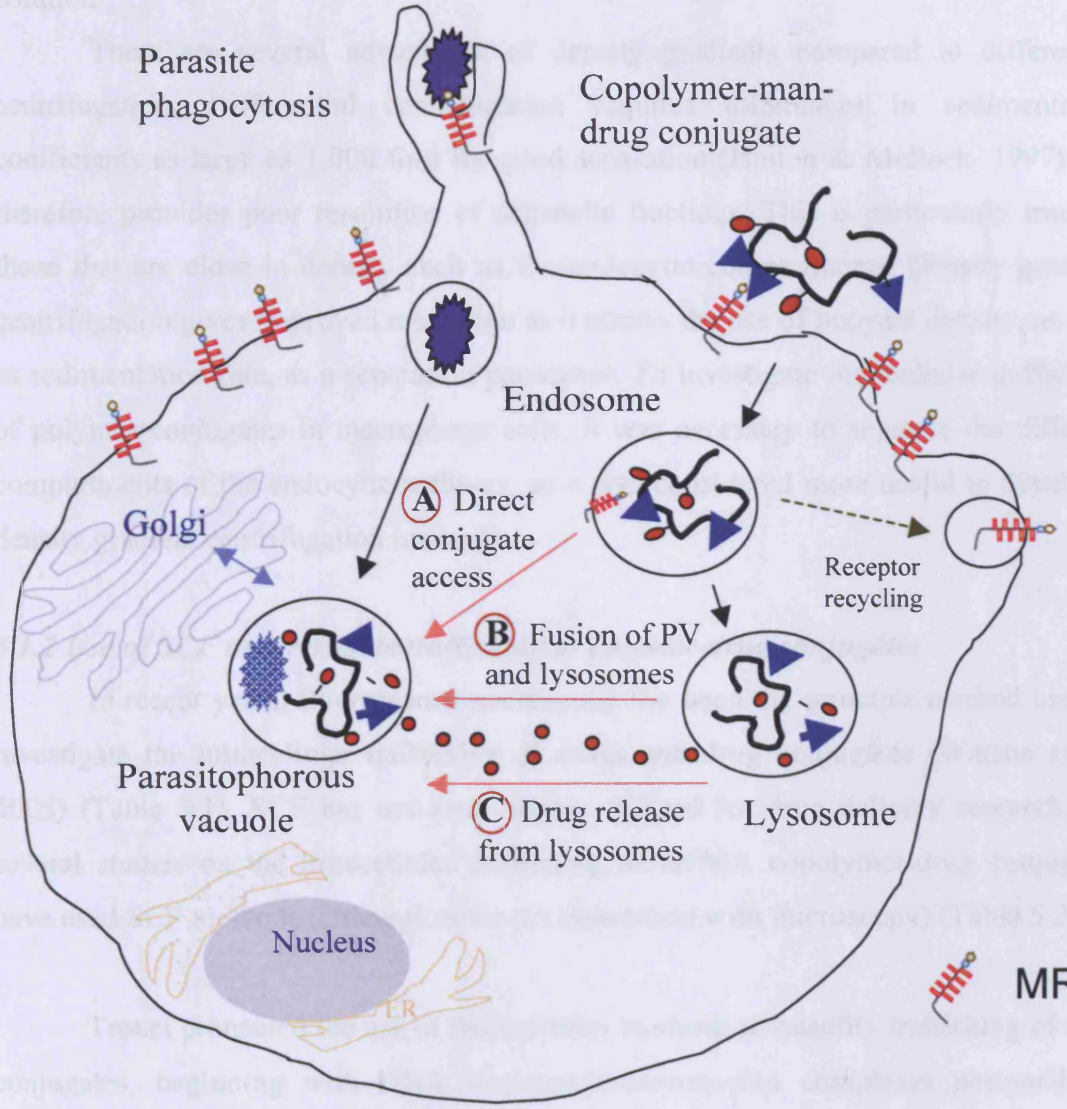

Figure 5.1 Potential intracellular fate of HPMA copolymer-drug conjugates.

Hogeboom, 1951). Generally, density gradient centrifugation uses isopycnic or equilibrium centrifugation. The solution is placed on top of the gradient and centrifuged at forces in excess of 150,000 x g. The organelles move through the gradient until they reach the point in the gradient at which their density matches that of the surrounding solution.

There are several advantages of density gradients compared to differential centrifugation. Differential centrifugation requires differences in sedimentation coefficients as large as 1,000 fold for good separation (Hinton & Mullock, 1997) and therefore provides poor resolution of organelle fractions. This is particularly true for those that are close in density such as the endocytic compartments. Density gradient centrifugation gives improved resolution as it allows the use of buoyant density, as well as sedimentation rate, as a separation parameter. To investigate intracellular trafficking of polymer conjugates in macrophage cells, it was necessary to separate the different compartments of the endocytic pathway, so it was considered more useful to develop a density gradient centrifugation method.

5.1.2 Use of SCF to investigate trafficking of polymer-drug conjugates

In recent years, fluorescence microscopy has been the principle method used to investigate the intracellular trafficking of drugs and drug conjugates (Watson et al., 2005) (Table 5.1). SCF has not been widely utilised for drug delivery research, but several studies on the intracellular trafficking of HPMA copolymer-drug conjugates have used SCF methods (although often in conjunction with microscopy) (Table 5.2).

Trouet pioneered the use of fractionation methods to quantify trafficking of drug conjugates, beginning with DNA-daunorubicin/adriamycin complexes designed for lysosomotropic delivery (Trouet et al., 1972). Early studies on HPMA copolymer-drug conjugates used subcellular fractionation to investigate their intracellular fate. Duncan et al. (1986) first demonstrated the fate of HPMA copolymer-drug conjugates (PK2) in liver cells using density gradient fractionation. They showed that, with time, the radiolabelled conjugate was transported to lysosomes and then Dox was released and accumulated in the nucleus. More recently, Nori et al., (2003a; 2003b) and Tijerina et al., 2001; 2003) have used density gradient centrifugation to study the fate of peptide-targeted HPMA copolymer conjugates of Dox or monoethylenediamine (Mce_6) in

Table 5.1 Intracellular trafficking studies using microscopy to monitor HPMA copolymer drug delivery systems

Conjugate	Methodology to investigate trafficking	Cell line	Reference
HPMA copolymer-ADR-GalN HPMA copolymer-ADR-OV-TL16	Live fluorescence microscopy and PFA fixed confocal microscopy (lysosomes labelled with neutral red or α_2-macrosialin)	HEP-G2 OVCAR-3	Omenyalenko et al., 1998
HPMA copolymer-Mce_6 -NLS	Live fluorescence confocal microscopy	A2780	Tijerina et al., 2003
HPMA copolymer-Dox-TAT HPMA copolymer-TAT	Live fluorescence confocal microscopy	A2780	Nori et al., 2003
HPMA copolymer-Dox	Fixed and live cell fluorescence and confocal microscopy (lysosomes labelled with FITC-Dextran)	B16F10	Seib et al., 2006

Table 5.2 Intracellular trafficking studies using SCF to monitor HPMA copolymer drug delivery systems

Conjugate	Methodology	Cell line	Reference
HPMA copolymer-Dox-Gal	Percoll density gradient, 26 fractions	Rat liver	Duncan et al., 1986
Cationic HPMA copolymer	Percoll density gradient	Rat Liver	McCormick et al., 1986
HPMA copolymer-Daunomycin-Gal	Differential centrifugation	Rat liver	Wedge et al., 1991
HPMA copolymer-Mce_6 -NLS	23 % Percol density gradient, 4 fractions	A2780	Tijerina et al., 2003
HPMA copolymer-Dox-TAT HPMA copolymer-TAT	23 % Percol density gradient, 4 fractions	A2780	Nori et al., 2003
HPMA copolymer-Dox	Differential centrifugation	B16F10	Seib et al., 2006

cultured A2780 ovarian carcinoma cells. These studies relied mainly fluorescence microscopy but they corroborated the results of cytosolic or lysosomal localisation by SCF. However, the fractionation method was limited as it only separated 4 fractions (lysosomal, plasma membrane, cytosolic and nuclear). Also, using these methods, they had poor resolution of the different endocytic compartments. Also, their studies used Percoll, a neutral, highly branched, high-mass, hydrophilic polysaccharide, which, although it can produce good purity of fractions, does not have good resolving power (Graham et al., 1994). A large overlap between mitochondria and lysosomes has been reported, with up to 50 % of the lysosomes being lost to the lower fractions (Arai et al., 1991).

These early studies demonstrate the potential of using SCF to monitor the intracellular fate of drug conjugates. Our group have recently been developing improved differential centrifugation (Seib et al., 2006) and density gradient (Manunta, 2007) methods with the specific aim of quantifying the intracellular distribution of polymer therapeutics.

Differential centrifugation of B16F10 cells showed quantitative and time-dependent accumulation of HPMA copolymer-Dox in lysosomes with subsequent transfer of free Dox to the nuclear fraction. The fractions were carefully characterised with high fraction purity (Seib et al., 2006). This study also underlined the unreliability of fluorescence microscopy due to both fluorescence quenching of Dox as a fluorophore, and the artefacts produced as a result of cell fixation. However, there was no separation of the endocytic compartments, the 'lysosomal' compartment likely also contained endosomes, mitochondria and peroxisomes. Subsequently, a novel density gradient centrifugation method was then developed in HepG2 cells as a means of gaining greater resolution of the endosomal compartments (Manunta, 2006). This density gradient subcellular fractionation, combined with fluorescence labelling of organelles, was also designed for characterisation of endocytic traffic of polymer therapeutics. However, it was clear from this study that further work was necessary to optimise separation of early endosomal and late endosomal/lysosomal compartments, and to apply the technique to polymer trafficking.

5.1.3 Advantages and disadvantages of SCF and fluorescence microscopy for drug/conjugate trafficking studies

SCF has a number of advantages compared to fluorescence microscopy. The limitations of fluorescence microscopy are mainly related to the lack of resolution and fluorophore-associated artefacts. Well-characterised SCF methods have the advantage that they can be used to quantitate drug trafficking and fate. Also, the results obtained can be more representative of the whole cell population rather than just the few cells visualised with a microscope. SCF is however not without its disadvantages. The methods must be tailored to each specific cell line used and there is a need to carefully characterise the fractions obtained. It is almost impossible to purify each organelle type to complete homogeneity. There is also a danger of vesicle rupture and redistribution of the contents. As well as being technically difficult, SCF is very labour intensive, and requires large numbers of cells. Despite this, it is the most simple and quantitative method by which to measure intracellular localisation of drugs and conjugates, and their redistribution with time.

5.1.4 Establishment of an SCF method in THP-1 cells to study intracellular trafficking of HPMA copolymer conjugates

It was decided here to develop the SCF method of Manunta et al. (2007) for uninfected THP-1 cells. It was hoped that this could then be used to monitor the trafficking of HPMA copolymer-OG-Man and later the HPMA copolymer-drug conjugates. Uptake mechanisms and endocytic compartmentalisation are highly complex, so it was hoped that a better picture of the intracellular trafficking should be obtained. Confocal microscopy techniques were also established for THP-1 cells (reported in Richardson et al., 2008) to allow comparison of the SCF results and the visual images.

First it was necessary to optimise the cell breakage. It was essential to achieve a high breakage efficiency so that the lysate was representative of the whole cell population. This must be done without disrupting the organelle structure. A ball bearing homogeniser (cell cracker) was used to achieve a reproducible, standardised homogenate, the breakage efficiency measured by the release of cytosol (Aubry & Klein, 2006; Manunta, 2007; Seib et al., 2006). Iodinated media in conjunction with

sucrose allows the required densities to be reached in media of lower viscosity and osmotic pressure than can be done with sucrose alone, resulting in good separation and little organelle damage. A density gradient of 5 – 20 % Optiprep (iodixanol solution) in a sucrose solution was chosen to allow sufficient separation of endosomes and lysosomes (Graham et al., 1994; Manunta, 2006).

It was essential to reliably identify the THP-1 fractions using organelle-specific markers. The enzyme assays chosen used here have been the standard for identifying subcellular fractions since the 50's, and were previously validated for linearity by Seib et al. (2006). The marker enzymes used were N-acetyl-β-glucosaminidase (lysosomes), alkaline phosphatase (plasma membrane) and lactate dehydrogenase (cytosol) as the assays are linear over a wide range of incubation times and protein content. There also appears to be little variation between different cell types (Seib et al., 2006; Tulkens et al., 1974). It was decided to use additional markers to label the endosomal compartments. Immunolabelling, common in fluorescence microscopy, can also be used to delineate the different endosomal compartments in the fractions.

The markers chosen were:

- Alkaline phosphatase (plasma membrane marker) (Graham, 1993).
- N-acetyl-β-glucosaminidase (late endosome/lysosome marker) (Klemm et al., 1998).
- Immunolabelling using a LAMP-1 antibody (late endosome/lysosome marker).
- A 5 min incubation with Texas Red labelled-Transferrin (Tf-TxR) (early endosome marker).
- Immunolabelling using EEA-1 antibody (early endosome marker).

Once the subcellular compartments within the fractions have been characterised, the distribution of HPMA copolymer-OG-Man conjugates, as described in Chapter 4, was investigated.

5.1.5 Establishment of a confocal fluorescence microscopy technique for THP-1 cells to study intracellular trafficking of HPMA copolymer conjugates

The distribution of HPMA copolymer-OG-Man conjugates was then visualised using confocal fluorescence microscopy. Many fixation techniques that permeabilise the membrane to allow antibody labelling lead to movement or loss of linear structures such as HPMA copolymers. Therefore, Texas Red-labelled BSA was used here to label the endocytic pathway and confirmed using antibody labels. Using a protein marker that can be endocytosed negates the need for antibody markers (Richardson et al., 2008).

5.1.6 Summary of aims

In summary, the specific technical aims were as follows:

- To establish a new density gradient SCF method for THP-1 macrophages
    - To optimise cell breakage and to ensure minimal lysosomal rupture by measuring the lactate dehydrogenase release.
    - To characterise the fractions obtained for the early endosomal markers Tf-TxR and EEA-1 antibody; and also the late endosome/lysosome markers N-acetyl-β-glucosaminidase and LAMP-1.
- To investigate the time-dependent trafficking of HPMA copolymer-OG-Man conjugates in THP-1 cells after 5 min, 4 h (1 h pulse with a 3 h chase) or 24 h incubations using the SCF method.
- To investigate the effect of leupeptin protease inhibitor on the distribution of the HPMA copolymer-OG-Man conjugates, and released OG using the SCF method.
- To establish fixation and confocal fluorescence microscopy techniques for THP-1 macrophages using BSA-TxR to label the endocytic pathway, and to visualise the localisation of the HPMA copolymer-OG-Man conjugates after a 4 h incubation.

5.2 Methods

5.2.1 Subcellular fractionation of THP-1 cells

5.2.1.1 Optimisation of cell breakage for THP-1 cells

The methods has been developed by Manunta et al. (2007) and Seib et al., (2006) showed that a 8.008 mm ball giving a clearance of 6 μm for the ball bearing in the cell cracker was ideal for cell breakage. It was decided to start with this and carefully validate it to ensure cells were broken, but organelles remained intact. The same number of cells (1 x 10^8) was used in each experiment. The THP-1 cell suspension was passed through the cell cracker (using the 6 μm gap ball) 1-20 times.

After each pass, a 100 μl aliquot was taken and placed on ice until all passes were complete. Then, 50 μl was used to assess the degree of cell breakage by measuring the lactate dehydrogenase release as described in section 2.3.5.1. Cell breakage was also assessed by eye using the light microscope coupled with a Trypan Blue exclusion assay (visible blue nuclei but no visible cells). Using the remaining 50 μl of the sample, the lysosomal breakage was assessed by measuring N-acetyl-β-glucosaminidase activity as described in section 2.3.5.3. The optimum number of passages through the cell cracker (10) was used in all subsequent fractionation experiments.

5.2.1.2 Gradient formation

The continuous gradients (5 - 20 % w/v Optiprep) were prepared in advance using a gradient master and cooled to 4 °C. Two ultracentrifuge tubes were etched at 5 ml using the marker block, one for the sample and one as a control. Solutions of Optiprep diluted in homogenisation buffer (HB) (comprising 250 mM sucrose, 6 mM EDTA, 60 mM HEPES, pH 7.4, and a 1 x protease inhibitor cocktail tablet) were made up at 5 % and 20 % Optiprep v/v. Then 5 ml of the 20 % Optiprep solution was layered under 5 ml of a 5 % solution using a syringe fitted with a long metal needle. The capped tubes were then placed into the automated gradient master which allows controlled mixing of the low- and high-density solutions by rotation at a preset angle of 80° at 17 rpm for 2 min.

5.2.1.3 Homogenisation and fractionation

The general procedure used is summarised in Figure 5.2. THP-1 cells were seeded at 10^6 cells per ml in five 150 cm^2 flasks and differentiated using PMA as

1. Cell harvest: washed with PBS (4˚C), scraped in 50 ml PBS, centrifuged (1200 rcf 5 min 4 ˚C) and resuspended in 1 ml HB

2. Breakage of cells: 10 passes through cell cracker, centrifuged (2000 rcf 2 min 4 ˚C) to remove nuclear pellet and obtain PNS

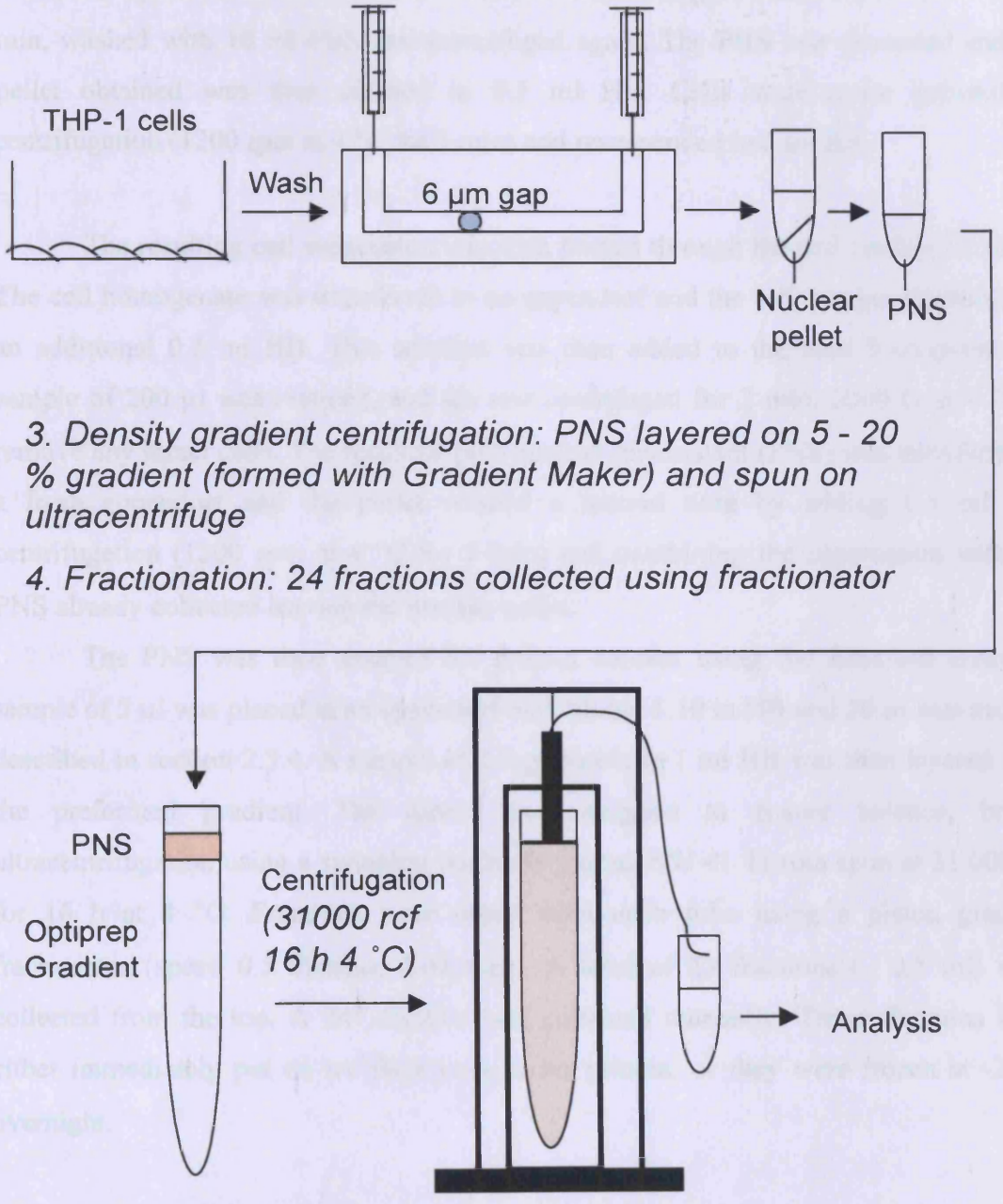

Figure 5.2 Scheme for fractionation scheme of THP-1 cells.

described previously (section 2.3.1.1). Cells were then washed three times with ice-cold PBS, leaving ~ 5 ml of fresh PBS in each flask. Cells were scraped using a cell scraper (or rubber policeman) and the flasks washed with 5 ml fresh PBS. The cell suspension were transferred from the flasks and pooled in a 50 ml falcon tube and the total volume was made up to 50 ml with PBS. The cells were centrifuged at 1200 rpm at 4 °C for 5 min, washed with 10 ml PBS and centrifuged again. The PBS was discarded and the pellet obtained was then washed in 0.5 ml HB. Cells were again pelleted by centrifugation (1200 rpm at 4 °C for 5 min) and resuspended in 1 ml HB.

The resulting cell suspension was then passed through the cell cracker 10 times. The cell homogenate was transferred to an eppendorf and the cell cracker washed with an additional 0.5 ml HB. This solution was then added to the total homogenate. A sample of 200 µl was retained, and the rest centrifuged for 2 min, 2000 G at 4 °C to remove any intact cells. The resultant post nuclear supernatant (PNS) was transferred to a fresh eppendorf and the pellet washed a second time by adding 0.5 ml HB, centrifugation (1200 rpm at 4 °C for 5 min) and combining the supernatant with the PNS already collected leaving the nuclear pellet.

The PNS was then assayed for protein content using the Bradford assay. A sample of 5 µl was placed in an eppendorf and diluted 1:10 in HB and 30 µl was used as described in section 2.3.4. A sample of 2 mg protein in 1 ml HB was then layered onto the preformed gradient. The tubes were weighed to ensure balance, before ultracentrifugation using a swinging bucket Beckman SW 41 TI rota spun at 31,000 rcf for 16 h at 4 °C. Fractions were taken from each tube using a piston gradient fractionator (speed 0.5 distance 3.41 mm). A total of 23 fractions (~ 0.5 ml) were collected from the top. A 24th fraction was collected manually. These fractions were either immediately put on ice then assayed for protein, or they were frozen at -20°C overnight.

5.2.1.4 Incubation of Tf-TxR protein marker in THP-1 cells to label the early endosomes

THP-1 cells were seeded at 10^6 cells per ml in five 150 cm^2 flasks and differentiated using PMA as described previously (section 2.3.1.1). Cells were washed with PBS, and then incubated with serum-free media with 0.2 % BSA for 20 min. To

label the early endosomes, cells were again washed with PBS then incubated with Tf-TxR (7.5 μg/ml) for 5 min before placing on ice. Cell homogenisation and fractionation was performed as described in section 5.2.1.3.

5.2.1.5 Measurement of the gradient density of the fractions

To determine the density profile of the gradient the blank gradient fractions (loaded with HB only) were measured using a refractometer. The refractive index, °Brix (which equates to % w/w sucrose) and the temperature of each sample was recorded. An adjustment was made to standardise the refractive index measurements for the temperature differences using the following equation (correction factor according to manufacturer):

$$(\text{temp} - 20) \times (7.8 \times 10^{-6}) + \text{measured R.I.} = \eta$$

The density was then be calculated using the following calculation:

$$\rho = A\eta - B$$

ρ=density (g/ml), η=refractive index (R.I.) and the value of A and B constants depending on the nature of the diluent used for preparing the solutions. In standard sucrose-iodixanol solutions A = 3.466 and B = 3.632 (Optiprep).

5.2.2 Characterisation of THP-1 cell fractions

5.2.2.1 Measurement of total protein and enzyme marker distribution in THP-1 cell fractions

The total cell lysate, PNS and all the fractions obtained from the gradient were assayed for total protein and marker enzymes. The total cell lysate and the PNS was diluted 1:10 in HB before use in the protein and enzyme assays. Enzyme assays can be carried out in the presence of Optiprep (Ford et al., 1994) and the activity of these enzymes in the presence of Tx-100 has been validated by Seib et al. (2006). Control samples (from the blank gradient) were included for each assay.

Protein recovery and distribution was assayed using 30 µl of the fractions or diluted cell lysate/PNS, and using the Bradford method as described in section 2.3.4.

The distribution of the cytosol marker lactate dehydrogenase was determined using 50 µl of the fractions or diluted cell lysate/PNS, as described in section 2.3.5.1.

The distribution of the plasma membrane marker alkaline phosphatase was determined using 25 µl of the fractions or diluted cell lysate/PNS, as described in section 2.3.5.2.

The distribution of the lysosomal marker N-acetyl-β-glucosaminidase was determined using 50 µl of the fractions or diluted cell lysate/PNS, as described in section 2.3.5.3.

5.2.2.2 Measurement of Tf-TxR protein marker distribution in THP-1 cell fractions

The fractions (50 µl) were resolved by SDS-PAGE as described in section 2.3.6. Following separation, the gels were directly placed on a Typhoon 9410 variable mode imager to detect TxR-Tf using the 532 nm excitation laser with 610 BP30 filter.

5.2.2.3 Measurement of antibody marker distribution in THP-1 cell fractions

Antibody markers were used as secondary markers for early endosome and late endosome/lysosome compartments. The fractions were again resolved by SDS-PAGE as described in section 2.3.6, and then transferred to nitrocellulose and labelled with antibodies using the western blotting procedure described in section 2.3.7. Primary antibody incubation was performed with α-EEA-1 (1:3000) and secondary antibody incubations were with Alexa 488 (1:1000). Alexa Fluor 488 was monitored using a 488 nm excitation with a 526 SP filter set on the Typhoon imager.

A semi-quantitative dot blot of the fractions was also performed as described in section 2.3.8 using 2 µl of the fractions or PNS (diluted 1:10) and an α-LAMP-1 antibody (1:1000 dilution). Secondary antibody incubations were with HRP conjugated anti-mouse antibodies (1:1000). HRP was monitored after incubation with ECL reagent for 5 min and exposure to film. The intensity of the band detected in each fraction was

quantified using Image J software (Rasband, 1997-2007) and the results expressed as the amount of fluorescence in each fraction as a percentage of the total fluorescence intensity.

5.2.3 Intracellular localisation of HPMA copolymer-OG-Man in THP-1 cells measured using SCF

THP-1 cells were seeded at 10^6 cells per ml in ten 150 cm^2 flasks and differentiated using PMA as described previously (section 2.3.1.1). The cells were then washed with PBS, the culture medium was aspirated and replaced with 10 ml of fresh RPMI media (10 % serum) containing HPMA copolymer-OG-Man conjugate (0.1 mg/ml). Cells were incubated for either 5 min (in 5 flasks) or a 4 h incubation (with 100 μM of the protease inhibitor leupeptin) (the remaining 5 flasks).

Following the incubation period, cells were placed on ice and cell homogenisation and fractionation was performed as described in section 5.2.1.3. The fractions obtained were immediately analysed for fluorescence. Samples of 100 μl were placed in a 96 well plate and measured using a fluorescence plate reader (excitation 480 nm and emission at 520 nm).

The above experiment was reproduced exactly, except the incubation times were adjusted to 24 h. The incubation was performed with (5 flasks) and without (5 flasks) 100 μM of leupeptin.

In addition, the cell culture media was collected after the 24 h incubation and free OG content was measured using a PD10 size exclusion column as described in section 4.2.5.

5.2.4 Confocal fluorescence microscopy imaging of HPMA copolymer-OG-Man in fixed THP-1 cells

A method was established to allow visualisation of HPMA copolymer-OG conjugates in fixed THP-1 cells that ensured retention of the water-soluble polymer with vesicles and avoided fixation artefacts (Richardson et al., 2008).

Cells were seeded at 5 x 10^5 cells/well on coverslips (ethanol immersed and washed in sterile PBS) in 6 well plates. To label the early endosomes and late

endosomes/lysosomes, THP-1 cells were incubated with 1 mg/ml BSA-TxR for either 5 min (to label the early endosomes) or a 1 h pulse with a 3 h chase (to label the late endosomes/lysosomes). The cells were subsequently washed 3 times with ice-cold PBS. Then the cells were fixed as described in section 2.3.9, and labelled with Tf-TxR (1:300), EEA-1 (1:600) and LAMP-1 (1:300) antibodies as described in section 2.3.10 (simplified scheme in Figure 5.3).

THP-1 cells were co-incubated with 1 mg/ml BSA-TxR and 1 mg/ml HPMA copolymer-OG-Man or HPMA copolymer-OG conjugates for a 1 h pulse with a 3 h chase. The cells were then fixed by incubation for 20 min in 3% w/v paraformaldehyde in PBS, and then washed 3 times with PBS.

The coverslips were mounted on slides with 40 µl Vectashield, the edges sealed with clear nail varnish, and stored at 4 °C for imaging within 72 h. Imaging was performed as described in section 2.3.11.

5.3 Results

5.3.1 Optimisation of cell breakage

Ten passes through the cell cracker gave a lactate dehydrogenase release of ~ 80 % (range 60 – 100 %) (Figure 5.4). Based on these results all subsequent cell lysates were prepared with 10 passes through the cell cracker. To ensure the organelles remained intact during cell breakage, at each pass the cell lysate was assayed for the lysosomal marker, N-acetyl-β-glucosaminidase. Though a small increase in lysosomal enzyme release was seen at each pass (0 - 0.5 nmol 4-methyumbelliferyl formed per fraction), this was negligible (~ 7 %) when compared to the total release seen with Triton X-100 (~ 6.8 nmol) (Figure 5.5).

5.3.2 Optiprep gradient

There was very high reproducibility of the gradient profile with respect to refractive index values of each fraction (Figure 5.6). While there was a slightly sharper increase in density in fractions 1–5, the gradient showed a near-linear increase in density (from 1.035 - 1.11 g/ml). As the last fraction was taken manually and had a non-

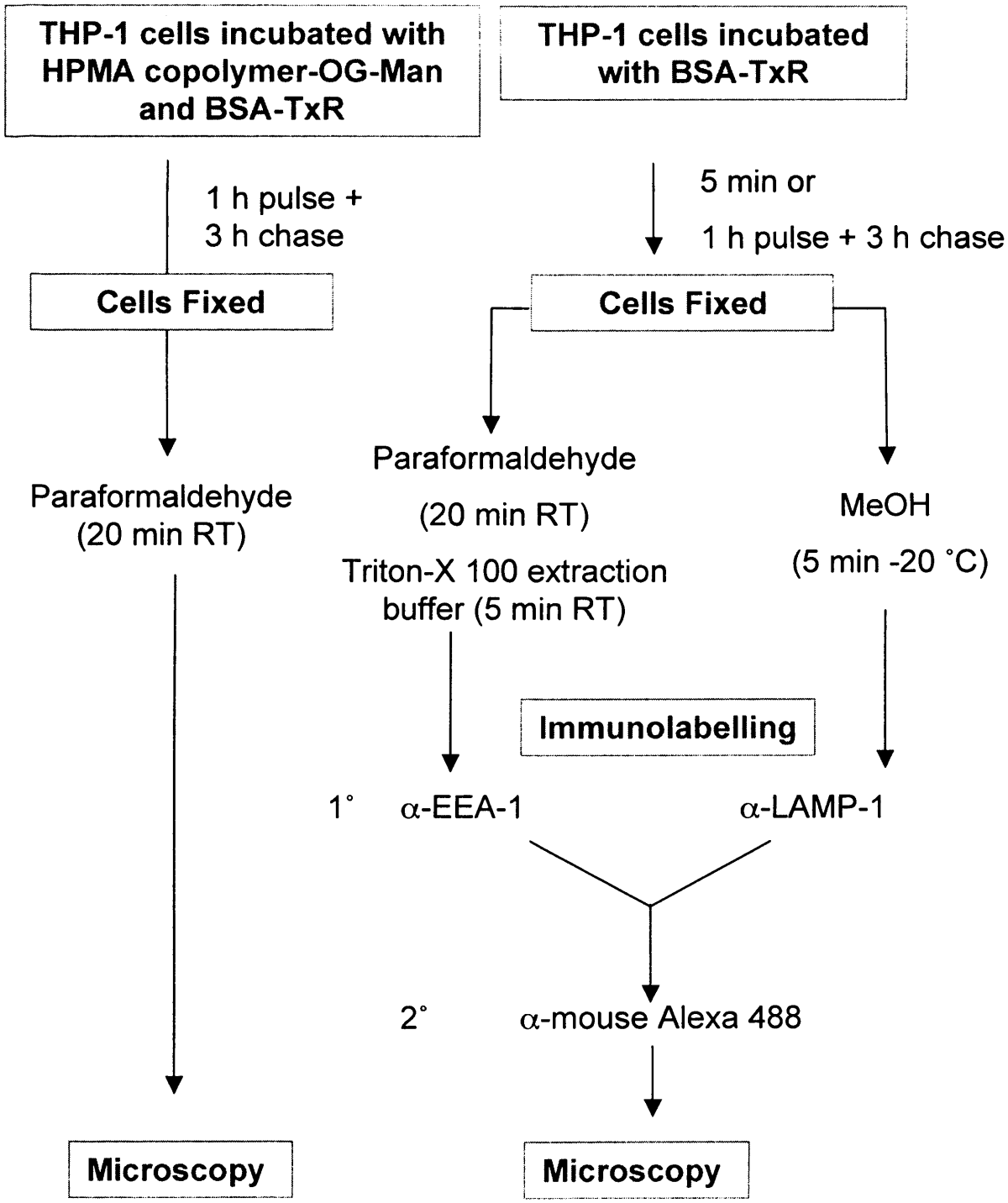

Figure 5.3 Scheme for confocal microscopy protocol. Incubation of THP-1 cells with BSA-TxR and/or HPMA copolymer-OG-Man, then fixation and co-labelling with EEA-1 and LAMP-1 antibodies used to label endosomes and lysosomes.

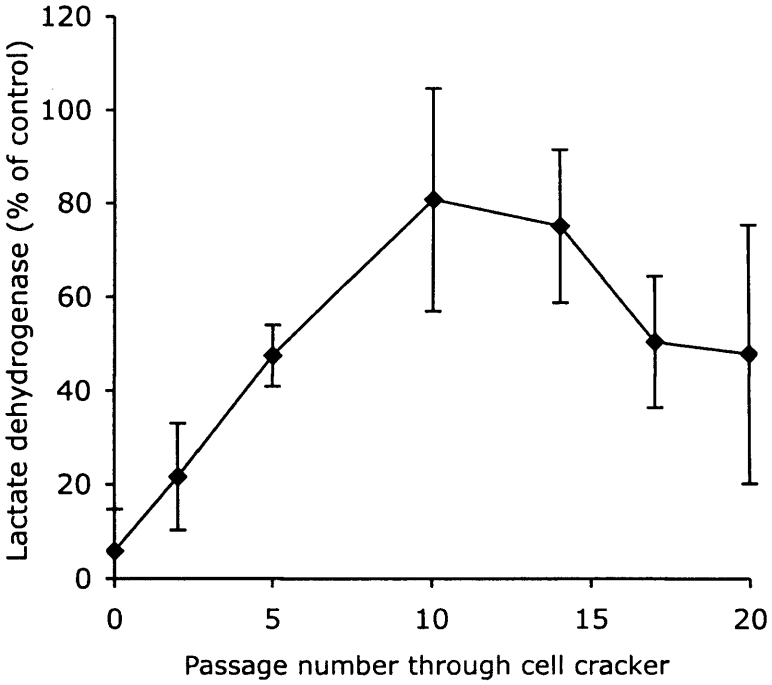

Figure 5.4 Optimisation of cell breakage of THP-1 cells. Effect of passage number through cell cracker on release of lactate dehydrogenase as a marker for cytosol. Data represent average ± S.D. (n=3).

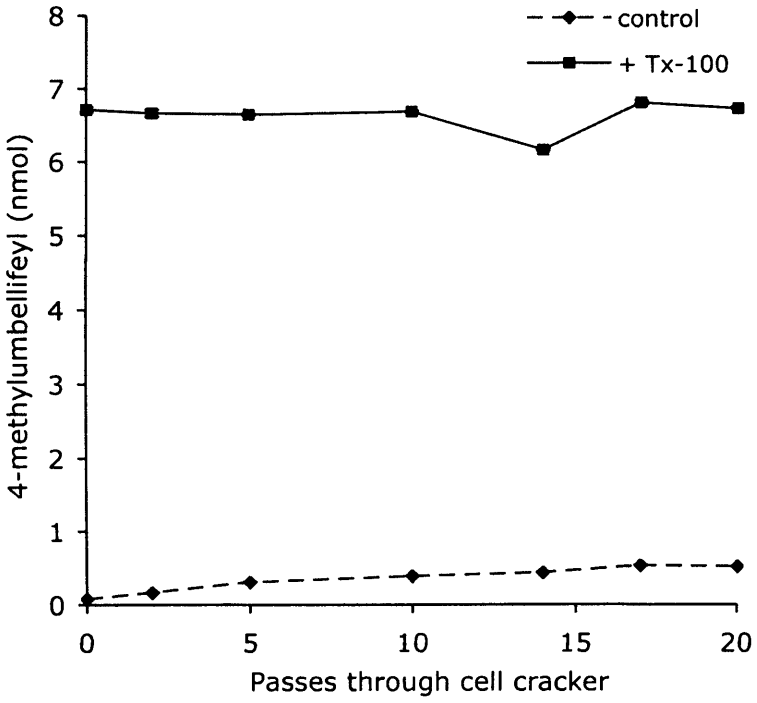

Figure 5.5 Effect of homogonisation and fractionation on lysosomal integrity of THP-1 cells. Lysosomal enzyme marker assay on homogenate after serial passes through cell cracker in the presence or absence of 0.1 % v/v Triton X-100 (n = 1).

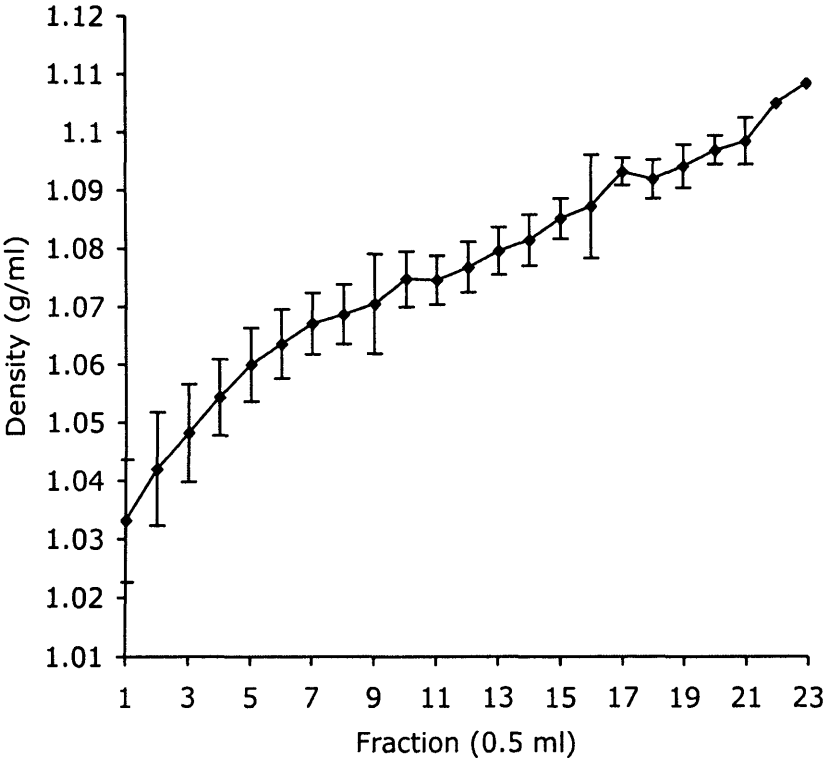

Figure 5.6 Gradient density of fractions calculated from the measured refractive index. Panel (a) shows profile of the total 24 fractions, panel (b) shows the profile with fraction 24 omitted. Data represent average ± S.D. (n=6).

linear increase in density with a large standard deviation, it was decided to exclude this fraction.

5.3.3 Characterisation of THP-1 subcellular fractions

The amount of total protein found in the PNS was between 2 – 5.2 mg/ml and the distribution between the fractions was reproducible. The gradient was loaded with 2 mg protein in 1ml of HB. There was between 20-300 μg of protein in each fraction with a distinct peak of protein content in fractions 2 - 8 (Figure 5.7).

The plasma membrane marker (alkaline phosphatase) was enriched in fractions 12 and 19 (Figure 5.8). The lysosomal marker (N-acetyl-β-glucosaminidase) displayed one major peak at fractions 14-18, though this was fairly broad, and a smaller peak in the lighter fraction 7 (Figure 5.9a).

When the N-acetyl-β-glucosaminidase content of the fractions was measured without Triton X-100, no enrichment was seen, with a basal level of about ~ 0.5 nmol (Figure 5.9b). With Triton X-100 was added the basal level was raised to about ~ 2 nmol and showed enrichment of about 4 times in fraction 17 (8 nmol). The dot blot for the lysosomal marker LAMP-1 showed a very broad peak with particular enrichment in fractions 14-16, and a smaller one in fraction 7 (Figure 5.10).

Cells that had been incubated with Tf-TxR for 5 min to label the early endosomes showed fluorescence as a single band at 80 kDa on the Typhoon imager after SDS PAGE. This was almost exclusively detected in fractions 4, 5 and 6 (Figure 5.11a). Antibodies used to probe for EEA-1 after western blotting detected a band at 180 kDa in fractions 4-10 (Figure 5.11b).

5.3.4 Intracellular localisation of HPMA copolymer-OG-Man using SCF

SCF of THP-1 cells after incubation with HPMA copolymer-OG-Man showed no alteration in the protein distribution in the fractions compared to the control (Figure 5.12). After a 5 min incubation, fluorescence was detected mainly in fractions 1-6 (50 % of the total fluorescence) with a small enrichment in fractions 12-22 (13 % of the total) (Figure 5.13).

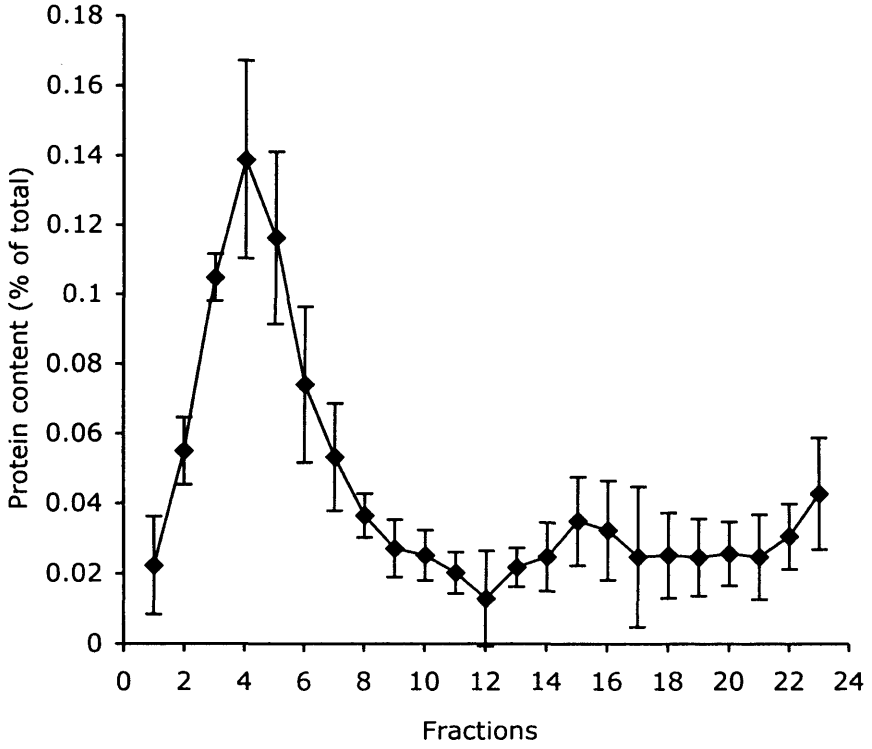

Figure 5.7 Protein content of THP-1 fractions. Measured using the Bradford assay, and displayed as a percentage of the total protein measured. Data represent average ± S.D. (n=5).

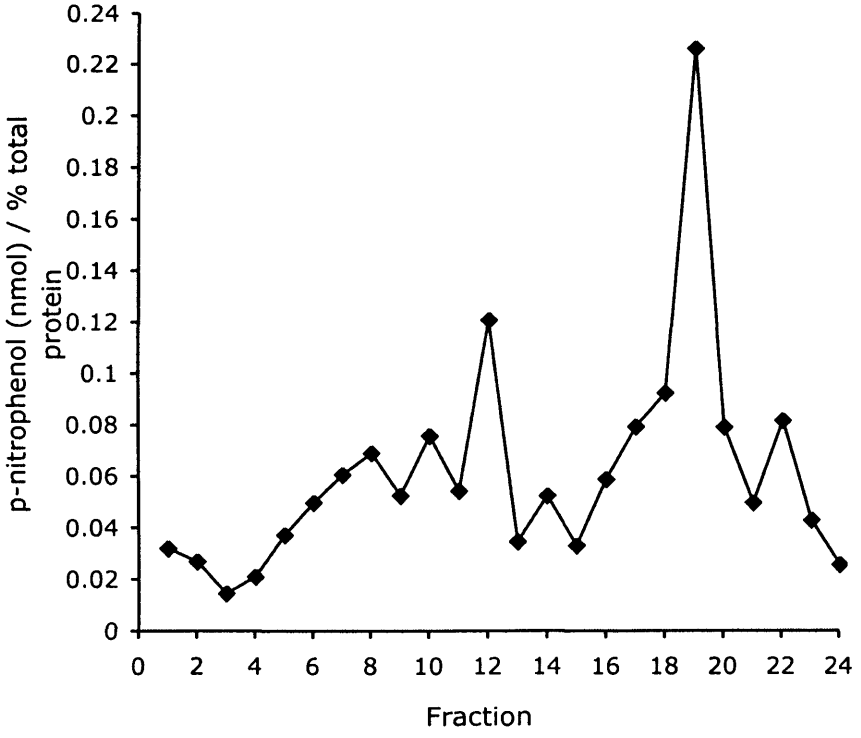

Figure 5.8 Enrichment in THP-1 fractions of plasma membrane (alkaline phosphatase assay) (n=1).

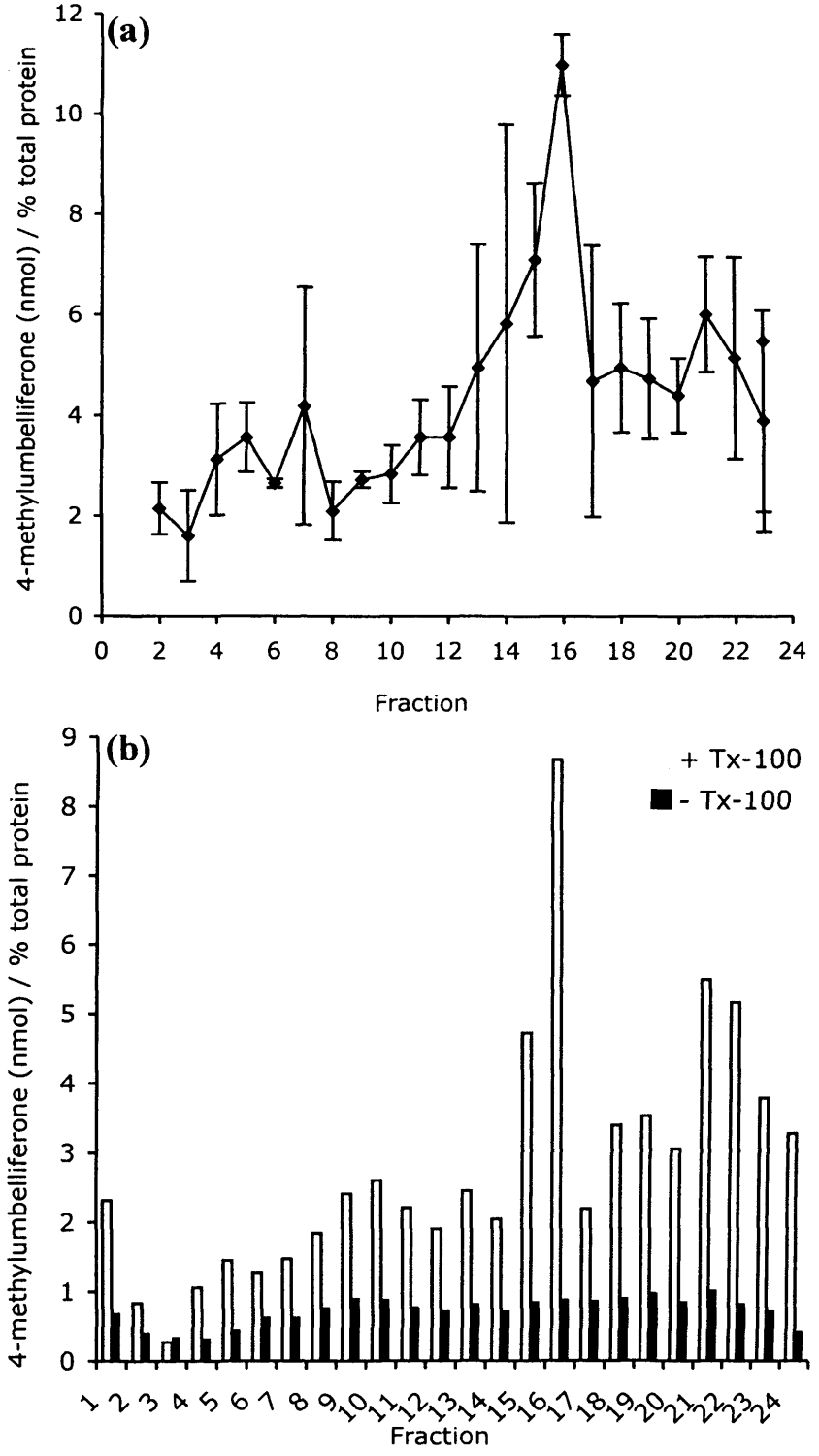

Figure 5.9 Enrichment in THP-1 fractions of lysosomes (N-acetyl-β-glucosaminidase assay). Panel (a) Lysosomal enzyme marker assay after fractionation. Data represent average ± S.D. (n = 3). Panel (b) shows the effect of homogenisation and fractionation on lysosomal integrity of THP-1 cells by performing the lysosomal enzyme marker assay after fractionation in the presence or absence of 0.1 % v/v Triton X-100 (n=1).

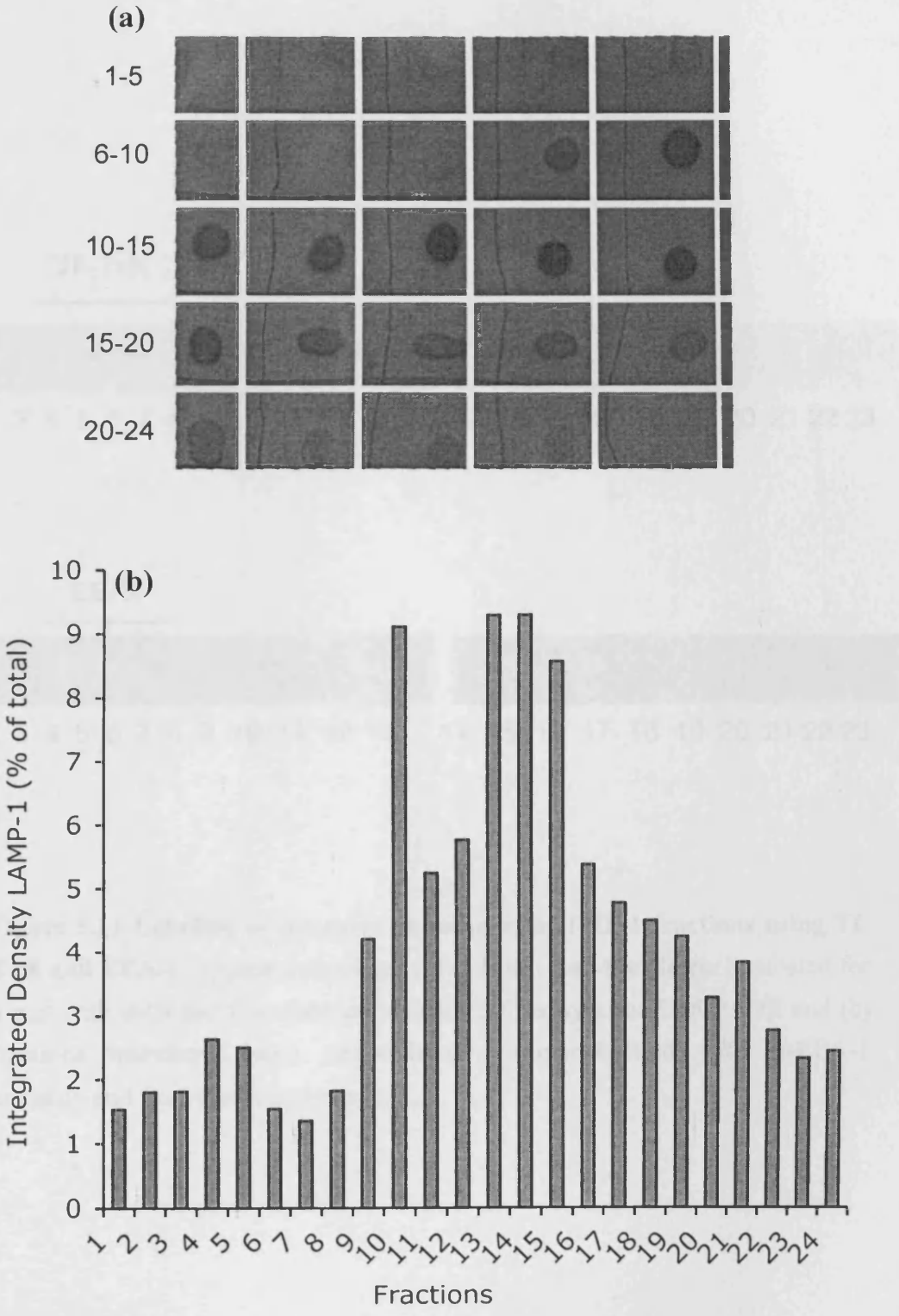

Figure 5.10 Dot blot of fractions with α-LAMP-1 antibody to determine lysosome distribution. Panel (a) dot blot (b) plotted integrated density of fractions (n=1).

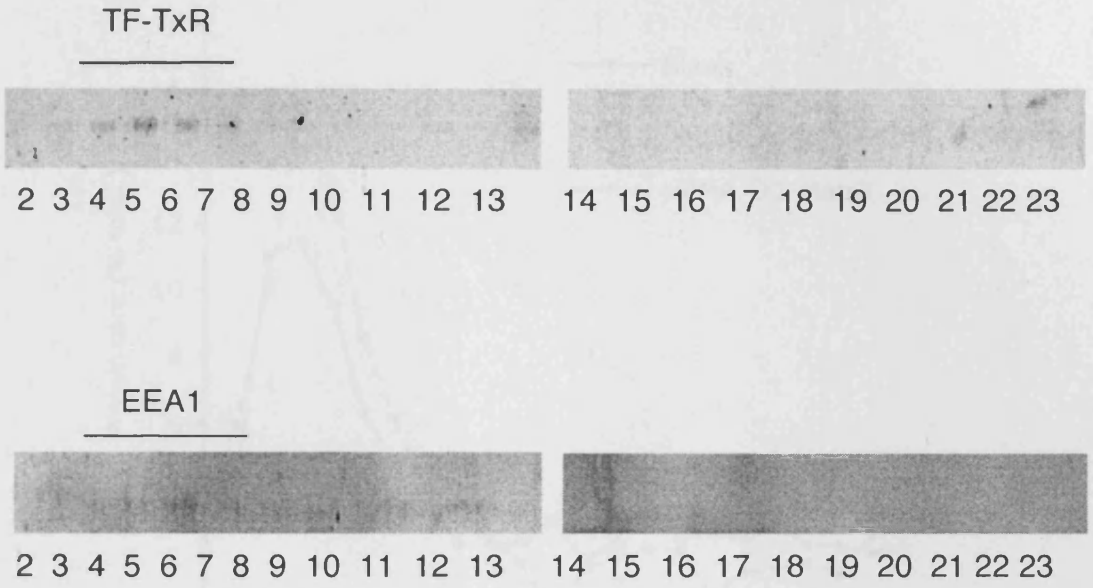

Figure 5.11 Labeling of the early endosomes in THP-1 fractions using Tf-TxR and EEA-1. Typical gels of panel (a) Texas Red-transferrin incubated for 5 min with cells and fluorescence visualised directly after SDS PAGE and (b) fractions transferred onto nitrocellulose, immunoblotted with α-EEA-1 antibody and fluorescent secondary.

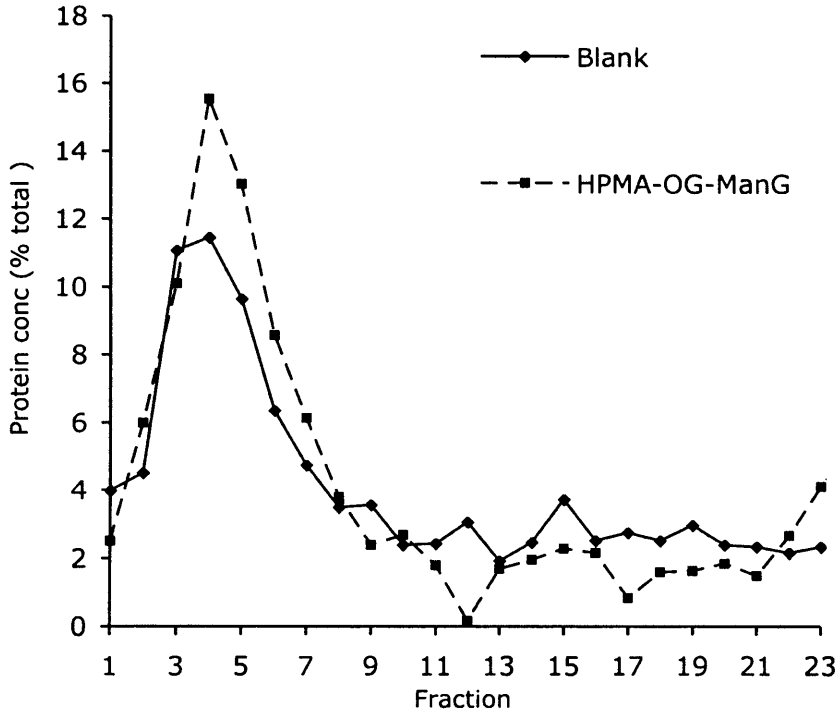

Figure 5.12 Distribution of protein in THP-1 cell fractions after 1 h incubation with HPMA copolymer-OG-Man. Protein measured in both control cell fractions (average ± standard deviation n = 3) and and those incubated with HPMA copolymer-OG-Man (n = 1) for 24 h using the Bradford assay and displayed as a percentage of the total protein measured.

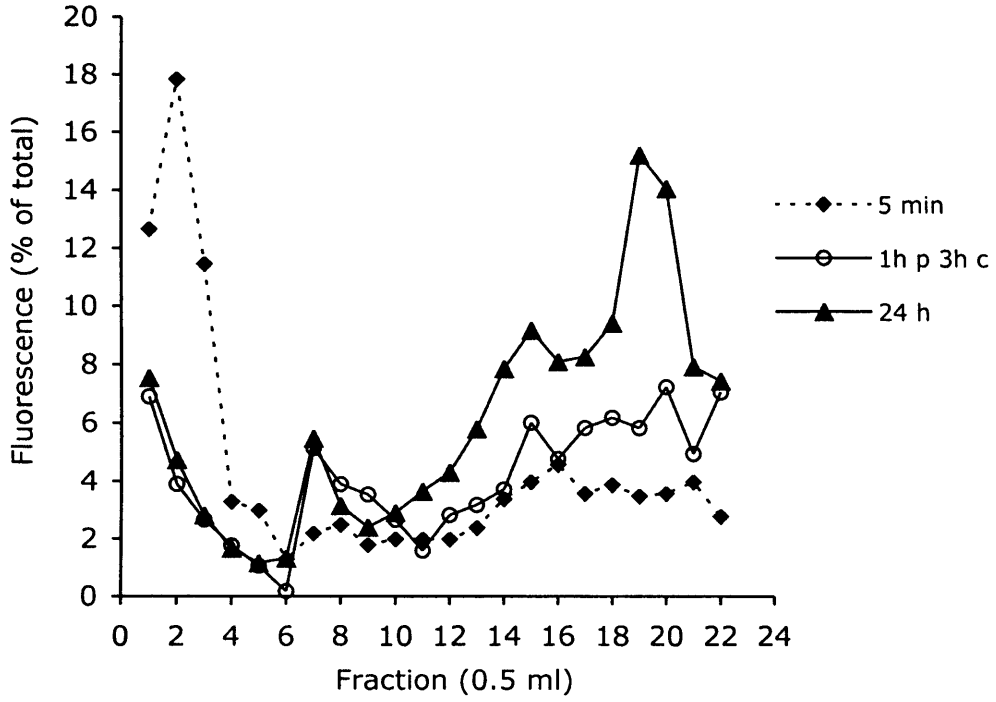

Figure 5.13 Time dependence of HPMA copolymer-OG-Man distribution after incubation in THP-1 cells. THP-1 cells were incubated for 5 min, 1 h pulse with a 3 h chase or for 24 h (with 100 μM leupeptin) before fractionation (n=1).

However, after a 4 h incubation, this pattern was reversed and the fluorescence was shifted to the later fractions. There was a small enrichment in fractions 1-6 (15 % of the total), but fluorescence was mainly seen in fractions 12-22 (66 % of the total). A smaller peak was also seen in fraction 7. This distribution of HPMA copolymer-OG-Man correlated well with the lysosomal markers N-acetyl-β-glucosaminidase and LAMP-1.

The distribution of fluorescence after a 24 h incubation showed a similar pattern to that seen in the cells after a 4 h incubation. There was enrichment in fractions 12 – 22 (71 % of the total), but showed a slightly greater accumulation in fractions 19 and 20, and a peak at fraction 7. However, when the cells were incubated with HPMA copolymer-OG-Man in the absence of leupeptin for 24 h, the fluorescence was mainly detected in the first 6 fractions (~50 % of the total) (Figure 5.14).

The amount of free OG in the media before incubation with THP-1 cells was 2.8 %. After 24 h incubation in the presence of leupeptin this had increased to ~ 30 % free OG. After 24 h incubation of cells with HPMA copolymer-OG-Man in the absence of leupeptin there was ~ 60 % free OG (Figure 5.15). This indicates OG is released from the conjugate over 24 h.

5.3.5 Intracellular localisation of HPMA copolymer-OG-Man using confocal fluorescence microscopy

When THP-1 cells were incubated with BSA-TxR the fluorescence was seen in distinct vesicular structures (Figures 5.16 and 5.17). After a 5 min incubation, BSA-TxR co-localised with EEA-1 and partially with Tf-TxR, but not with LAMP-1 (Figure 5.16). After the 4 h incubation BSA-TxR co-localised with LAMP-1 but not with EEA-1 or Tf-TxR (Figure 5.17).

When THP-1 cells were incubated with HPMA copolymer-OG and HPMA copolymer-OG-Man conjugates and BSA-TxR for 4 h they had completely co-localised in the lysosomal structures (Figure 5.18). No evidence of plasma membrane, nuclear or cytosolic labelling was seen. There was no difference in localisation between the conjugates ± Man.

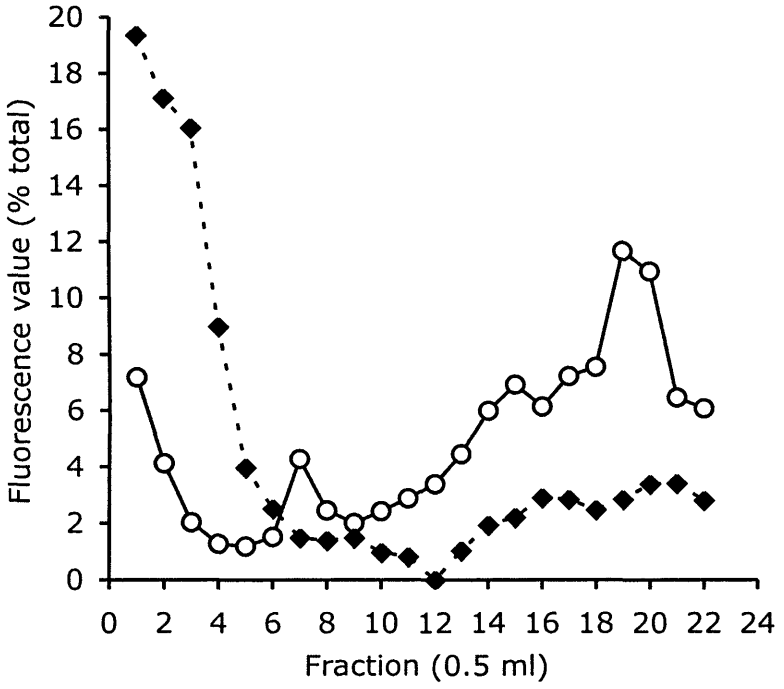

Figure 5.14 Distribution of fluorescence in THP-1 cell fractions after 24 h incubation with HPMA copolymer-OG-Man (± leupeptin). The dotted line represents fluorescence of fractions without leupeptin and solid line with 100 μM leupeptin (n=1).

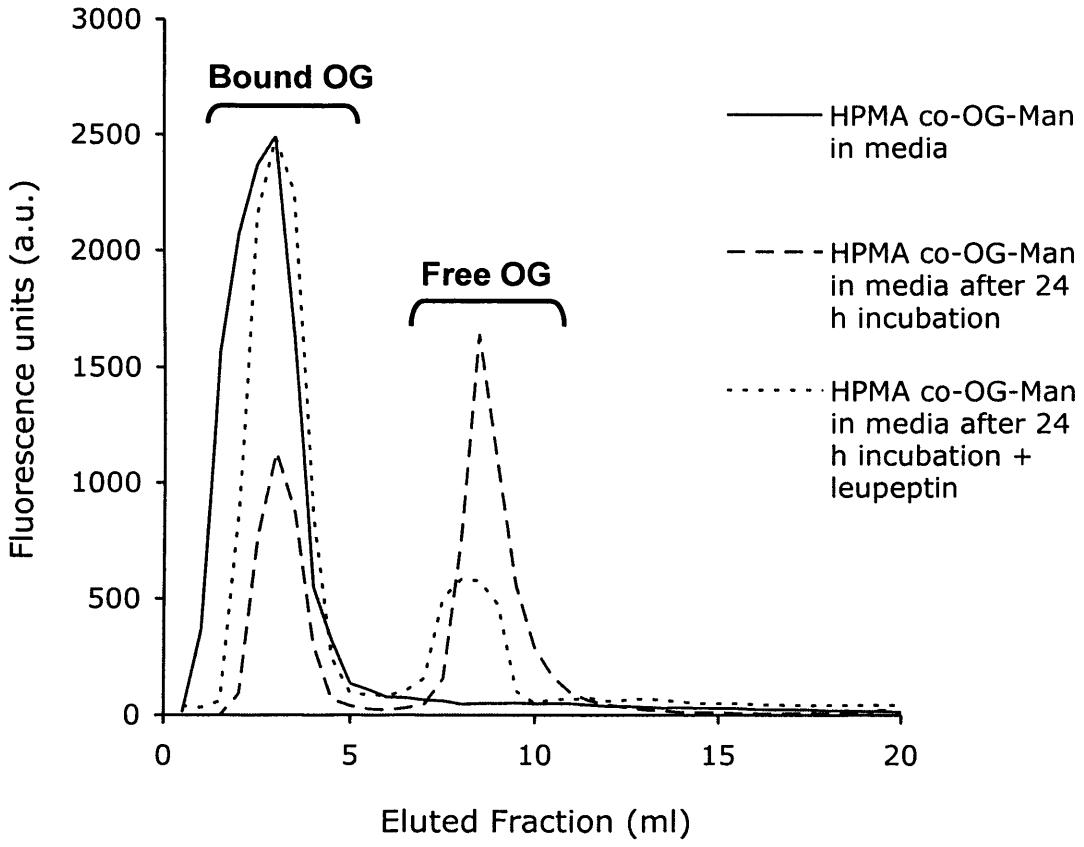

Figure 5.15 PD10 chromatography of tissue culture media obtained after a 24 h incubation of HPMA-OG conjugates with THP-1 cells. PD-10 profiles of HPMA copolymer-OG-Man conjugate after 24 h incubation with THP-1 cells (± leupeptin) at 37 °C were obtained by elution in PBS and the fractions collected were assayed for fluorescence measured (Abs 494 nm Em 520 nm).

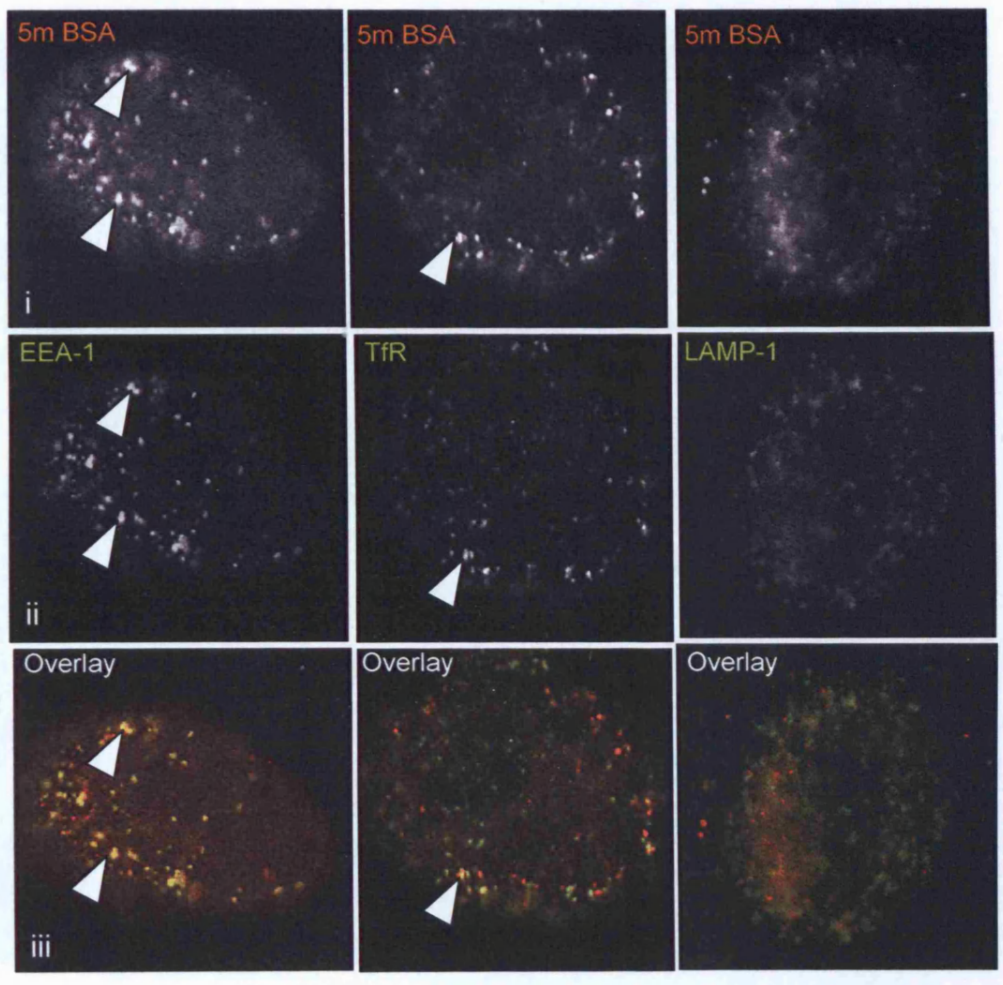

Figure 5.16 Representative confocal images of fixed THP-1 cells to demonstrate BSA-TxR-labeled early endosomes. Cells were incubated with BSA-TxR for 5 min and co-labeled with endosome (EEA-1 and Transferrin) and lysosome (LAMP-1) markers. Examples of co-localisation between compartment marker and BSA-TxR are indicated using white arrows.

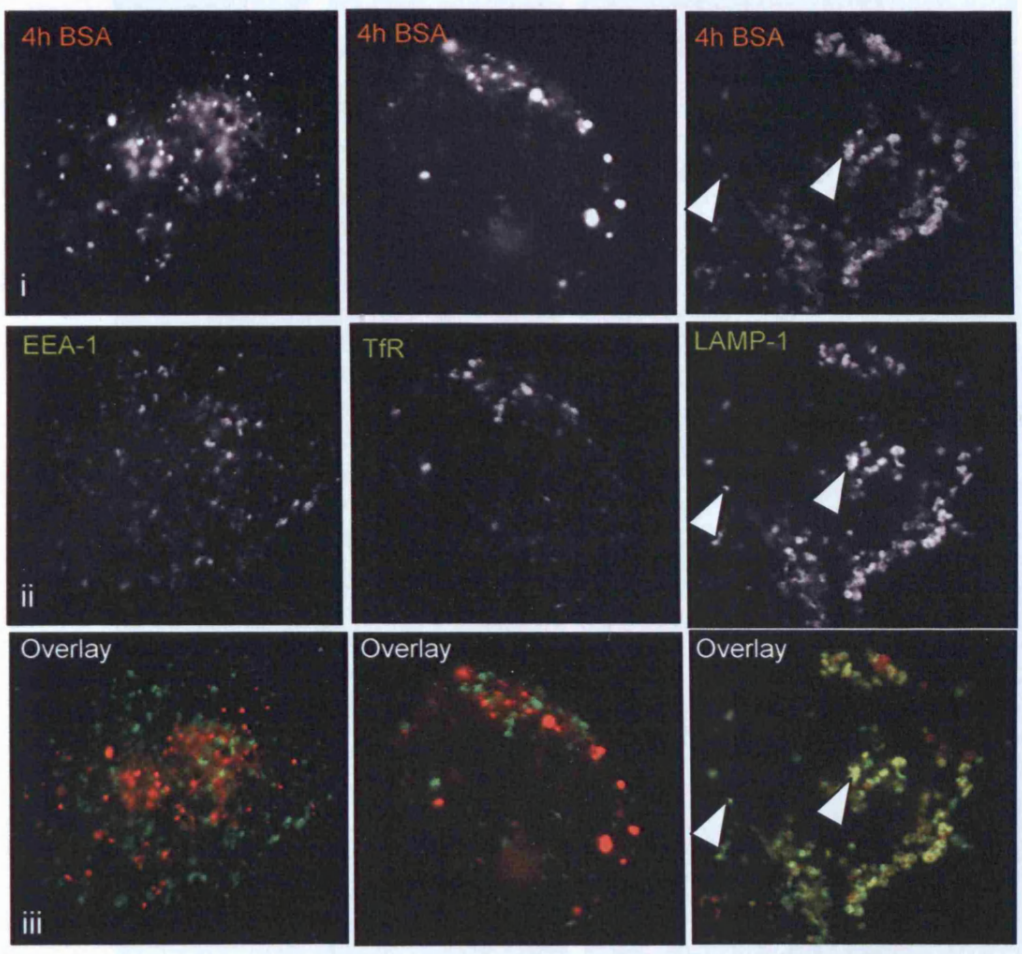

Figure 5.17 Representative confocal images of fixed THP-1 cells to demonstrate BSA-TxR-labeled lysosomes. Cells were incubated with BSA-TxR for 1 h (plus 3 h chase) co-labeled with endosome (EEA-1 and Transferrin) and lysosome (LAMP-1) markers. Examples of co-localisation between compartment marker and BSA-TxR are indicated using white arrows.

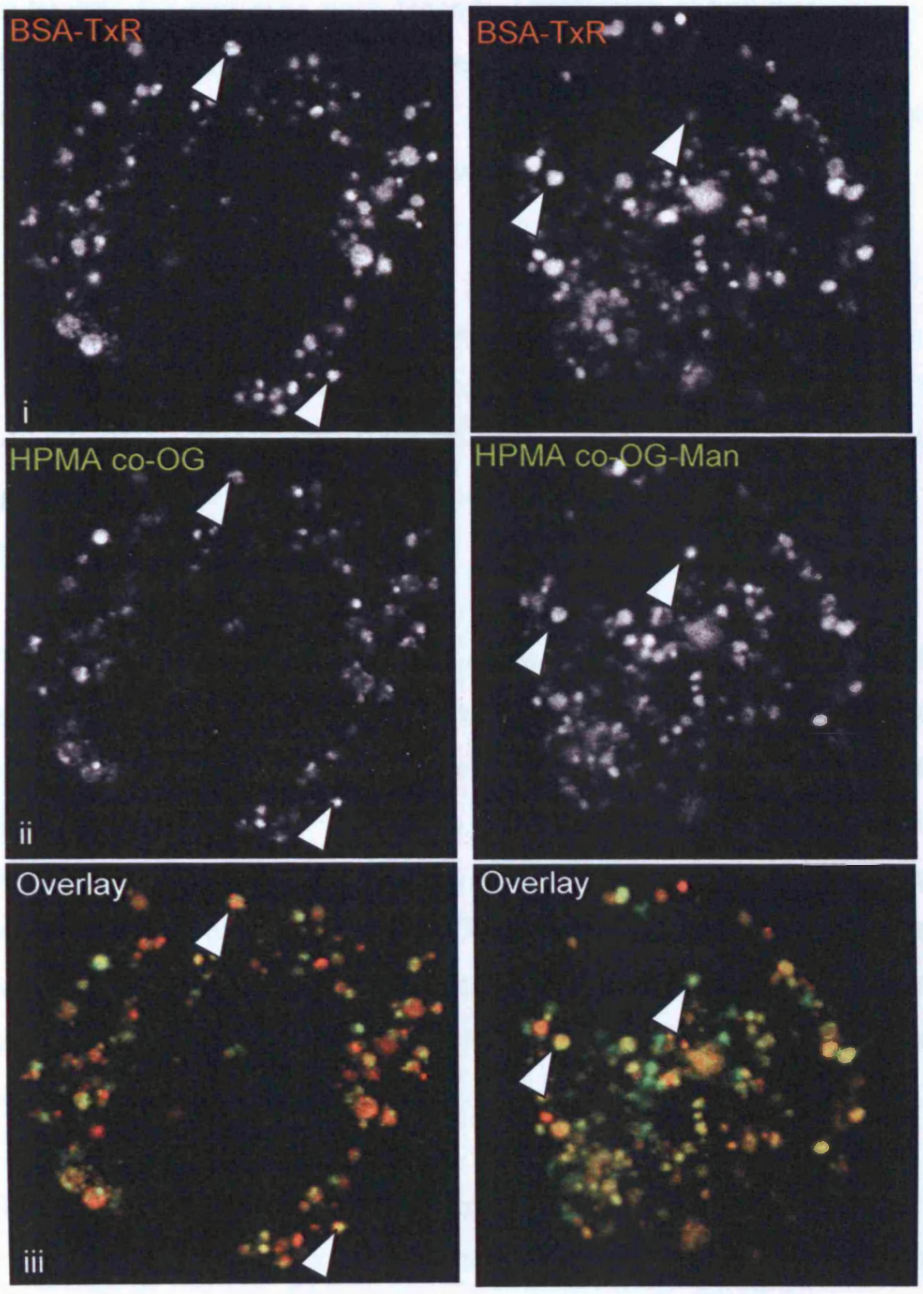

Figure 5.18 Investigation of the effect of Man on the intracellular localisation of HPMA copolymer-OG ± Man conjugates after 1 h (plus 3 h chase) in THP-1 cells with BSA-TxR labeled lysosomes. Examples of co-localisation between endocytic probe (BSA-TxR) and HPMA copolymer-OG are indicated using white arrows.

5.4 Discussion

5.4.1 Establishment of an SCF method for THP-1 cells

A novel quantitative fractionation method has been developed for THP-1 cells, which can be used to investigate time-dependent trafficking of polymer conjugates and potentially other drug delivery systems. Knowing that liposomes, lipidic carriers and nanoparticles are being widely explored as drug delivery systems for anti-leishmanial drugs this method could provide useful comparisons.

The average cell breakage efficiency was > 80 % after 10 passes through the cell cracker. The apparent breakage decreased with greater than 10 passages. This may be due cell damage and/or to release of organelle contents and inhibition of enzyme activity, despite the presence of protease inhibitors in the medium. Also, the lysosomes were largely intact after 10 passes therefore this protocol was used for all further experiments.

The Optiprep density gradient was linear and reproducible (Figure 5.6). This was important as it is necessary to ensure a reproducible separation of the cell components. The density gradient used here was found to be different to that reported by Manunta et al. (2007). Even though the density range was similar (from 1.035 to 1.11 g/ml compared to 1.045 – 1.11 g/ml), Manunta et al. (2007) reported a gradient profile that was steeper at higher density. This would be a limitation, as organelles of similar density (the early endosomal and late endosomal/lysosomal fractions) would not be easily separated. The linear gradient achieved here gives better separation of organelles at higher densities.

The protein content of the homogenate varied between ~ 2 and 5 mg/ml, therefore it was decided to use a constant amount of protein for the SCF (2 mg in 1 ml). This was applied to each gradient, and the distribution of protein subsequently obtained in the fractions was very reproducible, with the low-density fractions containing most of the protein (Figure 5.7). This was probably cytosolic. This protein distribution profile for THP-1 cells also differed from that reported by Manunta et al. (2007) for the HepG2 cells. They found a second, higher, protein enrichment in the heavier fractions (16 - 18), close to the lysosomal marker (N-acetyl-β-glucosaminidase) enrichment.

The plasma membrane marker (alkaline phosphatase) mainly showed enrichment in the later fraction (19) (Figure 5.8). This did not correspond to the cytosol or early endosomes. The peak showed a similar distribution to, but at a slightly higher density than, the late endosomes/lysosomes. Previous studies have shown that larger fragments of plasma membrane, possibly reformed into vesicles can be present depending on the cell type and homogenisation method used (Tulkens et al., 1974). However, this assay was only performed on one fractionation experiment, and would need to be repeated to confirm the enrichment.

The LAMP-1 antibody staining and N-acetyl-β-glucosaminidase enzyme activity showed the same distribution throughout the fractions (Figures 5.9 and 5.10). They both co-localised in the higher density fractions. Importantly, the lack of enrichment when Triton X-100 was absent showed that the lysosomes were intact after homogenisation and fractionation.

The lysosomes were recovered over a broad banding density of 1.07-1.11 g/ml (Figures 5.9 and 5.10), in agreement with the pattern reported by Manunta et al. (2007) (1.07 – 1.12 g/ml). A broad banding density for lysosomes was also reported by Graham et al. (1994) when using mouse liver separated on self-generated Optiprep gradients (1.10 – 1.13). The recovery of lysosomes over a broad density range may be due to the fairly shallow gradient, and/or the heterogeneity of the vesicles. The second peak, seen with both lysosomal markers, was at a much lower density (fraction 6/7, ~1.065 g/ml). However, this was at a higher density than early endosomal peak, and therefore unlikely to be cytosolic. Also, enrichment was seen in the same fractions using both the late endosome/lysosome markers, the membrane bound LAMP-1 and the intracellular enzyme N-acetyl-β-glucosaminidase.

The endocytic compartments are complex, with continuous fusion producing heterogeneity in the organelles population. For example, transient hybrid organelles, with intermediate densities between endosomes and lysosomes, have been reported, and may account for the apparent lysosomal enrichment in fractions of different densities (Mullock et al., 1998).

Both the early endosome markers (Tf-TxR and EEA-1) were found in fractions of a low density (~ 1.05 g/ml) (Figure 5.11). Using the HepG2 cells Manunta et al.

(2006) had reported EEA-1 localised in the same density fractions, but they had also found EEA-1 in higher density fractions. However Tf-TxR was found only in the lower density fractions. EEA-1 is cycled on and off the endosomal membrane, so a proportion will be cytoplasmic. In their study the lower density fraction was therefore attributed to the cytosolic portion of EEA-1, and the higher density fraction to the membrane-bound portion. In fact, two distinct, high and low density populations of early endosomal markers have been shown in previous studies (Chin et al., 2001; Hamasaki et al., 2004; Sheff et al., 1999). Surprisingly, in the present study using THP-1 cells, the Tf-TxR positive fractions co-localised with the EEA-1 positive fractions at low density, and no fluorescence was seen in the higher density fractions. Therefore, it was assumed that the low-density EEA-1/Tf-TxR positive fractions were not cytosolic and contained early endosomes.

Using the markers chosen, it was possible to clearly identify the early endosomes and the late endosomal/lysosomal compartments, and these were well differentiated.

5.4.2 Investigation of intracellular localisation of HPMA copolymer-OG-Man using SCF

The SCF method was able to show the time-dependent trafficking to lysosomes of the HPMA copolymer-OG-Man conjugates in THP-1 cells incubated with leupeptin. After a 5 min incubation, the conjugate was co-localised with the early endosomal markers, although there was also a small amount of conjugate found in the later fractions. It is unlikely that the fluorescence seen after 5 min was cytosolic as this would require free OG to have been released from the polymer. At this time it also did not co-localise with the plasma membrane enrichment. Therefore the conjugate appeared not to be surface bound. Consistent with the SCF, the microscopy also showed clear vesicular accumulation after 5 min.

After either a 4 h incubation, or a 24 h incubation, of THP-1 cells with the conjugate the distributions of fluorophore seen using SCF were very similar (Figure 5.13). The conjugate was transferred to lysosomes within 30 – 60 min. There was no change in distribution after 24 h compared to the 4 h, except there was a more

pronounced peak in the higher density fractions (late endosomes/lysosomal compartments), as would be expected. The total accumulation of conjugate in the lysosomes would be expected to be much greater after the longer continuous incubation unless there was degradation and/or exocytosis occurring. As shown by the analysis of free OG in the incubation medium, ~ 30 % of the total OG was released from the cells after 24 h, indicating degradation and exocytosis. The uptake of the conjugates measured using flow cytometry (Fig 4.16), showing that uptake slowed over the 1 h incubation, although it did not reach a plateau, consistent with these SCF results.

Seib et al. (2006) reported that after incubation of B16F10 murine melanoma cells with PK1, using differential centrifugation, the lysosomal accumulation was calculated to show a 3-5 times enrichment of Dox. The uptake of HPMA copolymer-OG-Man is receptor-mediated and therefore showed greater accumulation than the studies on non-specific fluid-phase uptake. The lysosomal enrichment would therefore be highly significant.

To study cleavage of the HPMA copolymer-GFLG side chain, free OG could be viewed as a drug model. When THP-1 cells were incubated with HPMA copolymer-OG-Man without leupeptin in the medium, the distribution of fluorescence after a 24 h incubation was very different from the distribution when leupeptin was included (Figure 5.14). In fact, the distribution was almost indistinguishable from that seen after a 5 min incubation (thought to be early endosomal). There was however a reduction in fluorescence in the first fraction. As there was no chase time, there would presumably be some fluorescence (HPMA copolymer-OG-Man) in the early endosomes, as well as some free OG in the cytoplasm. However, the amount of OG fluorescence in the early endosomes would be expected to be relatively small in comparison to the total cellular fluorescence. Therefore it is suggested that the fluorescence found in the early fractions after 24 h incubation is mainly cytosolic. Using a pulse-chase in this experiment would have perhaps helped delineate the two from each other, however the measured free OG content of 60 % confirms that significant OG release has occurred. Together these experiments indicate that side chain cleavage occurred and resulted in OG escape from the lysosome into the cytoplasm and out of the cell.

The results obtained here show trafficking of HPMA copolymer-OG-Man conjugates to lysosomes and this is consistent with previous studies on HPMA copolymers. As discussed earlier, Duncan and colleagues first demonstrated the time-dependent lysosomal transfer of ^{125}I-labelled HPMA copolymer-galactose in rat liver cells using a density gradient fractionation method (Duncan et al., 1986). After 10 min radioactivity was recovered in fractions that contained the plasma membrane marker enzyme 5'-nucleotidase (densities of approximately 1.03-1.05 g/ml), thought to represent the early endosomal vesicles. After 60 min there was an obvious shift of radioactivity into heavier fractions (density of approximately 1.10 g/ml) that contained arylsulphatase and therefore thought to represent secondary lysosomes. Time-dependent delivery to lysosomes has also been demonstrated for HPMA copolymer-daunomycin conjugates in rat liver cells (Wedge et al., 1991).

Tijerina et al. (2001; 2003) and Nori et al. (2003a; 2003b) used SCF to study the fate and drug release from HPMA copolymer-Dox conjugates targeted with TAT peptide, and HPMA copolymer-Mce_6 conjugates targeted with NLS, in A2780 ovarian carcinoma cells. They found that after 4 h, 90 % of the HPMA copolymer-GG-FITC conjugates without a targeting residue were endocytosed and localised to the lysosomes. However, the HPMA copolymer-GFLG-FITC conjugates were equally distributed between the lysosomal and cytosolic fractions, indicating lysosomal escape, somewhat in agreement with these studies. By comparison, the TAT-targeted HPMA copolymer-GG-Dox conjugates localised to the cytosol and the NLS-targeted HPMA copolymer-GG- Mce_6 conjugates were delivered to the nucleus.

It should be noted that vesicle payload might alter the vesicle density. In fact, this property has been purposefully used in the past to modify the density of lysosomes and aid the purification (Arai et al., 1991). However, the distribution of the HPMA copolymer-OG-Man was shown to be almost identical to the lysosomal distribution, and so it might be concluded that the polymer conjugate does not cause a significant change in lysosomal density.

5.4.3 Comparison of SCF and confocal microscopy of HPMA copolymer-OG-Man

Fluorescence was clearly visible in vesicles, and co-localised with the late endosome/lysosome markers, when the HPMA copolymer-OG ± Man conjugates were

incubated for 4 h with THP-1 cells (with leupeptin). There was no difference observed between the localisation of conjugates ± Man.

It was interesting to compare the semi-quantitative SCF results to the qualitative confocal fluorescence microscopy images. Cell fixation usually involves either detergent or solvent extraction that leads to permeabilisation of the intracellular membranes so that non-fixed material diffuses out. The method used here was developed to fix cells in a way that ensured retention of the water-soluble polymers in the intracellular vesicles (Richardson et al., 2008). It should be noted that there is likely to be some bleed-through of the green channel into the red, which could account for the apparent colocalisation. Using the appropriate antibody controls this could have been be ruled out. However, the SCF data and fluorescence microscopy images are in agreement and show that the HPMA copolymer-OG-Man conjugates co-localise to the late endosome/lysosome over the same time frame.

5.4.4 Transfer of this SCF method to Leishmania-infected THP-1 macrophage cells

To really understand the fate of HPMA copolymer conjugates in *Leishmania*-infected macrophages it is necessary to set up the method for that model. However, a number of modifications may be needed. The density of the PV is unknown. It contains many of the same markers as lysosomes (LAMP-1, N-acetyl-β-glucosaminidase), so will be needed to distinguish the endosomal, lysosomal and phagosomal (PV) compartments. Differences in trafficking in infected and non-infected cells might also be expected and this could impact on the ability of the conjugate to gain access to the PV.

The general nature of the PV is discussed in detail in Chapter 1. Ability of HPMA copolymer conjugates to access the PV will depend on fusion of endosomal or lysosomal vesicles with the PV. The PV is known to be a type of phagosome, which fuse with lysosomes (Geisow & Evans, 1984), but it does not express normal phagosomal characteristics, however it does contain LAMP-1, cathepsin B, D, H and L (Lang et al., 1994). There is a growing body of evidence showing considerable fusion between lysosomes and the PV for several *Leishmania* species (*L. donovani* in human monocyte-derived macrophages, *L. mexicana* in murine peritoneal macrophages and *L. amazonensis* in murine bone marrow-derived macrophages (Berman et al., 1979; Brazil,

1984; Courret et al., 2002)). However, in the J774 macrophage cell line there is some evidence of reduced fusion of the *L. donovani*-infected PV with lysosomes (Holm et al., 2001; Scianimanico et al., 1999), even though ultrastructural studies of *L. donovani*-infected macrophages from hamster liver incubated with liposomes have shown that the liposome-containing lysosomes fused readily with the PV (Weldon et al., 1983; Heath et al., 1984). Taken together, these studies strongly suggest that a polymer-drug conjugate delivered to the lysosome, as seen in the THP-1 cell model, should then be able to then enter the PV, and have direct access to the parasite.

Preliminary confocal microscopy studies on the uptake of the HPMA copolymer-OG-Man conjugates (2 h 30 min incubation) into *L. donovani*-infected THP-1 cells have shown some indication that the co-localisation of HPMA copolymer-OG-Man conjugates with the parasite (Seifert, 2007, unpublished, Figure 5.19). It must be stressed that these are only preliminary experiments, and this work is ongoing. However, this suggests that the HPMA copolymer-drug-Man conjugates will be able to enter the L. donovani-infected THP-1 cells in order to kill the parasite.

5.5 Conclusions

The aim of this study was to establish a SCF method that could be used to investigate the intracellular trafficking of MR-targeted HPMA copolymer-drug conjugates in subsequent studies. The results showed that this new SCF method could be used to investigate the time-dependent trafficking of HPMA copolymer-OG-Man conjugates and potentially of other polymer therapeutics in THP-1 cells (Wallom et al., 2008). There was good linear separation of the intact components of the endocytic pathway, using a combination of markers (enzymes, endocytosed fluorescent ligands and antibody markers) and direct imaging. The lysosomal accumulation of HPMA copolymer-OG-Man conjugates was supported by the fluorescence microscopy images. This method was also carefully optimised to confirm localisation of the HPMA copolymers in the endocytic vesicles without the problem of artefacts (Richardson et al., 2008).

Finally, these results have demonstrated the lysosomotropic delivery of HPMA copolymer-OG-Man and the release of OG as a model drug from the HPMA

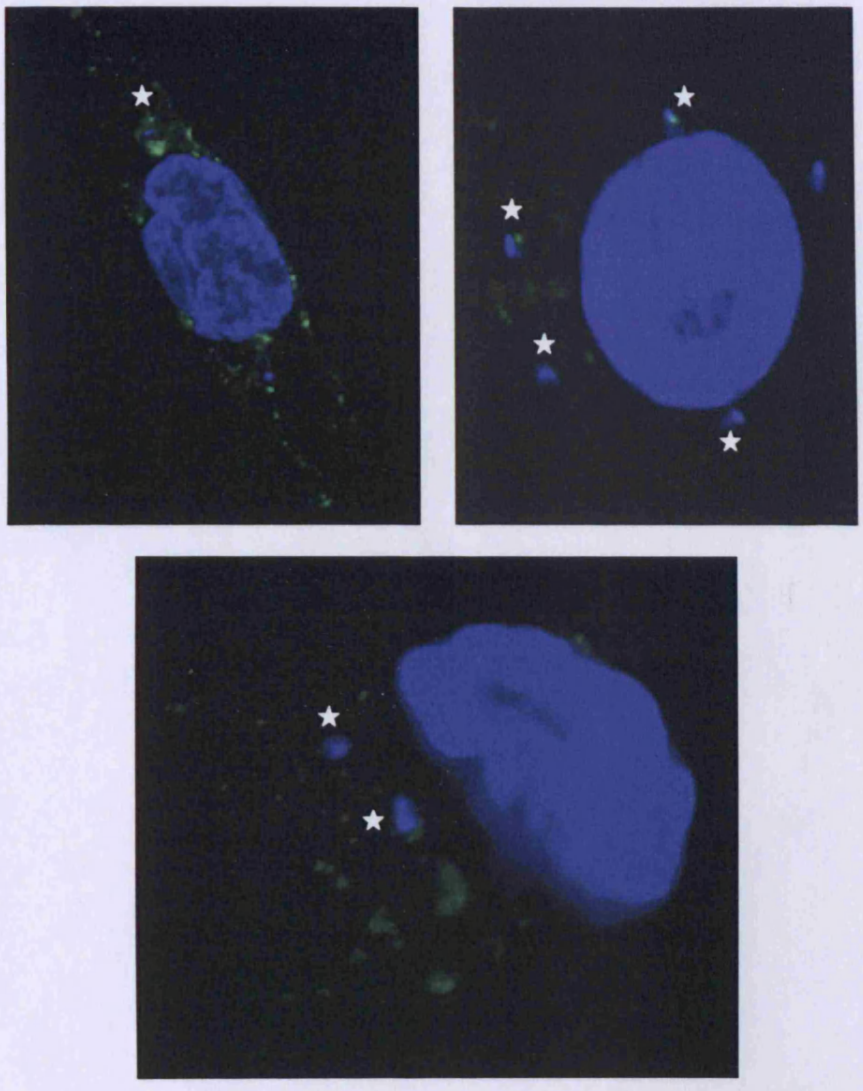

Figure 5.19 Preliminary live cell confocal images of the intracellular localisation of HPMA copolymer-OG-Man conjugates with *L. donovani*-infected THP-1 cells. *L. donovani* infected THP-1 cells were incubated with 0.1 mg/ml polymer solution in complete medium for 2 h 30 min. Examples of the parasite (blue nuclear stain DAPI) and HPMA copolymer-OG-Man (green) in close proximity are indicated using white stars. Seifert, 2007, unpublished.

copolymer-GFLG side chains as would been expected. There is clearly potential to develop a method for quantitative measurement of drug trafficking. Using this SCF method, in the next Chapter the synthesis, intracellular trafficking and toxicity of HPMA copolymer-Man-AmB conjugates will be studied.

Chapter 6

Synthesis of HPMA copolymer-AmB conjugates and determination of activity and intracellular fate

6.1 Introduction

The preceding studies have demonstrated that MR-targeted HPMA copolymer conjugates could be used to increase uptake into macrophages and also that these conjugates traffic to lysosomes (Chapters 3 - 5). In this study preliminary experiments were undertaken to evaluate a potential anti-leishmanial polymer-drug conjugate. As discussed in Chapter 1, AmB, a commonly used second line treatment for VL, was chosen as the model drug. The aim here was to synthesise and characterise a mannose-containing HPMA copolymer conjugate of AmB, and determine its cytotoxicity in comparison to free AmB. The intracellular trafficking of the HPMA copolymer-AmB conjugate was also investigated in uninfected THP-1 cells using the SCF method established in Chapter 5 to gain insight into the likely fate of such conjugates.

Most novel AmB delivery systems have been investigated as antifungals. Those that have been tested against *Leishmania* have shown variable results though none have proved more effective than the commercial formulations. The ideal delivery system would solubilise AmB, have low cytotoxicity and haemolytic activity towards mammalian cells, actively target macrophages, achieve co-localisation with the *Leishmania* parasite and have high anti-leishmanial activity. HPMA copolymer-Man has shown macrophage targeting, endocytosis and delivery to the lysosome. The choice of AmB and the properties of AmB formulations, both the clinically available formulations and those in the literature, are discussed below.

6.1.1 Amphotericin B

AmB (Figure 6.1) and its mode of action were described in section 1.4.2. It was chosen here because it is highly potent and it is the only anti-leishmanial drug not to have shown clinical resistance, although resistance has been demonstrated *in vitro* (Ouellette et al., 2004). The clinical use of AmB is limited by problems such as insolubility, low selectivity for the parasite membrane, acute toxicity (primarily severe nephrotoxicity) and drug instability (Kleinberg, 2006).

AmB exerts its anti-leishmanial effect by binding to sterols and inserting into the membrane, forming pores. This quickly leads to cell death. It displays some selectivity for the parasite membranes as they contain ergosterol, however non-specific toxicity

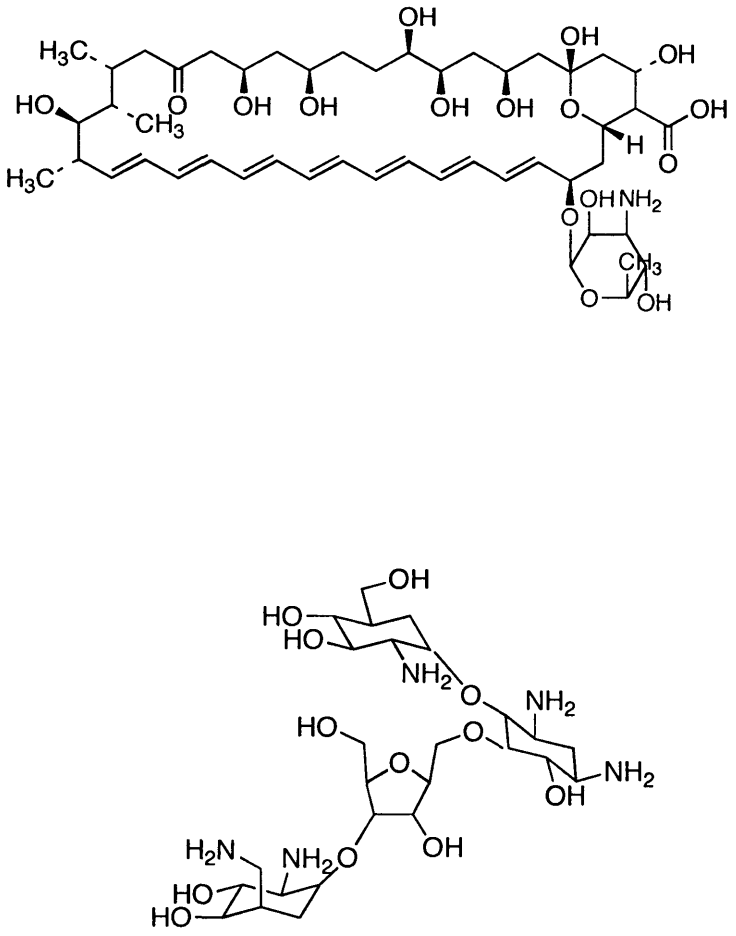

Figure 6.1 Chemical structures of amphotericin B and paromomycin

occurs due to interaction with cholesterol in normal cell membranes (Gruszecki et al., 2003). The aggregation of AmB in aqueous solution is related to the membrane interaction and consequent toxicity. The behaviour of AmB in solution is discussed below and related to the possible benefits of the various formulations.

AmB is very poorly soluble in aqueous solutions at physiological pH. It has better solubility at the pH extremes of < 2 or > 7; however at these pHs it then becomes unstable. In aqueous solutions, at concentrations > 0.2 μg/ml, AmB self-associates due to its amphipathic nature, giving rise to a mixture of water-soluble monomeric and dimeric structures and insoluble aggregates (Milhaud et al., 2002). The degree of aggregation depends on the AmB concentration, the solvent, the temperature, and the presence of serum proteins. Previous studies have examined the effect of the AmB aggregation state on the bioactivity following entrapment of AmB in albumin microspheres (Ordonez-Gutierrez et al., 2007). Preparations of free and encapsulated AmB in monomeric, dimeric and multi-aggregated forms were prepared and their activity against *Leishmania infantum*-infected J774 macrophages and against the free promastigotes was compared. Free AmB (in any form) did not kill the extracellular promastigote, however all the albumin microsphere encapsulated forms did. Free AmB in its monomeric and dimeric form was most toxic to the intracellular amastigote, but only the encapsulated drug was able to completely eliminate infection. The free AmB in multi-aggregated form was most toxic to host J774 macrophage cells, but interestingly, none of the encapsulated forms showed toxicity against these macrophages.

This study highlights both the affect of the AmB aggregation state and the ability of a drug delivery system to modulate AmB toxicity and activity (therapeutic index). It is thought that AmB binding to low-density lipoproteins (LDL) actually leads to the non-specific cellular toxicity, and that it is the aggregated form that causes non-specific haemolysis (Legrand et al., 1992; Ridente et al., 1999). Thus, encapsulation can reduce protein binding and consequently non-specific toxicity (Croft et al., 2006). This is also one potential mechanism by which liposomal encapsulation reduces the non-specific toxicity of AmB. Polymer conjugation of AmB could also potentially reduce toxicity by this mechanism.

6.1.2 Commercially available AmB products

A variety of AmB delivery systems have shown improved clinical benefit compared to free AmB. This is almost always due to reduced toxicity allowing administration of higher doses, rather than higher activity. Some delivery systems are actually less active. The commercially available AmB formulations are summarised in Table 6.1.

Since 1958 Fungizone® has been second line treatment for leishmaniasis, after the antimonials. Fungizone® is AmB solubilised with deoxycholate and it is delivered as an infusion, However this often leads to infusion-related reactions, and as the AmB dissociates quickly, it causes acute toxicity. Amphotec® and Abelcet® are lipid formulations primarily used for treatment of fungal infections. The liposomal AmB Ambisome® (see Section 1.5) is not in general use for leishmaniasis due its high cost. However, it is increasingly used for the treatment of fungal infections, particularly in Europe. A recent *in vitro* study compared the activity of Fungizone®, Amphocil®, Ambisome® and Abelcet®, against *Leishmania donovani* and it was found that their activity depended on the cell model used (Yardley & Croft, 2000). In the peritoneal macrophage (PEM) model Fungizone® and Amphocil® had higher activity than Ambisome® and Abelcet®. In contrast in THP-1 cells Amphocil® and Abelcet® had higher activity than Ambisome®, with Fungizone® showing the lowest activity. However, Ambisome® clearly showed higher clinical activity compared with Fungizone®, and this has been attributed to higher plasma concentrations, and slower elimination times compared to AmB (Bekersky et al., 2002). Liposomal AmB allows an administration of 5 times higher dose than conventional AmB (Fungizone®) *in vivo* due to the greatly reduced side effects (Lemke et al., 2005).

The disadvantages of liposomes (summarised in section 1.5) means that there is still scope for improved, cheaper AmB therapies, particularly those targeted to *Leishmania*-infected macrophages, rather than disseminated fungal infections, which require very different pharmacokinetic design. Reduced uptake into macrophages means that the drug is not removed from the circulation. This is advantageous for fungal infections. The drug either needs to be slowly released from the delivery system in the circulation or at the site of fungal infection (e.g. exploiting lowered pH). In contrast

Table 6.1 Characteristics of different drug delivery systems designed for AmB that are on the market.

Name	Delivery method/formulation	Indication	Dose mg/kg/day	Plasma half life (h)/C_{max}(μg/ml)	AmB Wt %	Reference
Fungizone	Micellar colloidal complex with sodium deoxycholate (oligomeric)	Fungal infections Leishmaniasis	0.6 - 1	24-48 / 1.4	12.5	Cheron et al., 2003
Abelcet (ABLC)	Ribbon-like lipid complex (Intralipid)	Fungal infections	5	20-24/1.7	50	Wingard et al., 2000
Amphotec/ Amphocil (ABCD)	Disk shaped cholesterol sulphate colloidal dispersion	Fungal infections	3 - 4	22/3.1	65	Bowden et al., 2002
AmBisome	Unilamellar liposome (monomeric) (60-70nm)	Fungal infections Leishmaniasis	2 - 5	24 / 23-83	12.5	Bekersky et al., 2002

macrophage uptake is essential for activity against *Leishmania*. Ideally the drug should be released specifically inside the macrophage in the vicinity of the parasite.

6.1.3 Novel AmB formulations in pre-clinical development

Ongoing studies on alternative AmB formulations and delivery systems have shown varying degrees of success (Table 6.2). They have been primarily been designed for controlled release or for better targeting of disseminated fungal infections, but some have also shown activity against leishmaniasis.

6.1.3.1 Heat aggregated Fungizone®

Second generation formulations of Fungizone® have been developed. Heated Fungizone® produces 'super-aggregated' AmB which showed lower toxicity but similar activity against *L.donovani* compared to conventional Fungizone® (Petit et al., 1999). Also, it has shown increased uptake into J774 macrophages (Cheron et al., 2003). However, results have suggested it is actually less kinetically stable and dissociates into monomers more quickly than Fungizone® (Baas et al., 1999).

6.1.3.2 Targeted AmB liposomes

Liposomes exploit AmB's high affinity for lipids (sterols and phospholipids). However, none of these lipid formulations have yet surpassed Ambisome®, which is still considered the gold standard anti-leishmanial formulation.

To further increase the anti-leishmanial activity, macrophage-targeted AmB liposomes have been explored. In fact, the only targeted delivery systems to incorporate AmB have been MR-targeted liposomal vesicles (Vyas & Sihorkar, 2000). Recently, multilameller vesicles (MLVs) containing AmB with macrophage-specific ligands, employing p-aminophenyl-mannopyranoside (PAM) and O-palmitoyl mannan (OPM), have been designed (Vyas et al., 2000). After intravenous administration to rats, PAM showed liver and spleen targeting, and OPM, in comparison, resulted in alveolar macrophage accumulation. The same group also designed an OPM targeted MLV for aerosolised delivery (Vyas et al., 2005) and a trilaurin-based nanoparticle targeted with OPM for liver targeting (emulsome) (Gupta et al., 2007; Gupta & Vyas, 2007).

Table 6.2 Characteristics of different drug delivery systems designed for AmB against *Leishmania* that are in the literature.

Delivery method/formulation	Specifications	Targeting	Reference
Heated deoxycholate complex	Superaggregated Fungizone	-	Petit et al., 1999
Liposomes	Fungizome	-	Kshirsagar et al., 2005
	PEGylated liposome	-	Moribe et al., 1999
	PC and cholesterol liposome	OPM/PAM	Vyas et al., 2005; 2000
Polymer conjugates	PEG	-	Sedlak et al., 2007 a+b; Conover et al., 2003
	Dendrimer	-	Gupta et al., 2007
	Arabinogalactan	-	Falk et al., 1999; Ehrunfreund-kleinman et al., 2004; Nishi et al., 2007
Nanoparticle/micelle/ other	Chitosan/Dextran nanoparticle	-	Tiyaboonachai and Limpeanchob, 2007
	Polyaxomer 188 coated poly(epsilon-capolactone)	-	Espuelas et al., 2003
	Emulsomes	OPM	Gupta et al., 2007
	PVP	-	Charvalos et al., 2006
	Albumin/PLGA/poly(sebacic anhydride) microspheres	-	Sanchez-Brunete et al., 2005
	Lipid nanosphere	-	Otsubo et al., 1999

Table 6.2 continued Characteristics of different drug delivery systems designed for AmB against *Leishmania* that are in the literature.

Delivery method/formulation	Specifications	Targeting	Reference
Nanoparticle/micelle/other	Egg lecithin-bile salt micelle	-	Brajtburg et al., 1994
	Sucrose ester	-	Gruda et al., 1991
	Block copolymer micelle	-	Lavasanifar et al., 2002
	Poly(ethylene oxide)-block-poly(L-amino acid) micelle	-	Adams et al., 2003
	PEG-block-poly(ε-caprolactone-co-trimethylenecarbonate)micelle	-	Vakil et al., 2005 Vandermeulen et al., 2006
	PEG micelle	-	Moreno et al., 2001, 2003;
	Lecithin based oil-in-water emulsion	-	Brime et al., 2004
	Cochleate lipid cylinder	-	Zarif et al., 2005
	Carbon nanotube	-	Wu et al., 2005

However, these targeted AmB preparations have not been tested specifically against *Leishmania.*

6.1.3.3 Polymer-AmB conjugates

Several PEG conjugates of AmB have been designed and have demonstrated reduced toxicity in comparison to conventional AmB *in vivo*, but have not yet been tested against *Leishmania.* The first PEG-AmB conjugate contained two molecules of AmB attached to PEG (Mw 40,000 g/mol) by a labile carbamate linkage (Conover et al., 2003). Though this conjugate achieved a 6 times reduction in toxicity *in vivo*, the relatively fast rate of hydrolysis of 1-3 h and release in blood plasma could lead to fast accumulation in the kidneys, and this is a potentially serious disadvantage as nephrotoxicity is a primary concern with AmB. A second PEG-AmB conjugate with a pH sensitive imine linkage was then investigated (Sedlak et al., 2007b). The conjugate was designed for site-directed drug release at pHs ≤ 5.5, either in the intracellular compartments or at sites of localised fungal infection. PEG molecular weight did not affect the rate of drug release but a notable disadvantage of the PEG conjugates is their low drug carrying capacity. Subsequently, a AmB-PEG-*b*-poly(L-lysine) conjugate was designed, again using an imine linkage, containing 12 AmB molecules per polymer conjugate (Mw 26,700 g/mol) (Sedlak et al., 2007a). This conjugate was 5 times less toxic *in vivo* than AmB delivered as Fungizone®, with a maximum tolerated dose (MTD) of 45 mg/kg, whilst maintaining *in vivo* antifungal effectiveness against *Candida albicans.*

Conjugates of AmB bound to arabinogalactan (an oxidised polysaccharide, Mw 23,000 g/mol) via an amine or imine bond have demonstrated reduced toxicity *in vivo* (Ehrenfreund-Kleinman et al., 2002; Falk et al., 1999; Falk et al., 2004). Only one has been tested against *Leishmania (major)* and had similar activity to Fungizone®, however it contained potentially toxic contaminants from the synthesis. An AmB conjugate of gum arabic (90% arabinogalactan, Mw ~ 250,000 g/mol) showed good activity against *L. donovani,* but only against the promastigotes (Nishi et al., 2007). Also, the MTD was 20 mg/kg in comparison to 45 mg/kg for PEG and arabinogalactan conjugates, most likely to the large size, and show slow release of AmB in plasma.

Succinylated dextrin (α-1,4 polyglucose) has also been developed as a drug carrier as it is degraded by α-amylase slowly in the blood plasma (Hreczuk-Hirst et al., 2001). Dextrin-AmB conjugates showed similar haemolytic activity to fungizone and greater non-specific cytotoxicity (against B16F10 cells) compared to Fungizone®. Also, these conjugates had a very low loading of AmB (0.006 wt %) (German et al., 2000).

The potential of polymers as AmB-delivery systems is clear, however the optimal conjugate should have a high carrying capacity with the ability to target the AmB conjugates to the macrophages and optimal release kinetics for intracellular delivery.

6.1.4 Techniques used to study HPMA copolymer-AmB-Man conjugates

6.1.4.1 Chemical characterisation of the conjugates

It was decided in Chapter 4 to use conjugates containing 4 mol % mannose for the drug conjugates. AmB could be conjugated via the amino group on the mycosamine sugar of AmB, therefore the methods described in Chapter 4 were modified and used here to prepare HPMA copolymer-AmB, HPMA copolymer-AmB-Man and HPMA copolymer-OG-AmB-Man conjugates. It was decided to load 4 mol % of AmB onto the conjugate, making full use of the available side chains to try and achieve a high drug loading. The conjugates were characterised for AmB content using UV absorbance.

The unusual absorbance properties of AmB have been used to study the aggregation state and the stability of AmB (Hargreaves et al., 2006). The absorbance peak at 415 nm is related to the monomeric form of AmB, and the peak at 348 nm related to the aggregated form. Therefore, the aggregation state can be assessed by using the ratio of $A_{348/415}$ (a higher ratio = greater aggregation). The aggregation state of the conjugate was measured using the ratio of $A_{348/415}$ in comparison with free AmB, Also, AmB displays thermal instability. The absorbance decreased by 50% over 24 h when incubated under physiological conditions at 37 °C (Ehrenfreund-Kleinman et al., 2002; Ehrenfreund-Kleinman et al., 2004). Therefore, the UV absorbance was used to monitor the stability of the conjugates over time under physiological conditions (pH 7.4, 37 °C) as this may affect the drug release and activity of the conjugates.

6.1.4.2 Biological characterisation of the conjugates

An important factor was the cytotoxicity of the conjugates. The AmB formulations discussed previously have all been shown to significantly reduce the cytotoxicity and haemolytic activity of AmB. The cell viability of THP-1 cells incubated with the HPMA copolymer-AmB and HPMA copolymer-AmB-Man conjugates was compared to free AmB using the MTT assay. The haemolysis assay was used to see if the degree of RBC lysis was reduced by conjugation to HPMA.

To show whether HPMA copolymer-OG-AmB conjugates ± Man showed different degrees of uptake (in THP-1 cells), flow cytometry was used. Also, preliminary studies to investigate the intracellular distribution of the HPMA copolymer-AmB-Man conjugates in THP-1 cells, the SCF method developed in Chapter 5, together with confocal fluorescence microscopy, were used. The protease inhibitor leupeptin was used to prevent linker degradation and therefore investigate the fate of the HPMA copolymer-OG conjugates without release of free OG.

6.1.5 Summary of aims

The specific technical aims were as follows:

- Synthesis of HPMA copolymer-AmB, HPMA copolymer-AmB-Man and HPMA copolymer-OG-AmB-Man.
- Characterise the conjugates for free and total AmB content using the measured UV absorbance and high performance liquid chromatography (HPLC).
- To study the aggregation state of the conjugate and the stability at 37 °C in comparison to free AmB measured using the UV absorption spectra.
- To determine the cell viability of THP-1 cells incubated with the HPMA copolymer-AmB-Man conjugates compared to free AmB using the MTT assay.
- To measure the RBC lysis caused by HPMA copolymer-AmB-Man conjugates compared to free AmB using the haemolysis assay.
- To study the cell association of the HPMA copolymer-OG-AmB and HPMA copolymer-OG-AmB-Man conjugates using flow cytometry.

- To visualise the intracellular fate of the HPMA copolymer-OG-AmB-Man conjugates using confocal FM.
- To apply the SCF method developed in Chapter 5 to investigate the intracellular localisation of HPMA copolymer-AmB-Man conjugate.

6.2 Methods

The general methods for used in these studies have already been described in chapter 2. The RAW 264.7 and THP-1 cells were maintained as in section 2.3.1.1. The MTT assay, flow cytometry and confocal fluorescence microscopy methods were performed using the methods described in sections 2.3.1.3, 2.3.3, 2.3.9, and the SCF procedure as described in sections 5.2.1, 2 and 3. The TLC reactions to monitor conjugation of mannose and OG to HPMA copolymer-GFLG was performed as described in section 4.2.1.

6.2.1 Synthesis and characterisation of HPMA copolymer-AmB ± Man conjugates

General method for preparation of HPMA copolymer-AmB conjugates

HPMA copolymer-AmB conjugates were synthesised as shown in Figure 6.2 Typically, HPMA copolymer-GFLG-ONp (9.03 mol % side chains) was dissolved in DMSO (63.7 mg in 1 ml). After stirring at room temperature for 30 min, a solution of AmB in dry DMSO (248 µl, 32 mg/ml) was added to this solution. This reaction mixture was then stirred at room temperature in the dark for 16 h under a nitrogen atmosphere. Then an excess of aminopropanol (2 µl) was added to remove any remaining ONp groups.

General method for preparation of HPMA copolymer-AmB-Man conjugates

Typically, HPMA copolymer containing GFLG-ONp side chains (9.03 mol %) was dissolved in DMSO (63.7 mg in 1 ml). To this solution, after stirring at room temperature for 30 min, a solution of mannosamine.HCl in dry DMSO (130 µl, 24 mg/ml), along with 2 molar equivalents (2 µl) of triethylamine was added. This reaction mixture was stirred at room temperature for 4 h. A solution of AmB in dry DMSO (248 µl, 32 mg/ml) was then added. This reaction mixture was stirred in the dark for 16 h at room temperature under a nitrogen atmosphere and then an excess of aminopropanol (2 µl) was added to remove any remaining -ONp groups.

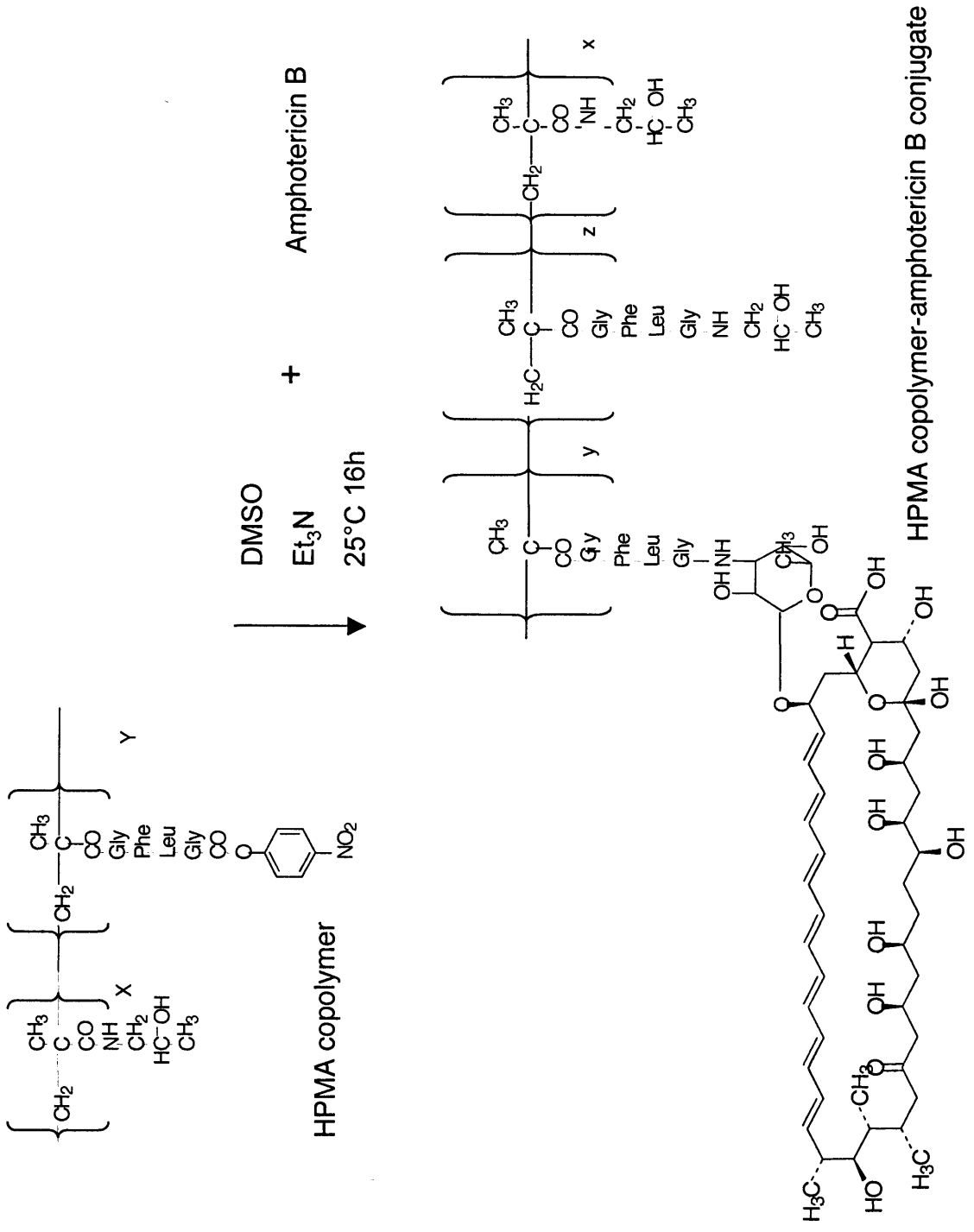

Figure 6.2 Reaction scheme for the conjugation of AmB to HPMA copolymer-GFLG-ONp (Mw 37,427 g/mol, Mw/Mn 1.58). x = 90.07 mol %; y + x = 9.03 mol %.

General method for preparation of HPMA copolymer-OG-AmB ± Man conjugates

OG labelled HPMA copolymer-AmB ± Man conjugates were also prepared using the methods described above. However, immediately after the 16 h incubation with AmB, a solution of OG-cadaverine in dry DMSO (340 µl, 5 mg/ml) was added. The mixture was again stirred at room temperature in the dark for 16 h under a nitrogen atmosphere and then an excess of aminopropanol (2 µl) was added to remove any remaining -ONp groups. Subsequently all conjugates were purified as described in section 4.2.4.

6.2.2 Characterisation of the conjugates in respect of total and free OG, and total AmB

Conjugates were characterised for total and free OG content using the methods described in section 4.2.5. It was decided not to measure the total mannose content of these conjugates due to the limitations of the method found in chapter 4, and the time limitations on developing an alternative method.

The total AmB content of the conjugates was measured by UV. A calibration curve of AmB was prepared over a concentration range of 0 - 200 µg/ml and the absorbance at 300 – 600 nm measured. The absorbance at 420 nm was plotted to create a calibration curve. Each conjugate was also dissolved in MeOH and the absorbance at 300 – 600 nm was measured. HPMA copolymer in MeOH was used as a background control. The absorbance of the conjugates at 420 nm was then used to determine the total AmB content from the calibration curve.

6.2.3 Determination of free AmB using HPLC

A HPLC method was set up to determine the free AmB content of the HPMA copolymer-AmB-Man conjugate. A calibration curve of AmB (2 – 80 µg/ml) was made up in DMSO. Samples (100 µl) containing the internal standard 1-amino-4-nitronaphthalene (1 µg/ml) were injected into a µBondpak reverse phase C18 column, at a flow rate of 1 ml/min using 40:28:32 methanol:acetonitrile:5mM EDTA as eluent, and a UV detector wavelength set at 407 nm.

To determine the amount of free AmB in the HPMA copolymer-AmB-Man conjugate, a solution of the conjugate in DMSO was injected (100 μl, 250 μg/ml). To assess the sensitivity the injection was repeated with a spike of AmB (20 ng/ml).

6.2.4 Characterisation of the HPMA copolymer-AmB-Man conjugate aggregation state and stability

The absorbance spectra of free AmB and of the HPMA copolymer-AmB-Man conjugates was determined in MeOH and media (0.1 mg/ml) and an absorbance spectrum measured for each (300 – 500 nm). Then the absorbance spectra of free AmB and of the HPMA copolymer-AmB-Man conjugates was determined in MeOH/water mixtures over the range of 300 – 500 nm. Solutions were prepared by diluting a 0.6 mg/ml stock solution of AmB or HPMA copolymer-AmB-Man conjugate in varying ratios of MeOH to water (0 - 100 % v/v MeOH) at 0.1 mg/ml. The aggregation state was assessed by determining the ratio of $A_{348/415}$.

The change in absorbance of HPMA copolymer-AmB conjugates was used to investigate the stability under physiological conditions. The conjugates and free AmB were dissolved in clear media at 37 °C, and the absorbance spectra (300 – 500 nm) was measured every hour for 5 h. Again the ratio of $A_{338/415}$ was calculated and plotted with time.

6.2.5 Measurement of the cytotoxicity of AmB, paromomycin and the HPMA copolymer-AmB ± Man conjugates against THP-1 cells using the MTT assay

Preliminary cytotoxicity experiments were performed using both differentiated THP-1 and RAW 264.7 cells with paromomycin and AmB.

Cells were seeded at 10^5 cells (100 μl) per well, and then were incubated for 24 h before the media was removed and replaced with fresh media. Stock solutions of drugs were made up at 20 mM (AmB in DMSO and paromomycin in media). Solutions of drugs were then made up at 81 μg/ml of AmB and 210 μg/ml of paromomycin in complete media. To the first row of wells 50 μl of each drug solution was added (3 wells for each drug). Serial dilutions were then made by pipetting 50 μl of the top solution to the next row, mixing and taking 50 μl to the next well. The 50 μl taken from the last well was discarded. The final concentration ranges were 1 - 70 μg/ml of

paromomycin and 0 – 27 μg/ml of AmB in 100 μl per well. One row of blank wells was filled with 100 μl of complete media only.

The plates were then incubated for 67 h before adding the MTT and the cells were incubated for a further 5 h (total 72 h) and the MTT assay was performed as described in section 2.3.1.3. Data was expressed as a percentage of the control (blank wells).

The same assay was used to investigate the cytotoxicity of the conjugates in comparison to free AmB. Stock solutions of HPMA copolymer-AP, HPMA copolymer-AmB, HPMA copolymer-AmB-Man and free AmB were dissolved in DMSO at 20 mg/ml. Solutions were then made up at an AmB equivalent of 1 mg/ml in complete media. These solutions were added to the first wells and the method described above repeated exactly. The final AmB equivalent concentrations were 0.46 μg/ml – 1 mg/ml.

The effect of leupeptin on the cytotoxicity of the conjugates on THP-1 cells was also investigated. Solutions of HPMA copolymer-OG-Man and free AmB were made up at AmB-equivalents of 0.1, 0.5 and 1 mg/ml in complete media, with and without leupeptin (100 μM) and the assay performed as described above. The results were then used to decide the concentration used for the subcellular fractionation experiments.

6.2.6 Measurement of the haemolytic activity of AmB and the HPMA copolymer-AmB ± Man conjugates

The haemolytic activity of the HPMA copolymer, HPMA copolymer-AmB, HPMA copolymer-AmB-Man conjugates and free AmB was assessed using isolated rat red blood cells (RBCs) *in vitro* (Duncan & Spreafico, 1994). Samples were dissolved in DMSO before being made up at appropriate concentrations in clear media in a 96 well plate (100 μl). The conjugates were diluted in clear media to give an AmB equivalent concentration of 0.46 μg/ml – 1 mg/ml. A control of PBS with Triton X-100 (0.5% v/v) was also included on the plate for each conjugates/drug tested. Plates were stored in the dark at 4 °C whilst the RBCs were prepared.

Healthy male Wistar rats (250 to 300 g) were killed by vertebral dislocation, and whole blood was taken immediately by cardiac puncture. Blood was placed into heparin bead-containing tubes on ice, and resupsended in 2 ml ice-cold PBS. The RBC's were

then prepared by washing three times. Tubes were washed by centrifugation (10 min, 1500 RCF at 4 °C), removal of the PBS, and addition of 2 ml fresh cold PBS and centrifugation, two more times. The RBCs were then weighed and finally resuspended in a PBS solution at 2 % w/v.

To start the assay, the RBC solution (100 µl) was added to each well and the plates were incubated at 37 °C for 1 h in the dark. The plates were then centrifuged (1500 x g for 10 min) and the supernatant (100 µl) was carefully pipetted into a new 96 well plate without disturbing the cells debris layer. The haemoglobin release from the RBCs was measured using the absorbance at 550 nm against a PBS blank measured using a microtitre plate reader. Data were expressed as the percentage haemolysis observed compared with total haemolysis induced by Triton X-100, adjusted to take into account the background observed with the PBS blanks.

6.2.7 Derived cell association and studies on the intracellular fate of HPMA copolymer-AmB ± Man

Flow cytometry

Differentiated THP-1 cells were seeded at 5 x 10^5 cells per ml per well in clear media in 6 well plates overnight. The derived cell association of HPMA copolymer-OG-AmB-Man and HPMA copolymer-OG-AmB was measured by incubation of the THP-1 cells with solutions of the conjugates in clear media (at 1 µg/ml of OG-equivalent) over 60 min. Derived cell association was measured every 10 min for 60 min by flow cytometry as described in sections 2.3.3. A total of 10 000 cells were counted, and data expressed as (the % of positive cells x geometric mean of the fluorescence)/100.

Subcellular fractionation

The intracellular localisation of the HPMA copolymer-AmB-Man in THP-1 cells was then investigated using subcellular fractionation. Differentiated THP-1 cells were seeded at 10^6 cells per ml in clear media in five 150 cm^2 flasks overnight. The cells were then washed with PBS, the culture medium was aspirated and replaced with 10 ml of fresh RPMI media (containing 10 % serum and 100 μM leupeptin) containing HPMA copolymer-OG-Man conjugate (100 μg/ml AmB-equivalent). Cells were incubated for 24 h.

Following the incubation period, cells were placed on ice and cell homogenisation and fractionation was performed as described in section 5.2.1.3. The fractions obtained were then immediately analysed for UV absorbance. Samples of standards (0 – 2.5 μg/ml free AmB in HB solution) and fractions (100 μl) were placed in a 96 well plate and measured using a microtitre plate reader (420 nm).

A dot blot of the fractions was performed using the protocol described in section 2.3.8, with an α-AmB primary antibody (1:50 dilution/0.028 μg/ml). A semi-quantitative calibration curve was made using standards of free AmB and AmB conjugates in HB over a concentration range of 0 – 100 μg/ml AmB equivalent. Samples of 2 μl of the standards, fractions or PNS (diluted 1:10) were used. Secondary antibody incubations were with HRP conjugated anti-mouse antibodies (1:1000). HRP was monitored after incubation with ECL reagent for 5 min and exposure to film. The intensity of the band detected in each fraction was quantified using Image J software (Rasband, 1997-2007) and the results expressed as the amount of fluorescence in each fraction as a percentage of the total fluorescence intensity.

Confocal microscopy

Confocal microscopy was used to visualise the intracellular localisation of HPMA copolymer-OG-AmB ± Man. Differentiated THP-1 cells were seeded at 5 x 10^5 cells per ml per well on coverslips as described in section 2.3.9. Cells were then co-incubated with BSA-TxR (1 mg/ml) and HPMA copolymer-OG-AmB or HPMA copolymer-OG-AmB-Man conjugates (1 mg/ml) in clear media containing leupeptin (100 μM) for either 4 h or 24 h. The cells were then fixed by incubation for 20 min in 3% w/v paraformaldehyde in PBS, and then washed 3 times with PBS (as described in section 5.2.4). The coverslips were mounted on slides with 40 μl Vectashield, the edges sealed with clear nail varnish, and stored at 4 °C for imaging within 72 h. Imaging and analysis was performed using the protocol described in section 2.3.11.

6.3 Results

6.3.1 Characteristics of HPMA copolymer-OG-AmB-Man conjugates

The characteristics of the HPMA copolymer-AmB conjugates synthesised are summarised in Table 6.3.

Table 6.3 Characteristics of HPMA copolymer-AmB conjugates.

Code number	Conjugate structure	AmB content †		Mannose content (theoretical mol %)	OG content ††	
		mol %	wt %		mol %	wt %
AC1	HPMA copolymer-GFLG-AP	NA	NA	NA	NA	NA
AC2	HPMA copolymer-GFLG-Man	NA	NA	4	NA	NA
AC3	HPMA copolymer-GFLG-AmB	3.5	17.7	NA	NA	NA
AC4	HPMA copolymer-GFLG-AmB-Man	3.1	15.8	4	NA	NA
AC5	HPMA copolymer-GFLG-OG-AmB	3.7	18.8	NA	0.62	1.68
AC6	HPMA copolymer-GFLG-OG-AmB-Man	3.2	16.4	4	0.54	1.47

† Estimated by UV absorbance at 415 nm †† Estimated by UV absorbance at 494 nm

The total OG content of the OG-labelled conjugates (AC5 and 6) was 0.62 and 0.54 mol % (1.68 and 1.47 wt %). It was not possible to measure the free OG content using PD10 columns as the AmB conjugates stuck to the column (as a visible yellow band), and could not be eluted with aqueous solutions.

Free AmB in DMSO had an absorbance maximum of 415 nm (Figure 6.3a) and the AmB calibration curve had a linear dependence (r^2 = 0.9989) over the range of concentrations tested (0 – 200 μg/ml). The sensitivity was 1 μg/ml (Figure 6.3b). The AmB content of the conjugates was in the range of 15.8 – 18.8 wt % (3.1 – 3.7 mol %).

After HPLC elution, free AmB had a retention time (t_r) of ~ 7 min. A smaller peak was also visable at ~ 4 min (Figure 6.4a). The internal standard 1-amino-4-nitronaphthalene eluted too close to the solvent front and so was not used in further studies. The calibration curve for AmB was linear (r^2 = 0.999) up to concentrations of > 80 μg/ml with a maximum sensitivity (3 x baseline) of 2 ng (20 ng/ml) (Figure 6.4b).

When HPMA copolymer-AmB conjugates were injected into this system, no peak was seen, however when the conjugate solution was spiked with free AmB (20 ng/ml), the drug could be detected (Figure 6.5). The peak of the spiked HPMA copolymer-AmB was greater than the peak for the free AmB alone, equating to 90 ng/ml.

6.3.2 Conjugate aggregation state and stability

The UV spectra of AmB and HPMA copolymer-AmB did not significantly differ (Figure 6.6). In MeOH, the peak maxima of AmB and conjugate are identical (348, 370, 390 and 415 nm), though the 415 nm peak is slightly reduced. The AmB peaks in media (345, 363, 385 and 419 nm) showed the conjugate peaks were identical except for the first peak, which had shifted to 352 nm. The ratios of $A_{348/415}$ were found to be 0.28 (AmB) and 0.74 (conjugate) in MeOH indicating a monomeric state; and 3.3 (AmB) and 2.9 (conjugate) in media indicating an aggregated state.

The spectra of both AmB and HPMA copolymer-AmB-Man showed a clear but gradual change in spectra with increasing MeOH concentration. The absorbance

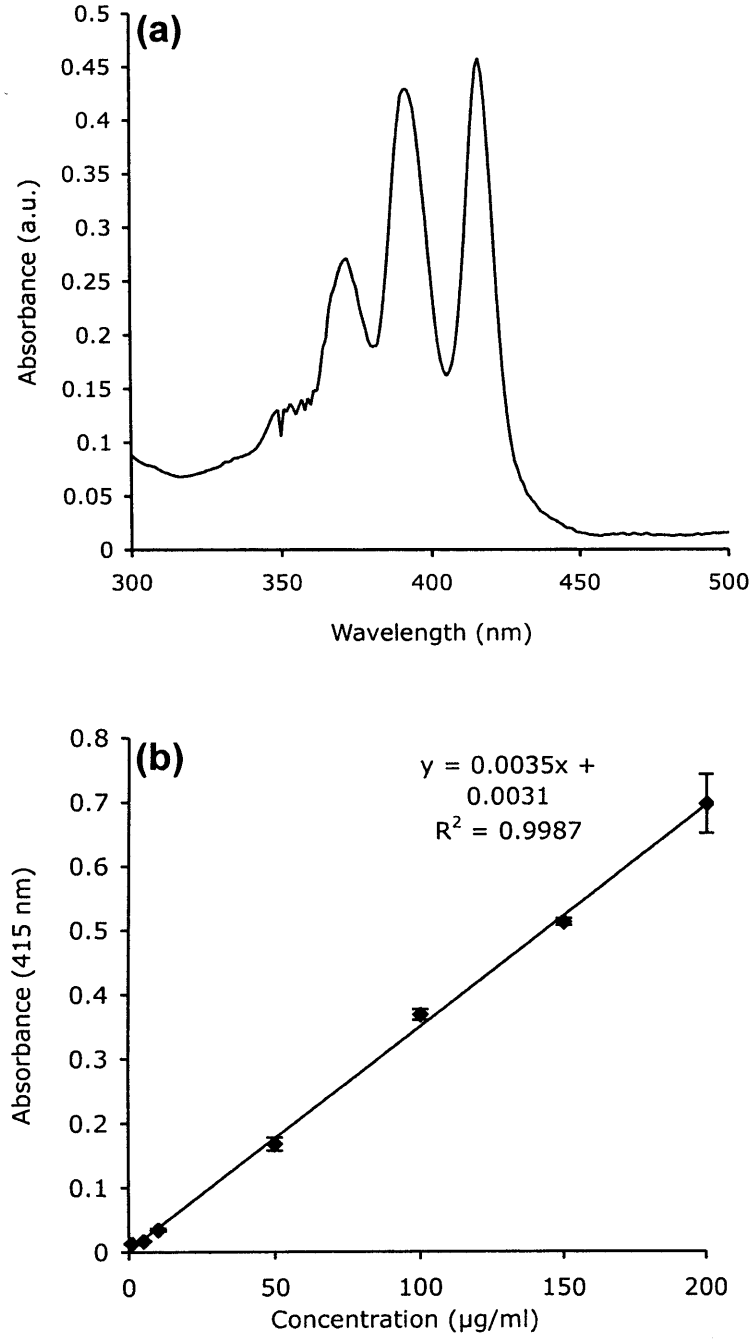

Figure 6.3 Calibration curve for AmB. Panel (a) shows the absorbance spectra of AmB in DMSO (0.1 mg/ml). Panel (b) calibration curve measured in MeOH at 415 nm. The data represent the mean ± SD (n = 3) and where the error bars are not visible they fall within the data points.

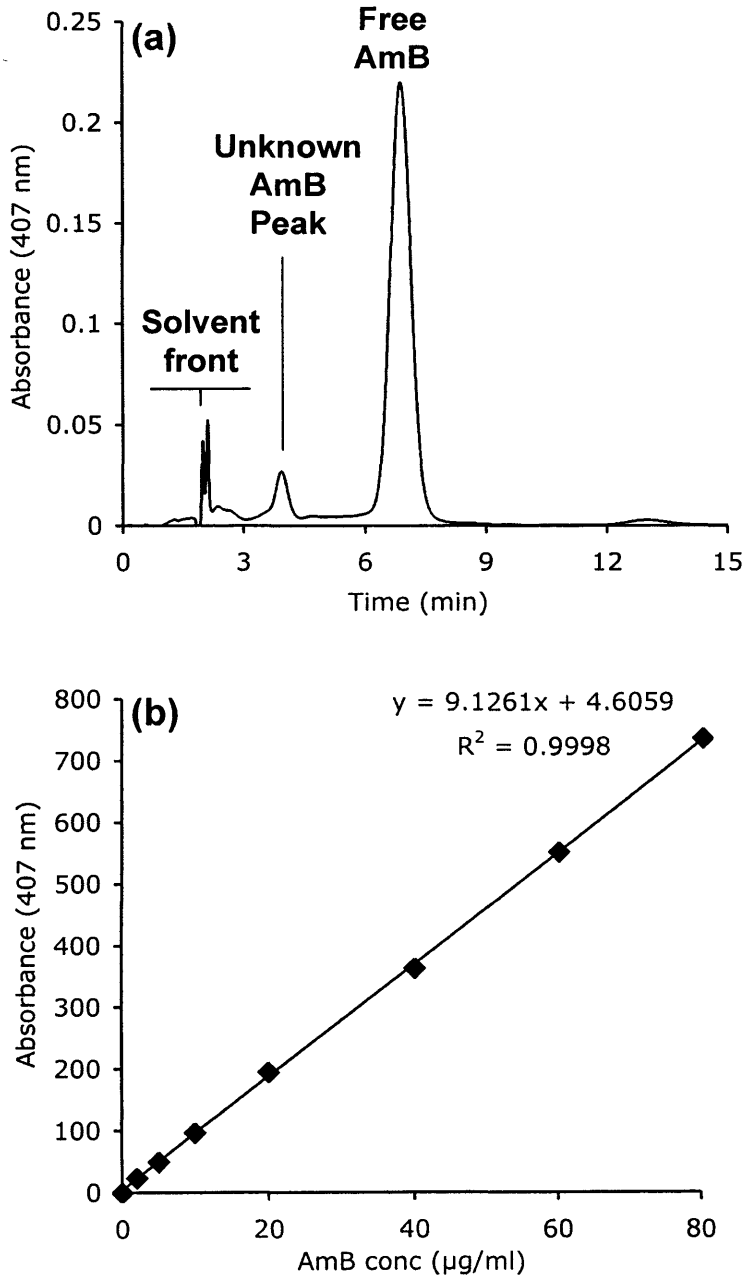

Figure 6.4 HPLC analysis of free AmB. Panel |(a) shows the chromatogram of AmB, panel (b) shows the calibration curve. The data represent the mean ± SD (n =3) and where the error bars are not visible they fall within the data points.

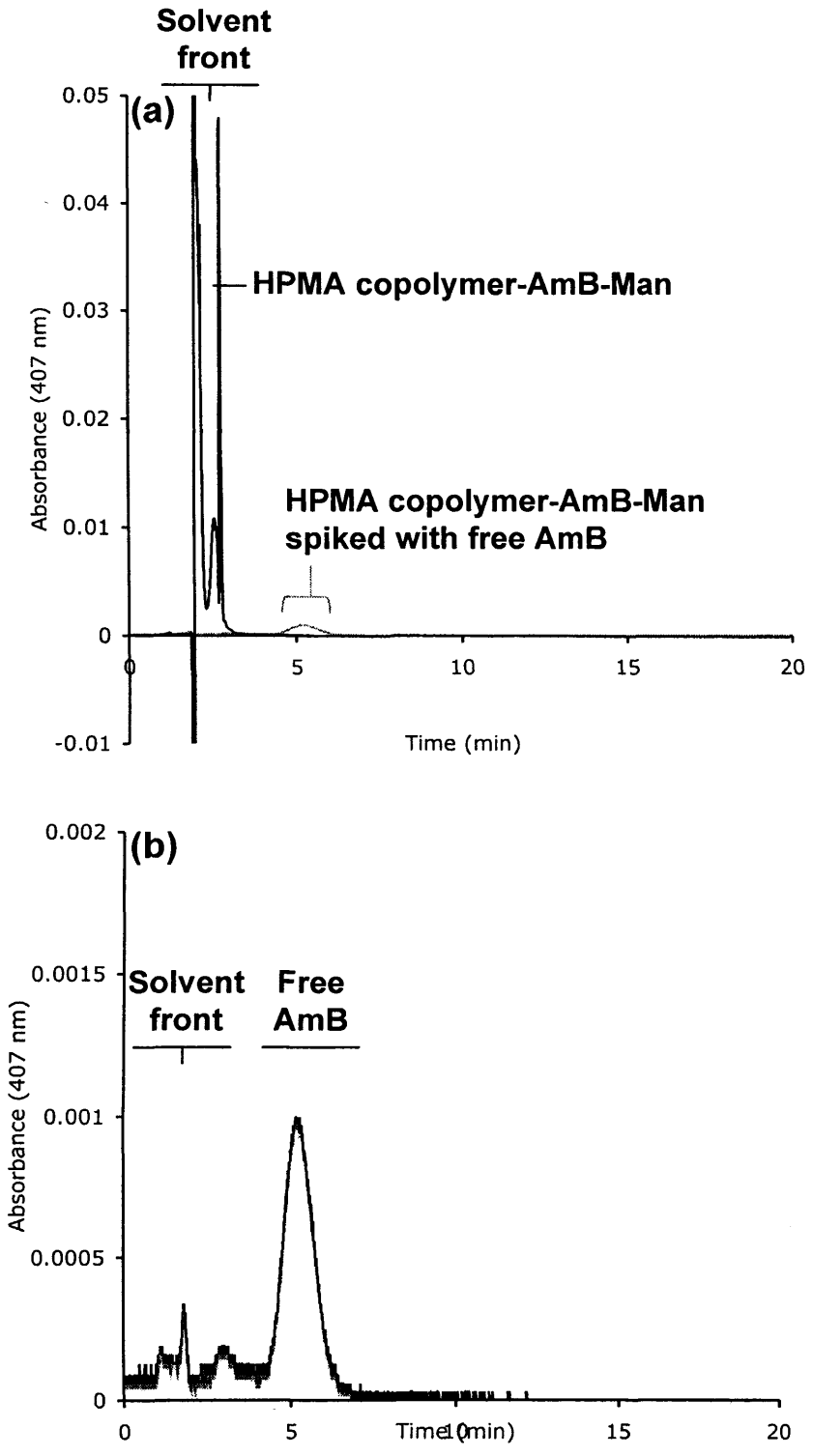

Figure 6.5 HPLC analysis of HPMA coploymer-AmB-Man conjugates. Panel (a) shows the chromatogram when injected with HPMA coploymer-AmB compared with HPMA coploymer-AmB spiked with 2 ng free AmB, and panel (b) shows the chromatogram when injected with HPMA coploymer-AmB spiked with 2 ng free AmB alone.

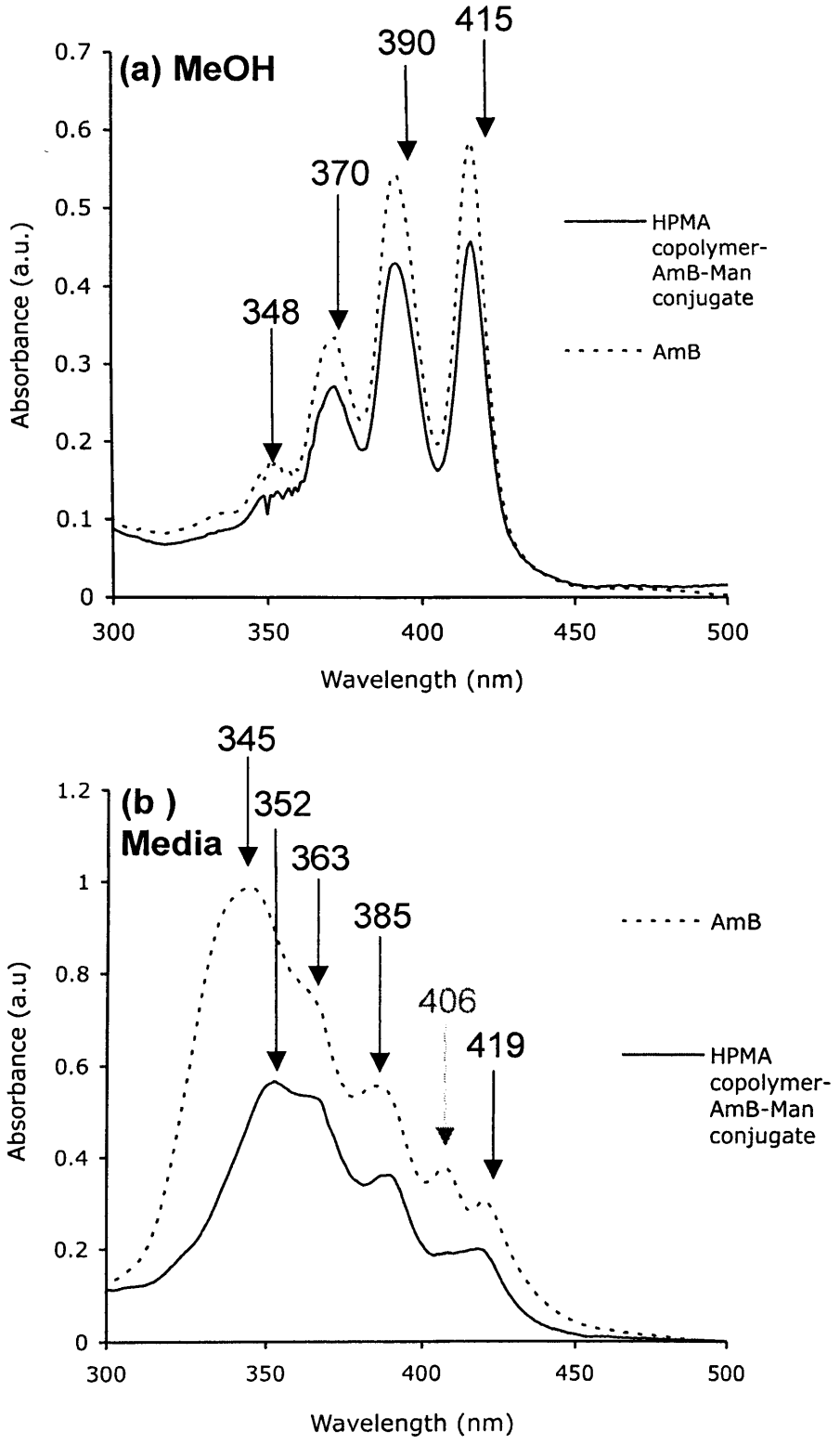

Figure 6.6 Comparison of the UV spectra of HPMA copolymer-AmB-Man conjugates and AmB in MeOH and tissue culture media. UV scans were taken of HPMA copolymer-AmB and AmB at 0.1 mg/ml AmB equivalent. Panel (a) 100 % MeOH, and panel (b) 100 % RPMI tissue culture media.

maxima was 407 nm in MeOH shifting to 330 nm in water (Figures 6.7 and 6.8). The minimum MeOH concentration to give the completely monomeric form of AmB was 50% (Figure 6.7b). However, the change in absorbance spectra of the conjugate was less rapid and did not reach complete monomeric form until the MeOH concentration was > 70 % (Figure 6.8b).

There was no change in the $A_{348/415}$ ratio of free AmB measured over 5 h at 4 °C, with the value remaining constant at ~ 3.9 (Figure 6.9a). However, the $A_{348/415}$ ratio measured at 37 °C decreased significantly. Compared to AmB, the HPMA copolymer-AmB values measured at 37 °C were relatively stable at ~ 3.9 (Figure 6.9b).

6.3.3 Cytotoxicity of AmB, paromomycin and the HPMA copolymer-AmB conjugates

Preliminary studies with AmB indicated IC_{50} values of ~ 2 μg/ml in THP-1 cells, and 5 μg/ml in RAW 264.7 cells (Figure 6.10). Paromomycin however was not very cytotoxic over the concentration range tested, however, it caused a greater reduction in cell viability in THP-1 cells (~ 20 % at 80 μg/ml).

The HPMA copolymer-AmB ± Man conjugates were significantly less toxic than AmB ($p < 0.05$, students t-test) (Figure 6.11). AmB was toxic at concentrations above 0.001 mg/ml and had an IC_{50} value of 0.01 mg/ml. Both conjugates showed no toxicity at < 0.004 mg/ml AmB-equivalent, but cell viability was reduced by ~ 40 % at 1 mg/ml AmB equivalent (as opposed to > 80 % by free AmB). Therefore it was not possible to estimate IC_{50} values. There was no difference in toxicity seen between HPMA copolymer-AmB and HPMA copolymer-AmB-Man.

The cell viability of HPMA copolymer-AmB-Man after incubation with THP-1 cells for 4 h at 1 mg/ml AmB-equivalent was reduced by > 30 % (Figure 6.12). However, when the incubation media contained leupeptin there was no cytotoxicity. After 24 h the cell viability had also reduced in the 0.5 mg/ml incubation, by ~ 10 %. Leupeptin had no effect after 24 h. Incubation with 0.1 mg/ml HPMA copolymer-AmB-Man had no effect on cell viability at either time point. It was therefore decided to use this non-toxic concentration (0.1 mg/ml AmB-equivalent) for incubation of THP-1 cells with HPMA copolymer-AmB-Man in the subcellular fractionation studies.

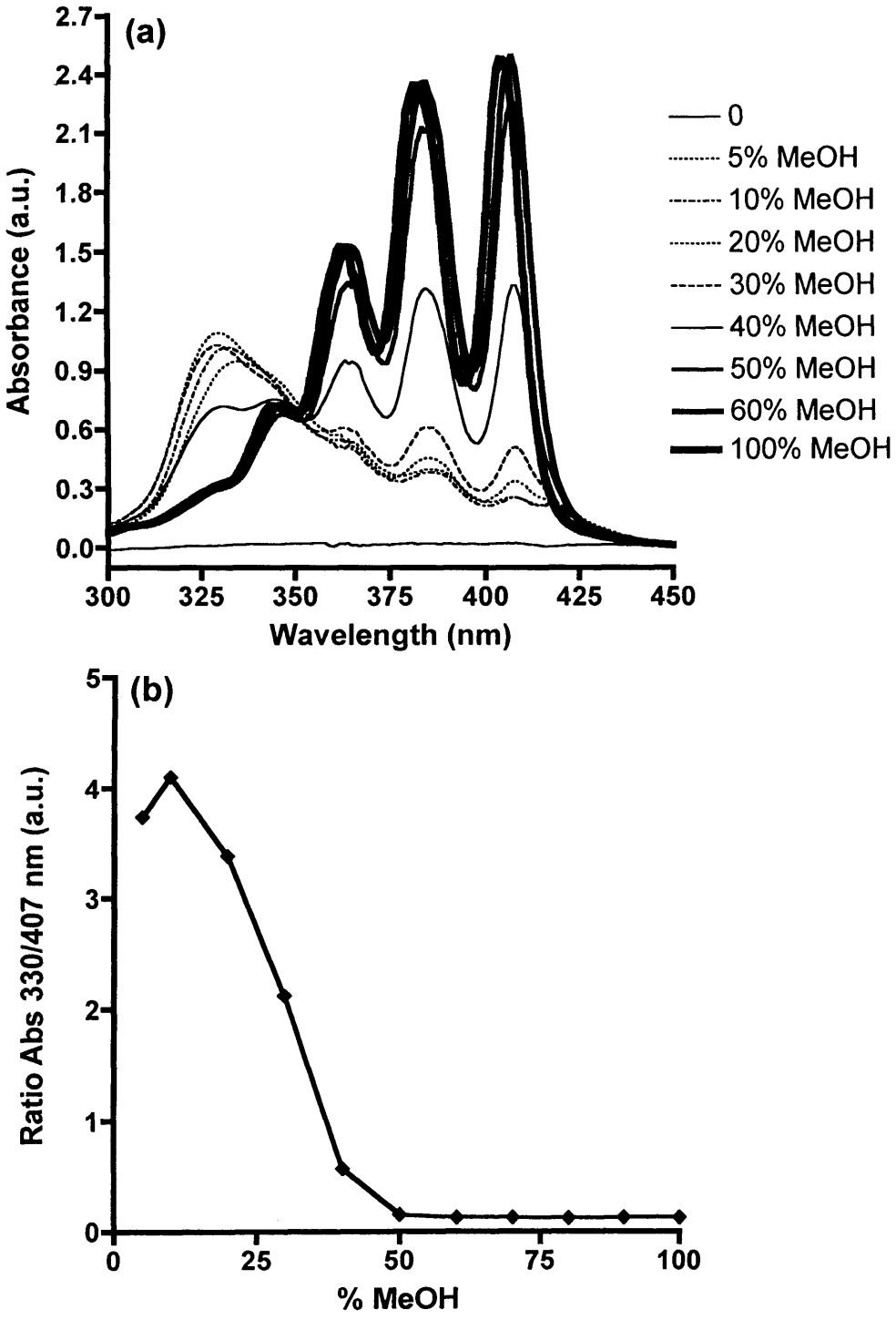

Figure 6.7 Effect of MeOH concentration on the absorbance of AmB. Panel (a) the UV absorbance scans of AmB in different ratios of H_2O:MeOH, panel (b) the ratio monomeric/aggregate peak as a measure of aggregation.

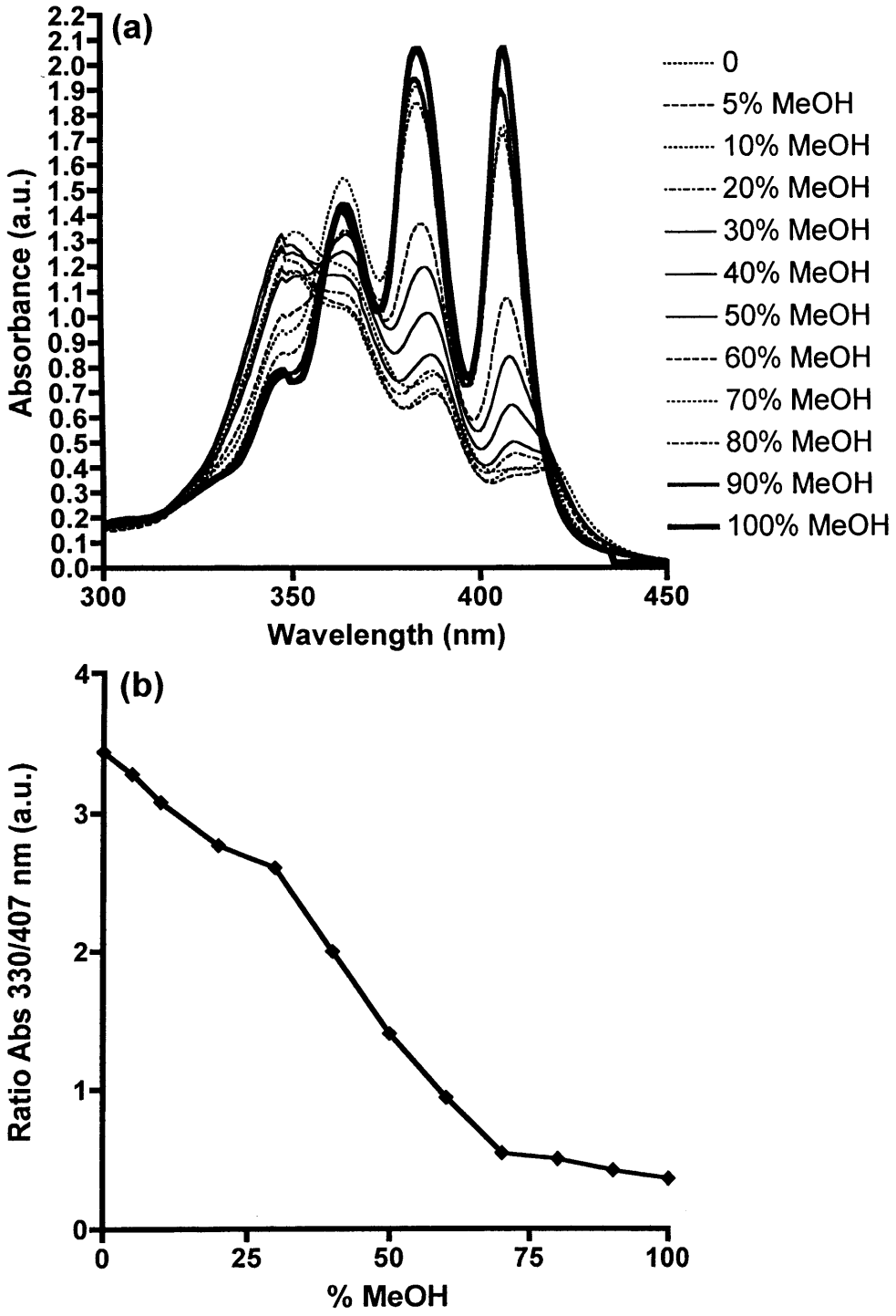

Figure 6.8 Effect of MeOH concentration on the absorbance of HPMA copolymer-AmB-Man. Panel (a) the UV absorbance scans of conjugate in different ratios of H_2O:MeOH, panel (b) the ratio monomeric/aggregate peak as a measure of aggregation.

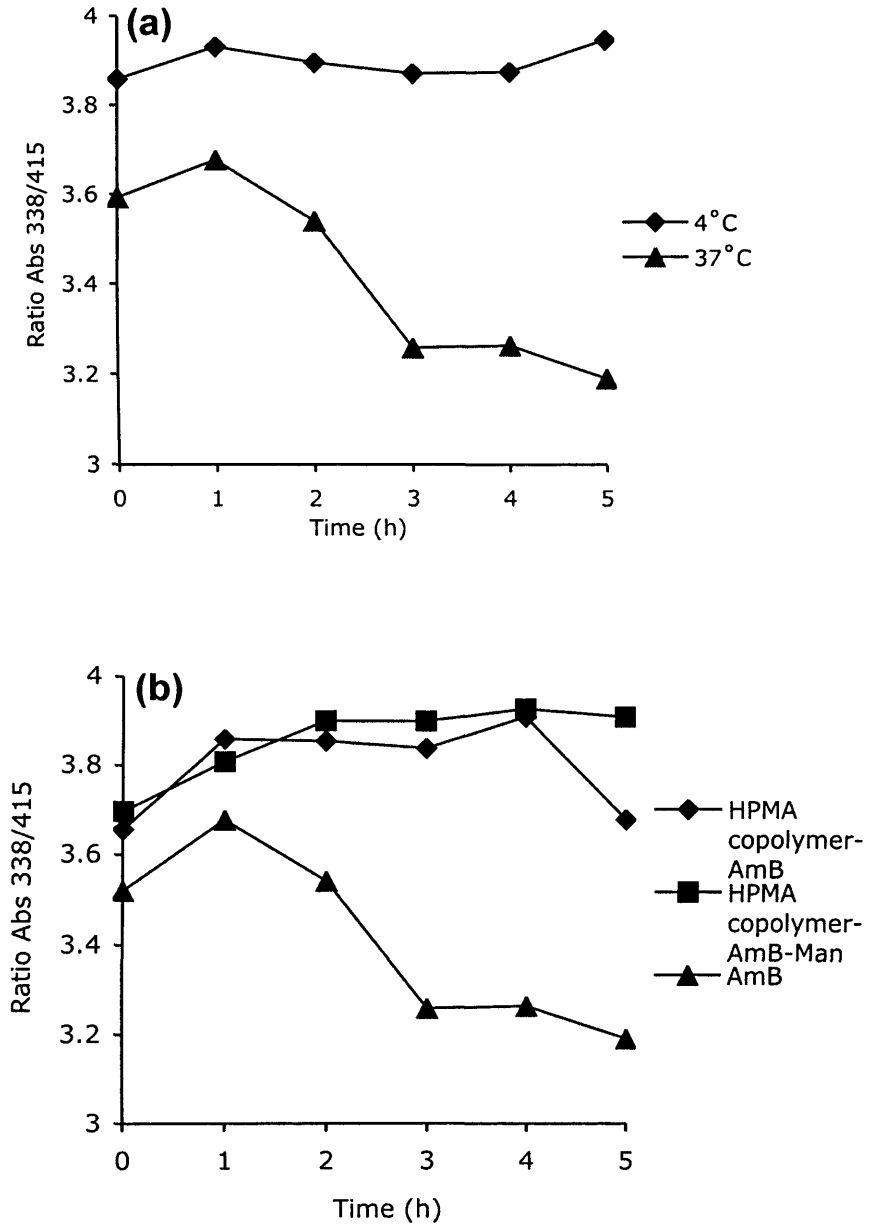

Figure 6.9 Effect of incubation time and temperature (37 and 4 °C) on the absorbance ratio of HPMA copolymer-AmB ± Man and AmB. Panel (a) shows the ratio $Abs_{348/415}$ of AmB in media at 4 and 37 ° C, panel (b) HPMA copolymer-AmB conjugates in media at 37 °C over 5 h and panel (c) HPMA copolymer-AmB over 72 h (n=1).

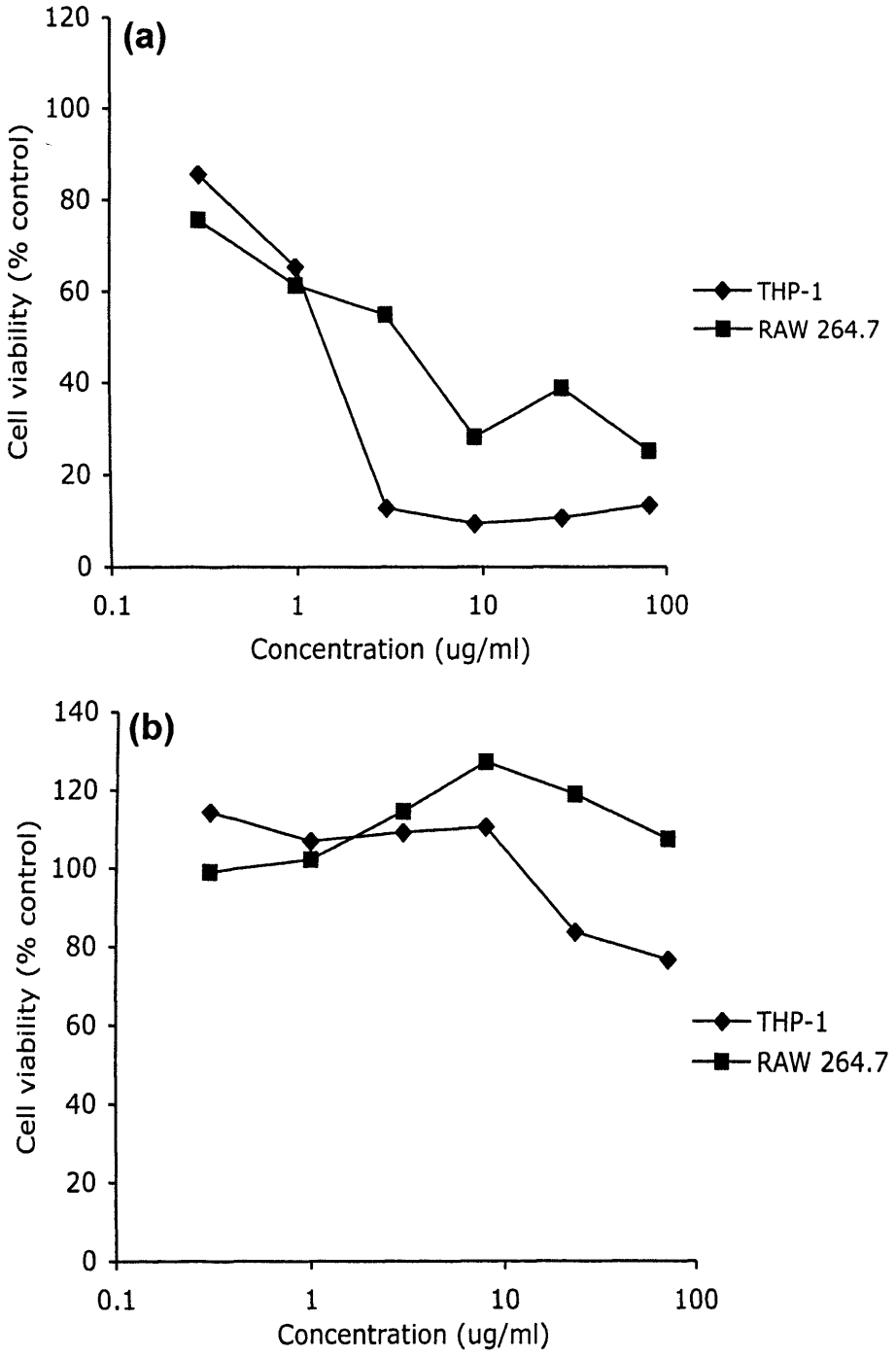

Figure 6.10 Cytotoxicity of AmB and paromomycin against THP-1 and RAW 264.7 cells. Panel (a) AmB and panel (b) paromomycin (72 h and the cell viability measured by the MTT assay). The data represent the mean ± SD (n = 6) and where the error bars are not visible they fall within the data points.

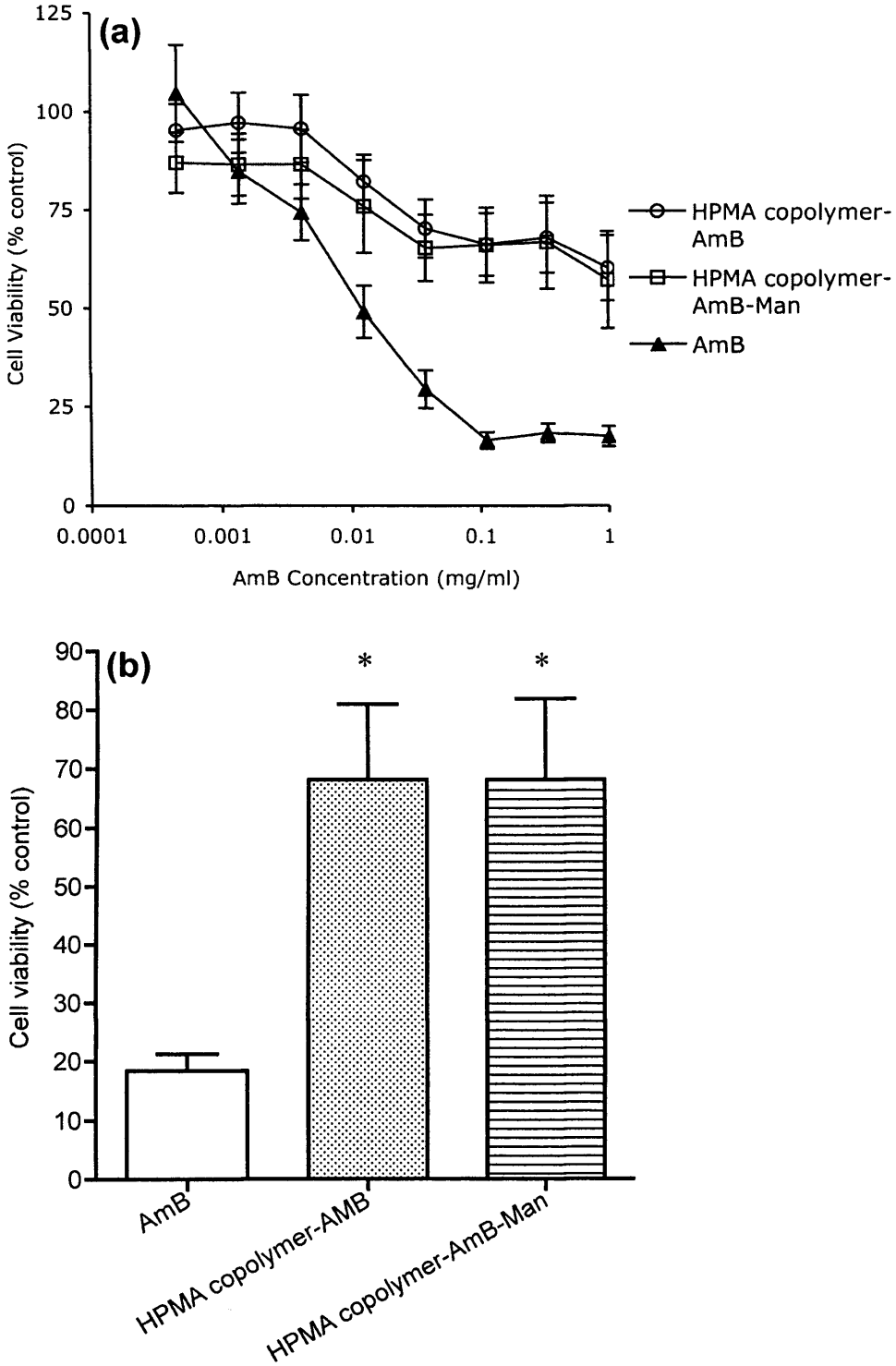

Figure 6.11 Cytotoxicity of HPMA copolymer-AmB conjugates in THP-1 cells. Panel (a) effect of concentration and panel (b) comparison at an AmB equivalent concentration of 1 mg/ml. The data represent the mean ± SEM (n = 4) and where the error bars are not visible they fall within the data points. Statistical significance (*) between conjugates and free drug was determined at $p < 0.05$ (students t-test).

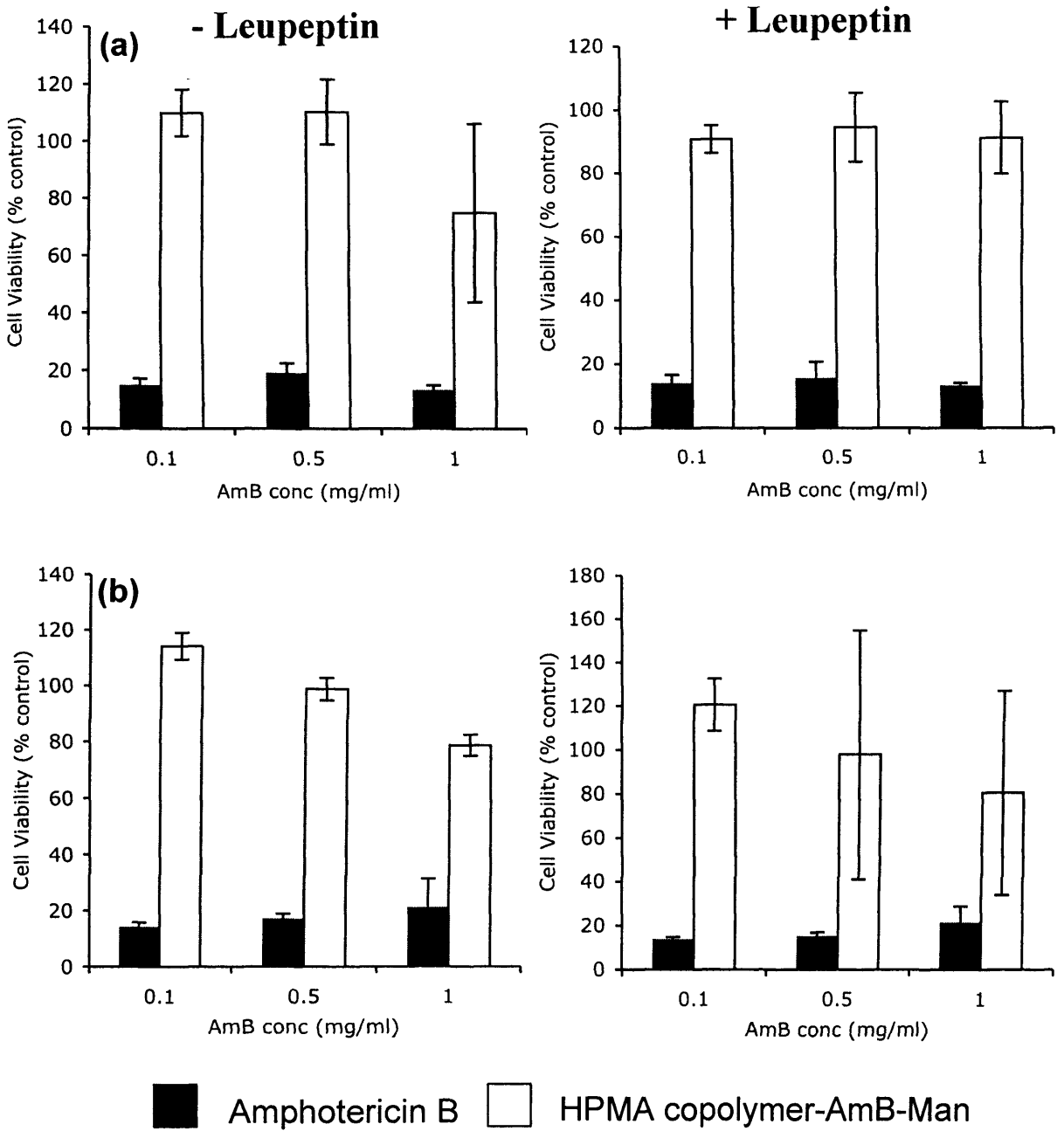

Figure 6.12 The effect of leupeptin on the cytotoxicity of HPMA copolymer-AmB-Man compared with AmB. THP-1 cells were incubated with HPMA copolymer-AmB-Man for panel (a) 4 h and panel (b) 24 h, and the cell viability measured by the MTT assay (n=3).

6.3.4 Haemolytic activity of the HPMA copolymer-AmB conjugates

AmB showed a high degree of haemolysis (~ 40 % at 0.03 mg/ml) after 1 h, but the HPMA copolymer-AmB ± Man conjugates did not show any haemolytic activity up to a concentration of 1 mg/ml AmB-equivalent (Figure 6.13). Therefore, no Hb_{50} values (concentrations at which there was 50 % Hb release) could be determined. The PBS blank gave a value of ~ 20 % haemolysis, though this differed greatly between experiments and between individual microtitre plates. The blank values were therefore subtracted as background from the sample values.

6.3.5 Cell accumulation of HPMA copolymer-AmB-Man in THP-1 cells

THP-1 cells showed a clear increase in THP-1 derived cell-associated fluorescence with time when incubated with the HPMA copolymer-OG-AmB and HPMA copolymer-OG-AmB-Man conjugates for 1 h (Figure 6.14a). This uptake was rapid over the first 10 min and then slowed, but it did not reach a plateau. Derived cell-associated fluorescence was 2-fold greater for the HPMA copolymer-OG-AmB-Man conjugate compared to HPMA copolymer-OG-AmB and statistically significant at all time-points ($p < 0.05$, paired t-test) (Figure 6.14b).

When compared with the derived cell association of HPMA copolymer-OG ± Man (4 mol %), discussed in chapter 4, there was no difference in derived cell association of HPMA copolymer-OG-Man ± AmB in THP-1s (Figure 6.15). However there was a two-fold increase in derived cell association of HPMA copolymer-OG-AmB compared to HPMA copolymer-OG.

6.3.6 Intracellular fate of HPMA copolymer-AmB-Man in THP-1 cells

When the cell were visualised using confocal microscopy the conjugates showed a high degree of co-localisation (yellow) with the BSA-TxR-labelled lysosomes after a 4 h incubation with HPMA copolymer-OG-AmB and HPMA copolymer-OG-AmB-Man (Figure 6.16). The amount of OG-fluorescence was greater but still largely co-localised after 24 h (Figure 6.17). No difference could be seen in distribution of the HPMA copolymer-OG-AmB conjugates with and without Man. Also, no change in cell morphology was seen at these concentrations and time points.

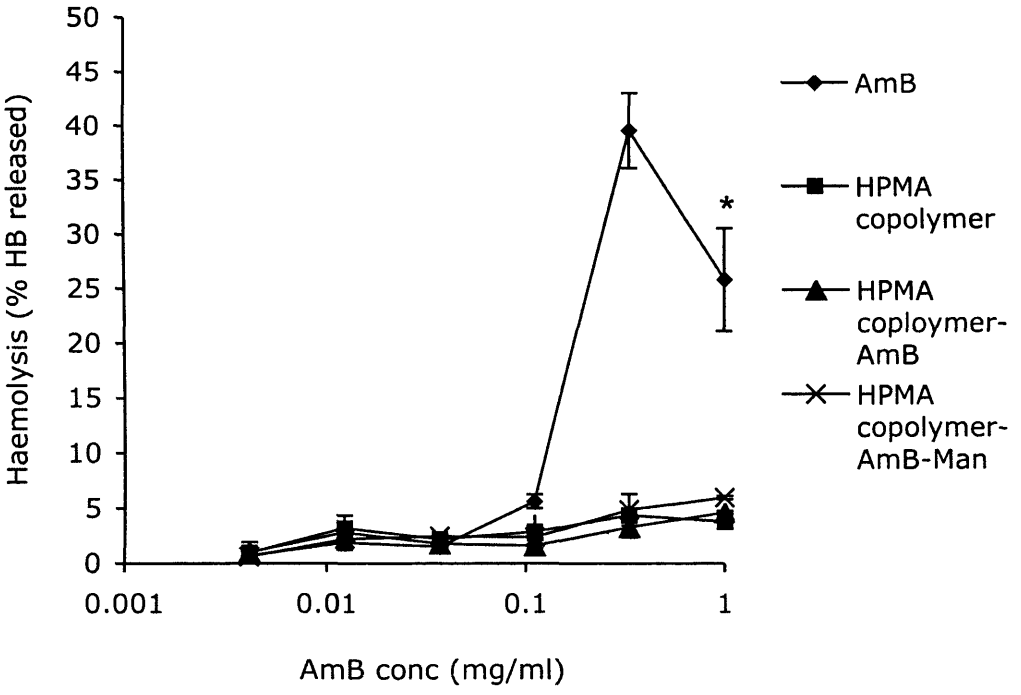

Figure 6.13 Haemolytic activity of HPMA copolymer-AmB ± Man conjugates on on rat RBCs. RBCs were incubated with AmB, HPMA copolymer-AP, HPMA copolymer-AmB and HPMA copolymer-AmB-Man, and the degree of haemolysis measured after 1 h. The data represent the mean ± SD (n =3) and where the error bars are not visible they fall within the data points. Statistical significance (*) at 1 mg/ml was determined at $p < 0.05$ (students t-test).

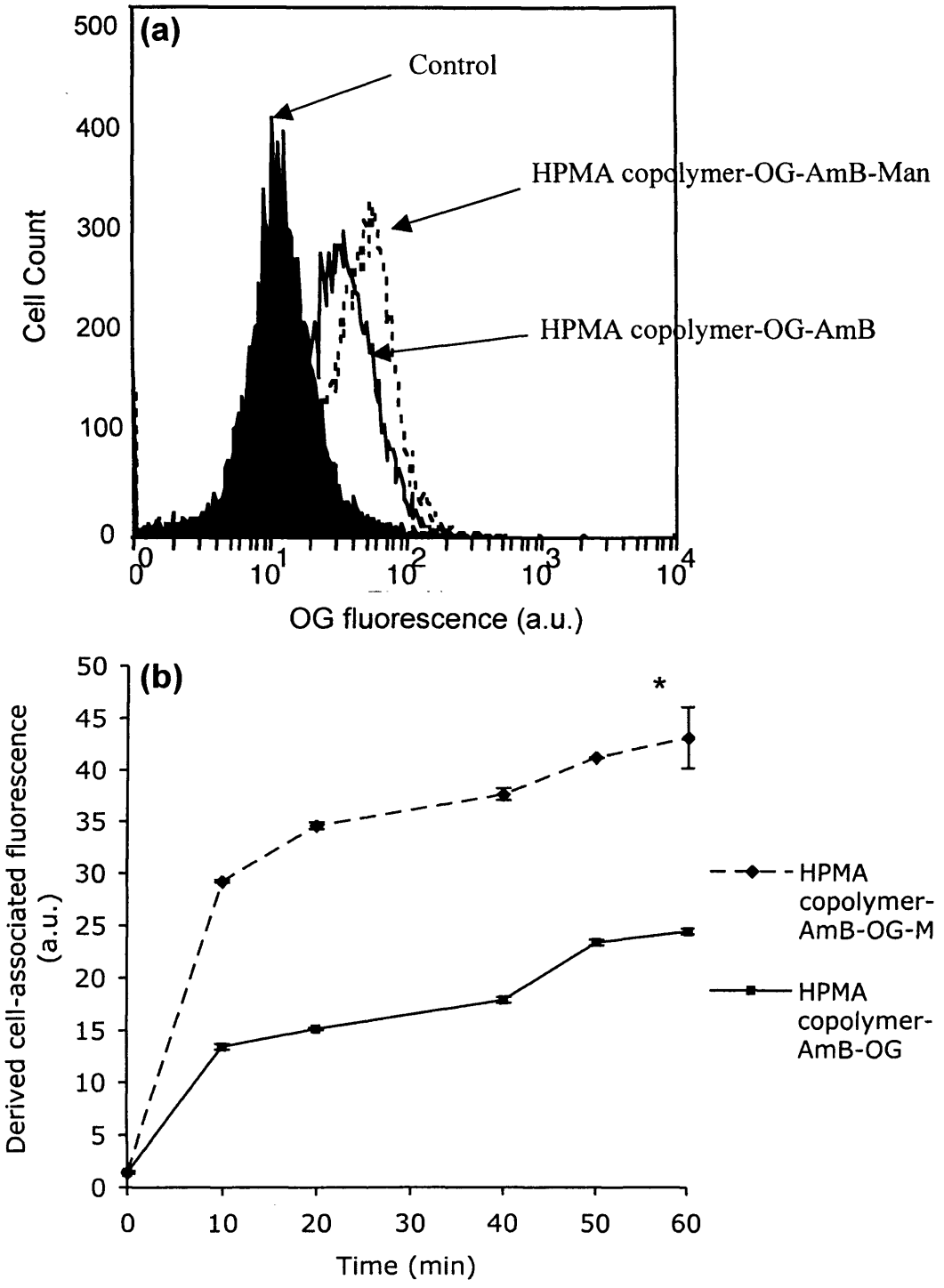

Figure 6.14 Time-dependent uptake of HPMA copolymer-AmB ± Man conjugates by THP-1 cells at 37 °C. Panel (a) flow cytometry raw data and (b) cell-associated fluorescence. The data represent the mean ± SD (n =3) and where the error bars are not visible they fall within the data points. Statistical significance (*) was determined at $p < 0.05$ (paired t-test).

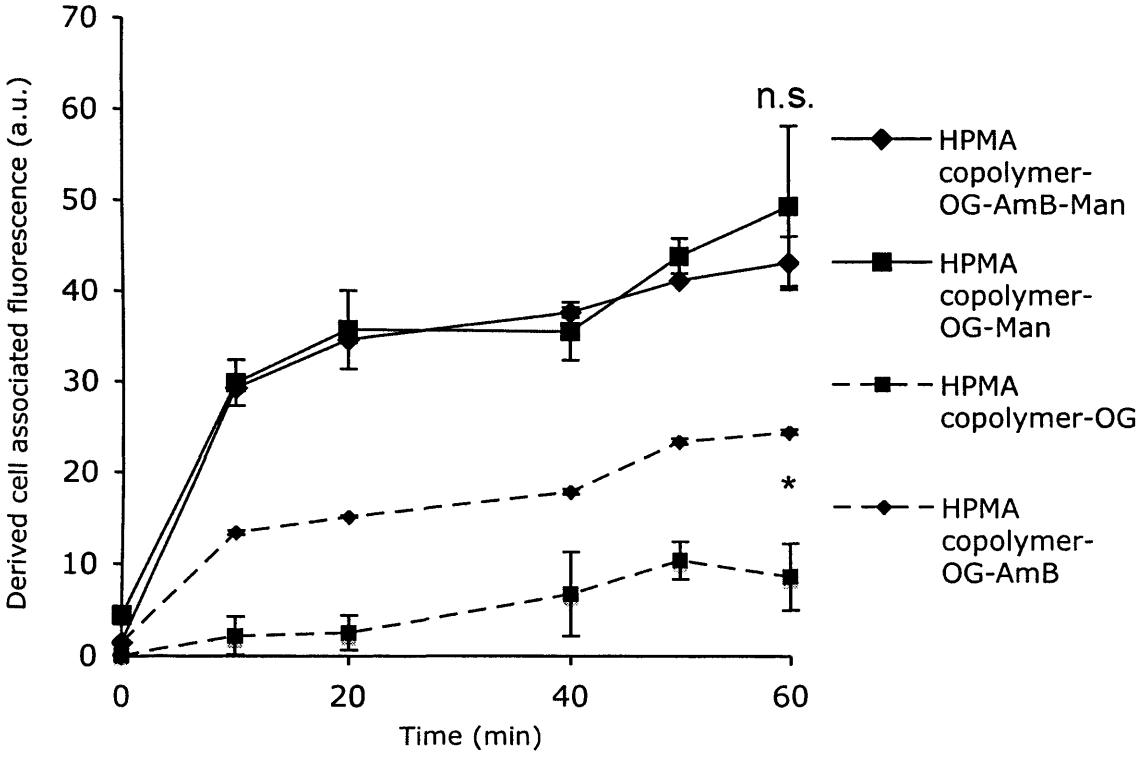

Figure 6.15 Time-dependent uptake of HPMA copolymer-OG ± Man ± AmB in THP-1 cells at 37 °C. Cell associated fluorescence measured by flow cytometry. The data represent the mean ± SD (n =3) and where the error bars are not visible they fall within the data points. Statistical significance (*) between HPMA copolymer-OG ± AmB was determined at $p < 0.05$ (ANOVA plus Bonferoni *post hoc* test).

(a) HPMA copolymer-OG-AmB

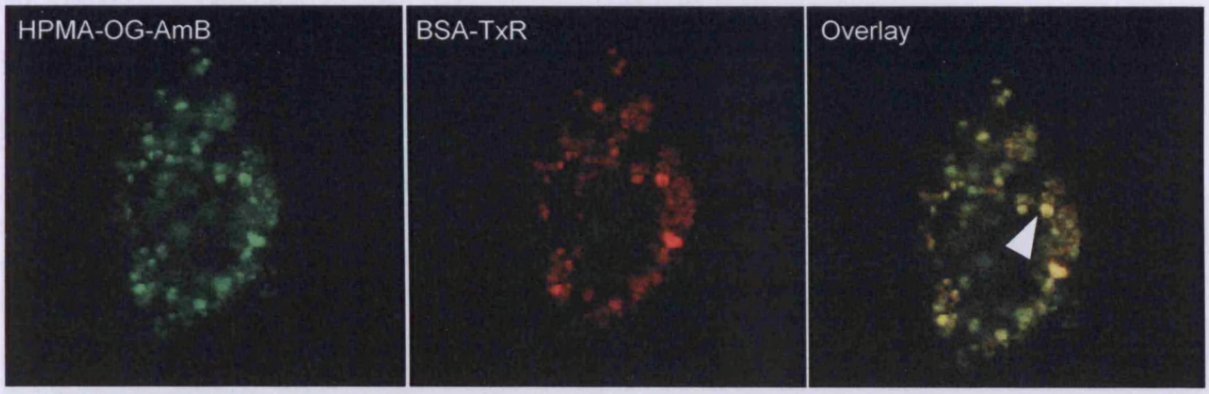

(b) HPMA copolymer-OG-AmB-Man

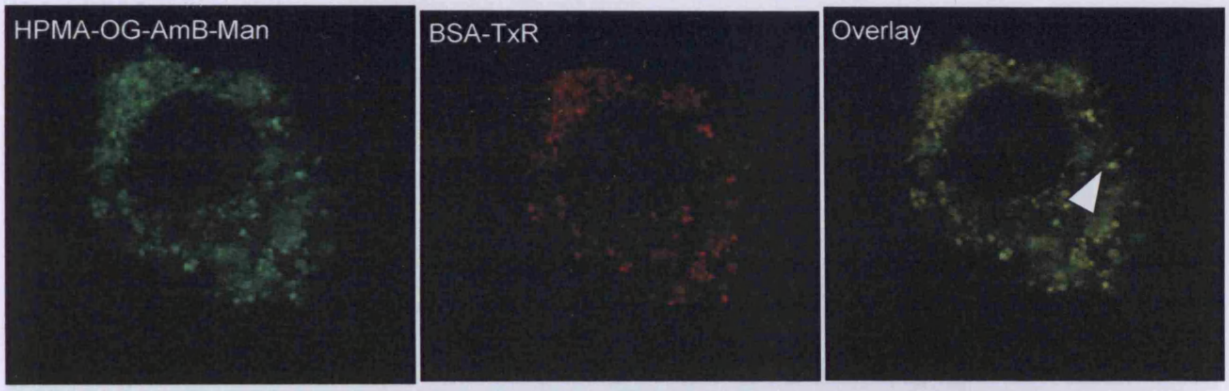

Figure 6.16 Confocal fluorescent microscope images of THP-1 cells incubated for a 24 h with AmB conjugates. Panels represent cells labelled with BSA-TxR and co-labelled with (a) HPMA copolymer-OG-AmB and (b) HPMA copolymer-OG-AmB-Man. Examples of co-localisation between compartment marker and BSA-TxR are indicated using white arrows.

(a) HPMA copolymer-OG-AmB

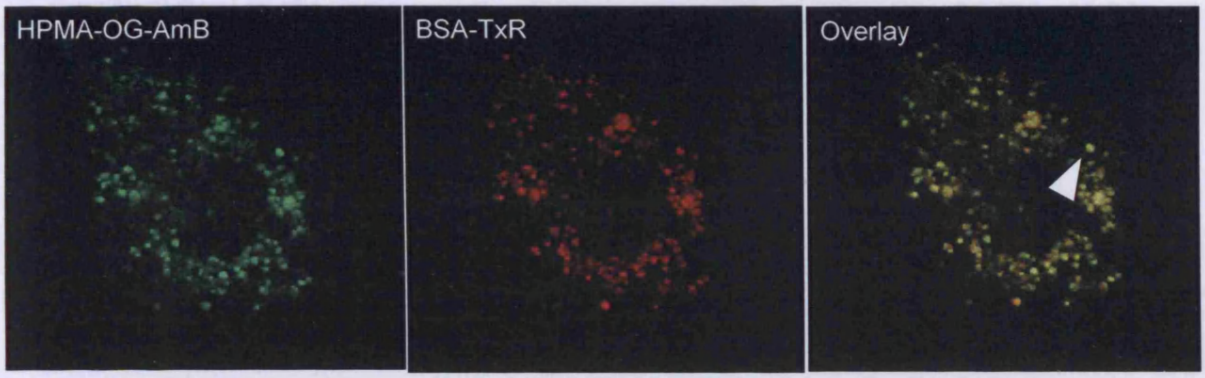

(b) HPMA copolymer-OG-AmB-Man

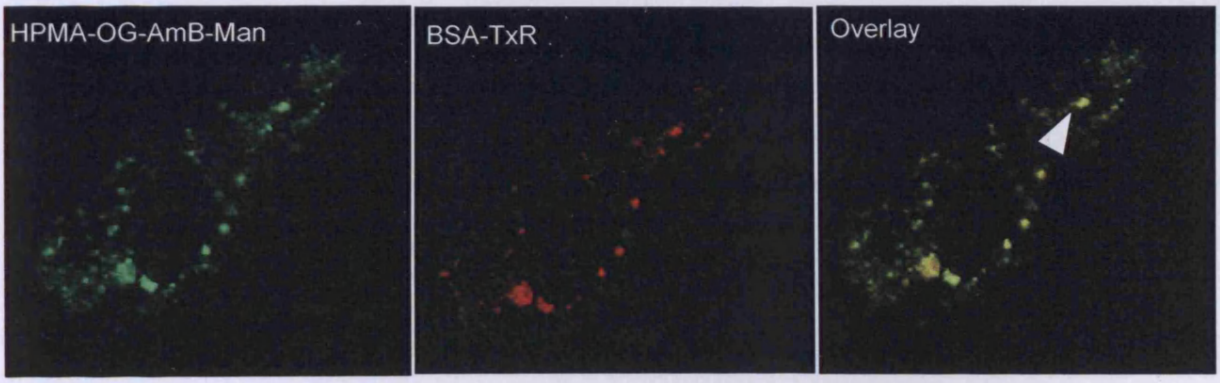

Figure 6.17 Confocal fluorescent microscope images of THP-1 cells incubated for a 1 h pulse and a 3 h chase with AmB conjugates. Panels represent cells labelled with BSA-TxR and co-labelled with (a) HPMA copolymer-OG-AmB and (b) HPMA copolymer-OG-AmB-Man. Examples of co-localisation between compartment marker and BSA-TxR are indicated using white arrows.

After incubation of THP-1 cells with the HPMA copolymer-AmB-Man conjugate and SCF, the UV absorbance was used to measure the AmB distribution in the fractions. The measured absorbance was at the lower end of the calibration curve (~ 0.05 mg/ml close to the limit of detection 0.01 mg/ml), so results were shown as % of total absorbance (Figure 6.18). After 24 h incubations the AmB UV absorbance was found predominantly in two groups of fractions, ~ 15 % in 3-5, and ~ 35 % in 14-22. A smaller peak was also seen in fraction 10. This distribution correlated somewhat with the lysosomal enrichment, however a larger proportion was in fractions correlating with the early endosomal compartments.

The AmB dot blot was used to gain better resolution of the intracellular distribution. The method was able to detect < 1 μg/ml free AmB or AmB-equivalent on the conjugates, and had a linear increase up to 50 μg/ml (Figure 6.19). However, it was not possible to measure the AmB in the fractions due to problems with detection. An example of a dot blot of the fractions shows dark spots in fractions 4 – 8, and clear spots in fractions 16 - 20 (Figure 6.20). The possible reasons for this and possible solutions will be discussed in the next section.

6.4 Discussion

The primary aim of these preliminary studies was to synthesise and characterise the HPMA copolymer-AmB-Man conjugates and evaluate them for the biological compatibility and potential for targeting macrophages.

Synthesis and chemical characterisation of the conjugates

These studies show preliminary results on HPMA copolymer-AmB-Man conjugates, but greater characterisation of the conjugates is needed before further development is possible.

A high loading of AmB was achieved (~ 17 wt%) in comparison to both Fungizone and Ambisome (~ 12 wt %). Importantly, improved solubility was shown, which would be essential for safe delivery of a therapeutic, and appropriate for IV administration. If a higher loading was necessary, then this could be achieved by using a HPMA copolymer with higher number of GFLG side chains. However, aqueous solubility may be reduced with higher AmB loadings. The solubility was not tested due

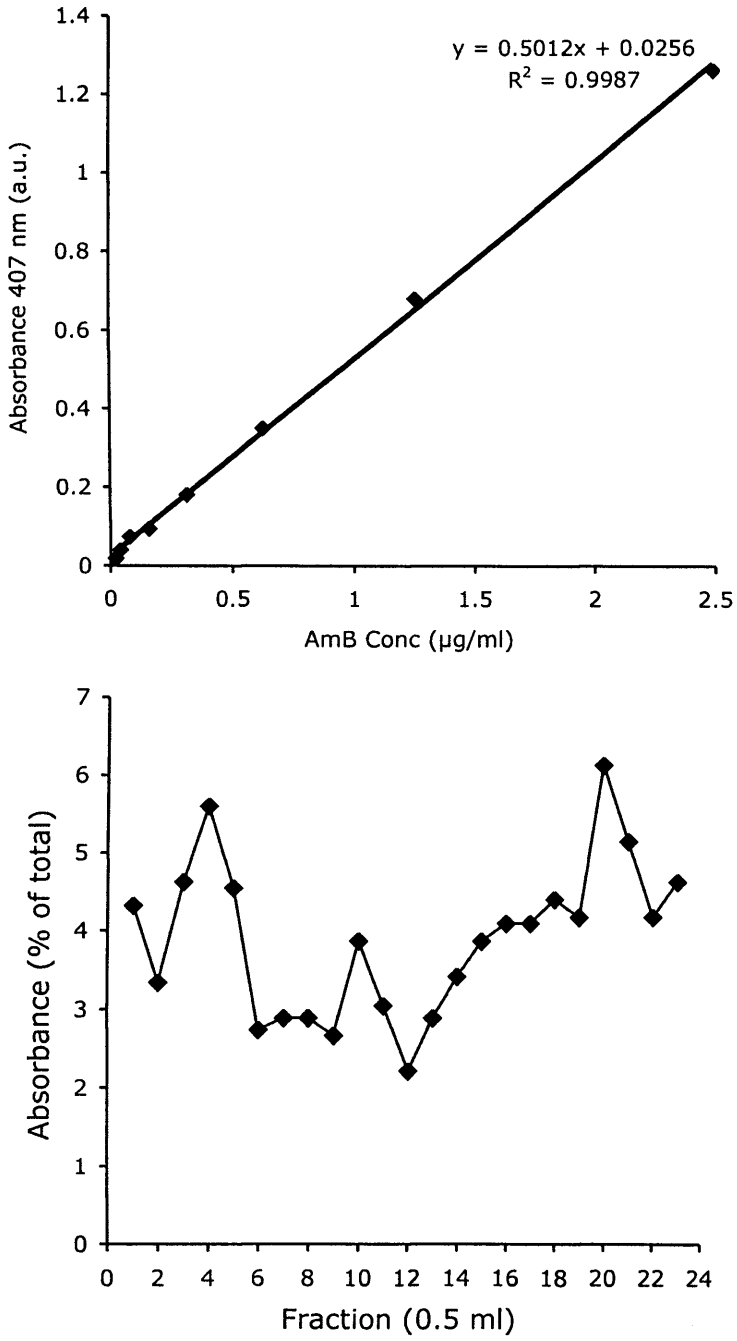

Figure 6.18 Distribution AmB in THP-1 cell fractions after 24 h incubation with HPMA copolymer-OG-Man (with leupeptin). Panel (a) calibration curve of AmB in MeOH, panel (b) UV absorbance of AmB measured in fractions (n=1).

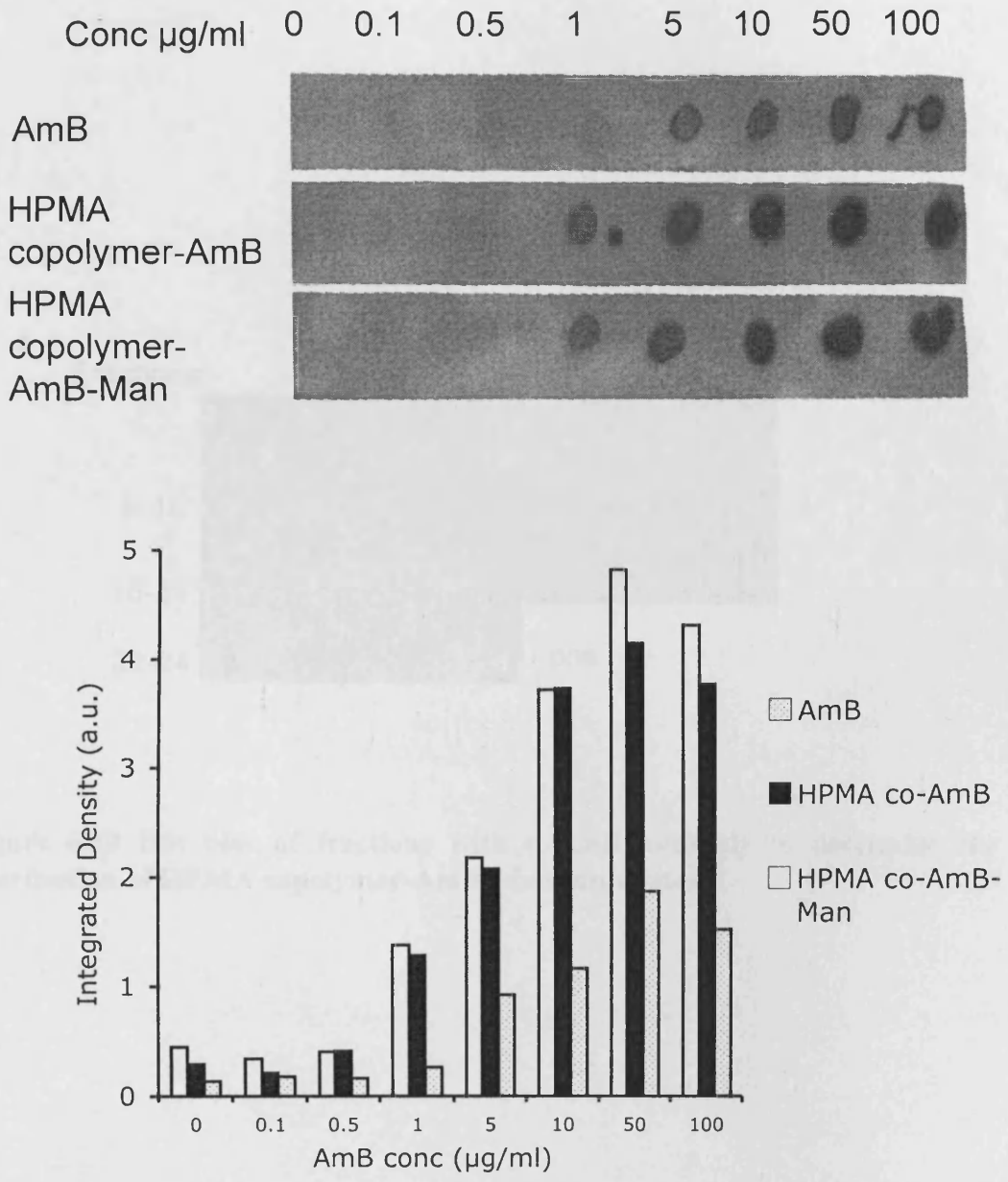

Figure 6.19 Dot blot of AmB. Calibration using α-AmB antibody (1:50 dilution/0.028 µg/ml). Panel (a) dot blot (b) plotted integrated density of fractions (n=1).

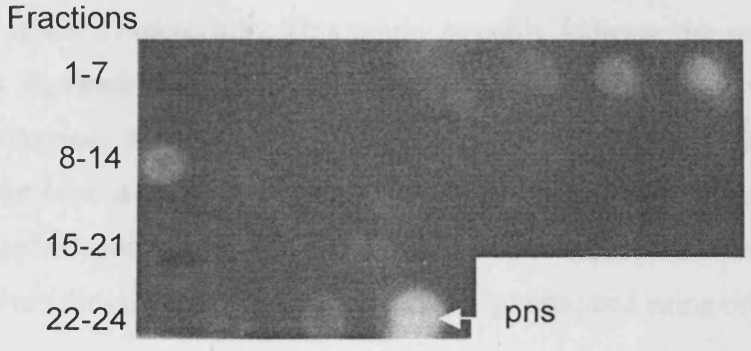

Figure 6.20 Dot blot of fractions with α-AmB antibody to determine the distribution of HPMA copolymer-AmB-Man conjugates.

to lack of product but the conjugate was clearly soluble in cell culture media at the concentrations used.

The sensitivity of the HPLC method (20 ng/ml) compared well with the published sensitivity values, which vary between 1 and 100 ng / ml in plasma and tissues (Table 6.4). The unknown peak seen at about 4 min (Figure 6.4) probably corresponds to impurities (other polyene compounds) that are found in all commercial preparations of AmB, such as amphotericin A (Cleary et al., 2007).

When the HPMA copolymer-AmB conjugate was applied to the column no free AmB was detected, but in the spiked sample the AmB detected was greater than the amount spiked (Figure 6.5). This could possibly indicate the presence of free AmB, however the results indicate the amount would be minimal in any case (>1% of total). This discrepancy may be due to measuring at the limit of sensitivity of the method. Had more time been available, the amount of free drug would be measured using a more robust method, such as using a different column to separate the free AmB, and the drug release from the conjugates would have been investigated using this method.

The Man content of these conjugates was not measured due to the problems with the method (discussed in section 4.4.1), and the limited time available to develop a new method. However, the theoretical Man contents were supported by the biological results in chapter 4.

For further development of the HPMA copolymer-AmB-Man conjugates, it would be necessary to better characterize the conjugates for the total Man, the free OG, and most importantly the free AmB content. The time limitation on these studies and the length of time needed to validate new methods meant that only preliminary characterisation could be performed. Had more time been available, the free AmB content would have been measured using an LH20 chromatography column, and then using either UV or HPLC analysis. However, the latter studies (the different stability and cytotoxicity profiles of the conjugates compared to free AmB) support the assumption that AmB was bound to HPMA copolymer and there was limited free AmB.

Table 6.4 Methods for AmB extraction and measurement by HPLC reported in the literature.

Reference	Extraction method	Recovery	HPLC method	Sensitivity
Granich et al., 1986	Cells homogenised and extracted with MeOH. SPE C18 column, conditioned with acetonitrile, sodium acetate buffer (pH7.2), 200µl sample, washed with MeOH-sodium acetate buffer (I:1), eluted with MeOH	92%	HPLC + N-acetyl AmB standard, A382, 1.5ml/min, C18 RP column, mobile phase acetonitrile:0.01 M EDTA (40:60 v/v pH4.2), retention time 4.9 min	0.04-10 µg/ml
Wang et al., 1992	Blood/ tissues homogenised and extracted with MeOH. SPE C18 column conditioned with MeOH, water, 10mM phosphate buffer pH7.4; washed with MeOH:phos buf (40:60 v/v); elution acetonitrile:2.5mM Na_2EDTA	92, 69, 76% (plasma, blood tissues)	HPLC + N-acetyl AmB standard, A382, 100µl sample injected, 1ml/min, C18 RP column, mobile phase acetonitrile:2.5mM Na_2EDTA (45:55 v/v pH4.2), retention time 6-7 min	5 ng/ml (P) 25 ng/ml (B) 2.5 ng/ml (U) 50 ng/ml (T)
Lopez-Galera et al., 1995	Serum samples diluted 200:600µl in MeOH, 10500g 5 min, 80 µl supernatant injected directly	90.2%	HPLC + A405, 1ml/min, short C18 RP column, mobile phase acetonitrile:2.5mM Na_2EDTA (30:70 v/v), retention time 1.5 min	50 ng/ml

Table 6.4 continued Methods for AmB extraction and measurement by HPLC reported in the literature.

Reference	Extraction method	Recovery	HPLC method	Sensitivity
Lambros et al., 1996	Serum or tissues homogenised and extracted with MeOH-acetic acid (9:1 v/v), the supernatant filtered and 100 µl injected directly	91.5, 74, 70 % (plasma, lungs, liver)	HPLC + A383, 1ml/min, C18 RP column, mobile phase acetonitrile:acetate buffer (37:63 v/v pH 4), retention time 15 min	100 ng/ml
Walsh et al., 2000	as Granich et al.	90%	as Granich et al.	25 ng/ml
Campanero et al., 2000	J774.2 cells lysed with TnX100 (1%) then diluted 2:1 v/v with MeOH and 150 µl samples injected directly	~ 99 %	HPLC at A408, 1ml/min, C8 RP column, mobile phase acetonitrile:water:0.05 M ammonium acetate, 0.02 M triethylamine, 4% acetic acid buffer (40:14.5:45.5 v/v pH6.6), retention time 4.01 min	1 ng/ml

Table 6.4 continued Methods for AmB extraction and measurement by HPLC reported in the literature.

Reference	Extraction method	Recovery	HPLC method	Sensitivity
Eldem & Arican-Cellat, 2001	Plasma diluted 1:1 in PBS. SPE C18 column conditioned with MeOH, water, phosphate buffer; 1 ml sample; washed with MeOH-phosphate buffer (40:60 v/v); eluted with acetonitrile-disodium edetate (2.5mM, 60:40 v/v, pH 4.2)	98%	HPLC at 407 nm, 100µl sample, 1ml/min, C8 RP column, mobile phase acetonitrile:disodium edetate 45:55 v/v pH5), retention time 6.27 min	10 ng/ml
Bekersky et al., 2002	Plasma samples < 2 mg/ml, extracted with MeOH and supernatant injected	66-77 %	HPLC at 405 nm, 1ml/min, RP column, mobile phase acetonitrile:0.05 N sodium acetate (34:66 v/v), retention time 4.9 min	
Espanuelas et al., 2003	as Campanero et al. - J774.2 cells		as Campanero et al. but 100µl injected and mobile phase pH3	1 ng/ml
Vogelsinger et al., 2006	Tissue homogenised, extracted with MeOH. SPE C18 column conditioned with MeOH, 45% MeOH; 0.5 ml sample; washed with 45 % MeOH; eluted with 60% acetonitrile.	55.2±4%	Reversed-phase HPLC using a RP C8 column, 405 nm, mobile phase acetonitrile-MeOH 10 mM NaH_2PO_4 buffer (41:10:49, v/v). Retention time 6.7 min.	5 ng/ml

As the toxicity of AmB is related to the aggregation state of the drug, the UV absorbance under different conditions could reveal information about the conformation of the conjugates, in relation to free AMB and other delivery methods, such as Ambisome®. In MeOH the conjugate spectrum was typical of monomeric AmB and of aggregated AmB in aqueous media (Figure 6.6). AmB aggregated in a solution of ≥ 50 % MeOH (Figure 6.7), as previously demonstrated by Adams & Kwon (2004). Although there was no large difference between the absorbance spectra in aqueous solution, the MeOH concentration at which the HPMA copolymer conjugate bound AmB aggregated was lower (70 – 100 % MeOH) (Figure 6.8). This and the altered stability profile suggested there was a different product, and that AmB was covalently bound rather than free AmB associated with the polymer.

Therefore, the hydrophobic interaction of AmB in aqueous solution was not impaired by the conjugation to the polymer. In agreement with studies on other polymer conjugates such as PEG-AmB and gum Arabic-AmB conjugates (Nishi et al., 2007; Sedlak et al., 2007a; Sedlak et al., 2007b). The structure of the HPMA copolymer is postulated to be a dynamic unimolecular micelle and the hydrophobic AmB could cause a change in conformation allowing the AmB to aggregate and may effect drug release. This has been proposed for HPMA copolymer-Dox, which showed a reduced rate of drug release with increased drug loading due to the effect of the hydrophobic interaction of Dox (Vicent et al., 2005).

It was important that therapeutics were stable at 37 °C, but free AmB has little stability in aqueous solutions at this temperature. The problems of AmB instability may be amplified in preparations of AmB designed to have an increased plasma half-life. However, the reduction in absorbance of the HPMA-conjugated AmB occurred at a slower rate and to a lesser degree than that of free AmB (Figure 6.9). Similar results were observed with arabinogalactan-AmB conjugates (Ehrenfreund-Kleinman et al., 2002; Ehrenfreund-Kleinman et al., 2004). These data suggest that the covalent binding of AmB to the polymer leads to stabilisation of the drug in aqueous solution. The increased stability shown by the HPMA copolymer-AmB conjugates should mean a greater percentage of the drug delivered to the parasite would still be active.

Biological characterisation of the conjugates

The success of these delivery methods is dependent on the mechanism of action, e.g. the state of aggregation, and this may influence the choice of delivery method. These preliminary studies have shown that HPMA copolymer conjugation produced a stable AmB therapeutic with reduced haemolytic activity and reduced cytotoxicity against human macrophage cells. Methods to investigate the intracellular fate of the AmB conjugates were also set up and demonstrated the potential of these methods to study the intracellular trafficking of other polymer-drug conjugates.

The haemolysis assay is most commonly used to assess the non-specific toxicity of AmB. However, the toxicity of AmB to macrophages has been attributed to a different mechanism than that for the RBCs, and involves binding to serum LDL and uptake via the LDL receptor, therefore it was considered important to also assess the toxicity in the THP-1 cells (in the presence of serum).

First, the cytotoxicity of AmB and paromomycin was investigated. AmB was, as expected, much more toxic to both THP-1 and RAW 264.7 cells than paromomycin In fact, paromomycin did not show toxicity against the RAW 264.7 cells, although a small amount of cytotoxicity was seen against the THP-1 cells (Figure 6.10). Clinical trials of paromomycin (at 11 mg/kg/day for 21 days) have shown it to have activity against VL equal to AmB (at ~ 1 mg/kg/ every other day for 30 days) though required higher doses (Sundar et al., 2007). It may be possible to achieve greater activity with lower doses when delivered to the specific site of action (the PV). Therefore, paromomycin was considered a possible alternative drug for conjugation if AmB proved not feasible, or in combination with AmB.

The cytotoxicity of the HPMA copolymer-AmB ± Man conjugates was significantly lower than the free AmB against the THP-1 cells (Figure 6.11). At AmB concentrations found in the blood of Fungizone-treated patients (~ 2 μg/ml) 95 % is bound to plasma proteins (Bekersky et al., 2002). In studies in renal cells, inhibition of LDL-AmB formation decreased toxicity (Barwicz et al., 1992), as did inhibition of LDL receptor expression (Wasan et al., 1994). Similar to other polymer-drug conjugates, HPMA copolymer conjugation significantly reduced toxicity to THP-1 cells. Therefore, it could be that binding to LDL is inhibited. The reduction in non-specific toxicity should increase the anti-leishmanial specificity.

The reduction in toxicity could also be due to polymer-bound AmB being sufficiently well hidden within the polymer coil to minimize membrane interaction. However, this does not prove that the AmB does not retain any activity when bound. Different mechanisms are thought to be responsible for cytotoxicity and anti-leishmanial activity. However activity is likely to be inhibited, as the amino group on the sugar to which the polymer is bound has been found to be essential to activity (Brajtburg et al., 1990). A rotatable β-glycosidic bond links the macrolide ring and the sugar, and the sugar orientation strongly affects the ergosterol selectivity and permeabilisation of the membrane (Matsumori et al., 2005). Although there was still some toxicity seen with the conjugate, this was completely prevented when leupeptin was added to the incubation medium (Figure 6.12). Leupeptin had no effect after 24 h, but this is likely to be due to degradation of the leupeptin. Therefore, this indicates that drug release is essential for activity.

Toxicity of AmB and its formulations is normally assessed in RBCs with no serum present. In studies on human RBCs, only the self-associated form of AmB caused K^+ leakage and subsequent haemolysis (Legrand et al., 1992). Therefore the haemolysis caused by AmB was probably due to this aggregation rather than LDL binding and uptake. The absence of haemolytic activity when incubated with the HPMA copolymer-AmB-Man conjugates further supported the conclusion that no free AmB was present. Although the UV absorbance studies showed the conjugates were in an aggregated state, this did not lead to toxicity. This property of the conjugated drug may lessen the risk of severe hepatic toxicity. Next it was important to investigate the uptake, to see if the AmB conjugates retained the increased derived cell association in macrophages seen in HPMA copolymer-Man conjugates espite possible changes in conformation (Chapter 4).

Increased cell surface binding of the AmB conjugates was considered a possibility due to the high loading of AmB. Also, the conformational change that may be induced by AmB conjugation may change the MR binding, the non-specific cell association and therefore the uptake. The conjugate solutions were standardised to contain the same amount of OG, rather than the amount of AmB. However the actual

amount of AmB used was almost identical (18.8 wt % in HPMA copolymer-AmB compared to 18.7 wt % in HPMA copolymer-AmB-Man). When the derived cell association in THP-1s was compared to that of the conjugates studied in chapter 4 (Figure 6.15), there was no difference between HPMA copolymer-OG-Man ± AmB, however there was a difference between HPMA copolymer-OG ± AmB. This would suggest that there was some enhanced non-specific binding or uptake due to the AmB, but this was not significant in comparison to the MR-specific uptake.

Specific uptake is likely to be related to efficacy. Heated Fungizone® showed higher uptake into macrophages, and was 2.5 times more effective against *Leishmania donovani* (but showed no difference in activity against fungal infections) (Cheron et al., 2003). Interestingly, Ambisome® actually has lower uptake into J774 macrophages than other liposomal AmB formulations (Legrand et al., 1996). Therefore it is hoped that MR targeting can increase uptake in comparison to Ambisome® without increasing non-specific toxicity, and result in greater activity.

Ambisome® is the gold standard of anti-leishmanial treatment, where cost is not a factor. The prolonged circulation times mean Ambisome is passively targeted to the macrophages. However, AmB is also slowly released in the blood plasma over time (Bekersky et al., 2001). Therefore its activity is not constrained to inside the macrophage. Specific targeted release of the drug from the HPMA copolymer-AmB-Man conjugates in the macrophage/PV may reduce the dose needed and result in even lower toxicities. However, further studies are needed on the pharmacokinetics of these conjugates before conclusions can be drawn.

The results from the cytotoxicity studies were used to determine concentrations and timings used for the SCF and confocal FM studies (0.1 mg/ml for 24 h). When Fungizone is administered *in vitro* only a small amount of AmB administered actually gets to the lysosome after 1 h (Vertut-Doi et al., 1994). This is dependent on concentration as high concentrations can block endosome-lysosome fusion. This further emphasises that a specific delivery method is needed. The high localisation of the HPMA copolymer-AmB-Man conjugate in lysosomes demonstrates the advantage of this system. Though the AmB was only partly found in the lysosomes using the SCF

method (Figure 6.18), the microscopy showed there was a high concentration of conjugate in the lysosomes. If more time were available, further studies including a pulse-chase incubation with HPMA copolymer-AmB-Man would have been performed to try to further investigate the trafficking. Also, if a shorter time frame had been used e.g. 4 h, this would eliminate the possibility that the leupeptin was degraded.

As AmB acts on surface it might not need to be released as long as it is delivered to PV. However, if there was inhibited fusion between the PV and the lysosome, then the drug must be able to diffuse across the vesicle membranes. For AmB this may lead to increased toxicity to the lysosomal membrane and lead to rupture of lysosomes. The studies with lysosomes discussed in section 5.1.1, and the microscopy studies showing HPMA copolymer-OG in close proximity to the parasite in the THP-1 cells in chapter 5, suggest fusion would allow direct access to the PV for the conjugate. However, the intracellular trafficking of the HPMA copolymer-drug conjugates must be carefully examined, and highlights the need for studies in infected cells.

One of the main difficulties of this study was that an accurate method for quantifying AmB was not available. Several attempts were made to measure AmB using dot blotting with an antibody against AmB. When calibrating the antibody, the method was found to be very sensitive, detecting both free AmB and HPMA copolymer-AmB-Man conjugates from ~ 0.1 – 50 μg/ml. However, difficulties arose when the fractions were blotted, giving a negative image on the film (clear spots rather than dark) (Figure 6.20). If more time were available, this method would be further investigated. Alternatively, the ideal quantitative method would have been to degrade the linker to then extract the free AmB and use the HPLC method to determine exact amounts of conjugate/AmB in each fraction.

Following this work, studies on efficacy would be needed, as well as studies on the intracellular trafficking in *Leishmania*-infected macrophages. A preliminary study on anti-leishmanial activity has been performed using these conjugates (by Karin Seifert, 2007, LSHTM). HPMA copolymer-AmB and HPMA copolymer-AmB-Man had significant anti-leishmanial activity (reduced infection completely at 0.56 μg/ml, and to ~ 20 % at 0.19 μg/ml) (Figures 6.21 and 6.22). The MR-targeted conjugate had

- THP-1 cells differentiated
- Promastigotes at late stage (infective)
- Infected ration 10:1

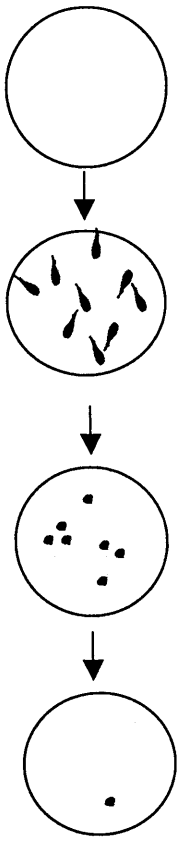

- After 24h infection control checked
- Cells washed and AmB/Conjugate added (0.19 - 5 µg/ml)
- After 72 h cells washed, MeOH fixed and stained with Giemsa (10% for 10m)
- Amastigote infected cells counted compared to negative control (100 %) and AmB-treated positive control (100 macrophages in quadruplate)

Figure 6.21 Scheme for investigation of efficacy of HPMA copolymer-AmB conjugates against *Leishmania donovani*-infected THP-1 cells.

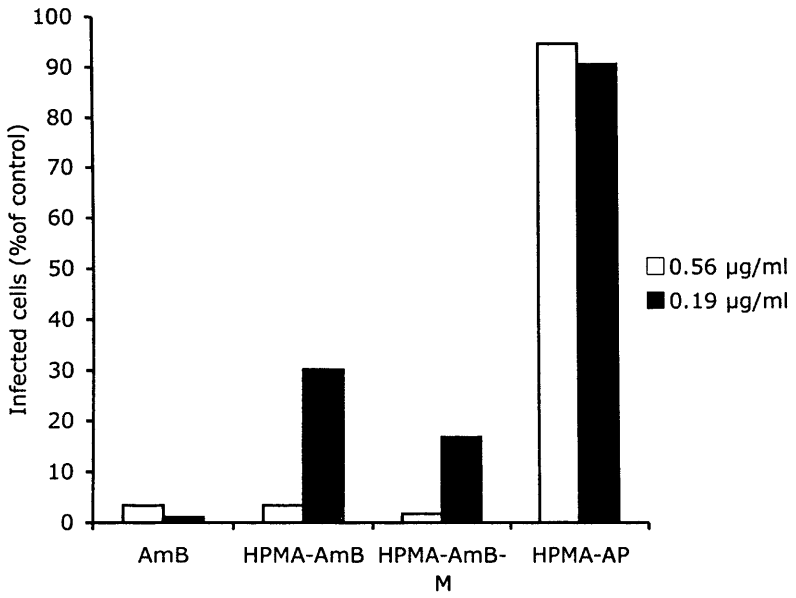

Figure 6.22 Efficacy of HPMA copolymer-AmB conjugates against *Leishmania donovani*-infected THP-1 cells. The amastigote infection level of the THP-1s was ~ 50 %. 100 cells were counted per quadruplate and the data expressed as a percentage of the control.

slightly higher activity, possibly supporting the idea of greater uptake and therefore drug release. These studies were only preliminary and ongoing, further work is needed to confirm these results and explore these effects in more detail. For comparison, the ED50's of Fungizone and Ambisome against *Leishmania donovani* against THP-1 cells were similar at 0.18 and 1 μg/ml (Yardley & Croft, 2000). However, it should be noted that these values differ depending on the cell line, and are also different *in vivo* (in PEM 0.13 and 1.5; *in vivo* 0.21, 0.73).

6.5 Conclusions

In conclusion, HPMA copolymer-AmB-Man conjugates have been synthesised with enhanced solubility and stability in comparison to free AmB. These conjugates have reduced the haemolysis and the non-specific toxicity against the human macrophage model THP-1. Enhanced MR-specific derived cell association and macrophage uptake, as well as subsequent trafficking to lysosomes have been shown. In order to develop the HPMA copolymer-AmB-Man conjugates for treatment of leishmaniasis further characterisation of the conjugates is required. However, these preliminary results have demonstrated the potential of these conjugates to provide a specific and potent treatment for leishmaniasis.

Chapter 7

General Discussion

7.1 Perspective and recent developments

Although the field of polymer therapeutics is relatively new, there has been an exponential increase in research in this area over the last few years (Duncan et al., 2006). This is presenting new opportunities to design novel, more therapeutically effective treatments for a number of diseases including intracellular infections such as leishmaniasis. The original idea behind this project was the need for new anti-leishmanial therapies. The main drugs currently in use are more than 50 years old and the therapeutic scenario has actually worsened over this time due to emerging resistance. The number of new drugs entering the pipeline is very low, mainly due to the lack of funding. Despite tropical diseases such as malaria, trypanosomiasis, leishmaniasis and tuberculosis accounting for 5% of the global disease burden, they accounted for only 0.1 % drugs brought to market between 1996 and 2006 (Date et al., 2007). However, according to the WHO, leishmaniasis remains a major health problem, and the distribution if not the actual number of cases has been on the increase since this study began (Boelaert, 2004).

Despite the numerous efforts to advance the diagnosis and treatment of *Leishmania,* there have been no significant advances. This situation has led to the formation of several not-for-profit product–development partnerships (Drugs for Neglected Diseases initiative (DNDi), The Medicines for Malaria Venture the Institute for One World Health, and the WHO Tropical Diseases Research Programme (TDR)). Specific initiatives include the clinical trials platform being organized by the DNDi in the Horn of Africa; and the draft agreement between the Bill and Melinda Gates Foundation and One World Health to carry out phase III/IV trials of paromomycin in India (Sundar et al., 2007). In 2005 health ministers formulated an ambitious VL elimination programme in the Indian subcontinent (Bhattacharya et al., 2006), spurred by the fact that, in this area, humans are the only reservoir and phlebotomus argentipes the only vector. However, the situation is less favourable in other areas and all these drugs have significant drawbacks.

A further boost to the anti-leishmanial effort came when some pharmaceutical companies agreed to reduce the prices of their drugs. An agreement between the WHO and Vestar in 2007 led to preferential pricing of Ambisome for VL patients of 10 GBP per 50 mg vial (as opposed to 96.69 GBP (BNF 2006)). However this price is valid for VL patients treated by not-for-profit organisations in East Africa only. The

Médecins Sans Frontières (MSF) claims that this is not enough to make Ambisome a cost effective alternative: "This is a significant and welcome reduction of the current private market price. However, treatment of VL with L-AMB according to WHO is done with a total dose of 20 mg/kg, with a flexible dosing schedule but an initial dose of at least 5 mg/kg. With the reduced price, for a patient of 35 kg, a full course with a total dose of 20 mg/kg still costs US$280. This price is too high for implementation in treatment programmes in developing countries."

Although considerable progress has been made in basic research into the biology of *Leishmania*, for example the *Leishmania* Genome Network has recently mapped the genome of *Leishmania major* (Ivens et al., 2005), the research in the area of therapeutics has not been so productive. However, the fact that since this study began, in 2004, no new anti-leishmanial therapies have been introduced to the market, makes polymer-drug conjugates of existing drugs a very interesting option for investigation. Since 2004, the number of polymer therapeutics entering clinical trials has increased greatly, and the continued clinical trials of HPMA copolymer-drug conjugates, including the targeted polymer drug conjugate PK2, have encouraged further research into novel therapeutics including for infectious agents.

7.2 Critical evaluation of study and future work

The design of the novel HPMA copolymer conjugates able to target anti-leishmanial drugs to the macrophage could contribute significantly, and provide improved therapeutics, less toxic than existing drugs and also better able to overcome resistance. One aim of this study was to design the HPMA copolymer-AmB-Man conjugates with increased macrophage targeting and reduced non-specific toxicity, and to eventually produce a candidate for clinical trial. A second objective was to investigate the *in vitro* intracellular trafficking of the conjugate and drug in uninfected macrophages. Therefore, a large amount of the work was establishing methods that could be used to study polymer therapeutics, specifically setting up the macrophage models, and the fluorescence microscopy and SCF methods.

Initial studies demonstrated that the THP-1 cell line was a suitable model for use in these mannose-targeting studies; expressing MR in sufficient numbers to study receptor specific targeting of polymer conjugates (Chapter 3). HPMA copolymer-Man

endocytosis was proportional to sugar content with a threshold of 4 mol % needed to achieve reproducible targeting to the THP-1 macrophages over the control conjugate (Chapter 4). A novel quantitative fractionation method was developed for THP-1 cells, along with a confocal microscopy method, which could be used to investigate time-dependent trafficking of HPMA copolymer conjugates (Richardson et al., 2008; Wallom et al., 2008) (Chapter 5). Using this SCF method, the lysosomotropic delivery of HPMA copolymer-OG-Man and the release of GFLG bound OG could be demonstrated. The established methods have the potential to be applied to the study of a variety of polymer therapeutics.

Finally, the first HPMA copolymer-AmB-Man conjugates were synthesised and investigation into their activity demonstrated reduced haemolysis and toxicity against the human macrophage model THP-1 (Chapter 6). Uptake and trafficking studies showed enhanced cell association, macrophage uptake and trafficking to lysosomes. However, one of the challenges of this method was achieving truly quantitative analysis of drug trafficking. The difficulty in measuring fluorescence or absorbance in a biological situation was a disadvantage. Had more time been available, methods would have been established to measure the absolute amounts of conjugate or AmB in the fractions. These studies have, though, begun to demonstrate the potential of these conjugates to provide a highly specific and effective treatment for leishmaniasis.

These results have underlined the advantages of using polymer-drug conjugates for the treatment of leishmaniasis, but have also highlighted a number of remaining questions. Further studies are needed to investigate the trafficking of the conjugates in infected cells to establish the localisation in relation to the parasite. The SCF method established in THP-1 cells here would have to be further optimised for infected cells, and the PV distinguished from the lysosomes. Although the current studies have demonstrated trafficking to the lysosomes in uninfected cells, in infected cells the likely altered trafficking of the conjugates could have a drastic effect on the original hypothesis. Few studies have attempted to study subcellular fractionation of *Leishmania*-infected macrophage cells (Kima & Dunn, 2005). None, to the author's knowledge, have studied intracellular trafficking of polymer drug conjugates in infected macrophages. However, current work at the LSHTM is developing this method in infected cells.

This research was necessarily informed by the success of Ambisome®, the current gold standard of treatment when cost is not a factor. AmB was a good choice for conjugation to HPMA copolymer, achieving a high loading of 16 - 19 wt%, in comparison to 12.5 wt% in Ambisome®. It is highly potent; preliminary activity studies showed that HPMA copolymer-AmB-Man conjugate (AmB dose of 0.56 μg/ml) produced almost 100 % parasite inhibition in *Leishmania donovani*-infected THP-1 cells, yet no non-specific toxicity against the macrophage at this dose. These results compare favourably with *in vitro* studies on Ambisome®, which had an IC_{50} of 1 μg/ml (Yardley & Croft, 2000) and show that HPMA copolymer-Man conjugates could provide a viable alternative. Whether activity could be increased beyond that of Ambisome® is beyond the scope of this study. Further studies on the *in vivo* activity are needed, as *in vitro* studies are limited as they do not take into account the different whole-body pharmacokinetics associated with polymer-drug conjugates.

To fully characterise the HPMA copolymer-AmB-Man conjugates and obtain a potential clinical candidate, pharmacokinetic studies would be needed to optimise the conjugate *in vitro*. Firstly, investigation of the polymer-drug linker to ensure optimal rates of intracellular release within the vacuole would be essential. Secondly, *in vivo* studies would be needed to ensure 4 mol % was still enough for targeting, and to establish pre-clinical activity and dosage data particularly in comparison to Ambisome®.

7.3 Potential applications for future development

Even if the afore-mentioned studies showed that HPMA copolymer-AmB-Man was highly effective against leishmaniasis, the potential for future development as an anti-leishmanial therapy will depend on a variety of factors such as the cost and patient compliance. Although formulated for IV administration, polymer drug conjugates are designed for long plasma circulation times, hence less frequent injections are needed. Interestingly, trials of single dose Ambisome® treatment with a 90 % cure rate have been reported (Sundar et al., 2001). A similar single dosage of the HPMA copolymer-AmB-Man conjugates could ensure high patient compliance and greatly reduce cost. Also, specific MR targeting reducing non-specific uptake could further reduce the required dose. Together, polymer-drug conjugates have the

potential advantage of reduced side effects, shorter treatment cycles and reduced dose, therefore increasing patient compliance and significantly reducing costs. The important comparison is against Ambisome®. Whether HPMA copolymer conjugates will be cheaper is difficult to calculate, however the active targeting could potentially decrease the dose needed in comparison to Ambisome®.

MSF suggest combination therapy could bring the price per treatment down but there is little data on combination therapies with Ambisome®. Combination therapy is desirable when resistance is a problem and this can be achieved neatly with a polymer conjugate. Indeed, recent studies have shown the potential breast cancer therapeutic HPMA copolymer-Dox-AGM conjugate has markedly enhanced cytotoxicity *in vitro* compared to HPMA copolymer-Dox, although mixtures of the two single drug conjugates did not have a synergistic effect (Greco et al., 2007; Vicent et al., 2005).

The choice of drug will be very important. The drug release rates of HPMA copolymer conjugates with a GFLG linker vary considerably depending on the drug conjugated and can greatly affect the activity. Combinations of drugs in simple mixtures may not necessarily improve the therapeutic effectiveness. Indeed the activity when mixed is likely to be very different to the activity when administered on the same polymeric chain. Miltefosine and AmB have shown synergy (Jha, 2006).The long ½ life (150h) of miltefosine means it needs careful regulation to prevent resistance developing (Chappuis et al., 2007). However, combination may reduce the treatment duration and prevent resistance (Bryceson, 2001). Paromomycin is attractive due to its low cost (US$10-20 per course), though side effects such as nephrotoxicity may limit its use. VL patients often have additional bacterial infections, and paromomycin has the advantage of being active against a number of bacterial infections. The current emerging problem of co-infection with HIV would benefit from intracellular delivery as well as combination therapy. Alternatively, the emergence of several new classes of drugs, for example dihydrofolate reductase inhibitors that have lower efficacy in vivo, presents an opportunity to generate several novel therapeutics.

Possible alternative applications of HPMA copolymer-Man's macrophage targeting, and the ability to tailor the intracellular trafficking and release of this sort of

system, are numerous. As discussed earlier, macrophages play a critically important role in host defence against many infectious agents, including bacteria, virus and parasites (Ahsan et al., 2002). Macrophages are also host's frontline defense against tumour cells. Therefore, targeting of drugs to macrophages could be an effective strategy for treatment of a variety of infectious diseases including schistosomiasis, leishmaniasis, brucellosis, salmonellosis, cancer, HIV, tuberculosis, influenza, herpes simplex e.g. in transplant patients, as well as rheumatoid arthritis, systemic lupus erythematosus, multiple sclerosis, enzyme replacement therapy e.g. gaucher disease. Since this study began, Ghandahari et al. have begun to develop the HPMA copolymer-Man platform for imaging, conjugating gadolinium for enhanced MRI of macrophages (Zarabi et al., 2006).

In conclusion, the presented work has advanced the methods needed for the design and the development of the ideal anti-leishmanial therapy. MR-targeted HPMA copolymer-AmB conjugates have shown potential for macrophage targeting and delivery to specific intracellular compartments. In addition, novel methods for investigating polymer therapeutics have been developed.

Bibliography

Adachi, Y., Ishii, T., Ikeda, Y., Hoshino, A., Tamura, H., Aketagawa, J., Tanaka, S. & Ohno, N. (2004). Characterization of beta-glucan recognition site on C-type lectin, dectin 1. *Infection and Immunity*, **72,** 4159-71.

Adams, M.L., Andes, D.R. & Kwon, G.S. (2003). Amphotericin B encapsulated in micelles based on poly(ethylene oxide)-block-poly(L-amino acid) derivatives exerts reduced in vitro hemolysis but maintains potent in vivo antifungal activity. *Biomacromolecules*, **4,** 750-7.

Aderem, A. & Underhill, D. (1999). Mechanisms of phagocytosis in macrophages. *Annual Reviews in Immunology*, **17,** 593-623.

Adler-Moore, J. & Proffitt, R.T. (2002). AmBisome: liposomal formulation, structure, mechanism of action and pre-clinical experience. *Journal of Antimicrobial Chemotherapy*, **49 Suppl 1,** 21-30.

Ahsan, F., Rivas, I.P., Khan, M.A. & Torres Suarez, A.I. (2002). Targeting to macrophages: role of physicochemical properties of particulate carriers-liposomes and microspheres-on the phagocytosis by macrophages. *Journal of Controlled Release*, **79,** 29-40.

Alexander, J., Satoskar, A.R. & Russell, D.G. (1999). *Leishmania* species: models of intracellular parasitism. *Journal of Cell Science*, **112,** 2993-3002.

Amer, A.O. & Swanson, M.S. (2002). A phagosome of one's own: a microbial guide to life in the macrophage. *Current Opinion in Microbiology*, **5,** 56-61.

Antoine, J.C., Prina, E., Lang, T. & Courret, N. (1998). The biogenesis and properties of the parasitophorous vacuoles that harbour *Leishmania* in murine macrophages. *Trends in Microbiology*, **6,** 392-401.

Arai, K., Kanaseki, T. & Ohkuma, S. (1991). Isolation of highly purified lysosomes from rat liver: identification of electron carrier components on lysosomal membranes. *Journal of Biochemistry*, **110,** 541-7.

Aramwit, P., Yu, B.G., Lavasanifar, A., Samuel, J. & Kwon, G.S. (2000). The effect of serum albumin on the aggregation state and toxicity of amphotericin B. *Journal of Pharmaceutical Sciences*, **89,** 1589-93.

Aubry, L. & Klein, G. (2006). Purification techniques of subcellular compartments for analytical and preparative purposes. *Methods in Molecular Biology*, **346,** 171-85.

Awasthi, A., Mathur, R.K. & Saha, B. (2004). Immune response to *Leishmania* infection. *Indian Journal of Medical Research*, **119,** 238-58.

Baas, B., Kindt, K., Scott, A., Scott, J., Mikulecky, P. & Hartsel, S.C. (1999). Activity and kinetics of dissociation and transfer of amphotericin B from a novel delivery form. *AAPS PharmSci*, **1,** E10.

Banerjee, G., Nandi, G., Mahato, S.B., Pakrashi, A. & Basu, M.K. (1996). Drug delivery system: targeting of pentamidines to specific sites using sugar grafted liposomes. *The Journal of Antimicrobial Chemotherapy*, **38,** 145-50.

Banuls, A.L., Hide, M. & Prugnolle, F. (2007). *Leishmania* and the leishmaniases: a parasite genetic update and advances in taxonomy, epidemiology and pathogenicity in humans. *Advances in Parasitology*, **64,** 1-109.

Barwicz, J., Christian, S. & Gruda, I. (1992). Effects of the aggregation state of amphotericin B on its toxicity to mice. *Antimicrobial Agents Chemotherapy*, **36,** 2310-5.

Basu, M.K. & Lala, S. (2004). Macrophage specific drug delivery in experimental leishmaniasis. *Current Molecular Medicine*, **4,** 681-9.

Basu, N., Sett, R. & Das, P.K. (1991). Down-regulation of mannose receptors on macrophages after infection with *Leishmania donovani*. *Biochemical Journal*, **277,** 451-456.

Bates, P.A. (2007). Transmission of Leishmania metacyclic promastigotes by phlebotomine sand flies. *International Journal of Parasitology*, **37,** 1097-106.

Bekersky, I., Fielding, R.M., Dressler, D.E., Kline, S., Buell, D.N. & Walsh, T.J. (2001). Pharmacokinetics, excretion, and mass balance of ^{14}C after administration of ^{14}C-cholesterol-labeled AmBisome to healthy volunteers. *Journal of Clinical Pharmacology*, **41,** 963-71.

Bekersky, I., Fielding, R.M., Dressler, D.E., Lee, J.W., Buell, D.N. & Walsh, T.J. (2002). Pharmacokinetics, excretion, and mass balance of liposomal amphotericin B (AmBisome) and amphotericin B deoxycholate in humans. *Antimicrobial Agents Chemotherapy*, **46,** 828-33.

Bensley, R.R. & Hoerr, N.L. (1934). Studies on cell structure by the freezing-drying method vi. The preparation and properties of mitochondria *The Anatomical Record*, **60,** 449-455.

Berman, J.D., Dwyer, D.M. & Wyler, D.J. (1979). Multiplication of *Leishmania* in human macrophages *in vitro*. *Infection and Immunity*, **26,** 375-9.

Berman, J.D., Fioretti, T.B. & Dwyer, D.M. (1981). *In vivo* and *in vitro* localization of *Leishmania* within macrophage phagolysosomes: use of colloidal gold as a lysosomal label. *Journal of Protozoology*, **28,** 239-42.

Berman, J.D., Hanson, W.L., Chapman, W.L., Alving, C.R. & Lopez-Berestein, G. (1986). Antileishmanial activity of liposome-encapsulated amphotericin B in hamsters and monkeys. *Antimicrobial Agents and Chemotherapy*, **30,** 847-51.

Bern, C., Adler-Moore, J., Berenguer, J., Boelaert, M., den Boer, M., Davidson, R.N., Figueras, C., Gradoni, L., Kafetzis, D.A., Ritmeijer, K., Rosenthal, E., Royce, C., Russo, R., Sundar, S. & Alvar, J. (2006). Liposomal amphotericin B for the treatment of visceral leishmaniasis. *Clinical Infectious Diseases*, **43,** 917-24.

Beyrer, C., Villar, J.C., Suwanvanichkij, V., Singh, S., Baral, S.D. & Mills, E.J. (2007). Neglected diseases, civil conflicts, and the right to health. *Lancet*, **370,** 619-27.

Bhatt, R., de Vries, P., Tulinsky, J., Bellamy, G., Baker, B., Singer, J.W. & Klein, P. (2003). Synthesis and in vivo antitumor activity of poly(l-glutamic acid) conjugates of 20S-camptothecin. *Journal of Medicinal Chemistry*, **46,** 190-3.

Bhattacharya, S.K., Sur, D., Sinha, P.K. & Karbwang, J. (2006). Elimination of leishmaniasis (kala-azar) from the Indian subcontinent is technically feasible & operationally achievable. *Indian Journal of Medical Research*, **123,** 195-6.

Bhattacharyya, S., Ghosh, S., Jhonson, P.L., Bhattacharya, S.K. & Majumdar, S. (2001). Immunomodulatory role of interleukin-10 in visceral leishmaniasis: defective activation of protein kinase C-mediated signal transduction events. *Infection and Immunity*, **69,** 1499-507.

Black, C.D., Watson, G.J. & Ward, R.J. (1977). The use of pentostam liposomes in the chemotherapy of experimental leishmaniasis. *Transactions of the Royal Society of Tropical Medicine and Hygiene*, **71,** 550-2.

Blackwell, J.M. (1985). Receptors and recognition mechanisms of *Leishmania* species. *Transactions of the Royal Society of Tropical Medicine and Hygiene*, **79,** 606-612.

Boelaert, M. (2004). Economic aspects of visceral leishmaniasis control. In *Report of the Scientific Working Group Meeting on Leishmaniasis* WHO: Geneva.

Bogdan, C. & Rollinghoff, M. (1999). How do protozoan parasites survive inside macrophages? *Parasitology Today*, **15,** 22-28.

Bowden, R., Chandrasekar, P., White, M.H., Li, X., Pietrelli, L., Gurwith, M., van Burik, J.A., Laverdiere, M., Safrin, S. & Wingard, J.R. (2002). A double-blind, randomized, controlled trial of amphotericin B colloidal dispersion versus amphotericin B for treatment of invasive aspergillosis in immunocompromised

patients. *Clinical Infectious Disease*, **35,** 359-66.

Bozeman, P.M., Hoidal, J.R. & Shepherd, V.L. (1988). Oxidant-mediated inhibition of ligand uptake by the macrophage mannose receptor. *Journal of Biological Chemistry*, **263,** 1240-7.

Bradford, M.M. (1976). A rapid and sensitive method for the quantitation of microgram quantities of protein utilizing the principle of protein-dye binding. *Analytical Biochememistry*, **72,** 248-54.

Brajtburg, J., Powderly, W.G., Kobayashi, G.S. & Medoff, G. (1990). Amphotericin B: current understanding of mechanisms of action. *Antimicrobial Agents Chemotherapy*, **34,** 183-8.

Brajtburg, J., Elberg, S., Kobayashi, G.S. & Bolard, J. (1994). Amphotericin B incorporated into egg lecithin-bile salt mixed micelles: molecular and cellular aspects relevant to therapeutic efficacy in experimental mycoses. *Antimicrobial Agents Chemotheapyr*, **38,** 300-6.

Brazil, R.P. (1984). *In vivo* fusion of lysosomes with parasitophorous vacuoles of *Leishmania*-infected macrophages. *Annals of Tropical Medicine and Parasitology*, **78,** 87-91.

Brime, B., Molero, G., Frutos, P. & Frutos, G. (2004). Comparative therapeutic efficacy of a novel lyophilized amphotericin B lecithin-based oil-water microemulsion and deoxycholate-amphotericin B in immunocompetent and neutropenic mice infected with Candida albicans. *European Journal of Pharmaceutical Science*, **22,** 451-8.

Brittingham, A., Morrison, C.J., McMaster, W.R., McGwire, B.S., Chang, K.P. & Mosser, D.M. (1995). Role of the *Leishmania* surface protease gp63 in complement fixation, cell adhesion, and resistance to complement-mediated lysis. *Journal of Immunology*, **155,** 3102-11.

Bryceson, A. (2001). Current issues in the treatment of visceral leishmaniasis. *Medical Microbiology and Immunology*, **190,** 81-4.

Caiolfa, V.R., Zamai, M., Fiorino, A., Frigerio, E., Pellizzoni, C., d'Argy, R., Ghiglieri, A., Castelli, M.G., Farao, M., Pesenti, E., Gigli, M., Angelucci, F. & Suarato, A. (2000). Polymer-bound camptothecin: initial biodistribution and antitumour activity studies. *Journal of Controlled Release*, **65,** 105-19.

Campanero, M.A., Espuelas, M.S., Azanza, J.R. & Irache, J.M. (2000). Rapid determination of intramacrophagic amphotericin B by direct injection HPLC. *Chromatographia*, **52,** 827-830.

Carrera, L., Gazzinelli, R.T., Badolato, R., Hieny, S., Muller, W., Kuhn, R. & Sacks, D.L. (1996). *Leishmania* promastigotes selectively inhibit interleukin 12 induction in bone marrow-derived macrophages from susceptible and resistant mice. *The Journal of Experimental Medicine*, **183,** 515-26.

Chakraborty, P., Bhaduri, A.N. & Das, P.K. (1990). Sugar receptor mediated drug delivery to macrophages in the therapy of experimental visceral leishmaniasis. *Biochemical and Biophysical Research Communications*, **166,** 404-10.

Chakraborty, R., Chakraborty, P. & Basu, M.K. (1998). Macrophage mannosyl fucosyl receptor: its role in invasion of virulent and avirulent *L. donovani* promastigotes. *Bioscience Reports*, **18,** 129-42.

Chappuis, F., Sundar, S., Hailu, A., Ghalib, H., Rijal, S., Peeling, R.W., Alvar, J. & Boelaert, M. (2007). Visceral leishmaniasis: what are the needs for diagnosis, treatment and control? *Nature Reviews Microbiology*, **5,** 873-82.

Charvalos, E., Tzatzarakis, M.N., Van Bambeke, F., Tulkens, P.M., Tsatsakis, A.M., Tzanakakis, G.N. & Mingeot-Leclercq, M.P. (2006). Water-soluble amphotericin B-polyvinylpyrrolidone complexes with maintained antifungal activity against

Candida spp. and Aspergillus spp. and reduced haemolytic and cytotoxic effects. *Journal of Antimicrobial Chemotherapy*, **57,** 236-44.

Chaudhuri, G., Chaudhuri, M., Pan, A. & Chang, K.P. (1989). Surface acid proteinase (gp63) of *Leishmania mexicana*. A metalloenzyme capable of protecting liposome-encapsulated proteins from phagolysosomal degradation by macrophages. *Journal of Biological Chemistry*, **264,** 7483-9.

Chaudhuri, G., Mukhopadhyay, A. & Basu, S.K. (1989). Selective delivery of drugs to macrophages through a highly specific receptor. An efficient chemotherapeutic approach against leishmaniasis. *Biochemical Pharmacology*, **38,** 2995-3002.

Cheng, P.W. & Boat, T.F. (1978). An improved method for the determination of galactosaminitol, glucosaminitol, glucosamine, and galactosamine on an amino acid analyzer. *Analytical Biochemistry*, **85,** 276-82.

Cheron, M., Petit, C., Bolard, J. & Gaboriau, F. (2003). Heat-induced reformulation of amphotericin B-deoxycholate favours drug uptake by the macrophage-like cell line J774. *Journal of Antimicrobial Chemotherapy*, **52,** 904-10.

Chin, L.S., Raynor, M.C., Wei, X., Chen, H.Q. & Li, L. (2001). Hrs interacts with sorting nexin 1 and regulates degradation of epidermal growth factor receptor. *Journal of Biological Chemistry*, **276,** 7069-78.

Claude, A. (1946). Fractionation of mammalian liver cells by differential centrifugation: I. Problems, methods, and preparation of extract. *Journal of Experimental Medicine*, **84,** 51-59.

Claude, A. (1946). Fractionation of mammalian liver cells by differential centrifugation: II. Experimental procedures and results. *Journal of Experimental Medicine*, **84,** 61-89.

Cleary, J.D., Chapman, S.W., Deng, J. & Lobb, C.J. (1996). Amphotericin B enzyme-linked immunosorbent assay. *Antimicrobial Agents Chemotherapy*, **40,** 637-41.

Configliacchi, E., Razzano, G., Rizzo, V. & Vigevani, A. (1996). HPLC methods for the determination of bound and free doxorubicin, and of bound and free galactosamine, in methacrylamide polymer-drug conjugates. *Journal of Pharmaceutical and Biomedical Analysis*, **15,** 123-9.

Conover, C.D., Zhao, H., Longley, C.B., Shum, K.L. & Greenwald, R.B. (2003). Utility of poly(ethylene glycol) conjugation to create prodrugs of amphotericin B. *Bioconjugate Chemistry*, **14,** 661-6.

Courret, N., Frehel, C., Gouhier, N., Pouchelet, M., Prina, E., Roux, P. & Antoine, J.C. (2002). Biogenesis of Leishmania-harbouring parasitophorous vacuoles following phagocytosis of the metacyclic promastigote or amastigote stages of the parasites. *Journal of Cell Science*, **115,** 2303-16.

Croft, S.L., Seifert, K. & Yardley, V. (2006). Current scenario of drug development for leishmaniasis. *Indian Journal of Medical Research*, **123,** 399-410.

Cunningham, A.C. (2002). Parasitic adaptive mechanisms in infection by *Leishmania*. *Experimental and Molecular Pathology*, **72,** 132-41.

Danhauser-Riedl, S., Hausmann, E., Schick, H.D., Bender, R., Dietzfelbinger, H., Rastetter, J. & Hanauske, A.R. (1993). Phase I clinical and pharmacokinetic trial of dextran conjugated doxorubicin (AD-70, DOX-OXD). *Investigational New Drugs*, **11,** 187-95.

Dasgupta, B., Roychoudhury, K., Ganguly, S., Akbar, M.A., Das, P. & Roy, S. (2003). Infection of human mononuclear phagocytes and macrophage-like THP1 cells with *Leishmania donovani* results in modulation of expression of a subset of chemokines and a chemokine receptor. *Scandinavian Journal of Immunology*, **57,** 366-374.

Date, A.A., Joshi, M.D. & Patravale, V.B. (2007). Parasitic diseases: Liposomes and polymeric nanoparticles versus lipid nanoparticles. *Advanced Drug Delivery Reviews*, **59,** 505-21.

David, A., Kopeckova, P., Minko, T., Rubinstein, A. & Kopecek, J. (2004). Design of a multivalent galactoside ligand for selective targeting of HPMA copolymer-doxorubicin conjugates to human colon cancer cells. *European Journal of Cancer*, **40,** 148-57.

Davidson, R.N., Croft, S.L., Scott, A., Maini, M., Moody, A.H. & Bryceson, A.D. (1991). Liposomal amphotericin B in drug-resistant visceral leishmaniasis. *Lancet*, **337,** 1061-2.

Dawson, M.C.D. (1986). *Data for Biochemical Research.* Oxford University Press: Oxford.

De Carvalho, P.B., Ramos, D.C.C., Cotrim, P.C. & Ferreira, E.I. (2003). Synthesis and *in vitro* evaluation of potential anti-leishmanial targeted drugs of pyrimethamine. *Journal of Pharmaceutical Sciences*, **92,** 2109-2116.

De Duve, D. (1969). The peroxisome: a new cytoplasmic organelle. *Proceedings of the Royal Society of London. Series B, Containing Papers of a Biological Character*, **173,** 71-83.

De Duve, C., de Barsy, T., Poole, B., Trouet, A., Tulkens, P. & Van Hoof, F. (1974). Commentary. Lysosomotropic agents. *Biochemical Pharmacology*, **23,** 2495-531.

De Duve, C. & Beaufay, H. (1981). A short history of tissue fractionation. *Journal of Cell Biology*, **91,** 293s-299s.

Desjeux, P. (2001). The increase in risk factors for leishmaniasis worldwide. *Transactions of the Royal Society of Tropical Medicine and Hygiene*, **95,** 239-43.

Diaz-Silvestre, H., Espinosa-Cueto, P., Sanchez-Gonzalez, A., Esparza-Ceron, M.A., Pereira-Suarez, A.L., Bernal-Fernandez, G., Espitia, C. & Mancilla, R. (2005). The 19-kDa antigen of Mycobacterium tuberculosis is a major adhesin that binds the mannose receptor of THP-1 monocytic cells and promotes phagocytosis of mycobacteria. *Microbial Pathogenesis*, **39,** 97-107.

Duncan, R., Lloyd, J.B. & Kopecek, J. (1980). Degradation of side chains of N-(2-hydroxypropyl) methacrylamide copolymers by lysosomal enzymes. *Biochemical and Biophysical Research Communications*, **94,** 284-90.

Duncan, R., Rejmanova, P., Kopecek, J. & Lloyd, J.B. (1981). Pinocytic uptake and intracellular degradation of N-(2-hydroxypropyl)methacrylamide copolymers. A potential drug delivery system. *Biochimica et Biophysica Acta*, **678,** 143-50.

Duncan, R., Cable, H.C., Lloyd, J.B., Rejmanova, P. & Kopecek, J. (1982). Degradation of side-chains of N-(2-hydroxypropyl)methacrylamide copolymers by lysosomal thiol-proteinases. *Bioscience Reports*, **2,** 1041-6

Duncan, R., Kopacek, J., Rejmanova, P. & Lloyd, J.B. (1983). Targeting of N-(2-hydroxypropyl)methacrylamide copolymers to liver by incorporation of galactose residues. *Biochemica et Biophysica Acta*, **755,** 518-52.

Duncan, R., Kopecek, J. & Lloyd, J.B. (1984). Drug targeting to lysosomes. *Biochemical Society Transactions*, **12,** 913-5.

Duncan, R., Seymour, L.C., Scarlett, L., Lloyd, J.B., Rejmanova, P. & Kopecek, J. (1986). Fate of N-(2-hydroxypropyl)methacrylamide copolymers with pendent galactosamine residues after intravenous administration to rats. *Biochimica et Biophysica Acta*, **880,** 62-71.

Duncan, R., Kopeckova-Rejmanova, P., Strohalm, J., Hume, I., Cable, H.C., Pohl, J., Lloyd, J.B. & Kopecek, J. (1987). Anticancer agents coupled to N-(2-hydroxypropyl)methacrylamide copolymers. I. Evaluation of daunomycin and

puromycin conjugates in vitro. *British Journal of Cancer*, **55,** 165-74.

Duncan, R., Kopeckova, P., Strohalm, J., Hume, I.C., Lloyd, J.B. & Kopecek, J. (1988). Anticancer agents coupled to N-(2-hydroxypropyl)methacrylamide copolymers. II. Evaluation of daunomycin conjugates in vivo against L1210 leukaemia. *British Journal of Cancer*, **57,** 147-56.

Duncan, R. & Spreafico, F. (1994). Polymer conjugates. Pharmacokinetic considerations for design and development. *Clinical Pharmacokinetics*, **27,** 290-306.

Duncan, R., Coatsworth, J.K. & Burtles, S. (1998). Preclinical toxicology of a novel polymeric antitumour agent: HPMA copolymer-doxorubicin (PK1). *Human and Experimental Toxicology*, **17,** 93-104.

Duncan, R. (2003). The dawning era of polymer therapeutics. *Nature Reviews Drug Discovery*, **5,** 347-60.

Duncan, R. (2005). N-(hydroxypropyl)methacrylamide copolymer conjugates. *Polymeric Drug Delivery Systems*, **1**.

Duncan, R., Ringsdorf, H. & Satchi-Fainaro, R. (2006). Polymer therapeutics-polymers as drugs, drug and protein conjugates and gene delivery systems: past, present and future opportunities. *Journal of Drug Targeting*, **14,** 337-41.

Duncan, R., Gilbert, H.R.P., Carbajo, R.J. & Vicent, M.J. (2008). Polymer Masked-Unmasked Protein Therapy. 1. Bioresponsive Dextrin-Trypsin and -Melanocyte Stimulating Hormone Conjugates Designed for alpha-Amylase Activation. *Biomacromolecules*, **In press.**

Dupont, B. (2002). Overview of the lipid formulations of amphotericin B. *Journal of Antimicrobial Chemotherapy*, **49,** 31-36.

Dye, C. & Wolpert, D.M. (1988). Earthquakes, influenza and cycles of Indian kala-azar. *Transactions of the Royal Society of Tropical Medicine and Hygiene*, **82,** 843-50.

Ehlers, M.R. (2000). CR3: a general purpose adhesion-recognition receptor essential for innate immunity. *Microbes and Infection*, **2,** 289-94.

Ehrenfreund-Kleinman, T., Azzam, T., Falk, R., Polacheck, I., Golenser, J. & Domb, A.J. (2002). Synthesis and characterization of novel water soluble amphotericin B-arabinogalactan conjugates. *Biomaterials*, **23,** 1327-35.

Ehrenfreund-Kleinman, T., Golenser, J. & Domb, A.J. (2004). Conjugation of amino-containing drugs to polysaccharides by tosylation: amphotericin B-arabinogalactan conjugates. *Biomaterials*, **25,** 3049-57.

Eldem, T. & Arican-Cellat, N. (2001). Determination of amphotericin B in human plasma using solid-phase extraction and high-performance liquid chromatography. *Journal of Pharmaceutical and Biomedical Analysis*, **25,** 53-64.

Elson, L.A. & Morgan, W.T. (1933). A colorimetric method for the determination of glucosamine and chondrosamine. *The Biochemical Journal*, **27,** 1824-8.

Engwerda, C.R., Ato, M. & Kaye, P.M. (2004). Macrophages, pathology and parasite persistence in experimental visceral leishmaniasis. *Trends in Parasitology*, **20,** 524-30.

Espuelas, M.S., Legrand, P., Campanero, M.A., Appel, M., Cheron, M., Gamazo, C., Barratt, G. & Irache, J.M. (2003). Polymeric carriers for amphotericin B: in vitro activity, toxicity and therapeutic efficacy against systemic candidiasis in neutropenic mice. *Journal of Antimicrobial Chemotherapy*, **52,** 419-27.

Falk, R., Domb, A.J. & Polacheck, I. (1999). A novel injectable water-soluble amphotericin B-arabinogalactan conjugate. *Antimicrobial Agents Chemotherapy*, **43,** 1975-81.

Falk, R., Grunwald, J., Hoffman, A., Domb, A.J. & Polacheck, I. (2004). Distribution of amphotericin B-arabinogalactan conjugate in mouse tissue and its therapeutic

efficacy against murine aspergillosis. *Antimicrobial Agents Chemotherapy*, **48,** 3606-9.

Fernandes, M.J., Finnegan, A.A., Siracusa, L.D., Brenner, C., Iscove, N.N. & Calabretta, B. (1999). Characterization of a novel receptor that maps near the natural killer gene complex: demonstration of carbohydrate binding and expression in hematopoietic cells. *Cancer Research*, **59,** 2709-17.

Ford, T., Graham, J. & Rickwood, D. (1994). Iodixanol: a nonionic iso-osmotic centrifugation medium for the formation of self-generated gradients. *Analytical Biochemistry*, **220,** 360-6.

Frankenberg, T., Kirschnek, S., Hacker, H. & Hacker, G. (2008). Phagocytosis-induced apoptosis of macrophages is linked to uptake, killing and degradation of bacteria. *European Journal of Immunology*, **38,** 204-15.

Fujiwara, R.T., Vale, A.M., Franca da Silva, J.C., da Costa, R.T., Quetz Jda, S., Martins Filho, O.A., Reis, A.B., Correa Oliveira, R., Machado-Coelho, G.L., Bueno, L.L., Bethony, J.M., Frank, G., Nascimento, E., Genaro, O., Mayrink, W., Reed, S. & Campos-Neto, A. (2005). Immunogenicity in dogs of three recombinant antigens (TSA, LeIF and LmSTI1) potential vaccine candidates for canine visceral leishmaniasis. *Veterinary Research*, **36,** 827-38.

Gebre-Hiwot, A., Tadesse, G., Croft, S.L. & Frommel, D. (1992). An in vitro model for screening antileishmanial drugs: the human leukaemia monocyte cell line, THP-1. *Acta Tropica*, **51,** 237-45.

Geisow, M.J. & Evans, W.H. (1984). pH in the endosome. Measurements during pinocytosis and receptor-mediated endocytosis. *Experimental Cell Research*, **150,** 36-46.

Gekle, M., Mildenberger, S., Freudinger, R. & Silbernagl, S. (1996). Functional characterization of albumin binding to the apical membrane of OK cells. *The American Journal of Physiology*, **271,** F286-91.

German, L.A., Tupper, J., Hreczuk-Hirst, D., Dagini, B., Humber, D.P., Shaunak, S. & Duncan, R. (2000). Dextrin-amphotericin B: a potential polymeric anti-infective or antiparasitic agent. *Journal of Pharmacy and Pharmacology*, **52,** 37.

Gilbert, I.H. (2002). Inhibitors of dihydrofolate reductase in *Leishmania* and *trypanosomes. Biochimica et Biophysica Acta*, **1587,** 249-257.

Giri, O.P. (1994). Treatment of visceral leishmaniasis unresponsive to pentamidine with amphotericin B. *Journal of Association of Physicians of India*, **42,** 688-9.

Golenser, J., Frankenburg, S., Ehrenfreund, T. & Domb, A.J. (1999). Efficacious treatment of experimental leishmaniasis with amphotericin B-aribinogalactan water soluble derivatives. *Antimicrobial Agents and Chemotherapy*, **43,** 2209-2214.

Gordon, S. (2003). Alternative activation of macrophages. *Nature Reviews Immunology*, **3,** 23-35.

Gordon, S., Fraser, I., Nath, D., Hughes, D. & Clarke, S. (1992). Macrophages in tissues and *in vitro. Current Opinion in Immunology*, **4,** 25-32.

Graham, J., Ford, T. & Rickwood, D. (1994). The preparation of subcellular organelles from mouse liver in self-generated gradients of iodixanol. *Analytical Biochemistry*, **220,** 367-73.

Graham, J.M. (1993). The identification of subcellular fractions from mammalian cells. In *Methods in Molecular Biology, Biomembrane protocols: I. Isolation and Analysis*, Graham, J.M. & J.A., H. (eds), Vol. 19. pp. 1-18. Humana Press Inc.: Totowa.

Granich, G.G., Kobayashi, G.S. & Krogstad, D.J. (1986). Sensitive high-pressure liquid

chromatographic assay for amphotericin B which incorporates an internal standard. *Antimicrobial Agents Chemotherapy*, **29,** 584-8.

Greco, F., Vicent, M.J., Gee, S., Jones, A.T., Gee, J., Nicholson, R.I. & Duncan, R. (2007). Investigating the mechanism of enhanced cytotoxicity of HPMA copolymer-Dox-AGM in breast cancer cells. *Journal of Controlled Release*, **117,** 28-39.

Gruda, I., Milette, D., Brother, M., Kobayashi, G.S., Medoff, G. & Brajtburg, J. (1991). Structure-activity study of inhibition of amphotericin B (Fungizone) binding to sterols, toxicity to cells, and lethality to mice by esters of sucrose. *Antimicrobial Agents Chemotherapy*, **35,** 24-8.

Gruszecki, W.I., Gagos, M., Herec, M. & Kernen, P. (2003). Organization of antibiotic amphotericin B in model lipid membranes. A mini review. *Cellular and Molecular Biology Letters*, **8,** 161-70.

Gupta, S., Dube, A. & Vyas, S.P. (2007). Antileishmanial efficacy of amphotericin B bearing emulsomes against experimental visceral leishmaniasis. *Journal of Drug Targeting*, **15,** 437-44.

Gupta, S. & Vyas, S.P. (2007). Development and characterization of amphotericin B bearing emulsomes for passive and active macrophage targeting. *Journal of Drug Targeting*, **15,** 206-17.

Hamasaki, M., Araki, N. & Hatae, T. (2004). Association of early endosomal autoantigen 1 with macropinocytosis in EGF-stimulated A431 cells. *The Anatomical Record. Part A, Discoveries in Molecular, Cellular and Evolutionary Biology*, **277,** 298-306.

Handman, E. & Bullen, D.V. (2002). Interaction of *Leishmania* with the host macrophage. *Trends in Parasitology*, **18,** 332-4.

Hargreaves, P.L., Nguyen, T.S. & Ryan, R.O. (2006). Spectroscopic studies of amphotericin B solubilized in nanoscale bilayer membranes. *Biochimica et Biophysica Acta*, **1758,** 38-44.

Hartnell, A., Steel, J., Turley, H., Jones, M., Jackson, D.G. & Crocker, P.R. (2001). Characterization of human sialoadhesin, a sialic acid binding receptor expressed by resident and inflammatory macrophage populations. *Blood*, **97,** 288-96.

Heath, S., Chance, M.L. & New, R.R. (1984). Quantitative and ultrastructural studies on the uptake of drug loaded liposomes by mononuclear phagocytes infected with *Leishmania donovani*. *Molecular and Biochemical Parasitology*, **12,** 49-60.

Henry, R., Hoppe, A., Joshi, N. & Swanson, J. (2004). Uniformity of phagosome maturation in macrophages. *Journal of Cell Biology*, **164,** 185-94.

Herwaldt, B.L. (1999). Leishmaniasis. *Lancet*, **354,** 1191-9.

Hinton, R.H. & Mullock, B.M. (1997). Isolation of Subcellular Fractions. In *Subcellular Fractionation: A Practical Approach.*, Graham, J.M. & Rickwood, D. (eds) pp. 31-69. IRL Press Limited: Oxford.

Hogeboom, G.H., Schneider, W.C. & Palade, G.E. (1948). Cytochemical studies of mammalian tissues. I. Isolation of intact mitochondria from rat liver; some biochemical properties of mitochondria and submicroscopic particulate material. *Journal of Biological Chemistry*, **172,** 637-650.

Holm, A., Tejle, K., Magnusson, K.E., Descoteaux, A. & Rasmusson, B. (2001). *Leishmania donovani* lipophosphoglycan causes periphagosomal actin accumulation: correlation with impaired translocation of PKCalpha and defective phagosome maturation. *Cellular Microbiology*, **3,** 439-47.

Hopewel, J.W., Duncan, R., Wilding, D. & Chakrabarti, K. (2001). Preclinical evaluation of the cardiotoxicity of PK2: a novel HPMA copolymer-doxorubicin-

galactosamine conjugate antitumour agent. *Human and Experimental Toxicology*, **20,** 461-70.

Hreczuk-Hirst, D., Chicco, D., German, L. & Duncan, R. (2001). Dextrins as potential carriers for drug targeting: tailored rates of dextrin degradation by introduction of pendant groups. *International Journal of Pharmaceutics*, **230,** 57-66.

Hunter, C.A., Dolan, T.F., Coombs, G.H. & Baillie, A.J. (1988). Vesicular systems (niosomes and liposomes) for delivery of sodium stibogluconate in experimental murine visceral leishmaniasis. *Journal of Pharmacy and Pharmacology*, **40,** 161-5.

Ilg, T. (2000). Proteophosphglycans of leishmania. *Parasitology Today*, **16,** 489-497.

Inoue, K., Kumazawa, E., Kuga, H., Susaki, H., Masubuchi, N. & Kajimura, T. (2003). CM-dextran-polyalcohol-camptothecin conjugate: DE-310 with a novel carrier system and its preclinical data. *Advances in Experimental Medicine and Biology*, **519,** 145-53.

Ivens, A.C., Peacock, C.S., Worthey, E.A., Murphy, L., Aggarwal, G., Berriman, M., Sisk, E., Rajandream, M.A., Adlem, E., Aert, R., Anupama, A., Apostolou, Z., Attipoe, P., Bason, N., Bauser, C., Beck, A., Beverley, S.M., Bianchettin, G., Borzym, K., Bothe, G., Bruschi, C.V., Collins, M., Cadag, E., Ciarloni, L., Clayton, C., Coulson, R.M., Cronin, A., Cruz, A.K., Davies, R.M., De Gaudenzi, J., Dobson, D.E., Duesterhoeft, A., Fazelina, G., Fosker, N., Frasch, A.C., Fraser, A., Fuchs, M., Gabel, C., Goble, A., Goffeau, A., Harris, D., Hertz-Fowler, C., Hilbert, H., Horn, D., Huang, Y., Klages, S., Knights, A., Kube, M., Larke, N., Litvin, L., Lord, A., Louie, T., Marra, M., Masuy, D., Matthews, K., Michaeli, S., Mottram, J.C., Muller-Auer, S., Munden, H., Nelson, S., Norbertczak, H., Oliver, K., O'Neil, S., Pentony, M., Pohl, T.M., Price, C., Purnelle, B., Quail, M.A., Rabbinowitsch, E., Reinhardt, R., Rieger, M., Rinta, J., Robben, J., Robertson, L., Ruiz, J.C., Rutter, S., Saunders, D., Schafer, M., Schein, J., Schwartz, D.C., Seeger, K., Seyler, A., Sharp, S., Shin, H., Sivam, D., Squares, R., Squares, S., Tosato, V., Vogt, C., Volckaert, G., Wambutt, R., Warren, T., Wedler, H., Woodward, J., Zhou, S., Zimmermann, W., Smith, D.F., Blackwell, J.M., Stuart, K.D., Barrell, B., et al. (2005). The genome of the kinetoplastid parasite, *Leishmania major*. *Science*, **309,** 436-42.

Jha, T.K. (1983). Evaluation of diamidine compound (pentamidine isethionate) in the treatment resistant cases of kala-azar occurring in North Bihar, India. *Transactions of the Royal Society of Tropical Medicine and Hygiene*, **77,** 167-70.

Jha, T.K. (2006). Drug unresponsiveness & combination therapy for kala-azar. *Indian Journal of Medical Research*, **123,** 389-98.

Kanbe, E., Emi, N., Abe, A., Tanaka, H., Kobayashi, K. & Saito, H. (2001). Novel synthesized trimannose conjugate induces endocytosis and expression of immunostimulatory molecules in monocytic leukemia cells. *International Journal of Hematology*, **74,** 309-15.

Kayser, O. & Kiderlen, A.F. (2003). Delivery strategies for antiparasitics. *Expert Opinion on Investigational Drugs*, **12,** 197-207.

Kery, V., Krepinsky, J.J., Warren, C.D., Capek, P. & Stahl, P.D. (1992). Ligand recognition by purified human mannose receptor. *Archives of Biochemistry and Biophysics*, **298,** 49-55.

Kishore, K., Kumar, V., Kesari, S., Dinesh, D.S., Kumar, A.J., Das, P. & Bhattacharya, S.K. (2006). Vector control in leishmaniasis. *The Indian Journal of Medical Research*, **123,** 467-72.

Kleinberg, M. (2006). What is the current and future status of conventional amphotericin

B? *International Journal of Antimicrobial Agents*, **27 Suppl 1,** 12-6.

Klemm, A.R., Young, D. & Lloyd, J.B. (1998). Effects of polyethyleneimine on endocytosis and lysosome stability. *Biochemical Pharmacology*, **56,** 41-6.

Koczan, G., Ghose, A.C., Mookerjee, A. & Hudecz, F. (2002). Methotrexate conjugate with branched polypeptide influences Leishmania donovani infection in vitro and in experimental animals. *Bioconjugate Chemistry*, **13,** 518-24.

Kohro, T., Tanaka, T., Murakami, T., Wada, Y., Aburatani, H., Hamakubo, T. & Kodama, T. (2004). A comparison of differences in the gene expression profiles of phorbol 12-myristate 13-acetate differentiated THP-1 cells and human monocyte-derived macrophage. *Journal of Atherosclerosis and Thrombosis*, **11,** 88-97.

Kopecek, J., Rejmanova, P., Strohalm, J., Ulbrich, K., Rihova, B., Chytry, V., Duncan, R. and Lloyd, J.B. Synthetic polymeric drugs. European Patent 0186547 (1986).

Kopecek, J. (1977). Soluble biomedical polymers. *Polimery W Medycynie*, **7,** 191-221.

Kopecek, J. & Bazilova, H. (1973). Poly[N-(hydroxypropyl)methacrylamide] - I. Radical polymerisation and copolymerisation. *European Polymer Journal*, **9,** 7-14.

Kovar, M., Strohalm, J., Ulbrich, K. & Rihova, B. (2002). In vitro and in vivo effect of HPMA copolymer-bound doxorubicin targeted to transferrin receptor of B-cell lymphoma 38C13. *Journal of Drug Targeting*, **10,** 23-30.

Kshirsagar, N.A., Pandya, S.K., Kirodian, G.B. & Sanath, S. (2005). Liposomal drug delivery system from laboratory to clinic. *J Postgrad Med*, **51 Suppl 1,** S5-15.

Laguna, F. (2003). Treatment of leishmaniasis in HIV-positive patients. *Annals of Tropical Medicine and Parasitology*, **97 Suppl 1,** 135-42.

Lambros, M.P., Abbas, S.A. & Bourne, D.W. (1996). New high-performance liquid chromatographic method for amphotericin B analysis using an internal standard. *Journal of Chromatography. B Biomedical Applications*, **685,** 135-40.

Lang, T., Hellio, R., Kaye, P.M. & Antoine, J.C. (1994). *Leishmania donovani*-infected macrophages: characterization of the parasitophorous vacuole and potential role of this organelle in antigen presentation. *Journal of Cell Science*, **107 (Pt 8),** 2137-50.

Lavasanifar, A., Samuel, J., Sattari, S. & Kwon, G.S. (2002). Block copolymer micelles for the encapsulation and delivery of amphotericin B. *Pharmaceutical Research*, **19,** 418-22.

Le Cabec, V., Emorine, L.J., Toesca, I., Cougoule, C. & Maridonneau-Parini, I. (2005). The human macrophage mannose receptor is not a professional phagocytic receptor. *Journal of Leukocyte Biology*, **77,** 934-43.

Lee, Y.C. & Lee, R.T. (1995). Carbohydrate-Protein Interactiuons: Basis of Glycobiology. *Accounts of Chemical Research*, **28,** 321-327.

Legrand, P., Romero, E.A., Cohen, B.E. & Bolard, J. (1992). Effects of aggregation and solvent on the toxicity of amphotericin B to human erythrocytes. *Antimicrobial Agents Chemotherapy*, **36,** 2518-22.

Legrand, P., Vertut-Doi, A. & Bolard, J. (1996). Comparative internalization and recycling of different amphotericin B formulations by a macrophage-like cell line. *Journal of Antimicrobial Chemotherapy*, **37,** 519-33.

Lemke, A., Kiderlen, A.F. & Kayser, O. (2005). Amphotericin B. *Applied Microbiology and Biotechnology*, **68,** 151-62.

Lennartz, M.R., Cole, F.S. & Stahl, P.D. (1989). Biosynthesis and processing of the mannose receptor in human macrophages. *Journal of Biolical Chemistry*, **264,** 2385-90.

Lewis, D.H. & Peters, W. (1977). The resistance of intracellular *Leishmania* parasites to

digestion by lysosomal enzymes. *Annals of Tropical Medicine and Parasitology*, **71,** 295-312.

Li, C., Yu, D.F., Newman, R.A., Cabral, F., Stephens, L.C., Hunter, N., Milas, L. & Wallace, S. (1998). Complete regression of well-established tumors using a novel water-soluble poly(L-glutamic acid)-paclitaxel conjugate. *Cancer Research*, **58,** 2404-9.

Li, J., Sutterwala, S. & Farrell, J.P. (1997). Successful therapy of chronic, nonhealing murine cutaneous leishmaniasis with sodium stibogluconate and gamma interferon depends on continued interleukin-12 production. *Infection and Immunity*, **65,** 3225-30.

Lin, X., Zhang, Q., Rice, J.R., Stewart, D.R., Nowotnik, D.P. & Howell, S.B. (2004). Improved targeting of platinum chemotherapeutics. the antitumour activity of the HPMA copolymer platinum agent AP5280 in murine tumour models. *European Journal of Cancer*, **40,** 291-7.

Linehan, S.A., Martinez-Pomares, L. & Gordon, S. (2000). Macrophage lectins in host defence. *Microbes and Infection*, **2,** 279-288.

Lodge, R. & Descoteaux, A. (2005). *Leishmania donovani* promastigotes induce periphagosomal F-actin accumulation through retention of the GTPase Cdc42. *Cellular Microbiology*, **7,** 1647-58.

Lodge, R. & Descoteaux, A. (2005). Modulation of phagolysosome biogenesis by the lipophosphoglycan of *Leishmania*. *Clinical Immunology*, **114,** 256-65.

Lodge, R., Diallo, T.O. & Descoteaux, A. (2006). *Leishmania donovani* lipophosphoglycan blocks NADPH oxidase assembly at the phagosome membrane. *Cellular Microbiology*, **8,** 1922-31.

Loegering, D.J. & Lennartz, M.R. (2004). Signaling pathways for Fc gamma receptor-stimulated tumor necrosis factor-alpha secretion and respiratory burst in RAW 264.7 macrophages. *Inflammation*, **28,** 23-31.

Lopez-Berestein, G. (1988). Liposomes as carriers of antifungal drugs. *Annals of the New York Academy of Sciences*, **544,** 590-7.

Lopez-Galera, R., Pou-Clave, L. & Pascual-Mostaza, C. (1995). Determination of amphotericin B in human serum by liquid chromatography. *Journal of Chromatography. B Biomedical Applications*, **674,** 298-300.

Luo, Y., Bernshaw, N.J., Lu, Z.R., Kopecek, J. & Prestwich, G.D. (2002). Targeted delivery of doxorubicin by HPMA copolymer-hyaluronan bioconjugates. *Pharmaceutical Research*, **19,** 396-402.

Luzio, J.P., Pryor, P.R. & Bright, N.A. (2007). Lysosomes: fusion and function. *Nature Reviews Molular Cell Biology*, **8,** 622-32.

Malhotra, R. (1993). Collectin receptor (C1q receptor): structure and function. *Behring Institute Mitteilungen*, 254-61.

Mammen, M., Choi, S. & Whitesides, G.M. (1998). Polyvalent interactions in biological systems: implications for design and use of multivalent ligands and inhibitors. *Angewandte Chemie*, **37,** 2754-2794.

Manunta, M., Izzo, L., Duncan, R. & Jones, A.T. (2007). Establishment of subcellular fractionation techniques to monitor the intracellular fate of polymer therapeutics II. Identification of endosomal and lysosomal compartments in HepG2 cells combining single-step subcellular fractionation with fluorescent imaging. *Journal of Drug Targeting*, **15,** 37-50.

Marodi, L., Korchak, H. & Johnston, R.J. (1991). Mechanisms of host defence against Candida species: phagocytosis by monocytes and monocyte derived macrophages. *Journal of Immunology*, **146,** 2783-9.

Matsumori, N., Sawada, Y. & Murata, M. (2005). Mycosamine orientation of amphotericin B controlling interaction with ergosterol: sterol-dependent activity of conformation-restricted derivatives with an amino-carbonyl bridge. *Journal of the American Chemical Society*, **127,** 10667-75.

Matsumura, Y. & Maeda, H. (1986). A new concept for macromolecular therapeutics in cancer chemotherapy: mechanism of tumoritropic accumulation of proteins and the antitumor agent smancs. *Cancer Research*, **46,** 6387-92.

Meerum Terwogt, J.M., ten Bokkel Huinink, W.W., Schellens, J.H., Schot, M., Mandjes, I.A., Zurlo, M.G., Rocchetti, M., Rosing, H., Koopman, F.J. & Beijnen, J.H. (2001). Phase I clinical and pharmacokinetic study of PNU166945, a novel water-soluble polymer-conjugated prodrug of paclitaxel. *Anti-cancer Drugs*, **12,** 315-23.

Milhaud, J., Ponsinet, V., Takashi, M. & Michels, B. (2002). Interactions of the drug amphotericin B with phospholipid membranes containing or not ergosterol: new insight into the role of ergosterol. *Biochimica Biophysica Acta*, **1558,** 95-108.

Minko, T., Kopeckova, P., Pozharov, V. & Kopecek, J. (1998). HPMA copolymer bound adriamycin overcomes MDR1 gene encoded resistance in a human ovarian carcinoma cell line. *Journal of Controlled Release*, **54,** 223-33.

Miralles, G.D., Stoeckle, M.Y., McDermott, D.F., Finkelman, F.D. & Murray, H.W. (1994). Th1 and Th2 cell-associated cytokines in experimental visceral leishmaniasis. *Infection and Immunity*, **62,** 1058-63.

Mishra, J., Saxena, A. & Singh, S. (2007). Chemotherapy of leishmaniasis: past, present and future. *Current Medicinal Chemistry*, **14,** 1153-69.

Mitra, A., Nan, A., Papadimitriou, J.C., Ghandehari, H. & Line, B.R. (2006). Polymer-peptide conjugates for angiogenesis targeted tumor radiotherapy. *Nuclear Medicine and Biology*, **33,** 43-52.

Monsigny, M., Roche, A.C. & Midoux, P. (1984). Uptake of neoglycoproteins via membrane lectin(s) of L1210 cells evidenced by quantitative flow cytofluorometry and drug targeting. *Biology of the Cell*, **51,** 187-96.

Moreno, M.A., Frutos, P. & Ballesteros, M.P. (2001). Lyophilized lecithin based oil-water microemulsions as a new and low toxic delivery system for amphotericin B. *Pharmaceutical Research*, **18,** 344-51.

Moribe, K., Maruyama, K. & Iwatsuru, M. (1999). Molecular localization and state of amphotericin B in PEG liposomes. *International Journal Pharmaceutics*, **193,** 97-106.

Morris, R.V., Shoemaker, C.B., David, J.R., Lanzaro, G.C. & Titus, R.G. (2001). Sandfly maxadilan exacerbates infection with *Leishmania major* and vaccinating against it protects against L. major infection. *Journal of Immunology*, **167,** 5226-30.

Mosmann, T. (1983). Rapid colorimetric assay for cellular growth and survival: application to proliferation and cytoxicity assays. *Journal of Immunological Methods*, **65,** 55-63.

Mukherjee, S., Das, L., Kole, L., Karmakar, S., Datta, N. & Das, P.K. (2004). Targeting of parasite-specific immunoliposome-encapsulated doxorubicin in the treatment of experimental visceral leishmaniasis. *The Journal of Infectious Diseases*, **189,** 1024-1034.

Mukherjee, S., Ghosh, R.N. & Maxfield, F.R. (1997). Endocytosis. *Physiological Reviews*, **77,** 759-803.

Mullock, B.M., Bright, N.A., Fearon, C.W., Gray, S.R. & Luzio, J.P. (1998). Fusion of lysosomes with late endosomes produces a hybrid organelle of intermediate density and is NSF dependent. *Journal of Cell Biology*, **140,** 591-601.

Murray, H.W. (2000). Treatment of visceral leishmaniasis (kala-azar): a decade of

progress and future approaches. *International Journal of Infectious Disease*, **4,** 158-77.

Murray, H.W. (2004). Progress in the treatment of a neglected infectious disease: visceral leishmaniasis. *Expert Review Anti-Infective Therapy*, **2,** 279-92.

Murray, H.W., Berman, J.D., Davies, C.R. & Saravia, N.G. (2005). Advances in leishmaniasis. *Lancet*, **366,** 1561-77.

Nan, A., Nanayakkara, N.P., Walker, L.A., Yardley, V., Croft, S.L. & Ghandehari, H. (2001). N-(2-hydroxypropyl)methacrylamide (HPMA) copolymers for targeted delivery of 8-aminoquinoline antileishmanial drugs. *Journal of Controlled Release*, **77,** 233-43.

Nan, A., Croft, S.L., Yardley, V. & Ghandehari, H. (2004). Targetable water-soluble polymer-drug conjugates for treatment of visceral leishmaniasis. *Journal of Controlled Release*, **94,** 115-127.

Murray, H.W., Berman, J.D., Davies, C.R. & Saravia, N.G. (2005). Advances in leishmaniasis. *Lancet*, **366,** 1561-77.

Negre, E., Chance, M.L., Hanboula, S.Y., Monsigny, M., Roche, A.C., Mayer, R.M. & Hommel, M. (1992). Antileishmanial drug targeting through glycosylated polymers specifically internalized by macrophage membrane lectins. *Antimicrobial Agents Chemotherapy*, **36,** 2228-32.

New, R.R., Chance, M.L. & Heath, S. (1981). Antileishmanial activity of amphotericin and other antifungal agents entrapped in liposomes. *The Journal of Antimicrobial Chemotherapy*, **8,** 371-81.

New, R.R., Chance, M.L., Thomas, S.C. & Peters, W. (1978). Antileishmanial activity of antimonials entrapped in liposomes. *Nature*, **272,** 55-6.

Nishi, K.K., Antony, M., Mohanan, P.V., Anilkumar, T.V., Loiseau, P.M. & Jayakrishnan, A. (2007). Amphotericin B-gum arabic conjugates: synthesis, toxicity, bioavailability, and activities against *Leishmania* and fungi. *Pharmaceutical Research*, **24,** 971-80.

Nori, A., Jensen, K.D., Tijerina, M., Kopeckova, P. & Kopecek, J. (2003). Subcellular trafficking of HPMA copolymer-Tat conjugates in human ovarian carcinoma cells. *Journal of Controlled Release*, **91,** 53-9.

Nori, A., Jensen, K.D., Tijerina, M., Kopeckova, P. & Kopecek, J. (2003). Tat-conjugated synthetic macromolecules facilitate cytoplasmic drug delivery to human ovarian carcinoma cells. *Bioconjugate Chemistry*, **14,** 44-50.

North, A.J. (2006). Seeing is believing? A beginners' guide to practical pitfalls in image acquisition. *Journal of Cell Biology*, **172,** 9-18.

Ogunkolade, B.W., Colomb-Valet, I., Monjour, L., Rhodes-Feuillette, A., Abita, J.P. & Frommel, D. (1990). Interactions between the human monocytic leukaemia THP-1 cell line and Old and New World species of *Leishmania*. *Acta Tropica*, **47,** 171-6.

O'Hare, K.B., Duncan, R., Strohalm, J., Ulbrich, K. & Kopeckova, P. (1993). Polymeric drug-carriers containing doxorubicin and melanocyte-stimulating hormone: in vitro and in vivo evaluation against murine melanoma. *Journal of Drug Targeting*, **1,** 217-29.

Omelyanenko, V., Kopeckova, P., Gentry, C. & Kopecek, J. (1998). Targetable HPMA copolymer-adriamycin conjugates. Recognition, internalization, and subcellular fate. *Journal of Controlled Release*, **53,** 25-37.

Opanasopit, P., Higuchi, Y., Kawakami, S., Yamashita, F., Nishikawa, M. & Hashida, M. (2001). Involvement of serum mannan binding proteins and mannose receptors in uptake of mannosylated liposomes by macrophages. *Biochimica et Biophysica*

Acta, **1511,** 134-45.

Ordonez-Gutierrez, L., Espada-Fernandez, R., Dea-Ayuela, M.A., Torrado, J.J., Bolas-Fernandez, F. & Alunda, J.M. (2007). In vitro effect of new formulations of amphotericin B on amastigote and promastigote forms of *Leishmania infantum*. *International Journal of Antimicrobial Agents*, **30,** 325-9.

Otsubo, T., Maesaki, S., Hossain, M.A., Yamamoto, Y., Tomono, K., Tashiro, T., Seki, J., Tomii, Y., Sonoke, S. & Kohno, S. (1999). In vitro and in vivo activities of NS-718, a new lipid nanosphere incorporating amphotericin B, against Aspergillus fumigatus. *Antimicrobial Agents Chemotherapy*, **43,** 471-5.

Ouellette, M., Drummelsmith, J. & Papadopoulou, B. (2004). Leishmaniasis: drugs in the clinic, resistance and new developments. *Drug Resistance Updates*, **7,** 257-266.

Paul, M., Durand, R., Boulard, Y., Fusai, T., Fernandez, C., Rivollet, D., Deniau, M. & Astier, A. (1998). Physicochemical characteristics of pentamidine-loaded polymethacrylate nanoparticles: implication in the intracellular drug release in Leishamnia major infected mice. *Journal of Drug Targeting*, **5,** 481-90.

Perez-Victoria, F.J., Sanchez-Canete, M.P., Seifert, K., Croft, S.L., Sundar, S., Castanys, S. & Gamarro, F. (2006). Mechanisms of experimental resistance of *Leishmania* to miltefosine: Implications for clinical use. *Drug Resistance Updates*, **9,** 26-39.

Petit, C., Yardley, V., Gaboriau, F., Bolard, J. & Croft, S.L. (1999). Activity of a heat-induced reformulation of amphotericin B deoxycholate (fungizone) against *Leishmania donovani*. *Antimicrobial Agents Chemotherapy*, **43,** 390-2.

Pluddemann, A., Neyen, C. & Gordon, S. (2007). Macrophage scavenger receptors and host-derived ligands. *Methods*, **43,** 207-17.

Pontow, S.E., Kery, V. & Stahl, P.D. (1992). Mannose receptor. *International Review of Cytology*, **137B,** 221-44.

Posey, J.A., 3rd, Saif, M.W., Carlisle, R., Goetz, A., Rizzo, J., Stevenson, S., Rudoltz, M.S., Kwiatek, J., Simmons, P., Rowinsky, E.K., Takimoto, C.H. & Tolcher, A.W. (2005). Phase 1 study of weekly polyethylene glycol-camptothecin in patients with advanced solid tumors and lymphomas. *Clinical Cancer Research*, **11,** 7866-71.

Raay, B., Maedda, S., Mukhopadhyay, S. & Basu, M.K. (1999). Targeting of piperine intercalated in mannose-coated liposomes in experimental leishmaniasis. *Indian Journal of Biochemistry and Biophysics*, **36,** 248-51.

Rabinovitch, M., Topper, G., Cristello, P. & Rich, A. (1985). Receptor-mediated entry of peroxidases into the parasitophorous vacuoles of macrophages infected with *Leishmania Mexicana amazonensis*. *Journal of Leukocyte Biology*, **37,** 247-61.

Rademaker-Lakhai, J.M., Terret, C., Howell, S.B., Baud, C.M., De Boer, R.F., Pluim, D., Beijnen, J.H., Schellens, J.H. & Droz, J.P. (2004). A Phase I and pharmacological study of the platinum polymer AP5280 given as an intravenous infusion once every 3 weeks in patients with solid tumors. *Clinical Cancer Research*, **10,** 3386-95.

Radtke, O.A., Foo, L.Y., Lu, Y., Kiderlen, A.F. & Kolodziej, H. (2003). Evaluation of sage phenolics for their antileishmanial activity and modulatory effects on interleukin-6, interferon and tumour necrosis factor-alpha-release in RAW 264.7 cells. *Zeitschrift fur Naturforschung C*, **58,** 395-400.

Rasband, W.S. (1997-2007). Image J. National Institutes of Health: Bethesda, Maryland, USA.

Raschke, W.C., Baird, S., Ralph, P. & Nakoinz, I. (1978). Functional macrophage cell lines transformed by Abelson leukemia virus. *Cell*, **15,** 261-7.

Raveh, D., Kruskal, B.A., Farland, J. & Ezekowitz, R.A. (1998). Th1 and Th2 cytokines

cooperate to stimulate mannose-receptor-mediated phagocytosis. *Journal of Leukocyte Biology*, **64,** 108-13.

Rejmanova, P., Kopecek, J., Duncan, R. & Lloyd, J.B. (1985). Stability in rat plasma and serum of lysosomally degradable oligopeptide sequences in N-(2-hydroxypropyl) methacrylamide copolymers. *Biomaterials*, **6,** 45-8.

Rejmanova, P., Labsky, J. & Kopacek, j. (1977). Aminolysis of monomeric and polymeric 4-nitrophenyl esters of N-methacryloylamino acids. *Die Makromolekulare Chemie*, **178,** 2159-2168.

Richardson, S.C., Wallom, K.L., Ferguson, E.L., Deacon, S.P., Davies, M.W., Powell, A.J., Piper, R.C. & Duncan, R. (2008). The use of fluorescence microscopy to define polymer localisation to the late endocytic compartments in cells that are targets for drug delivery. *Journal of Control Release.*

Ridente, Y., Aubard, J. & Bolard, J. (1999). Absence in amphotericin B-spiked human plasma of the free monomeric drug, as detected by SERS. *FEBS Letters*, **446,** 283-6.

Ringsdorf, H. (1975). Structure and properties of pharmacological active polymers. *Journal of Pharmaceutical Science Polymer Symposium*, **51,** 135-153.

Rittig, M.G. & Bogdan, C. (2000). *Leishmania*-host-cell interaction: complexities and alternative views. *Parasitology Today*, **16,** 292-7.

Rouleux-Bonnin, F., Monsigny, M. & Legrand, A. (1995). Transcriptional expression of mannose receptor gene during differentiation of human macrophages. *Biochemical and Biophysical Research Communications*, **217,** 106-12.

Russell, D.G., Xu, S. & Chakraborty, P. (1992). Intracellular trafficking and the parasitophorous vacuole of *Leishmania mexicana*-infected macrophages. *Journal of Cell Science*, **103,** 1193-1210.

Sacks, D.L. (1989). Metacyclogenesis in *Leishmania* promastigotes. *Experimental Parasitology*, **69,** 100-3.

Sallusto, F., Cella, M., Danieli, C. & Lanzavecchia, A. (1995). Dendritic cells use macropinocytosis and the mannose receptor to concentrate macromolecules in the major histocompatibility complex class II compartment: downregulation by cytokines and bacterial products. *Journal of Experimental Medicine*, **182,** 389-400.

Sanchez-Brunete, J.A., Dea, M.A., Rama, S., Bolas, F., Alunda, J.M., Torrado-Santiago, S. & Torrado, J.J. (2005). Influence of the vehicle on the properties and efficacy of microparticles containing amphotericin B. *Journal of Drug Targeting*, **13,** 225-33.

Sano, H., Hsu, D.K., Apgar, J.R., Yu, L., Sharma, B.B., Kuwabara, I., Izui, S. & Liu, F.T. (2003). Critical role of galectin-3 in phagocytosis by macrophages. *Journal of Clinical Investigation*, **112,** 389-97.

Saraiva, E.M., de Figueiredo Barbosa, A., Santos, F.N., Borja-Cabrera, G.P., Nico, D., Souza, L.O., de Oliveira Mendes-Aguiar, C., de Souza, E.P., Fampa, P., Parra, L.E., Menz, I., Dias, J.G., Jr., de Oliveira, S.M. & Palatnik-de-Sousa, C.B. (2006). The FML-vaccine (Leishmune) against canine visceral leishmaniasis: a transmission blocking vaccine. *Vaccine*, **24,** 2423-31.

Satchi-Fainaro, R., Puder, M., Davies, J.W., Tran, H.T., Sampson, D.A., Greene, A.K., Corfas, G. & Folkman, J. (2004). Targeting angiogenesis with a conjugate of HPMA copolymer and TNP-470. *Nature Medicine*, **10,** 255-61.

Schneider, W.C. (1948). Intracellular distribution of enzymes. III. The oxidation of octanoic acid by rat liver fractions. *Journal of Biological Chemistry*, **176,** 259-276.

Schneider, W.C. & Hogeboom, G.H. (1951). Cytochemical studies of mammalian tissues; the isolation of cell components by differential centrifugation: a review. *Cancer Research*, **11,** 1-22.

Screiber, F. (2004). BSA ribbon. In *www.physchem.ox.ac.uk/~fs/images/BSA_ribbon.gif*, (accessed 2006).

Schwende, H., Fitzke, E., Ambs, P. & Dieter, P. (1996). Differences in the state of differentiation of THP-1 cells induced by phorbol ester and 1,25-dihydroxyvitamin D3. *Journal of Leukocyte Biology*, **59,** 555-61.

Scianimanico, S., Desrosiers, M., Dermine, J.F., Meresse, S., Descoteaux, A. & Desjardins, M. (1999). Impaired recruitment of the small GTPase rab7 correlates with the inhibition of phagosome maturation by *Leishmania donovani* promastigotes. *Cellular Microbiology*, **1,** 19-32.

Sedlak, M., Pravda, M., Kubicova, L., Mikulcikova, P. & Ventura, K. (2007). Synthesis and characterisation of a new pH-sensitive amphotericin B--poly(ethylene glycol)-b-poly(L-lysine) conjugate. *Bioorganic Medicinal Chemistry Letters*, **17,** 2554-7.

Sedlak, M., Pravda, M., Staud, F., Kubicova, L., Tycova, K. & Ventura, K. (2007). Synthesis of pH-sensitive amphotericin B-poly(ethylene glycol) conjugates and study of their controlled release *in vitro*. *Bioorganic Medicinal Chemistry Letters*, **15,** 4069-76.

Seib, P.F., Jones, A.T. & Duncan, R. (2006). Establishment of subcellular fractionation techniques to monitor the intracellular fate of polymer theraputics I. Differential centrifugation fractionation of B16F10 cells and use to study the intracellular fate of HPMA copolymer-doxorubicin. *Journal of Drug Targeting*, **14,** 375-390.

Seifert, K. (2007). Confocal microscope images of *L. donovani*-infected THP-1 cells incubated with HPMA copolymer-OG-Man.

Seifert, K. (2007). *In vitro* activity of of HPMA copolymer-AmB ± Man conjugates against *L. donovani*-infected THP-1 cells.

Sett, R., Sarkar, K. & Das, P.K. (1993). Pharmacokinetics and biodistribution of methotrexate conjugated to mannosyl human serum albumin. *Journal of Antimicrobial Chemotherapy*, **31,** 15109.

Sett, R., Sarkar, K. & Das, P.K. (1993). Macrophage-directed delivery of doxorubicin conjugated to neoglycoprotein using leishmaniasis as the model disease. *Journal of Infectious Diseases*, **168,** 994-9.

Seymour, L.W., Duncan, R., Strohalm, J. & Kopecek, J. (1987). Effect of molecular weight (Mw) of N-(2-hydroxypropyl)methacrylamide copolymers on body distribution and rate of excretion after subcutaneous, intraperitoneal, and intravenous administration to rats. *Journal of Biomedical Materials Research*, **21,** 1341-58.

Seymour, L.W., Ferry, D.R., Anderson, D., Hesslewood, S., Julyan, P.J., Poyner, R., Doran, J., Young, A.M., Burtles, S. & Kerr, D.J. (2002). Hepatic drug targeting: phase I evaluation of polymer-bound doxorubicin. *Journal of Clinical Oncology*, **20,** 1668-76.

Seymour, L.W., Ulbrich, K., Wedge, S.R., Hume, I.C., Strohalm, J. & Duncan, R. (1991). N-(2-hydroxypropyl)methacrylamide copolymers targeted to the hepatocyte galactose-receptor: pharmacokinetics in DBA2 mice. *British Journal of Cancer*, **63,** 859-66.

Sheff, D.R., Daro, E.A., Hull, M. & Mellman, I. (1999). The receptor recycling pathway contains two distinct populations of early endosomes with different sorting functions. *Journal of Cell Biology*, **145,** 123-39.

Shepherd, V.L., Abdolrasulnia, R., Garrett, M. & Cowan, H.B. (1990). Down-regulation

of mannose receptor activity in macrophages after treatment with lipopolysaccharide and phorbol esters. *The Journal of Immunology*, **145,** 1530-1536.

Shiah, J.G., Sun, Y., Kopeckova, P., Peterson, C.M., Straight, R.C. & Kopecek, J. (2001). Combination chemotherapy and photodynamic therapy of targetable N-(2-hydroxypropyl)methacrylamide copolymer-doxorubicin/mesochlorin e(6)-OV-TL 16 antibody immunoconjugates. *Journal of Controlled Release*, **74,** 249-53.

Sindermann, H., Croft, S.L., Engel, K.R., Bommer, W., Eibl, H.J., Unger, C. & Engel, J. (2004). Miltefosine (Impavido): the first oral treatment against leishmaniasis. *Medical Microbiology and Immunology*, **193,** 173-80.

Skeiky, Y.A., Kennedy, M., Kaufman, D., Borges, M.M., Guderian, J.A., Scholler, J.K., Ovendale, P.J., Picha, K.S., Morrissey, P.J., Grabstein, K.H., Campos-Neto, A. & Reed, S.G. (1998). LeIF: a recombinant *Leishmania* protein that induces an IL-12-mediated Th1 cytokine profile. *Journal of Immunology*, **161,** 6171-9.

Sprincl, L., Exner, J., Sterba, O. & Kopecek, J. (1976). New types of synthetic infusion solutions. III. Elimination and retention of poly-[N-(2-hydroxypropyl)methacrylamide] in a test organism. *Journal of Biomedical Materials Research*, **10,** 953-63.

St-Denis, A., Caouras, V., Gervais, F. & Descoteaux, A. (1999). Role of protein kinase C-alpha in the control of infection by intracellular pathogens in macrophages. *Journal of Immunology*, **163,** 5505-11.

Stahl, P. & Gordon, S. (1982). Expression of a mannosyl-fucosyl receptor for endocytosis on cultured primary macrophages and their hybrids. *Journal of Cell Biology*, **93,** 49-56.

Stahl, P., Schlesinger, P.H., Sigardson, E., Rodman, J.S. & Lee, Y.C. (1980). Receptor-mediated pinocytosis of mannose glycoconjugates by macrophages: characterization and evidence for receptor recycling. *Cell*, **19,** 207-15.

Stahl, P.D. (1992). The mannose receptor and other macrophage lectins. *Current Opinion in Immunology*, **4,** 49-52.

Stahl, P.D., Rodman, J.S., Miller, M.J. & Schlesinger, P.H. (1978). Evidence for receptor-mediated binding of glycoproteins, glycoconjugates, and lysosomal glycosidases by alveolar macrophages. *Proceedings of the National Academy of Sciences of the United States of America*, **75,** 1399-403.

St'astny, M., Ulbrich, K., Strohalm, J., Rossmann, P. & Rihova, B. (1997). Abnormal differentiation of thymocytes induced by free cyclosporine is avoided when cyclosporine bound to N-(2-hydroxypropyl)methacrylamide copolymer carrier is used. *Transplantation*, **63,** 1818-27.

Sterba, O., Paluska, E., Jozova, O., Spunda, J., Nezvalova, J., Sprincl, L., Kopecek, J. & Cinatl, J. (1976). New types of synthetic infusion solutions. Basic biological properties of poly N-(2-hydroxypropyl) methacrylamide. *Review of Czechoslovak Medicine*, **22,** 152-6.

Sundar, S., Rosenkaimer, F., Makharia, M.K., Goyal, A.K., Mandal, A.K., Voss, A., Hilgard, P. & Murray, H.W. (1998). Trial of oral miltefosine for visceral leishmaniasis. *Lancet*, **352,** 1821-3.

Sundar, S., More, D.K., Singh, M.K., Singh, V.P., Sharma, S., Makharia, A., Kumar, P.C. & Murray, H.W. (2000). Failure of pentavalent antimony in visceral leishmaniasis in India: report from the center of the Indian epidemic. *Clinical Infectious Diseases*, **31,** 1104-7.

Sundar, S., Agrawal, G., Rai, M., Makharia, M.K. & Murray, H.W. (2001). Treatment of Indian visceral leishmaniasis with single or daily infusions of low dose liposomal

amphotericin B: randomised trial. *British Medical Journal*, **323,** 419-22.

Sundar, S., Jha, T.K., Thakur, C.P., Bhattacharya, S.K. & Rai, M. (2006). Oral miltefosine for the treatment of Indian visceral leishmaniasis. *Transactions of the Royal Society of Tropical Medicine and Hygiene*.

Sundar, S. & Chatterjee, M. (2006). Visceral leishmaniasis - current therapeutic modalities. *Indian Journal of Medical Research*, **123,** 345-52.

Sundar, S., Jha, T.K., Thakur, C.P., Sinha, P.K. & Bhattacharya, S.K. (2007). Injectable paromomycin for visceral leishmaniasis in India. *New England Journal of Medicine*, **356,** 2571-81.

Swanson, J.A. & Baer, S.C. (1995). Phagocytosis by zippers and triggers. *Trends in Cell Biology*, **5,** 89-93.

Teitelbaum, R., Cammer, M., Maitland, M.L., Freitag, N.E., Condeelis, J. & Bloom, B.R. (1999). Mycobacterial infection of macrophages results in membrane-permeable phagosomes. *Proceedings of the National Academy of Science*, **96,** 15190-5.

Tempone, A.G., Perez, D., Rath, S., Vilarinho, A.L., Mortara, R.A. & de Andrade, H.F., Jr. (2004). Targeting Leishmania (L.) chagasi amastigotes through macrophage scavenger receptors: the use of drugs entrapped in liposomes containing phosphatidylserine. *Journal of Antimicrobial Chemotherapy*, **54,** 60-8.

Thakur, C.P., Kanyok, T.P., Pandey, A.K., Sinha, G.P., Messick, C. & Olliaro, P. (2000). Treatment of visceral leishmaniasis with injectable paromomycin (aminosidine). An open-label randomized phase-II clinical study. *Transactions of the Royal Society of Tropical Medicine and Hygiene*, **94,** 432-3.

Tijerina, M., Kopeckova, P. & Kopecek, J. (2001). The effects of subcellular localization of N-(2-hydroxypropyl)methacrylamide copolymer-Mce(6) conjugates in a human ovarian carcinoma. *Journal of Controlled Release*, **74,** 269-73.

Tijerina, M., Kopeckova, P. & Kopecek, J. (2003). Correlation of subcellular compartmentalization of HPMA copolymer-Mce6 conjugates with chemotherapeutic activity in human ovarian carcinoma cells. *Pharmaceutical Research*, **20,** 728-37.

Tiyaboonchai, W. & Limpeanchob, N. (2007). Formulation and characterization of amphotericin B-chitosan-dextran sulfate nanoparticles. *International Journal of Pharmaceutics*, **329,** 142-9.

Tremblay, M., Olivier, M. & Bernier, R. (1996). *Leishmania* and the pathogenesis of HIV infection. *Parasitology Today*, **12,** 257.

Trouet, A., Deprez-de Campeneere, D. & De Duve, C. (1972). Chemotherapy through lysosomes with a DNA-daunorubicin complex. *Nature: New Biology*, **239,** 110-2.

Tsuchiya, S., Yamabe, M., Yamaguchi, Y., Kobayashi, Y., Konno, T. & Tada, K. (1980). Establishment and characterization of a human acute monocytic leukemia cell line (THP-1). *International Journal of Cancer*, **26,** 171-6.

Tulkens, P., Beaufay, H. & Trouet, A. (1974). Analytical fractionation of homogenates from cultured rat embryo fibroblasts. *Journal of Cell Biology*, **63,** 383-401.

Ulbrich, K. & Subr, V. (2004). Polymeric anticancer drugs with pH-controlled activation. *Advanced Drug Delivery Reviews*, **56,** 1023-1050.

Vakil, R. & Kwon, G.S. (2005). PEG-phospholipid micelles for the delivery of amphotericin B. *Journal of Controlled Release*, **101,** 386-9.

Vandermeulen, G., Rouxhet, L., Arien, A., Brewster, M.E. & Preat, V. (2006). Encapsulation of amphotericin B in poly(ethylene glycol)-block-poly(epsilon-caprolactone-co-trimethylenecarbonate) polymeric micelles. *International Journal of Pharmaceutics*, **309,** 234-40.

Vanlerberghe, V., Diap, G., Guerin, P.J., Meheus, F., Gerstl, S., Van der Stuyft, P. &

Boelaert, M. (2007). Drug policy for visceral leishmaniasis: a cost-effectiveness analysis. *Tropical Medicine & International Health*, **12,** 274-83.

Vasey, P.A., Kaye, S.B., Morrison, R., Twelves, C., Wilson, P., Duncan, R., Thomson, A.H., Murray, L.S., Hilditch, T.E., Murray, T., Burtles, S., Fraier, D., Frigerio, E. & Cassidy, J. (1999). Phase I clinical and pharmacokinetic study of PK1 [N-(2-hydroxypropyl)methacrylamide copolymer doxorubicin]: first member of a new class of chemotherapeutic agents-drug-polymer conjugates. Cancer Research Campaign Phase I/II Committee. *Clinical Cancer Research*, **5,** 83-94.

Vassault, A. (1983). Lactate dehydrogenase. In *Methods of Enzymatic Analysis: Enzymes I Oxidoreductases, Transferases*, Bergmeyer, H.U., Bergmeyer, J. & Graßl, M. (eds), Vol. 3. pp. 118 - 126. Verlag Chemie: Basel.

Venier-Julienne, M.C., Vouldoukis, I., Monjour, L. & Benoit, J.P. (1995). *In vitro* study of the anti-leishmanial activity of biodegradable nanoparticles. *Journal of Drug Targeting*, **3,** 23-9.

Vertut-Doi, A., Ohnishi, S.I. & Bolard, J. (1994). The endocytic process in CHO cells, a toxic pathway of the polyene antibiotic amphotericin B. *Antimicrobial Agents Chemotherapy*, **38,** 2373-9.

Vicent, M.J., Greco, F., Nicholson, R.I., Paul, A., Griffiths, P.C. & Duncan, R. (2005). Polymer therapeutics designed for a combination therapy of hormone-dependent cancer. *Angewandte Chemie International Edition*, **44,** 4061-6.

Vogelsinger, H., Weiler, S., Djanani, A., Kountchev, J., Bellmann-Weiler, R., Wiedermann, C.J. & Bellmann, R. (2006). Amphotericin B tissue distribution in autopsy material after treatment with liposomal amphotericin B and amphotericin B colloidal dispersion. *Journal of Antimicrobial Chemotherapy*, **57,** 1153-60.

Vyas, S.P., Katare, Y.K., Mishra, V. & Sihorkar, V. (2000). Ligand directed macrophage targeting of amphotericin B loaded liposomes. *International Journal of Pharmaceutics*, **210,** 1-14.

Vyas, S.P., Quraishi, S., Gupta, S. & Jaganathan, K.S. (2005). Aerosolized liposome-based delivery of amphotericin B to alveolar macrophages. *International Journal of Pharmaceutics*, **296,** 12-25.

Vyas, S.P. & Sihorkar, V. (2000). Endogenous carriers and ligands in non-immunogenic site-specific drug delivery. *Advanced Drug Delivery Reviews*, **43,** 101-64.

Wallom, K.L., Richardson, S.C., Duncan, R. & Gilbert, I.H. (2008). Establishment of a subcellular fractionation method for THP-1 cells: studies on the fate of HPMA copolymer conjugates. In *International Syposium on Polymer Therapeutics, Laboratory to Clinical Practice.*: Valencia, Spain.

Walsh, T.J., Jackson, A.J., Lee, J.W., Amantea, M., Sein, T., Bacher, J. & Zech, L. (2000). Dose-dependent pharmacokinetics of amphotericin B lipid complex in rabbits. *Antimicrobial Agents Chemotherapy*, **44,** 2068-76.

Wang, L.H., Smith, P.C., Anderson, K.L. & Fielding, R.M. (1992). High-performance liquid chromatographic analysis of amphotericin B in plasma, blood, urine and tissues for pharmacokinetic and tissue distribution studies. *Journal of Chromatography*, **579,** 259-68.

Wang, D., Sima, M., Mosley, R.L., Davda, J.P., Tietze, N., Miller, S.C., Gwilt, P.R., Kopeckova, P. & Kopecek, J. (2006). Pharmacokinetic and biodistribution studies of a bone-targeting drug delivery system based on N-(2-hydroxypropyl)methacrylamide copolymers. *Molecular Pharmacology*, **3,** 717-25.

Wasan, K.M., Morton, R.E., Rosenblum, M.G. & Lopez-Berestein, G. (1994). Decreased toxicity of liposomal amphotericin B due to association of amphotericin B with high-density lipoproteins: role of lipid transfer protein. *Journal of Pharmaceutical*

Sciences, **83,** 1006-10.

Wedge, S.R., Duncan, R. & Kopeckova, P. (1991). Comparison of the liver subcellular distribution of free daunomycin and that bound to galactosamine targeted N-(2-hydroxypropyl)methacrylamide copolymers, following intravenous administration in the rat. *British Journal of Cancer*, **63,** 546-9.

Weldon, J.S., Munnell, J.F., Hanson, W.L. & Alving, C.R. (1983). Liposomal chemotherapy in visceral leishmaniasis: an ultrastructural study of an intracellular pathway. *Zeitschrift fur Parasitenkunde*, **69,** 415-24.

WHO. (2003). In *www.who.int/tdr/tropical_diseases/databases/imagelib.pl*, (Accessed 2007).

WHO/CDS/CSR/ISR/2000. (2001). Leishmaniasis and *Leishmania*/HIV co-infection. WHO Report on Global Surveillance of Epidemic Prone Infectious Diseases.

WHO. (2006). Control of Leishmaniasis. Report by the Sectretariat. pp. 1-7. WHO.

Wileman, T., Boshans, R.L., Schlesinger, P. & Stahl, P. (1984). Monensin inhibits recycling of macrophage mannose-glycoprotein receptors and ligand delivery to lysosomes. *The Biochemical Journal*, **220,** 665-75.

Wileman, T.E., Lennartz, M.R. & Stahl, P.D. (1986). Identification of the macrophage mannose receptor as a 175-kDa membrane protein. *Proceedings of the National Academy of Sciences of the United States of America*, **83,** 2501-5.

Wilson, M.E. & Pearson, R.D. (1986). Evidence that *Leishmania donovani* utilizes a mannose receptor on human mononuclear phagocytes to establish intracellular parasitism. *Journal of Immunology*, **136,** 4681-8.

Wingard, J.R., White, M.H., Anaissie, E., Raffalli, J., Goodman, J. & Arrieta, A. (2000). A randomized, double-blind comparative trial evaluating the safety of liposomal amphotericin B versus amphotericin B lipid complex in the empirical treatment of febrile neutropenia. L Amph/ABLC Collaborative Study Group. *Clinical Infectious Disease*, **31,** 1155-63.

Wu, W., Wieckowski, S., Pastorin, G., Benincasa, M., Klumpp, C., Briand, J.P., Gennaro, R., Prato, M. & Bianco, A. (2005). Targeted delivery of amphotericin B to cells by using functionalized carbon nanotubes. *Angewandte Chemie International Edition English*, **44,** 6358-62.

Yamasaki, M., Takahashi, N. & Hirose, M. (2003). Crystal structure of S-ovalbumin as a non-loop-inserted thermostabilized serpin form. *Journal of Biolical Chemistry*, **278,** 35524-30.

Yardley, V. & Croft, S.L. (2000). A comparison of the activities of three amphotericin B lipid formulations against experimental visceral and cutaneous leishmaniasis. *International Journal of Antimicrobial Agents*, **13,** 243-248.

Zarabi, B., Nan, A., Zhuo, J., Gullapalli, R. & Ghandehari, H. (2006). Macrophage targeted N-(2-hydroxypropyl)methacrylamide conjugates for magnetic resonance imaging. *Molecular Pharmacology*, **3,** 550-7.

Zarif, L. (2005). Drug delivery by lipid cochleates. *Methods in Enzymology*, **391,** 314-29.

Zhao, C., Papadopoulou, B. & Tremblay, M.J. (2004). *Leishmania infantum* enhances human immunodeficiency virus type-1 replication in primary human macrophages through a complex cytokine network. *Clinical Immunology*, **113,** 81-88.

Zimmer, H., Riese, S. & Regnier-Vigouroux, A. (2003). Functional characterisation of mannose receptor expressed by immunocompetant mouse microglia. *Glia*, **41,** 89-100.

Zwier, J.M., Van Rooij, G.J., Hofstraat, J.W. & Brakenhoff, G.J. (2004). Image calibration in fluorescence microscopy. *Journal of Microscopy*, **216,** 15-24.

Appendix

PUBLICATIONS

Papers:

Richardson, S.C., Wallom, K.L., Ferguson, E.L., Deacon, S.P., Davies, M.W., Powell, A.J., Piper, R.C. & Duncan, R. (2008). The use of fluorescence microscopy to define polymer localisation to the late endocytic compartments in cells that are targets for drug delivery. *Journal of Controlled Release*, **127,** 1-11.

Wallom KL., Richardson S.C.W., Gilbert I., Duncan R. (2008) Establishment of a subcellular fractionation method for THP-1 cells: studies on the fate of HPMA copolymer conjugates. *Journal of Controlled Release* (in preparation).

Abstracts:

Wallom KL., Nicoletti S., Seifert K., Gilbert I., and Duncan R. (2007). Synthesis and biological characterisation of HPMA copolymer-mannose conjugates for macrophage targeting. *Proceedings of the 1st European Science Foundation Summer School on Nanomedicine, Cardiff.*

Wallom KL., Richardson S.C.W., Gilbert I., Duncan R. (2008) Establishment of a subcellular fractionation method for THP-1 cells: studies on the fate of HPMA copolymer conjugates. *Proceedings of the International Symposium on Polymer Therapeutics: Laboratory to Clinical Practice, Valencia, Spain.*